`

STUDY OF GROUNDWATER PROPERTIES AND BEHAVIOUR USING GEOSPATIAL TECHNIQUES

By

Vivek Agarwal

Thesis submitted to the University of Nottingham for the degree of Doctor of Philosophy

November 2021

`

Declaration

This is to declare that the contents of this thesis are my own work and were performed at the University of Nottingham from 2017 to 2021. This thesis has not been submitted to any other institution for another degree.

The thesis contains publication work that has been jointly written with co-authors. The contribution made by me and other authors has been explicitly indicated below each chapter where publication is presented, and appropriate credit is given to the contribution of others.

Vivek Agarwal

Faculty of Engineering, University of Nottingham

November 2021

Email: vivek.agarwal@nottingham.ac.uk, vacivil@gmail.com

`

Acknowledgements

This PhD is funded by the University of Nottingham Faculty of Engineering Research Excellence PhD scholarship, and the research has been undertaken at the Faculty of Engineering, University of Nottingham.

I want to express my sincere gratitude and appreciation to Prof. Stuart Marsh and Prof. Rachel L. Gomes for their guidance, motivation, support, and patience during my study. The completion of this work would be impossible without their continuous supervision.

I would like to thank the European Space Agency (ESA)-Eohops program for providing funding for ENVI-SARscape software in association with Harris Geospatial. I would also like to thank Environment Agency, UK and Central Ground Water Board, India, for providing the boreholes groundwater data.

I want to thank my colleague and friend, Mr Amit Kumar, for providing immense technical help and moral support. He engaged in long hours of discussions and was always present in hours of need for the last three years. Surviving the lockdown and finishing the work on time would be really difficult without his support.

I want to express sincere gratitude to Dr Stephen Grebby for providing valuable feedback during the yearly reviews and supporting the study in critical instances. I would also thank Dr David Gee for helping with InSAR processing and analysing the results.

I would like to thank all members of Nottingham Geospatial Institute, and Food Water Waste for their friendly and inclusive behaviour towards me. I would thank all my friends whose morale support and social skills motivated me to keep going, especially during the COVID lockdown period, namely Amit, Dr. Tamal, Tusharika, Dr. Utkarsh, Sweta, Zhengyuan, Vishal, Yusuf and Shahrukh.

I would like to thank my parents and family for always supporting me. I want to mention special gratitude to my grandmother Mrs. Kamla Devi and my uncle Mr. Hariom Agarwal, for their immense impact and contribution to my life.

`

Publications and Presentations

Publications

Agarwal, Vivek*; Kumar, Amit; L. Gomes, Rachel; Marsh, Stuart. 2021. '*Evaluating spatio-temporal decadal-scale changes in groundwater quality for London, 2000-2020'*. Journal of Hydrology: Regional Studies (In revision).

Agarwal, Vivek*; Kumar, Amit; Gee, David; Grebby, Stephen; L. Gomes, Rachel; Marsh, Stuart. 2021. '*"Comparative Study of Groundwater-Induced Subsidence for London and Delhi Using PSInSAR"*. Remote Sensing 13, no. 23: 4741. **https://doi.org/10.3390/rs13234741**

Agarwal, Vivek*; Kumar, Amit; L. Gomes, Rachel; Marsh, Stuart. 2020. '*Monitoring of Ground Movement and Groundwater Changes in London Using InSAR and GRACE*' Applied Sciences 10, no. 23: 8599**. https://doi.org/10.3390/app10238599**

Agarwal, Vivek*; Kumar, Amit; L. Gomes, Rachel; Marsh, Stuart. 2020. '*An Overview of Sar Sensors And Software And A Comparative Study Of Open Source (Snap) And Commercial (Sarscape) Software For DInSAR Analysis Using C-Band Radar Images*'. Asian Conference of Remote Sensing – 2020, November 9-11 online, hosted at Deqing city, China.

`

Conference Presentations

Agarwal, Vivek; Kumar, Amit; L. Gomes, Rachel; Marsh, Stuart. 2021. '*Investigating spatio-temporal changes in groundwater quality for London between 2000-2020'.* AGU Fall Meeting, New Orleans, Louisiana, 13-17 December 2021.

Agarwal, Vivek; Kumar, Amit; L. Gomes, Rachel; Marsh, Stuart. 2021. '*Mapping and modelling of groundwater and resulting subsidence'*. International Symposium of Resilient City & The 21st Annual General Meeting of UK-China Association of Resources and Environment (UK-CARE), 3-4 November 2021.

Agarwal, Vivek; Kumar, Amit; L. Gomes, Rachel; Marsh, Stuart. 2021. '*Comparison of groundwater induced Land subsidence in London and Delhi using PSInSAR*'. The European Geosciences Union, EGU General Assembly 2021, online, 19–30 Apr 2021, hosted at Vienna, Austria, EGU21-10707, https://doi.org/10.5194/egusphere-egu21-10707, 2021.

Agarwal, Vivek; L. Gomes, Rachel; Marsh, Stuart. 2019. '*Studying groundwater variation using geospatial techniques'*. The Geological Remote Sensing Group (GRSG) AGM -2019, December 9-12 at European Space Agency in Frascati, Italy.

Agarwal, Vivek; L. Gomes, Rachel; Marsh, Stuart. 2018. '*Open source DInSAR processing for Sentinal-1 data using ESA SNAP*'. The Geological Remote Sensing Group (GRSG) AGM -2018, December 9-12 at Geological society, Piccadilly, London.

`

Abstract

Groundwater contributes a significant proportion of the earth's freshwater and is essential to sustain life on earth, but its availability in spatial and temporal dimensions is not uniform. With the advent of efficient pumps and rural electrification, global groundwater extraction increased from 312 km^3/year in the 1960s to 800 km^3/year in 2000s; approximately 70% of this extraction is used for agriculture. About half of domestic human water consumption in urban areas is from groundwater. The ever-increasing dependence on groundwater has led to its depletion across various parts of the world. This trend must be reversed to sustain the critical role of groundwater. Groundwater monitoring based on validated data can provide information that can guide decision making to decrease groundwater stress on local and global scales. This thesis aims to monitor spatio-temporal changes in groundwater and related phenomena (like land subsidence) using geospatial techniques like InSAR, GRACE, GIS, data analysis and data visualisation.

The over-extraction or rebound of groundwater can lead to land deformation because of the change in effective stress of underground sediments. Groundwater-induced land movement can cause damage to property and resources, and hence it must be monitored for the safety and economics of a city. This thesis explores the suitability of Persistent Scatterer Interferometric Synthetic Aperture Radar (PSInSAR) to measure land deformation and different senor-software for InSAR processing. The groundwater quantity variation and resulting land deformation for London using InSAR and Gravity Recovery and Climate Experiment (GRACE) between 2002-2010 were analysed. Long-term, decreasing, complex, non-linear patterns in the spatial and temporal domains from both InSAR and GRACE datasets were observed. The land movement velocities varied from -6 to +6 mm/year, and their reliability was validated with observed GNSS data by conducting a two-sample t-test. The average groundwater loss estimated from GRACE was found to be 9.003 MCM/year. The results demonstrate that InSAR and GRACE complement each other and can be an excellent source of monitoring groundwater for hydrologists. Then groundwater induced subsidence for London and the National Capital Territory of Delhi (NCT-Delhi) between 2016 and 2020 were studied. The land movement velocities were found to vary between -24 mm/year to +24 mm/year for London and between -18 mm/year to +30 mm/year for NCT-Delhi. This land movement was compared with observed groundwater levels and spatio-temporal variation of groundwater. A 1-D mathematical model was used to quantify land deformation for a given change

`

in groundwater level. It was broadly observed that when large volumes of groundwater are extracted, it leads to land subsidence, and when groundwater is recharged, surface uplift is witnessed. However the local geology, did play an important role in the extent of subsidence, which was considered in the mathematical model.

The increased pressure on groundwater can cause spatio-temporal changes in its quality because of various atmospheric stimulations, varied geology, variation in subsurface mineralogy and factors controlling residence times. Moreover, the variation of groundwater quality is vital for the sustainable management and safety of groundwater. Thus, the variation in groundwater quality is analysed from observed data for London between 2000 and 2020. The data samples were used from 500 wells in the London basin, and the data is provided in the free open access domain by Environment Agency. The overall groundwater in London was found to be dominant magnesium bicarbonate type which typically represents shallow fresh groundwater, and spatio-temporal variations of hardness, sodium, and dissolved oxygen (DO) were also studied. Significant variations in the range of each constituent were found, which was attributed to variation in the geology of the London Palaeogene aquifers and anthropogenic activities.

All the case studies help better understand the phenomenon of spatio-temporal variation in groundwater behaviour and associated land deformation for urban cities. The research presented in this thesis can be used to determine whether groundwater is available and suitable for its intended purpose, discover pollutants, examine any spatio-temporal variations, and monitor land subsidence.

`

Table of Contents:

`

List of Figures

`

`

`

`

List of Tables

`

List of Abbreviations

BGS: British Geological Survey

CGWB: Central Ground Water Board, India

DInSAR: Differential Interferometry Synthetic Aperture Radar

EA: Environment Agency

ERS-1: European Remote Sensing Satellite-1

ESA: European Space Agency

ESD: Enhanced Spectral Diversity

FAO: Food and Agriculture Organisation

GARDIT: General Aquifer Research, Development and Investigation Team

GCPs: Ground Control Points

GIS: Geographical Information Systems

GNSS: Global navigation satellite system

GRACE: Gravity Recovery and Climate Experiment

GUI: Graphical User Interface

GVL: Geomatic Ventures Limited

IW: Interferometric Wide

NCT-Delhi: National Capital Territory of Delhi

NGI: Nottingham Geospatial Institute

NISAR: NASA-ISRO Synthetic Aperture Radar

PSInSAR: Persistent Scatterer Interferometric Synthetic Aperture Radar

RS: Remote Sensing

SLC: Single Look Complex

TOPSAR: Terrain observation with Progressive Scans SAR

TWS: Total Water Storage

UNESCO: United Nations Educational, Scientific, and Cultural Organisation

WHO: World Health Organisation

`

Chapter 1 Introduction

1.1 Preface

Water is vital for sustaining life on earth, but it is non-uniformly distributed across the globe, both spatially and temporally. According to World Health Organisation (WHO), 785 million people around the globe lack even an essential drinking-water service, including 144 million people who are dependent on surface water. At least 2 billion people use drinking water sources that are contaminated with faeces and, by 2025, half of the world's population will be living in water-stressed areas (WHO, 2017). Groundwater is the most significant freshwater source globally and contributes to 97% of freshwater on earth (Guppy et al., 2018). It not only meets the domestic and industrial water demand but also caters for a major portion of irrigation water (Siebert et al., 2010). Furthermore, groundwater is less susceptible to pollution than surface water because the soil and rocks through which ground water flows screen out most of the pollutants and so groundwater tends to be a clean source of water, sometimes being able to be used with no prior treatment.

Groundwater is also crucial for sustainable management of water crises, as climate change will enforce increased drought frequency (Famiglietti & Rodell, 2013; Lehner et al., 2006). In Europe, more than 40% of domestic water demand is met through groundwater (Wolf et al., 2015). In England, approximately 35% of public water demand is fulfilled using groundwater, and for south and east England, this contribution rises to around 70% (Bonì et al., 2016). In India, more than 60% of irrigated agriculture and 85% of drinking water supplies are accomplished by groundwater (Bank, 2012). It also contributes to maintaining baseflows to rivers and wetlands during dry seasons, thus ensuring a sustainable water cycle (Royse et al., 2012). The ever-increasing dependence on groundwater has led to its depletion across various parts of the world (Aeschbach & Gleeson, 2012; An et al., 2016; Jasechko et al., 2017).

With the increase in urbanisation and waste discharge, groundwater depletion in terms of quantity and quality has increased swiftly and has become a global issue because of its possible effects on humanity (Abelson, 1984; Bulut et al., 2020; Grimmeisen et al., 2017; Kaur & Garg, 2019; D. Liu et al., 2019). This degradation is causing double water stresses (both quantity and quality depletion) in most urban areas across the globe, especially in arid areas (Cheng et al., 2019; Das et al., 2019; S. Liu & Li, 2019). There is extra pressure on groundwater resources in metro cities

`

like London and NCT-Delhi, where population density is high. This extra pressure can lead to exploitation of local water bodies, aquifer depletion, disturbance of groundwater-surface water interactions, land subsidence, and groundwater pollution (Koster & Suarez, 2001; Kustu et al., 2010; Y. Wang et al., 2019; Zuoding, 2002). Therefore, ensuring good quality, potable groundwater in sufficient amounts is the primary concern of water resource management and related research (An et al., 2016; Cai et al., 2019).

Groundwater is a critical resource in terms of both risks and opportunities. Increasing urbanisation and industrialisation worldwide has led to over-exploitation of 20% of the earth's aquifers (Gleeson et al., 2012). These trends must be reversed to sustain the critical role of groundwater. To ensure a safe water supply and reduce the severity of groundwater quality degradation, it is essential to identify the status of groundwater quality and assess the suitability of groundwater for drinking (Edmunds et al., 2003; Mattos et al., 2018). Groundwater monitoring based on validated data can provide information that can guide decision making to decrease groundwater stress on local and global scales.

Over-abstraction (or rebound) of groundwater can cause land subsidence (or uplift). The land subsidence (or uplift) is caused due to compression (or decompression) of the sub-surface aquifer system because of loss (or gain) in pore pressure within the aquifer, which is caused due to excessive groundwater discharge (or recharge) (Zheng et al., 2018). This land movement can cause significant and recurrent harm to infrastructure, increase flood and water contamination risks, and adversely affect hydrogeological characteristics of the aquifer. This is particularly pertinent with globally growing urbanisation. Traditional methods like levelling, GNSS (Global navigation satellite system), 3D laser scanning, and similar provide accurate information to map the land movement. However, when surveying large (basin level) areas these approaches are time-consuming, expensive, and have low spatial extent (Huang et al., 2016; Zheng et al., 2018).

To overcome the demerits of traditional methods for monitoring land movement over large areas (city or country scale), the Persistent Scatterer Interferometric Synthetic Aperture Radar (PSInSAR) technique can be used. It discovers coherent and stable scattering targets and uses their phase history to measure land movement. Moreover, it can provide weather independence (radar penetrates cloud), sunlight independence (radar is an active sensor) and high (basin-level or greater) spatial coverage. Therefore, PSInSAR offers better accuracy and spatial coverage as

`

compared to other traditional methods of land surveying. Many researchers have used it to study land movement resulting from earthquakes (Fialko et al., 2001), glacial movements (Wang et al., 2015), landslides (Kang et al., 2017; Q. Sun et al., 2015; Zhang et al., 2020), volcanic bulging (Albino et al., 2020; Fournier et al., 2010), sand motion (Albino et al., 2020; Fournier et al., 2010), and subsidence (Dai et al., 2015; Fan et al., 2015; Huang et al., 2016).

An urban area, also known as a built-up area, is a human community with a high population density (~>500 people/km^2) and built-environment infrastructure. Urban areas are classified as cities, towns, conurbations, or suburbs based on their urban morphology. In terms of PSInSAR, phase measurements depends on successful selection of points that appear stable across a set of satellite images taken overtime. Urban areas provide multiple stable points, owing to its built-up infrastructure like houses, commercial buildings,, bridges, roads, railway lines, poles and others. During the urban revolution, the establishment of early precursors of urban areas led to the development of contemporary urban planning, which, combined with other human activities such as the exploitation of natural resources, resulted in a human influence on the environment. Since then, "agglomeration effects" have been listed as one of the key repercussions of rising business creation rates.

The changes in groundwater quantity can be monitored using in situ measurements from boreholes. Nevertheless, it can be labour intensive and expensive work when surveying over basin or continental areas for multiple years. For example, drilling borehole and getting continuous monitoring data for multiple years over continental areas could be very costly, tedious and difficult to maintain. ‘Gravity Recovery and Climate Experiment (GRACE) gravimetry’ is a remote sensing tool that maps gravity anomalies and can monitor water storage. This water may include surface water, groundwater, soil moisture, snow and ice (Ramillien et al., 2016; Rodell et al., 2009; Tiwari et al., 2009; Wang et al., 2011; Zaitchik et al., 2008). It provides continuous monthly data globally, thus making monitoring less labour intensive and more economical. GRACE has emerged as a vital information source for hydrologists, as it can be used for taking optimal groundwater observations at a regional scale. When there is a significant change in groundwater, the corresponding mass change causes change in gravity, which can be detected by GRACE due to its high signal to noise ratio (Guo et al., 2016; Longuevergne et al., 2013; Tourian et al., 2015). Therefore, GRACE data can be a good source of monitoring the variation in groundwater storage.

`

In addition to monitoring groundwater quantity, another aspect to consider is its quality, because the availability of groundwater in ample amounts does not guarantee that the water is safe for its various uses. Keeping track of spatio-temporal variations in groundwater quality is vital for sustainable management and monitoring of groundwater safety for its desirable use. To observe groundwater quality on a decadal scale at a particular place, consistent data at regular intervals is desirable, but getting such consistent data, especially in the open domain, is rare. Statistics and Geographical Information Systems (GIS) can be helpful tools to obtain desired groundwater quality information even from inconsistent data (Bearcock & Smedley, 2010). Statistical methods, such as arithmetic means, standard deviation, kurtosis, and box plots, could be used to assess individual groundwater quality parameters (Jamshidzadeh & Mirbagheri, 2011) and require very rigorous analysis especially when the data are bounded with variable uncertainty. Also, Piper-Trilinear plots can indicate the overall quality of the groundwater (Morris et al., 1983). To study the spatial distribution, thematic maps could be made at desired time intervals for each water quality parameter.

This thesis focuses on the groundwater resources of London, United Kingdom (UK), as it is a true representation of urban cities across the world in a developed nation. Chalk is the most vital aquifer in the UK as it provides approximately 60% of the groundwater consumed in the UK (BGS, 2013) and accounts for nearly 80% of water supply in the River Thames catchment and 20% in London alone (Bonì et al., 2016). The Chalk is one of the most supervised and controlled aquifer systems in the UK and has provided water in London for domestic and industrial use since the 19th century (Jones et al., 2012; Royse et al., 2012). During the early and mid-twentieth century, substantial groundwater abstraction took place because of anthropogenic development around central London. This abstraction led to a decrease in the water level to 88 m below sea level in the 1960s, resulting in a depression of the water table. Due to de-industrialisation since the 1980s, groundwater abstraction reduced and recovered by 3 m/year in the 1990s. This rise in groundwater level caused a threat to infrastructure in the London basin. To check this rise, the General Aquifer Research, Development and Investigation Team (GARDIT) strategy was implemented in 1992 (EA, 2017). The GARDIT strategy was implemented using groundwater withdrawal licensing and monitoring, which stabilised the groundwater around the year 2000. Since then, groundwater has been monitored regularly.

`

Historically, the data on groundwater quality of London has shown significant variations at spatial and temporal scales both between and within aquifers (Bearcock & Smedley, 2010). Anthropogenic activities are continuously changing the natural groundwater chemistry in London. The concentration of individual water quality parameters varies significantly on a local scale, and thus drawing basin-wide predictions becomes difficult (Shand et al., 2007). The groundwater chemistry for the London basin and its variability is discussed in Ineson and Downing (1963), which summarised that towards the centre of the London Basin, the carbonate and non-carbonate hardness decreased while sulphate and chloride concentration increased. Abnormally high values of sulphate, calcium, magnesium, iron and manganese were also noticed in 1970-80s for London groundwater (Flavin & Joseph, 1983). They also found a high sulphate concentration in the Lee catchment where London clay was thin or absent. In the late 20th century, high concentrations of iron, sulphate and, in some instances, manganese have caused concern for the groundwater aquifers in London, suggesting either drainage from the Basal Sands, or possibly dissolution occurring during artificial recharge (Flavin & Hawn, 1979; Flavin & Joseph, 1983). Some other studies on groundwater quality focused on the London basin are Kinniburgh et al. (1994) on the Lee valley and Edmunds et al. (1987) on the western end of the basin in Berkshire. Towards the end of the 20th century, it was found that areas with significantly less or no London clay witnessed pyrite oxidation as during dewatering oxygen can actively enter these areas (Rae & Parker, 1992). The oxidation of pyrite releases iron into pore waters and leads to other essential mineral transformations such as the dissolution of carbonates and the formation of iron oxides and hydroxides. The British Geological Survey (BGS) published a report on ‘Baseline groundwater chemistry: the Palaeogene of the Thames Basin’ in 2010 (Bearcock & Smedley, 2010), and found that London groundwater experienced problems related to pyrite oxidation, which occurred irregularly in Palaeogene deposits, and can cause acidic, complex, metal-rich waters.

NCT-Delhi, India represents urban cities across the world in developing nations, and also witness high population explosion in the last few decades. To provide a comparison to London, a major groundwater system in the developed world, this thesis also analyses NCT-Delhi, India in the developing world for its groundwater quantity changes. India is home to over 1.3 million people, and its ever-increasing population, urbanisation and non-uniform extraction have increased the depletion rate of groundwater resources (Central Ground Water Board, 2018). The National Capital Territory (NCT) of Delhi lies in the heart of India and forms the capital city of the country.

`

The subsurface geological features of NCT-Delhi determine its discrete landform units and are directly related to groundwater availability. The primary source of irrigation in NCT-Delhi is groundwater, although surface water is also available from Trans Yamuna Canal Network. The Central Ground Water Board (CGWB), India, monitors and publishes groundwater records for India. It took up the aquifer mapping program during the 12th five-year plan (2012-2017) for the entire country (including NCT-Delhi) for sustainable development and management of groundwater resources (Central Ground Water Board, 2016a). The groundwater level in NCT-Delhi is continuously declining and has reached a critical stage (Gupte, 2019), and this decline in groundwater level can pose the threat of land subsidence (Garg et al., 2020).

In this thesis, the sensors-software combinations for InSAR data processing are studied, to investigate which sensors and software are available and suitable for SAR data processing. Also the thesis addresses groundwater quantity variation and resulting subsidence for London using InSAR and GRACE between the years 2002-2010, to explore the interdependence of groundwater variation and land subsidence. Further, groundwater induced subsidence for London and NCT-Delhi between 2016 and 2020 is compared and a mathematical model to quantity the relation between groundwater and subsidence was suggested. The thesis also studies variation in groundwater quality from observed data for London for 2000 to 2020, to explore if the available groundwater is suitable for potable purposes. These case studies show the spatio-temporal variation in overall quality and quantity of groundwater and related subsidence, and set methodology for future research in groundwater.

1.2 Aims and Objectives

The overarching goal of the thesis is to use geospatial techniques like InSAR, GRACE, GIS, observed in-situ data, data analysis and data visualisation to study the spatial and temporal changes in groundwater (both quality-quantity aspects) and related phenomenon (like land subsidence).

In this thesis, a novel attempt has been made to explore InSAR and GRACE technologies and their application to study variation in groundwater resources in conjunction, for London. Also, land subsidence for UK (London) and India (Delhi) has been studied as both these cities are witnessing an ever-increasing population growth that has exerted excess pressure on groundwater resources. Despite their different sub-surface geology, this increasing pressure on groundwater poses a significant threat of land movement in these cities. No previous study has attempted to examine

`

the groundwater behaviour and resulting land-subsidence for both these cities simultaneously. Furthermore, For London, there has been no comprehensive work in the last two decades that studies spatiotemporal variation of groundwater quality parameters. A comprehensive assessment of groundwater quality focused on London has been done to help allocate resources to maintain potable-quality groundwater. The overall aim is supported by several objectives as outlined below:

1.2.1 Objectives

The thesis has the following research objectives:

i. Study the sensors and software available for InSAR data processing and identify the sensor–software combination to be used in this thesis for SAR analysis, based on availability, requirements, and performance (addressed in **Chapter 3**).

ii. Identify the potential applications and limitations of using InSAR data over an urban area (addressed in **Chapters 3, 4 and 5)**.

iii. Study the groundwater quantity variation in London and resulting land subsidence using InSAR and GRACE (addressed in **Chapters 4 and 5)**.

iv. Compare groundwater induced subsidence for London and Delhi using PSInSAR (addressed in **Chapter 5)**.

v. Propose and use a mathematical model to quantify subsidence for a given change in groundwater (addressed in **Chapter 5)**.

vi. Evaluate spatio-temporal decadal-scale changes in groundwater quality for London, 2000-2020, and indicate overall groundwater quality (addressed in **Chapter 6).**

1.3 Thesis overview

The thesis contains eight chapters and has been summarised in Figure 1.1. The first two chapters are an introduction and literature review, and the following four chapters are four different case studies on InSAR processing, groundwater quantity variations in London, the same problem in Delhi and water quality variations in London. The seventh chapter is discussion where it is evaluated if the objectives drawn are achieved, and wider aspects of the research work are discussed. Finally, the last chapters answer the research questions, highlight the research

`

contributions, and summarise brief conclusions and suggestions for future work. This section briefly describes the contents of the thesis to provide a simple guide to the reader.

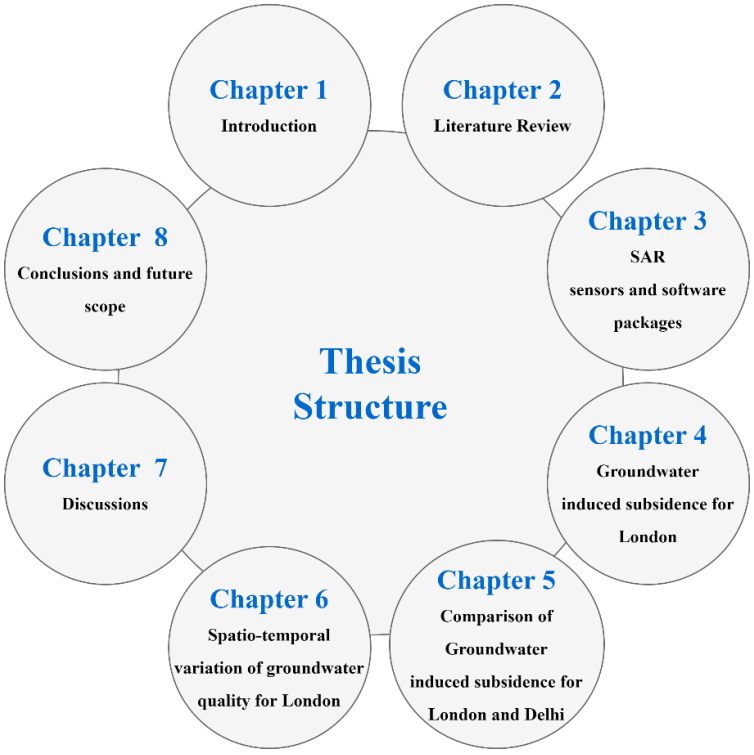

Figure 1.1: Summary of Thesis structure

Chapter One: introduces the research background and gives a general overview of the research problem. Accordingly, the research questions, aims, and objectives are set here. Also, the importance and motivation to undertake such topics are highlighted.

Chapter Two: reviews the existing studies in the literature and state of the art related to the topics of this research. It clarifies the importance of monitoring groundwater quantity and quality variation and the geospatial tools that could be used to study groundwater. The general background to the concept of radar, including a summary of the development of radar techniques from their initial conception, through to the most advanced SAR techniques, is discussed. It also contains the concept of GRACE satellite gravity measurements. Finally, statistical tools to study observed groundwater quality data are explained.

Chapter Three: comprises the first case study: It provides an overview of past, present and future SAR sensors and software packages. Differential Interferometry SAR (DInSAR) land displacement maps are created to understand the strengths and limitations of open source and

`

commercial SAR processing software. The open-source software SNAP and commercial software SARscape are used to generate the land displacement maps from Sentinel-1A data over London between April 2015 and April 2018.

Chapter Four: comprises the second case study: Groundwater-induced land movement is studied using InSAR and GRACE. ENVISAT ASAR C-band SAR images are used to obtain land movement using the PSInSAR technique and GRACE gravity anomalies to obtain groundwater variations between December 2002 and December 2010 for central London.

Chapter Five: comprises the third case study: The methodology developed in chapter four is extended to apply for the latest data available. PSInSAR methodology is used to study land movement for London and NCT-Delhi from October 2016 to December 2020 using Sentinel-1, C-band radar images. A mathematical model is used to quantify land deformation for a given change in groundwater.

Chapter Six: comprises the fourth case study: The spatio-temporal variation of groundwater quality for London is studied from 2000 to 2020. GIS, statistics, data analysis and data visualisation are used to monitor and evaluate the groundwater quality.

Chapter Seven: discusses various aspects of all the case studies, evaluating if aims and objectives could be achieved. This section examines the rationale of the study and its applicability in future research.

Chapter Eight: presents the conclusions on the various aspects of the research by restating the aims and objectives and summarising how each was achieved, which leads to a list of suggestions and recommendations for future work.

1.4 Summary

This chapter of the thesis provides background to the importance of groundwater for humankind, and the essence of monitoring spatio-temporal variation of groundwater. This chapter also briefly introduces the use of InSAR and GRACE in monitoring groundwater.The groundwater behaviour in London and NCT-Delhi is highlighted briefly, as these two cities form the study area for our case studies. Following this, the aims and objectives are then presented and finally, the thesis overview provides a brief description for each chapter.

`

Chapter 2 Literature Review

The literature review is divided into six subcategories. The first part of this chapter reviews the importance of groundwater and its monitoring for the survival of life on earth. It also summarises the various threats caused by groundwater depletion. This thesis extensively analysed land subsidence/uplift caused by groundwater depletion/recharge and its monitoring using PSInSAR. Thus, land subsidence and the basic phenomenon of InSAR are reviewed in the second section. Since land subsidence reflects the indirect groundwater movement based on aquifer compaction, another approach was used to study groundwater quantity change using GRACE satellite gravimetry, which is reviewed in the third section. After discussing the groundwater quantity variation using PSInSAR and GRACE, the groundwater quality for London was also studied using GIS and statistics, which is reviewed in the fourth section. The fifth section explains the suitability of the study areas selected for this thesis, London and NCT-Delhi. Finally, in the last section, the research gaps are discussed, emphasising what has been missed in the previous literature and what is contributed in this thesis to fill these missing points.

2.1 Groundwater and its depletion

Water is a marker for life on earth, and its uses are manifold. The earth stores approximately 1,460,000,000 cubic kilometres of water. The breakdown of global water distribution is shown in Figure 2.1 (USGS, 2021b).

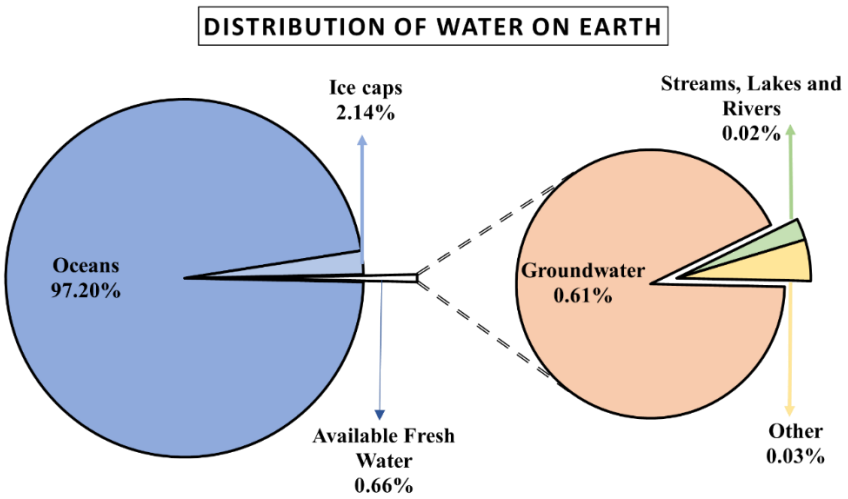

Figure 2.1: Breakdown of global water distribution

`

The most significant freshwater availability is in the form of groundwater, i.e. 8,906,000 cubic kilometres (USGS, 2021b). It is the water that lies beneath the surface of the land in saturated zones, and the uppermost part of this saturated zone is known as water table. Aquifers are rocks or sediments from which either groundwater flows naturally or from which it can be removed (in practical proportions) by pumping. In an aquifer, groundwater travels slowly, about 7-60 centimetres per day on average (USGS, 2021c), and thus water might last hundreds or thousands of years in an aquifer (Figure 2.2).

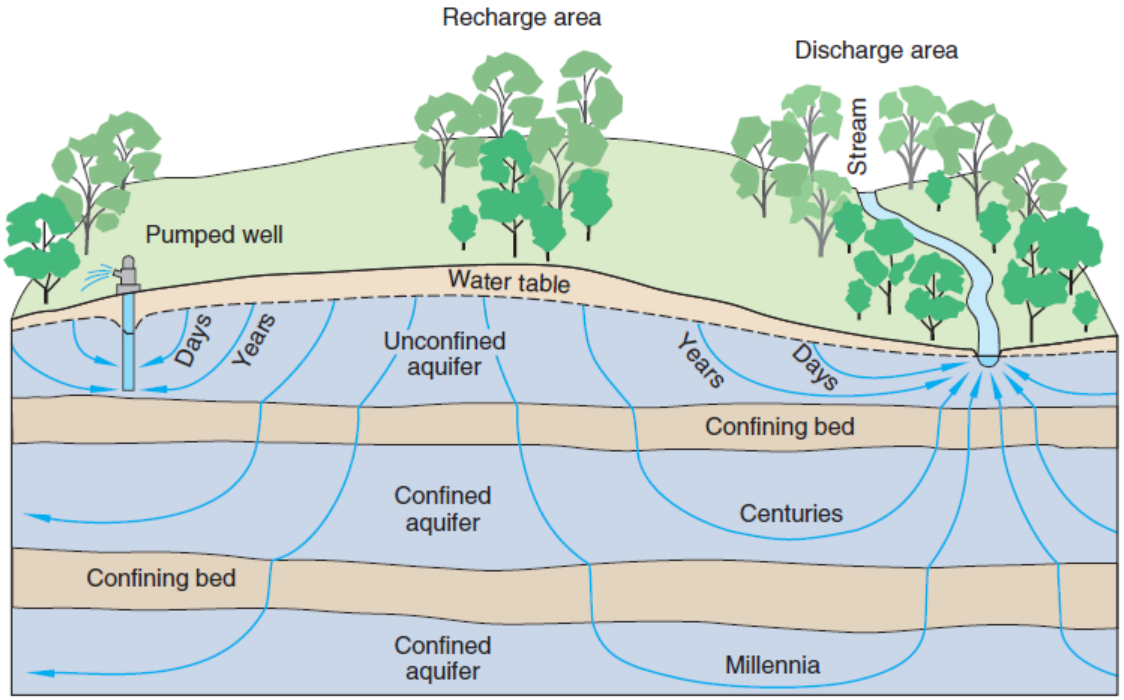

Figure 2.2: Groundwater system showing generalised flow paths of groundwater movement and the relative age of the water since the time of recharge (USGS, 2021a)

The diverse properties of aquifers and restricting strata of subterranean beds (which hinder water penetration) in the earth determine the velocity of groundwater movement, as shown in Figure 2.2. The ability of water to migrate below the ground is determined by permeability (the ability of the substance to transmit fluid) and porosity (the amount of free space that can store water in the substance) of the subsurface rock. Groundwater can travel substantial distances in many days if the underlying materials have features that permit water to travel reasonably easily through itself. However, groundwater can descend into deep aquifers, from which it may take hundreds of years

`

to return, or can even transform into deep groundwater storage, where it may remain for far longer lengths of time.

Groundwater contributes to roughly 30% of global freshwater, and only 0.2% of global freshwater is present in lakes, streams, or rivers, while 70% is locked as snow in mountainous and polar regions (UKGW, 2021). It supports rivers and lakes, and hence it is not an overstatement to say that nearly all the water used to sustain life is directly or indirectly related to groundwater. It plays several critical roles in our nature and economy as it supports rivers, lakes, and wetlands in the environment, especially during the drier months when rainfall is scarce, and also supports agricultural, domestic and industrial processes. It flows into rivers by seepage through the riverbed (base-flow), and it is critical for the survival of aquatic fauna and flora.

Groundwater contributes 33%, 98%, and 42% of the water for the public, home, and irrigation supply, respectively, in the United States (Kenny et al., 2009). For certain nations (e.g., Denmark, Malta, and Saudi Arabia), groundwater is the only resource to meet their water demand. In other European countries, groundwater accounts for over 70% of total water usage (Zektser & Everett, 2004). In comparison to surface water, groundwater has various advantages as a water source; it is usually of superior quality, safer from natural and anthropogenic pollution, less vulnerable to seasonal and permanent changes, and more consistently distributed across broad areas (Das et al., 2019). Groundwater is a good choice for a water source for a variety of reasons (BGS, 2013; UK Groundwater forum, 1998) :

- It is common in places where there are not many surface water sources.
- The contaminants are removed by the soil and rocks through which groundwater travels.
- It is usually of very high quality, and thus the treatment process is cheaper than that for the surface water.
- Its quality does not fluctuate significantly throughout the year, which is great for the human activitie that it supports.
- When there is no rainfall and streams dry up, poising threats of droughts, groundwater is often available as it is sluggish to respond to fluctuations in rainfall.

`

- Many sections of Africa and the developing world rely on groundwater since it is commonly located in the vicinity of villages and requires fewer expenses associated with gathering, purifying, and piping surface water.
- Groundwater does not necessitate the construction of costly water storage bodies before using it.

Groundwater accounts for 30% of the freshwater used by humans on average, but this figure can be as high as 100% in some regions (UKGW, 2021). Groundwater is a valuable natural resource that plays a vital part in a country's sustainability, as it is the primary water resource for irrigation and industries. Groundwater can be used flexibly, as more groundwater can be extracted when it is dry, and there is a greater demand, while less groundwater can be extracted when there is ample surface water (e.g., rainfall, lakes, ponds, rivers, reservoirs). Irrigation consumes 70% of the world's total water used, and groundwater provides 43% of this overall irrigation water (Ungureanu et al., 2020). The depletion of both surface and groundwater resources has resulted from rising water demands associated with urbanisation and industrialisation. The growth of the national economy and improving people's living standards are aided by using groundwater. However, since it is not adequately controlled, severe overexploitation in many locations has resulted in a slew of geological issues, including persistent groundwater depletion, seawater intrusion, land subsidence, and desertification, which are reviewed in section 2.1.1.

2.1.1 Problems associated with groundwater depletion

The previous section highlights the importance of groundwater and owing to these benefits, it is not surprising that it has been overexploited both regionally and globally. The gap between availability and requirement for groundwater is widening because of population growth leading to groundwater exploitation (Shah et al., 2003). The depletion of groundwater can cause various adverse effects, like exploitation of local water bodies, deterioration of the balance between aquifers and rivers, and variation in the regional heat flux and moisture flux responses at the land surface (Koster & Suarez, 2001; Kustu et al., 2010). The repercussions of overuse may also include water level decrease, aquifer depletion, disturbance of groundwater-surface water interactions, land subsidence, and saltwater intrusion into coastal aquifers (Zuoding, 2002). Some of these phenomena which are most harmful in present times have been defined below:

`

Land Subsidence/Uplift: Over-exploitation of groundwater causes a significant drop in water levels and results in land surface subsidence at various locations, primarily because of deep groundwater extraction. Land Subsidence/Uplift has severe consequences for the environment and economy, and thus it requires global technology and knowledge exchange (Aldiss et al., 2014; Bateson et al., 2009; Budhu & Adiyaman, 2010; Chatterjee et al., 2006; Cigna & Tapete, 2021; Ezquerro et al., 2017; Galloway & Burbey, 2011). Land subsidence/uplift is reviewed in detail in section 2.2.1.

Groundwater Pollution: Groundwater depletion speeds up the infiltration of surface water and its contaminants, resulting in polluted groundwater (Castellazzi et al., 2016; Changming et al., 2001). In addition, waste management practices lead to chemical and microbial contamination of aquifers, degrading water quality and rendering the water supply unsuitable for public and domestic use. Similarly, applications of fertilisers, pesticides, and herbicides for agricultural purposes adversely affect the water quality of aquifers on regional scales (Figure 2.3). It is hard to recover from once it takes place and many cities across the globe have reported that groundwater resources are now highly polluted (Donoso et al., 2020; Jabbari et al., 2020; Jia et al., 2020; Sharma, 2021). Pollution of groundwater is reviewed in detail in section 2.4.

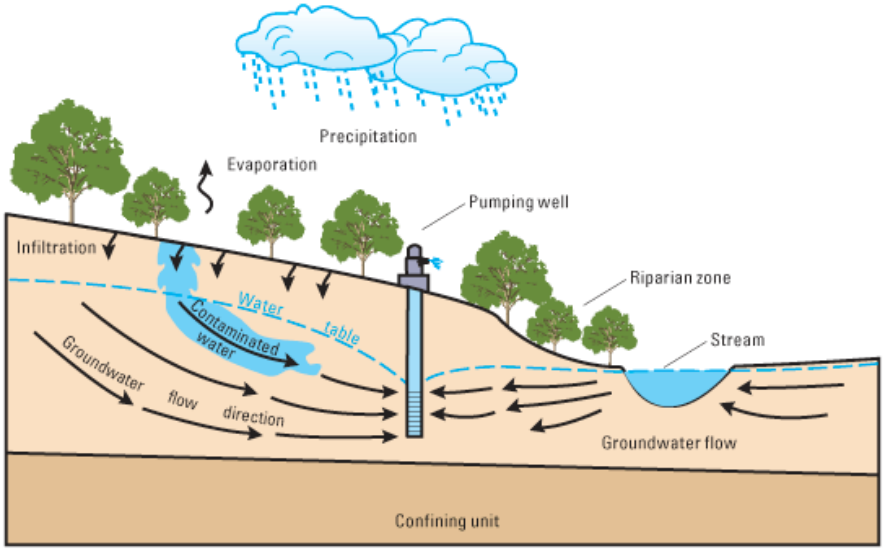

Figure 2.3: Schematic of a groundwater-flow system in an agricultural setting. In this figure, infiltration of water from either precipitation or irrigation can transport chemicals to the unsaturated zone and aquifer (USGS, 2012)

Regional groundwater depression continually: If aquifers cannot be recharged in time, then the depression cones grow more prominent because of the continuous and high-intensity over-

`

exploitation of groundwater in some regions, leading to the aquifer being drained, the water yield of wells being reduced, the wells being discarded as useless, and ultimately leading to the depletion of the water resource (Barlow & Clark, 2011; Berthold et al., 2004; Chen et al., 2020; Sidhu et al., 2021; Yang et al., 2021; Zhou et al., 2013).

Seawater Invasion: Seawater invasion occurs primarily in coastal areas around the world. This is because the seawater inflow arises because of widespread groundwater mining (Guo et al., 2019; Hounsinou, 2020; Ju et al., 2021; Kerrou et al., 2010; Rao et al., 2011; Zhou et al., 2003).

Ground collapse: Over-exploitation of groundwater in the bedrock region will cause geological problems, such as ground collapse and fissures. (Jia et al., 2021; Peng et al., 2016; Shao, 2019).

Soil desertification: The loss of groundwater can cause the degeneration of flora, and the destruction of the ecosystem, which is one of the causes of soil desertification (Hussin & Ghazal, 2020; Sidiropoulos et al., 2021).

From both quantity and quality perspectives, effective management of the groundwater resource is vital to the health of our economies, environment, and quality of life. To avoid any or all the above situations, groundwater monitoring across all spatial and temporal domains is very important. It shows the prevailing situation and can also indicate future scenarios, thus helping with decision-making to ensure a safe and ample supply of groundwater for present and future generations.

2.1.2 Importance of monitoring groundwater

Groundwater monitoring began in the twentieth century in several nations worldwide, and only after years of hard work groundwater monitoring networks could be set up globally. These networks provide evidence for groundwater resource management and sustainable development with a specific scale and primarily monitor groundwater level, groundwater quantity, and groundwater quality (Villholth et al., 2007). Groundwater observation wells are also laid out, and sites near water supply and depression cones are studied to monitor dynamic groundwater state. It integrates the demand for groundwater exploitation and management in the departments of city development and land resources. However, groundwater monitoring continues to be ineffective, making it impossible to meet the demands of water resource management and control. Many issues remain, including a low density of observation wells, a lack of monitoring wells in the water

`

depression zones, outdated monitoring equipment, a sluggish observation and transmission method that cannot guarantee the timely transmission of information, and a lack of funding for groundwater monitoring. These limitations of groundwater monitoring must be addressed in the near future, as effective monitoring can serve the following benefits (Alley, 2007):

- Monitor variations in groundwater levels to aid decision-makers in determining the long-term viability of an aquifer as a source of water and making appropriate policy decisions.
- Provide groundwater contamination information, such as pollutant identification and contaminant level measurements, and assist in identifying groundwater contamination sources.
- Assist decision-makers in better understanding the aquifer's water quality, potential impacts on human health and the ecology, and which sources require the most significant attention.
- Determine whether there are any current or potential changes in the flow because of groundwater depletion. This data can assist policymakers in making proper policy decisions to avoid damage such as saltwater intrusion or contamination migration towards a pumping station or well.
- Assess the effects of climate change on groundwater levels so that decision-makers can issue drought warnings or declarations on time and adopt necessary mitigation actions.

Ground-based monitoring is extensively employed but is restricted by geographies and is only effective for easily accessible small areas. This procedure takes a long time, is expensive, and requires a lot of effort. Remote sensing may swiftly capture regional and global areas because of large-scale and dynamic observation features, allowing many ecological indicators to be obtained through data modelling and retrieval but needs to be validated by in-situ observations. As a result, remote sensing has become an increasingly important tool for groundwater monitoring. Thus remote sensing tools like InSAR and GRACE are used in this study to monitor groundwater induced subsidence and groundwater quantity, respectively, reviewed in sections 2.2 and 2.3.

`

2.2 Subsidence and InSAR

2.2.1 Land subsidence

Land subsidence (or uplift) is the gentle to rapid settling (or rising) of distinct patches of the land surface because of the consolidation (or rebound) of underground sediments because of increasing (or decreasing) effective stress (Galloway & Burbey, 2011; Ma et al., 2018). According to Pratt & Johnson (1926), it maybe caused by the lowering of the piezometric surface owing to fluid extraction. It is caused by massive quantities of liquid removal from an aquifer. It has been witnessed in many parts of the world, and thus, it has been studied extensively by earlier scholars (Lewis & Schrefler, 1978; Poland & Davis, 1969; Pratt & Johnson, 1926). Figure 2.4 shows the relationship between surface and subsurface processes before and after land subsidence. The linkages to subsidence deformation are briefly summarised for surface water, landscape and groundwater flow processes. The potential changes in the movement of water before and after the linked effects of subsidence result in redirected or reduced runoff, reduced stream-flow and canal flows, the additional connection of root zone to capillary fringe above the water table, reduced aquifer thickness, and poor hydraulic properties (transmissivity and storativity) (Niroumand, 2021).

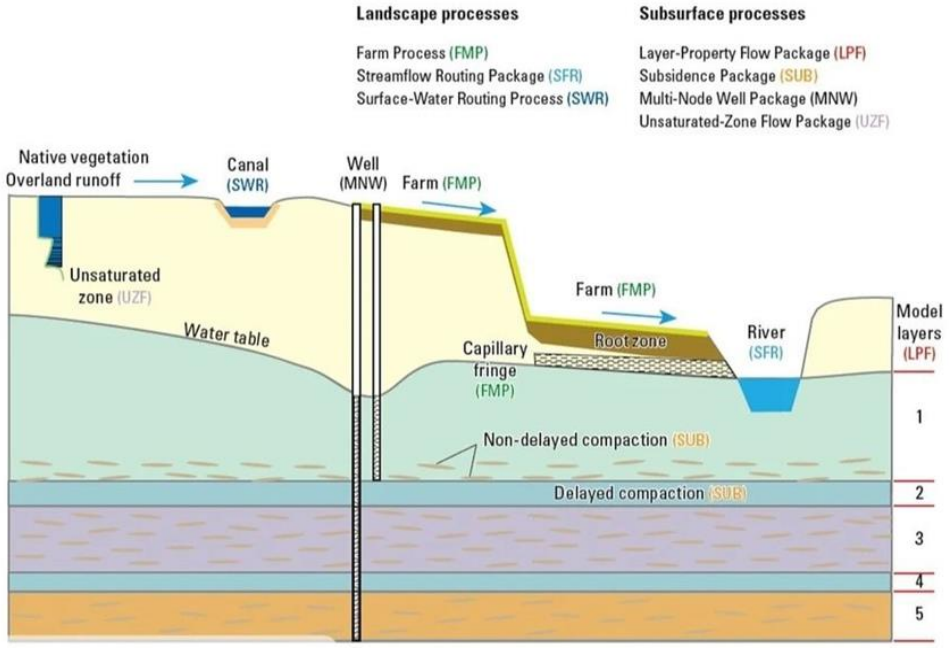

Figure 2.4: The relation between surface and subsurface processes before and after land subsidence [adopted from (Niroumand, 2021)].

`

The United Nations Educational, Scientific, and Cultural Organisation (UNESCO) took up land subsidence as an essential research topic in 1965 owing to its threats to the safety and economics of any city (UNESCO, 1970). In 1969, a study was carried out by Poland and Davis (1969) called 'land subsidence due to fluid withdrawal', and their publication in 1984 is probably the first mention of groundwater-induced land subsidence (Poland, 1984). To date, many academics have made significant efforts to analyse various essential components of land subsidence, such as causes, estimation, models, socioeconomic impacts, environmental impacts, monitoring and control. The monitoring, anticipation, and management of human-induced land subsidence enforced due to removal of fluids from underground layers (groundwater, oil, and gas) were studied by Gambolati in 2006 and again in 2015 (Gambolati et al., 2006; Gambolati & Teatini, 2015). Several regional studies on land subsidence have been published, e.g. China (Ye et al., 2016), Japan (Yamamoto & others, 1995), and Central Mexico (Figueroa et al., 2018). The adverse effects of land subsidence in heavily populated regions of Mexico City, Shanghai and Bangkok were frequently noted in 2020 (Lyu et al., 2020). The forecast and risk assessment of infrastructure losses caused by land subsidence is critical in mitigating the effects of this geohazard (Jin et al., 2016).

Land subsidence threatens eleven coastal cities across the globe with inundation before the start of 22nd century (Inbev et al., 2013), namely: Jakarta, Indonesia (17 cm per year); Lagos, Nigeria (up to 200 cm by the end of the century); Houston, USA (at a rate of 5 cm per year); Dhaka, Bangladesh; Venice, Italy (0.2 cm per year); Virginia Beach, Virginia (up to 360 cm by the end of the century); Bangkok, Thailand (1.0 cm per year); New Orleans, Louisiana (at a rate of 5 cm per year); Rotterdam, The Netherlands; Alexandria, Egypt (up to 60 cm by the end of this century); and Miami, Florida. Land Subsidence is a global anthropogenic and naturally induced geohazard and needs attention in various countries worldwide, e.g. Australia, China, Egypt, USA and European countries (France, Germany, Italy, Netherlands, Poland, Sweden, UK) (Liu et al., 2017). In areas with a lack of rainfall, the groundwater demand increases, especially in the case of industrial and agricultural development, and groundwater abstraction to meet this increased demand triggers the land subsidence (Motagh et al., 2008).

The centres of land subsidence in the Santa Clara Valley, California, USA, correlated to the centres of substantial pumping, and the historical growth of the subsidence coincided with the growing use of groundwater (Poland & Davis, 1969). Land subsidence in Jakarta, Indonesia, is closely

`

linked to the over-extraction of groundwater (Abidin et al., 2001). The threat evaluation caused by land subsidence is intriguing due to uncertainty associated with the land subsidence and harms caused by it (Lyu et al., 2019). Various mathematical models, such as the fuzzy analytic hierarchy process (Zou et al., 2013), Bayesian network rules (Jin et al., 2018; Sierra et al., 2018), and Gray method (Ishikawa et al., 1993; Wang et al., 2014) have been used to quantify the threats caused by land subsidence. The land subsidence varies in both spatial and temporal domains worldwide (Baum et al., 2008; Figueroa et al., 2018).

Traditional methods for mapping land motion, such as levelling, GNSS, 3D laser scanning, and others, give precise measurements. However, for surveying vast (basin level) areas they are time-consuming, costly, and have a limited spatial scope, making them unsuitable (Huang et al., 2016; Zheng et al., 2018). The PSInSAR approach is a better alternative, which can detect coherent and stable scattering targets and use their phase history to calculate land movement over vast areas (Ferretti et al., 2000b). It provides better spatial coverage and temporal resolution, cost-effective, time-saving, and reliable solution to monitor spatio-temporal variation of land deformation.

2.2.2 SAR remote sensing overview

The remote sensing which is carried out in the microwave (MW) region of the electromagnetic (EM) spectrum, is known as MW remote sensing. Synthetic Aperture Radar (SAR) remote sensing is an imaging active MW technique that provides spatial resolution data with millimeter level accuracy. It is used to create images of objects, such as landscapes, which can be 2D or 3D representations of the object. Microwave radiation can be classified into eight bands (Table 2.1). Generally, the K-band is not used for spaceborne sensors because its short wavelength will be blocked or disturbed by atmospheric particles or clouds (Kumar, 2017).

Table 2.1: Microwave radiation bands

Band	Wavelength (cm)	Applications
Ka	0.75 to 1.10	Glacial/ice, very high-resolution imagery
K	1.10 to 1.67	Glacial/ice, snow cover
Ku	1.67 to 2.40	Glacial/ice, snow cover
X	2.40 to 3.8	Ocean, agriculture, general surface investigation (high resolution)
C	3.75 to 7.50	Ocean, agriculture, general surface investigation
S	7.5 to 15	Agriculture, biomass, ocean

`

L	15 to 30	Agriculture/forestry, Soil moisture, ground penetration
P	30 to 100	Biomass, soil moisture, ground penetration
Higher wavelength	>100	Foliage / ground penetration, biomass

Active microwave sensors have their own source of energy which emits MW radiation to visualise the target. These can be broadly divided into two types: a) Imaging and b) non-Imaging. The sensor receives and detects only the backscattered portion of the signal. This backscattered portion depends on three critical characteristics: surface features - roughness, orientation, geometric structure; electrical characteristics - conductivity, dielectric constant, moisture content; and sensor frequency. Figure 2.5 explains the principle of SAR. In radar remote sensing, the length of antennae is inversely proportional to spatial resolution. Thus the resolution remains limited when an actual aperture is used, and to overcome this problem, SAR uses a long virtual antennae. As the aircraft or satellite moves forward, the same device antenna receives the returns from the ground surface at different locations in the direction of the flight track. These different locations are considered as parts of a single long antenna (Richards, 2009). The mechanism used here is based on the Doppler effect, which states that when there is relative movement between source and receiver, the sound frequency at source is different from the frequency of sound at the listener (Victor et al., 2006). Figure 2.5 shows that the length of virtual synthetic antennae (L_a), which is also called the synthetic aperture, is given by Equation 2.1:

$$L_a = R_0 \frac{\lambda}{l_a} \qquad \text{Equation 2.1}$$

Where,

L_a = length of virtual synthetic antennae, R_0 = Distance between target and aircraft, l_a = length of actual (Short) antennae, and λ = wavelength of RADAR beam

`

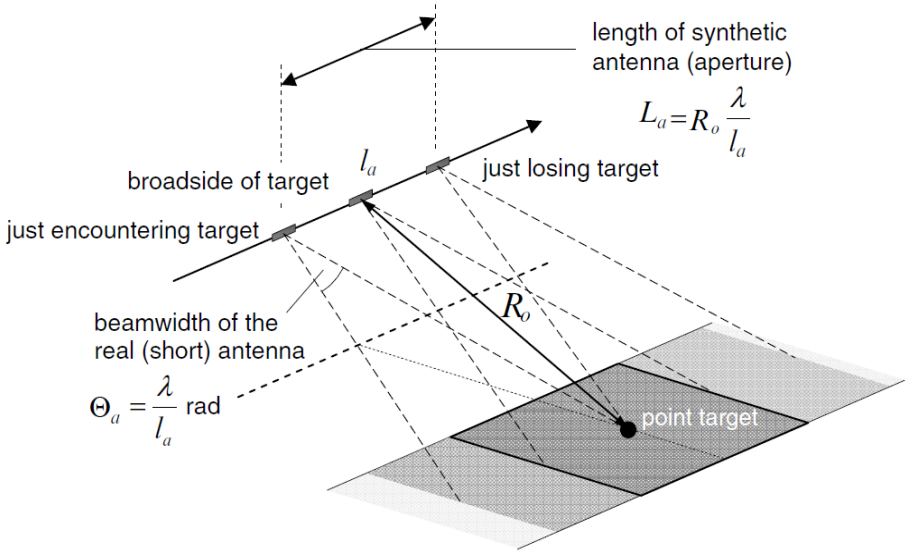

Figure 2.5: Synthetic Aperture Radar Principle (Richards, 2009)

Many geophysical investigations aiming to study subsurface processes have used data collected at the earth's surface or very close to it (Chang et al., 2010; Kusche & Schrama, 2005; Z. Li et al., 2006a; Peltier et al., 2010). To get meaningful information regarding subsurface phenomenon, proper sampling of spatial and temporal aspects is difficult using geospatial techniques like Global Positioning System (GPS), ground levelling, and others. It is laborious, time-consuming and expensive to survey multiple points manually for a large area and at regular fixed intervals. The InSAR technique provides a solution to this problem, as it allows the observation of the surface displacement field at high spatial resolutions (meters) and with a very high precision (millimetres) for large areas (1000s of km^2) (Gabriel et al., 1989).

2.2.3 SAR Interferometry

InSAR is an active radar technique in the MW region of the electromagnetic spectrum for measuring the earth's surface movements. InSAR can be utilised day and night (active senor), in all weather as SAR radiations can penetrate rain and cloud, because it transmits electromagnetic waves at a wavelength that can range from a few millimeters to tens of centimeters (Rosen, 2000). The governing principle behind SAR interferometric measurements lies in measuring the phase of the complex-valued radar signal (Osmanouglu et al., 2016). In this method, two or more SAR images are used to create surface deformation or elevation maps. Many researchers have used this technique to study land movement resulting from earthquakes (Fialko et al., 2001), glacial movements (Wang et al., 2015), landslides (Kang et al., 2017; Sun et al., 2015; Zhang et al., 2020),

`

volcanic bulging (Albino et al., 2020; Fournier et al., 2010), sand motion (Albino et al., 2020; Fournier et al., 2010), and subsidence (Dai et al., 2015; Fan et al., 2015; Huang et al., 2016).

2.2.3.1 History of InSAR

The interferometry concept was first discussed in the 1970s (Graham, 1974), and in the 1980s, InSAR applications become more popular (Andrew & Richard, 1988; Zebker & Goldstein, 1986). Both airborne and spaceborne InSAR applications were recognised and published. Airborne InSAR, for example, JPL/NASA TOPSAR, produced 1-3 m accurate digital elevation models (Madsen et al., 1995), while spaceborne InSAR could produce global DEMs, for example, Shuttle Radar Topography Mission (SRTM) DEM (30m spatial resolution) (Farr et al., 2007; Rabus et al., 2003).

Gabriel et al. (1989) first mapped displacement using repeat pass interferometry on Seasat data over an imaging site in Imperial Valley, California, where motion effects were observed that were ascribed to the expansion of water-absorbing clays. The European Remote Sensing satellite (ERS-1) was launched in 1991, and it led to a rapid increase in the use of InSAR as data became available. InSAR has since been used to measure displacements of millimetre level accuracy. For example, the displacement caused by the Landers earthquake in 1992 was detected by InSAR technology (Massonnet & Rabaute, 1993). Interferometry measures various geophysical processes like the motion associated with earthquakes (Junxiang et al., 2011; Massonnet et al., 1994; Wright et al., 2004), volcanic bulging before eruptions (Amelung et al., 2000; Lu & Dzurisin, 2010; Massonnet et al., 1995; Ofeigsson et al., 2011), and land subsidence (Buckley et al., 2003; Fielding et al., 1998; Massonnet et al., 1997; Osmanouglu et al., 2011).

Conventionally, many factors hinder the application of InSAR or affect the quality of measurements from interferometry. Atmospheric ambiguities (Zebker et al., 1997) like delay in signal propagation because of atmospheric conditions, thermal noise, changes in reflectivity characteristics of backscatters, and decorrelation (Zebker et al., 1992) can pose a challenge to InSAR technology. To overcome these challenges and to maximise interferometry's potential, several time series algorithms have been developed in the last two decades like Persistent Scattering Interferometry (PSInSAR) (Ferretti et al., 2001; Hooper et al., 2007), Small Baseline Interferometry (SBAS InSAR) (Berardino et al., 2002; Hooper, 2008) and SqueeSAR (Ferretti et al., 2011). Some additional important work has been published, like the use of independent

`

atmospheric water vapour data to correct atmospheric data, e.g. using MODIS (Li et al., 2006b), GPS (Li et al., 2006a; Webley et al., 2002), MERIS (Li et al., 2012), and numerical weather models (Foster et al., 2006; Wadge et al., 2002), where techniques allow a 50-60% reduction of the atmospheric effect.

2.2.3.2 Phase measurement

A single resolution cell contains many scatterers, and the phase and brightness value of the resolution cell is a coherent sum of all the scatterers. Thus the brightness value shown differs from the actual values of the object. This phenomenon is called the speckle effect, and it leads to a random signal phase (Lee et al., 1994). To avoid this randomness in the phase of SAR images, the phase difference between two or more acquisitions is used. When two separate radar acquisitions are obtained over the same area with similar geometry, then the total participation from each specific scatterer is mostly the same, so that difference in phase between the two acquisitions is not random (Curtis & Howard, 2001; Gens, 1999; Ghiglia & Pritt, 1998). This can be done by using either two physically different antennas fitted on the same platform or using the same antenna on two different passes (Figure 2.6). The first one is called Single-pass interferometry, and the latter is called Repeat-pass interferometry (Miyawaki et al., 2017).

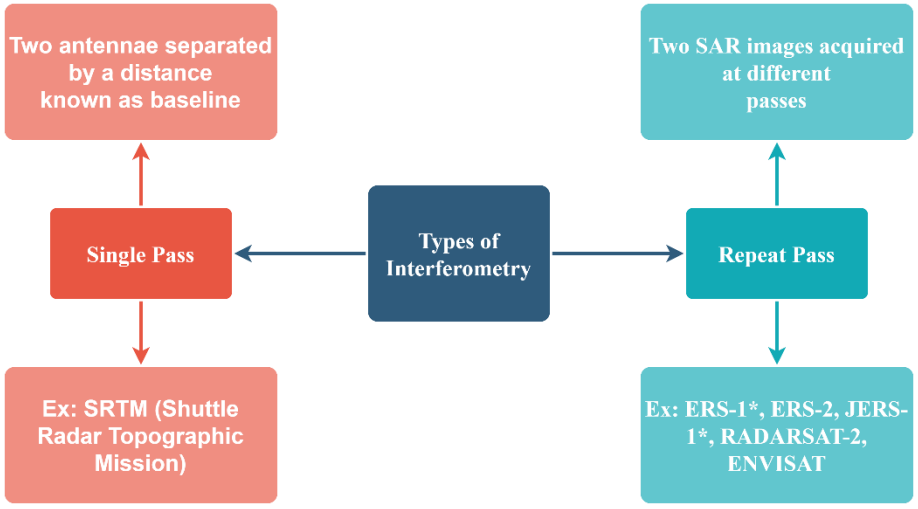

*Figure 2.6: Types of Interferometry. *ERS: European Remote Sensing satellite, *JERS: Japanese Earth Resource Satellite*

If I_1 and I_2 are two complex image signals, then an interferogram is formed by the following equation:

`

$$I = I_1 I_2^* = A_1 e^{i\phi 1} . A_2 e^{-i\phi 2} = A_1 A_2 . e^{i(\phi 1 - \phi 2)} = A . e^{i\phi} \quad \text{Equation 2.2}$$

where, $*$ represents the complex conjugate, $A = A_1 A_2$, is the amplitude of the interferogram and $\phi = \phi_1 - \phi_2$ is the interferometric phase, which is the most important observation in InSAR measurement. Apart from noise, acquisitions for the same surface and geometry should be identical and therefore $I_1 = I_2$ and hence InSAR phase should be nil everywhere. But this is not the case as the final phase is a combination of different parameters mentioned in Equation 2.3 (Ferretti et al., 2000; Zebker et al., 1994):

$$\phi = \phi_{def} + \phi_{topo} + \phi_{atm} + \phi_{orb} + \phi_n \quad \text{Equation 2.3}$$

where, ϕ_{topo} = phase contribution due to surface topography, ϕ_{def} = phase contribution due to deformation because of movement of the earth surface, ϕ_{atm} = phase contribution due to atmospheric screen due to various atmospheric conditions, ϕ_{orb} = orbit error due to inaccurate orbit information, and ϕ_n = phase noise. The first four terms might be considered as signal or noise, depending upon the condition. The interferometric baseline is the distance by which two antennae positions are separated in a plane perpendicular to the antennae motion. The contribution of phase because of viewing the topography from two (slightly) different angles can be given by Equation 2.4 (Hanssen, 2001; Zebker et al., 1994):

$$\phi_{topo} = -\frac{4\pi B_\perp}{\lambda r sin\theta}\, dz + \phi_{flat\_earth} \quad \text{Equation 2.4}$$

where, λ = radar wavelength, r = range (the distance between a point on the ground and SAR satellite), $B_\perp$ = perpendicular baseline, θ = look angle, dz is the elevation of the surface above a reference elevation, and ϕ_{flat_earth} is a deterministic phase contribution because of the reference surface, which for satellite systems is typically the reference ellipsoid. To compensate for topographic factors, a separate interferogram of the exact location is used when a DEM is not present (Zebker et al., 1994). These days, a zero displacement interferogram is synthesised using a DEM and InSAR geometry, which is subtracted from the measured interferogram to remove the topographic phase corrections (Massonnet & Feigl, 1998).

If the land surface position is changed between the two acquisitions, for reasons such as landslides, earthquakes, subsidence, and others , then the distance between the scattering points on the ground

`

and the antenna changes (i.e., the range). The area on the ground experiences this change in the range between acquisitions. Let Δr be the area displaced on the ground in line-of-sight direction, then the path difference between the two acquisitions will be 2Δr. This will cause an excess phase of:

$$\phi\text{def} = \frac{4\pi}{\lambda}.\Delta\text{r} \qquad \text{Equation 2.5}$$

It is only the precision to which orbits are known that can tell us about the absolute displacements of the radar scene's imaged area. However, the interferometric technique mainly uses observations of relative movements between areas within the radar image for deformation measurements.

2.2.3.3 Polarisation

SAR backscatter is largely affected by the polarisation, i.e. the direction of the wave projected from the radar, and then the direction of the wave returned after it has bounced off an object (Figure 2.7). For example, if a wave leaves a satellite, oscillates up and down (or vertically), hits an object on the ground, and returns with a beam oscillating vertically again, then a vertical-vertical (VV) polarization is achieved. When the polarisation is VV or HH it is called co-polarised, and when it is VH or HV it is called cross polarised (Table 2.2). Different polarisation will result from different ground surface characteristics, so the more polarisation options that can be measured, the more in-depth the analysis that can be undertaken.

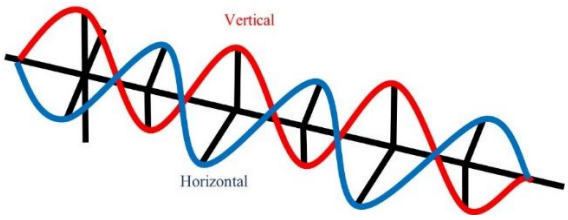

Figure 2.7 Vertical and horizontal modes of travel

Table 2.2: Polarisation

Polarisation	Physical Meaning	Mainly affected By
VV	Vertical wave, outgoing and incoming	Vegetation structure
HH	Horizontal wave, outgoing and incoming	Surface scattering
VH	Vertical wave outgoing, horizontal wave incoming	Volume Scattering
HV	Horizontal wave outgoing, vertical wave incoming	Volume Scattering

`

Polarisation plays a large part in the information that is obtained from SAR backscatter. So, depending on what information is needed, choosing the correct polarisation to start with is essential. For example, quad polarised SAR is needed to obtain comprehensive information on vegetation, which means all four polarisations VV, VH, HH and HV are desirable. However, availability is sometimes difficult due to sensor limitations, so dual polarisation (VV & VH or HH & HV) can still inform many agricultural aspects. Each polarisation is affected by different aspects of soil and vegetation interactions. For example, HH receives a significant response from the soil, so it is useful when information is desired on what is happening underneath the crop or when monitoring soil moisture. VH and HV are sensitive to volumetric scattering from the canopy of the vegetation, so detects changes from when the crops can grow leaves. VV backscatter is affected by the vegetation structure such as the stem, branches, leaves and flowers of the crops of interest. However, if the vegetation is dense enough, VV and VH will have the same responses, as they cannot penetrate through the canopy layer. The graph below (Figure 2.8) shows how Sentinel-1 VV and VH react over different vegetation types and structures.

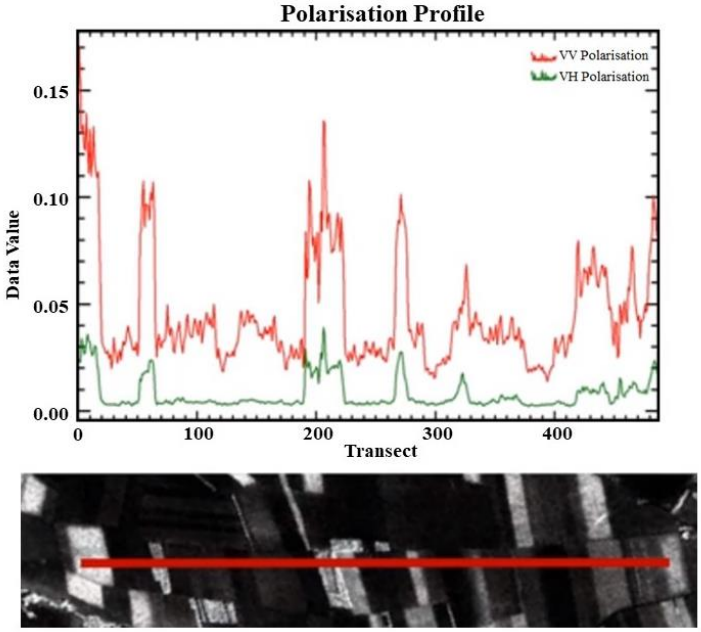

Figure 2.8: Polarisation effect: Image Source: Harris Geospatial Technologies

VH is always lower than VV, and VV is more sensitive to crops than VH. VV is shown to pick up a significant signal over the bright field areas and variations over the dark field, where it is detecting scattering from the soil or early plant crops. Until the mid-1990s, researchers focused on

`

adapting the new InSAR technology for geospatial applications without focusing on measurement reliability. However, with the increasing use of this technology, it has become essential to understand the errors affecting the measurements, as tiny errors can significantly impact results leading to erroneous data, thus affecting its reliability for essential applications. Some great attempts have been made to understand and treat the errors in radar interferometry (Hanssen, 2001; Jonsson, 2002).

2.2.3.4 Coherence

Coherence captures the relationship between the two images used to generate the interferogram i.e. it reflects how similar the images are. If both the scenes are similar, they will have very high coherence, indicating that not much has changed between them. However, if there is a significant change between the two acquisitions, such as during earthquakes or landslides, they will have low coherence, also referred to as decorrelation. Coherence change detection is essential for understanding the similarities in a image, while interferometry enables us to track changes in the image. The amount of deformation capable of being inferred is dependent on decorrelation. There are numerous affects that can reduce the coherence. For example, temporal decorrelation effects, which are caused due to different incidence angles of radar radiations (Zebker et al., 1992), land cover - vegetation growth/change, snow cover, and others. Between two SAR images, the complex coherence is given by Equation 2.6:

$$\gamma_c = \frac{E\{S_1 . S_2^*\}}{\sqrt{E\{S_1 . S_1^*\} . E\{S_2 . S_2^*\}}} \qquad \text{Equation 2.6}$$

where, γ_c = complex coherence, E{.} = expectation, * = complex conjugate, S_1 = first radar signal, S_2 = second radar signal

2.2.3.5 Data Structure for SAR Interferometry

SAR data is usually present in single look complex (SLC) format, and it can extract both the phase and amplitude information (Figure 2.9). For SCL images, SAR data can be represented as a+ib.

$$Amplitude = \sqrt{a^2 + b^2} \qquad \text{Equation 2.7}$$

`

$$phase = tan^{-1}\left(\frac{b}{a}\right)$$ Equation 2.8

Where, a= real part of the complex SAR image, and b= imagery part of the complex SAR image.

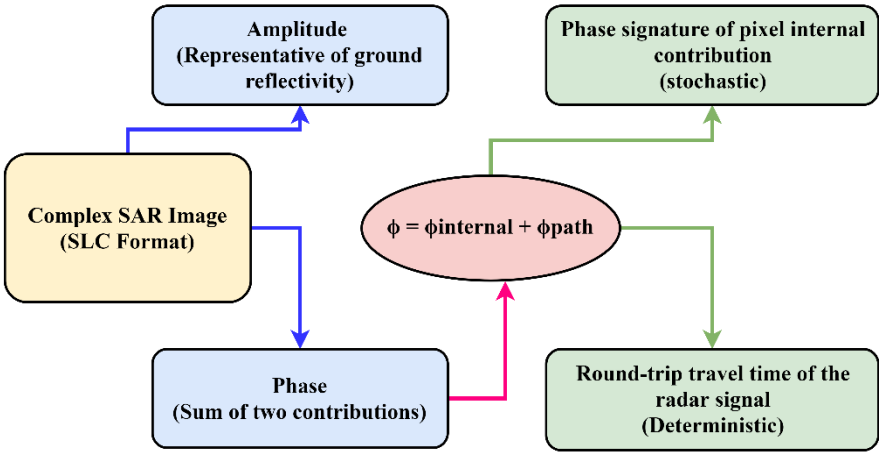

Figure 2.9: Interferometric SAR data structure

2.2.3.6 Differential InSAR

In differential InSAR, an interferogram is generated by registering two SLC images together very accurately and precisely in both the amplitude and phase (Schulz et al., 2017). The image registration means aligning the images by pixel-to-pixel match between common features in SAR image pairs. After co-registrating the images, their phases are deducted from each other, and the interferogram is produced. The following parameters affect the process of SAR Interferometry:

Ambiguity Height: $AH = \frac{\lambda R sin\theta}{4\pi Bn}$ Equation 2.9

Critical Baseline: $Bn(crictical) = \frac{\lambda R tan\theta}{2\ (RR)}$ Equation 2.10

Sensitivity: $S = \frac{\lambda}{2}$ Equation 2.11

where, λ = radar signal's wavelength, R = radar antennae's slant range distance, θ = radar's look angle, Bn = perpendicular baseline, and RR = range resolution. The flowchart (Figure 2.10) shows the processing steps for generating surface displacement maps from an interferometric pair i.e primary and secondary image. Here, raw data is taken as the input and a single look complex (SLC)

`

image is obtained, which needs to be registered with the other image. The primary image remains intact for all calculations, while the secondary image is modified according to the primary image. After the image registration, the next step is interferogram generation, wherein the single look complex primary (a+ib) is multiplied with conjugate single look complex secondary (a-ib). This gives pixel by pixel differences of phase between the two images. After interferogram generation, orbital flattening is performed, and after that, phase unwrapping is done. As phase values are calculated in [0, 2π] interval, they must be added to obtain the absolute phase differences between locations in the image. This process of phase integration is known as phase unwrapping (Curtis & Howard, 2001). Then the final steps are phase to height conversion and DEM generation.

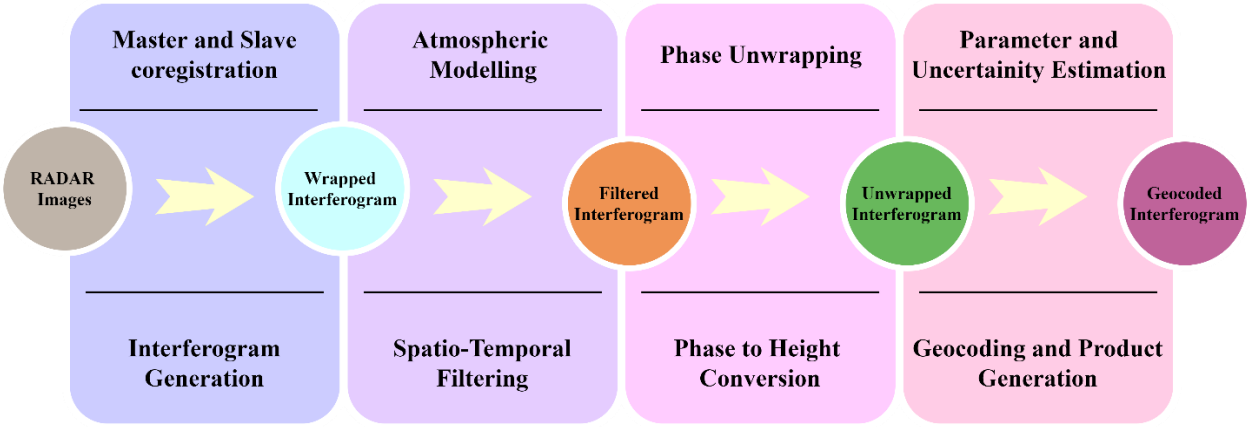

Figure 2.10: Steps for InSAR processing to obtain the Deformation map

When there is significant deformation in the area of interest, especially with good correlation (low noise), DInSAR with two images is sufficient to map deformation. However, the signal is often dominated by the atmosphere, orbit and DEM errors; and noise is larger than the actual signal (i.e. high decorrelation). In such a scenario, time series analysis of InSAR becomes important if map deformation is required with high accuracy.

In time series analysis multiple SAR images are used, (usually more than 25), while in DInSAR only two inages are used. Time series analysis of InSAR data, which observes the displacement of the Earth's surface over time, is an indispensable tool for many fields of Earth science. Several algorithms have been developed for time series analysis of InSAR data (in alphabetical order): Coherent Pixels Technique (CPT) (Blanco et al., 2008); Delft Persistent Scatterer Interferometry (DePSI) (Kampes, 2005); Interferometric Point Target Analysis (IPTA) (Werner et al., 2003); Permanent Scatterer InSAR (PSInSAR™) (Ferretti et al., 2001); Persistent Scatterer Pairs (PSP)

`

(Costantini et al., 2008); Quasi Persistent Scatterers (QPS) (Perissin & Wang, 2012); Small Baseline Subset (SBAS) (Berardino et al., 2002); Stable Points Network (SPN) (Crosetto et al., 2008); SqueeSAR™ (Ferretti et al., 2009, 2011) and Stanford Method for Persistent Scatterers (StaMPS) (Hooper et al., 2004; Hooper, 2008).

2.2.3.7 Persistent Scatterer InSAR

PSInSAR is different from conventional interferometry as it only uses pixels that demonstrate stability in phase for a number of interferograms. These stable pixels can be termed as persistent scatterers (PS) or permanent scatterers or slowly decorrelating filtered phase (SDFP) pixels (Hooper, 2008). The multi-temporal PSInSAR analysis allows us to better select coherent pixels, decrease atmosphere/orbit errors by filtering in space and time, calculate DEM errors, phase unwrapping and achieve sub-pixel resolution. Various factors contribute to the phase of an interferogram, such as the height of topography, deformation of the surface, atmospheric disturbance, and others. An efficient algorithm is used to consider all these factors and select the most reliable potential PS candidates. The phase contribution observations are wrapped and badly affected by several errors; hence, amplitude observations are used for PS points. For the selection of PS candidates, the present techniques can be broadly divided into three categories (Ketelaar, 2009):

- Signal to clutter ratio (SCR) (SCR, 1993)
- Normalised amplitude dispersion (D_a) (Ferretti et al., 2001) and
- Supervised classification (Humme, 2007)

For the calculation of signal to clutter ratio, a deterministic signal is present in persistent scatterer observations, which is distributed by random clutter of circular Gaussian distribution. The main principle is that the point scatterer is surrounded by distributed scatterers, which is reflected in the clutter. The signal to clutter ratio and phase variance are related as follows (SCR, 1993):

$$SCR = \frac{s^2}{c^2}$$ Equation 2.12

$$\sigma_{\psi}^2 = \frac{1}{2\ .SCR}\ (rad)$$ Equation 2.13

`

where, σ_{ψ}^{2} = phase variance of a single SAR observation, s = amplitude of the persistent scatterer, and c = clutter in the surroundings. A pixel is considered a persistent scatterer if it has a high signal to clutter ratio over time. For SCR, it is assumed that the neighbourhood of the dominant scatterer has stationary stochastic behaviour. This assumption may not always be accurate, especially in areas where multiple scatterers may be present close together and might interfere with PS, such as urban areas. The normalised amplitude dispersion method (Ferretti et al., 2001) also does not use spatial observations (like SCR) and uses only amplitude time-series observations.

$$D_a = \frac{\sigma_a}{\mu_a}, \qquad \text{Equation 2.14}$$

Point scatterers show a low phase dispersion if they have a low normalised amplitude dispersion, hence, they can be selected as persistent scatterer candidates. An empirical relationship exists between SCR and D_a (SCR, 1993):

$$D_a = \frac{1}{\sqrt{2.SCR}} \qquad \text{Equation 2.15}$$

A typical standard value for D_a is 0.25 (Ferretti et al., 2001), resulting in an SCR of 8. Both the signal to clutter ratio and normalised dispersion use amplitude analysis for PS candidate selection but phase analysis has been researched as well (Hooper et al., 2004). To investigate phase analysis for PS selection, it is assumed that deformation is spatially correlated. All the neighbouring pixel's phase is averaged, and the one with the lowest residual noise is selected. Lastly, to obtain PS candidates, supervised classification is researched (Humme, 2007). Here, pixels are manually selected to decrease the probability of missing a PS candidate, especially in areas where the distribution of PS is crucial.

2.2.4 Application of SAR/InSAR to hydrology

The "deformation" of the ground surface can be anything that moves the ground pixel between the two image acquisitions, such as crustal deformation caused by earthquakes and volcanoes, surface subsidence caused by groundwater exhaust or underground mining activities, changes in river water levels, and so on. As a result, InSAR has a wide range of applications. Seismology, surface water hydrology, groundwater hydrology, glaciology, mining, forestry, environmental, and structural engineering are only a few examples. This thesis mainly covers the hydrology aspects,

`

so the applications on InSAR related to hydrology is reviewed here, and a brief summary is provided in Table 2.3.

2.2.4.1 Land movement due to groundwater change:

Groundwater pumping can produce land subsidence, resulting in aquitard compaction during the slow process of aquitard drainage. Subsidence detected from interferogram can be used for parameter estimates in simulations of aquifer system compaction (Galloway et al., 1998). In California, subsidence caused by excessive groundwater withdrawal has made canal operation and design more expensive (Prokopovich & Marriott, 1983). InSAR can be used to monitor the spatial scale of land subsidence. For example, the city of Venice (Italy) had severe land subsidence from 1950 to 1970, with the highest rates owing to groundwater withdrawals (Carbognin et al., 2004; Teatini et al., 2005). To stop the subsidence caused by groundwater withdrawal, substantial measures to decrease both industrial and other artesian extractions have been adopted since 1970. However, subsidence as a result of consolidation processes may still be occurring. As obtained from interferogram images ERS-1/2 from 1992 to 1996, (Carbognin et al., 2004) found that the vertical displacement rates are between +1.0 and -2.0 mm/year. This demonstrates the quasi-stability of the sediments in the city's landward and central areas over time, while certain minor zones subsiding at a rate more than 1 mm/year in the city's western and eastern areas may still be undergoing consolidation processes. Subsidence caused by groundwater pumping has also been documented in other Italian cities (Raucoules et al., 2003).

In semi-arid and desert regions, groundwater is the principal supply of water for human use and agricultural irrigation. Excessive groundwater withdrawal might result in large-scale subsidence. In the coming decades, the InSAR application will be extremely valuable in monitoring ground subsidence owing to excessive withdrawal. During a wet season, groundwater recharge causes groundwater levels to rise. The granular skeleton expands and the surface uplifts as unsaturated sediment moves from the granular skeleton to the pressured pore fluid. (Hoffmann et al., 2001) used interferogram analysis to reveal seasonal subsidence and uplift in the Las Vegas valley, Nevada.

Using interferogram analysis of ERS-1 and ERS-2 pictures, (Lu & Danskin, 2001) successfully found a groundwater recharge uplift of several centimetres in the Bernardino basin in Southern California. These seasonal deformation data provide essential information on the aquifer system's

`

hydrogeologic features and are useful in evaluating the success of groundwater recharge schemes. (Bawden et al., 2001) used InSAR to show seasonal fluctuations in the Santa Ana basin, California, of 50 mm of basin uplift due to groundwater recharge during the wet winter season and 60 mm of subsidence due to groundwater withdrawal during the dry summer season, with the most significant fluctuations near the city of Santa Ana and at the basin's northwestern end.

Watson et al., (2002) confirmed that vertical motion owing to annual fluctuations in the elevation of the water table must be taken into consideration when interpreting geodetic data for tectonic motion in the Los Angeles basin. Schmidt & Bürgmann, (2003) studied the geographical and temporal pattern of uplift of the Santa Clara Valley aquifer using 115 differential interferograms from 1992 to 2000 in order to resolve both seasonal uplift and subsidence as well as long-term uplift.

The seasonal surface deformation reflects the constrained aquifer's poroelastic reaction to groundwater redistribution, but the long-term uplift indicates the net rise in pore fluid pressure. As inferred from the net regional uplift, the recovery of groundwater levels in the Santa Clara Valley, which began in the 1960s, appears to have continued until the 1990s, according to (Schmidt & Bürgmann, 2003) analysis. Understanding the mobility of groundwater within an aquifer, the distribution of permeable units, and the mechanics of the aquifer system will be aided by understanding the geographical and temporal pattern of deformation of the aquifer.

2.2.4.2 Hot springs or volcanic zones

Groundwater that is warm or hot, such as that found near hot springs or in volcanic zones, is a helpful source of energy. For geothermal energy, hot water is pumped. Excessive pumping of ground hot water at a rate faster than the recharging rate, like groundwater exhaust, causes vertical and horizontal ground subsidence, which can damage property and the environment (Hole et al., 2007; Narasimhan & Goyal, 1984). Land subsidence is caused by changes in volume or a decrease in subsurface pore pressure in geothermal reservoirs due to fluid storage depletion and thermal contraction. It's critical to keep track of subsidence in the geothermal field using a precise level network or interferogram so that damage to infrastructure and the environment can be avoided.

Massonnet et al., (1997) created an interferogram using ERS-1 radar images collected over a two-year period near the East Mesa geothermal facility in southern California, and discovered up to 90 mm of subsidence. The extraction of geothermal fluid produced by medium to fine-grained

`

quartzose sandstone is causing this sinking. The overall volume loss owing to subsidence was estimated to be 3.6106 m^3, which corresponds to a total fluid removal from the geothermal reservoir of roughly 5.0106 m^3. For other geothermal fields in Iceland (Vadon & Sigmundsson, 1997), Cerro Prieto, Mexico (Carnec & Fabriol, 1999), Coso, California (Fialko & Simons, 2000) , and the Taupo Volcanic Zone of New Zealand (Hole et al., 2007) the same technique to monitor deformation has been employed.

2.2.4.3 Glacial Water movement

Subglacial water movement has been inferred using vertical displacement characteristics generated from interferograms (Fatland & Lingle, 1998; Gray et al., 2005). Through DEM creation and height comparison, InSAR has also been utilised to infer the water level or volume change of supraglacial lakes (Furuya & Wahr, 2005; Smith et al., 2000). (Goldstein et al., 1993) used InSAR to determine the flow velocity field of the Rutford Ice Stream in Antarctica by combining two SAR phase images with a 6-day interval. InSAR was widely employed for mapping glacier surface velocity in the years after that (König et al., 2001; Massonnet & Feigl, 1998). To derive all three components of the displacement vector, (Joughin et al., 1998) and (Mohr et al., 1998) combined ascending and descending passes of the satellite and placed limitations on the ice flow. A 2D ice-flow velocity field can be derived by combining cross-correlation approaches with InSAR (Gray et al., 2001; Strozzi et al., 2002). Interferogram-derived glacier velocity data is utilised to aid in the location of supraglacial lakes for glacial hazard management (Quincey et al., 2007). The interferogram-derived glacier velocity field can also be used to detect the reasons of ice shelf acceleration (Vieli et al., 2007).

2.2.4.4 Water Level Measurement and Monitoring

In theory, simply geometric observations of river cross-sections, water levels, and surface slopes for both rivers and lakes or reservoirs can be used to determine temporal river outflow and water level fluctuations in lakes or reservoirs (Chow, 1959). Water level (stage) for lakes/reservoirs and major rivers can thus be recovered using spaceborne remote sensing sensors with geometric measuring capabilities (Bjerklie et al., 2003). Imaging radars are among these instruments. Spaceborne water level measurement is greatly improved with current measurement which was in turn demonstrated by using along-track InSAR (ATI) techniques (Bjerklie et al., 2005). For example, if there are persistently existing reflectors (e.g. leafless trees) sticking out of a water

`

surface, interferograms can be formed even over the water that can result in cm-scale estimates of changes in water level (Alsdorf et al., 2000).

2.2.4.5 Soil Moisture Monitoring

InSAR can be used to calculate erosion, deposition, soil moisture, water level change, and net volumetric change of discharges (Smith, 2002). The impact of soil moisture on the strength of backscattered signals has been well studied in the literature. However, very little research has been done on the signal phase's sensitivity to soil moisture conditions. Even though a simple relationship between the phase and the soil moisture profile could not be established (because the relationship varies depending on the frequency, roughness, moisture level, and shape of the moisture profile), a general trend of soil moisture influence on the correlation coefficient was highlighted.

The amplitude and phase of backscattered radar echoes are both influenced by the soil dielectric constant. Because water has a much larger dielectric constant than dry soil matrix, a difference in phase occurs when the two radar images needed to generate an interferogram are obtained due to the dielectric constant difference. Makkeasorn et al., (2006) used Radarsat-1 pictures and a genetic programming model to show that average volumetric soil moisture in the Choke Canyon Reservoir basin, Texas, was 15.5% in September 2004. It could be expanded in the future to use InSAR to detect the soil moisture difference.

From three radar images of the L band (25 cm) collected by Seasat on three distinct occasions spanning 12 days in 1978, (Gabriel et al., 1989) created a color-coded interferogram of agricultural areas in the Imperial Valley, California. The interferogram depicts phase shifts caused by irrigation. In the interval between radar photos, the phase of agricultural areas watered by irrigation canals altered by up to 0.3 cycles. The range shift of 3.75 cm is equivalent to the phase change. The dielectric constant difference generated by water content in the soil causes the phase change. The interferogram can be used to calculate a 1 cm equivalent range change. In a high-plains region of Colorado, (Nolan & Fatland, 2003) used ERS-2 interferogram data to show that millimetre-order changes in path length might be produced by fluctuations in soil moisture of a few volume percentages. The mechanism of soil moisture content on radar phase change is still debated (Gabriel et al., 1989; Massonnet & Feigl, 1998; Nolan & Fatland, 2003), however the equivalent range change is connected to the quantity of water content and could be a useful tool for soil moisture monitoring.

`

Table 2.3: SAR/InSAR application to hydrology

Parameter Measured	Country	Observation Period	SAR Sensor/ other data used	Result	Reference
Land uplift due to groundwater variation	San Bernardino, California	1992-1993	ERS 1,2	0.87 cm/month	(Lu & Danskin, 2001)
Land subsidence due to groundwater variation	Venice	1971–2002	ERS-1, 2 and others	3–5 mm/year	(Carbognin et al., 2004)
Discharge in rivers	The Tanana and Taku Rivers in Alaska, and the Iskut River in British Columbia	2002	Along track interferometric (ATI) SAR imager (AirSAR) and others	794 m^3/sec	(Bjerklie et al., 2005)
Land Subsidence and groundwater variation	Kolkata, India	Dec 1992 to July 98	ERS 1,2	5 mm/year	(Chatterjee et al., 2006)
Soil Moisture	Choke Canyon Reservoir Watershed (CCRW), Texas	April 2004 and September 2004	RADARSAT-1	average volumetric soil moisture is 16.3%	(Makkeasorn et al., 2006)
Glacier recession	Tama Koshi and Dudh Koshi river basins, Himalaya	1994-1996	ERS-1 and ERS-2	25–35 m/year	(Quincey et al., 2007)
Ice-shelf acceleration	Larsen B ice shelf (LBIS)	1995-1999	ERS-1 and ERS-2	− 1.46 ± 0.94 m/year	(Vieli et al., 2007)
Subsidence in the geothermal fields	Taupo Volcanic Zone (TVZ), New Zealand	1996 to 2005	ERS 1,2 and Envisat	− 10 and + 15 mm/year	(Hole et al., 2007)
Land Subsidence duw to groundwater and mining	Pangzhuang mining field, china	Sep 2004 – Dec 2010	ALOS PALSAR	42 ± 15 mm	(Fan et al., 2015)
Ground motion over Coalfield	South Wales Coalfield, United Kingdom	1992 and 1999	ERS-1/2	Uplift at center of coalfield 1 cm/yr.	(Bateson et al., 2015)
Land Subsidence and groundwater variation	Wuhan, China	April 2015 to April 2016	Sentinel-1A	−82 mm/year to 18 mm/year	(Zhou et al., 2017)
Groundwater depletion	Central Mexico	2006-2011	ALOS-1, GRACE, and others	3620 MCM/yr	(Castellazzi et al., 2018)
Structurally controlled land subsidence due to groundwater exploitation	Aguascalientes Valley, Mexico	1996-2020	ERS-1/2, ENVISAT, Sentinel-1	-10 cm/year to -14 cm/year	(Cigna & Tapete, 2021)

`

2.3 Grace Fundamentals

It is not convenient to directly estimate regional-scale water storage as it is labour intensive and expensive work. Many researchers have shown that Gravity Recovery and Climate Experiment (GRACE) gravimetry offers an alternative remote sensing tool (Ramillien et al., 2016; Rodell et al., 2009; Tiwari et al., 2009; Wang et al., 2011; Zaitchik et al., 2008), which is capable of monitoring water storage. This water may include surface water, groundwater, soil moisture, snow, and ice. GRACE has emerged as a vital information source to hydrologists, as it can be used for optimal groundwater observations at a regional scale. When there is a significant change in groundwater storage volume in a small area, GRACE can detect the corresponding mass change because of its high signal-to-noise ratio (Guo et al., 2016; Longuevergne et al., 2013; Tourian et al., 2015). Therefore, GRACE data can be an excellent source for monitoring the variation in groundwater storage.

GRACE is a joint venture of NASA, the USA and the German Aerospace Center (DLR) (Tapley, Bettadpur, Ries, et al., 2004). It was launched on a rocket launch vehicle from the Plesetsk cosmodrome in Russia on March 17th, 2002. The mission is operated by the German Space Operations Center (GSOC), and it consists of two similar satellites named GRACE-A and GRACE-B (Figure 2.11). With more than 15 years of operation, the predicted mission lifetime of 5 years was exceeded by nearly three times. To continue studying earth's gravitational field, the GRACE joint project was relaunched as the Gravity Recovery and Climate Experiment Follow-On (GRACE-FO) in May 2018. Despite the time gaps between GRACE and GRACE-FO, various new methods for bridging the gaps have been proposed, such as singular spectrum analysis (Li et al., 2019) and machine learning (Sahour et al., 2020; Sun et al., 2020).

`

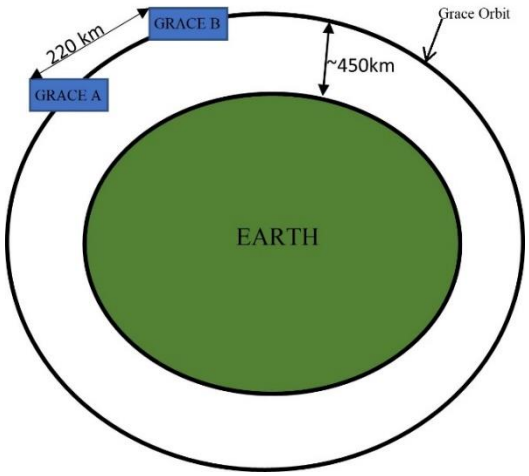

Figure 2.11: GRACE satellite visualisation

The mission's primary goal is the determination of the earth's temporal gravity field. GRACE can be considered as the most successful satellite mission for observing earth's gravity field due to its incredible impact on the broad spectrum of geosciences (Zhang et al., 2016). It consists of two satellites at an inclination of 89.5º and an altitude of about 500 km in near-circular orbits, with a distance of about 220 km along-track between them (Ramillien et al., 2016). The distance between the satellites is monitored using a K-band MW ranging system. There is no fixed pattern for repetition of the ground track, but the satellites are held in such a position that both the K-band antennas precisely point at each other.

There is attenuation and noise contamination in the signal detected by the GRACE satellites. There may be errors due to instruments and measurements also. The near-circular orbit with 89.5º inclination has north-south oriented ground track patterns. These lead to north-south stripes in gravity maps which bury most of the actual signal and thus require filtering.

2.3.1 GRACE working principle

The GRACE measurement principle is based on three fundamental techniques: precise orbit determination, inter-satellite ranging, and accelerometry. The gravity observation from space is based on the fact that the satellite's orbit is perturbed by the inhomogeneously distributed earth's mass attraction. Therefore, precise orbit determination is the primary observation technique (Bandikova, 2015).

`

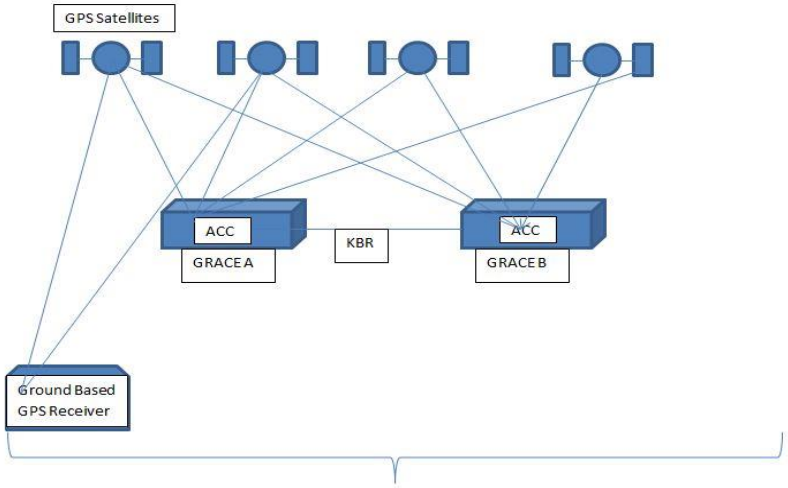

Figure 2.12: GRACE measurement principle

As the two satellites are flying in a co-planar orbit separated by 220±50 km, the sensed orbit perturbation is slightly different for each satellite, which results in continuous inter-satellite range variations. The relative range rates reflect the gravitational potential directly at the position of the satellites at the time of measurement. They are obtained from the inter-satellite ranging. It is the gravitational attraction of the earth and the gravitational attraction of the Sun, the Moon, and other celestial bodies, which perturb the satellite's orbit. All these forces have to be precisely modelled and removed from the observations. Along with the gravitational forces, non-gravitational forces such as air drag, solar radiation pressure and earth's albedo act on the satellite vehicle (Witkowski & Massmann, 2014). In order to obtain the orbit perturbations caused solely by the gravitational attraction of the earth's mass, these non-gravitational forces are sensed by ultra-sensitive accelerometers and subsequently reduced from the original observations.

2.3.2 GRACE Orbit

The GRACE satellites are placed in a low Earth orbit that is slowly decaying. The twins fly in a co-planar, nearly polar orbit with an inclination of 88.93° - 89.10° and nearly circular orbit with a characteristic eccentricity of 0.0010 - 0.0025. The right ascension of the ascending node is progressing very slowly with a period of ca. eight years. The orientation of the orbital plane relative to the Sun changes with a period of ca. 322 days.

It takes approximately 93 minutes to complete one revolution, which results in 15.5 revolutions per day. The orbit is selected to make sufficient spatial data coverage available within one month,

`

and an up-to-date gravity field model can be computed. The two satellites are separated by 220±50 km, which is maintained by regular orbital manoeuvres. Due to the separation distance, the trailing satellite passes over a particular region approximately 28s after the leading satellite.

2.3.3 Groundwater extraction from GRACE

GRACE provides gravity anomalies which can be used to obtain the Total Water Storage (TWS) anomaly, which is the total amount of water column thickness in and above the earth's crust, including surface water, soil moisture (water in soil up to 2 m depth), groundwater, and snow. To get groundwater from TWS, other quantities from TWS needs to be subtracted (Syed et al., 2008). Groundwater storage can be calculated by Equation 2.16:

$$GW = TWS_{GRACE} - (SW + SM + SP) \qquad \text{Equation 2.16}$$

where, GW = groundwater storage anomaly, TWS_{Grace} = Total water storage from GRACE, SW = Surface water storage anomaly, SM = Soil Moisture storage anomaly, and SP = Snowpack storage anomaly. SW, SM and SP components can be obtained either from the site and local bodies or from different models depending on the site conditions.

2.3.4 Applications of GRACE in hydrology

The GRACE monthly gravity maps (at ~110km spatial resolution) have wide application in oceanography, hydrology, glaciology, climatic and geological studies. Water distribution across the earth can be detected using GRACE data, and it is an emerging field in hydrology. It can be applied to sense water fluctuations on and beneath the earth's surface, measure sea-level changes, detect ocean currents near the surface and far beneath the waves, and understand the structural changes of the solid earth (Chinnasamy et al., 2013; Feng et al., 2012). Researchers have successfully performed mass balance studies of hydrological components through GRACE modelling. The components of the global water cycle, variation in the groundwater, snow cover and evapotranspiration contribution have all been quantified using the long-term GRACE data (Scanlon et al., 2012; Schmidt et al., 2008; Swenson et al., 2008; Wang et al., 2011).

Precise, accurate and reliable observations of aquifer levels are required to monitor changes in groundwater storage over time. The GRACE mission opened up new possibilities for monitoring the terrestrial phase of the hydrological cycle, which includes groundwater resources (Tapley, Bettadpur, Ries, et al., 2004). The GRACE project monitors minute changes in the earth's gravity

`

field linked to changes in TWS. TWS anomalies from GRACE are widely employed in hydrological applications at scales from regional to global (Frappart et al., 2016; Wouters et al., 2014). The GRACE data provide a new source of information on extreme climatic events, such as exceptional droughts and floods (Andersen et al., 2005; L. Chen et al., 2009; Long et al., 2014), and snow accumulation (Frappart et al., 2011). It also enables the analysis of basin-scale hydrological fluxes, such as freshwater discharge (Syed et al., 2008, 2009) or evapotranspiration (Ramillien et al., 2006; Rodell et al., 2004), either alone or in combination with external datasets.

Strassberg et al. (2009) demonstrated that GRACE-derived modelling could address the observational gap in monitoring groundwater storage changes over the river basins. Reager et al. (2014) determine the watershed wetness in response to precipitation and flood events. The water cycle components viz. surface water, soil moisture and groundwater and their storage capabilities were quantified to understand the hydrological state of the Missouri, Columbia, and Indus River basins. In the Ganga basin, Gleeson et al. (2012) applied GRACE data to estimate the stress on groundwater resources. The changes in groundwater level in Northern India were studied in detail in 2009, which evaluated that the groundwater is depleting at a rate of one foot per year due to unsustainable groundwater extraction in the Ganga Plains (Rodell et al., 2009; Tiwari et al., 2009). The study of Chinnasamy et al. (2013) shows the importance of GRACE data in studying the groundwater supply in the state of Gujarat, India. The results of the study were validated with direct measurement data of CGWB. Chen et al. (2014) demonstrated that groundwater storage changes in Northwest India are strongly correlated with the precipitation anomalies as the monsoon is a significant source for groundwater renewal and thus holds control over groundwater level in India. Hussain et al. (2020) reported that the TWS reduced in the upper Indus basin at the rate of 4.47 ± 0.38 mm/year from 2003 to 2016.

Rodell et al. (2009) studied GRACE data around the Northern Indian region between 2002 and 2008. They found that more than 109 km^3 of groundwater disappeared during the period, double the capacity of India's largest surface water reservoir, the upper Wainganga. The study concluded that groundwater is being pumped and consumed by human activities, principally to irrigate cropland, faster than natural processes can replenish the aquifers. Though the absolute volume of water in the Northern Indian aquifers is unknown, GRACE provides strong evidence that current water extraction rates are not sustainable. The region has become dependent on irrigation to maximise agricultural productivity and this is behind the water crisis. The loss is particularly

`

alarming because it occurred when there were no unusual trends in rainfall; instead, it was above average for the period. Castle et al. (2014) applied the GRACE gravity data in the Colorado River basin and revealed that the parched western US uses significant amounts of groundwater. The study concluded that the Colorado River basin lost nearly 53-million-acre feet of freshwater between December 2004 to November 2013, almost double the volume of the nation's largest reservoir, Nevada's Lake Mead. The study further concluded that more than 75% of the water loss in the drought-stricken Colorado River basin since late 2004 came from underground resources. Famiglietti et al. (2011) studied the GRACE data around the California region between September 2011 and September 2014. The study revealed that around 11 trillion gallons of water would be required to replenish California drought losses. The TWS changes using GRACE has been interpreted from the basin (Sun et al., 2020), regional (Zhu et al., 2021) and continental scales (Humphrey et al., 2016). Furthermore, GRACE measurements have shown tremendous promise in measuring groundwater levels globally (Döll et al., 2014; Feng et al., 2018; Frappart & Ramillien, 2018) and exploring climate and human interactions (Hosseini et al., 2020). Table 2.44 summarises annual rates of groundwater depletion in the significant aquifers located in arid and semi-arid regions based on the decomposition of GRACE-based TWS.

Table 2.4: Annual rates of groundwater depletion in the major aquifers located in arid and semi-arid regions based on the decomposition of GRACE-based TWS [Modifed from (Frappart & Ramillien, 2018)].

Region	Area 10^6 km^2	Country	Ref	Estimated Depletion Rate		GRACE Product and Release	SM Product	SW Product	Snow Product	Period (MM/YYYY–MM/YYYY)
				mm/ year	km^3/ year					
North-western Sahara Aquifer System	1	Algeria, Lybia, Tunisia	(Gonçalvès et al., 2013)	−0.54 ±1.40	−0.54 ±1.40	NA	GLDAS	None	None	01/2003 – 12/2007
			(Ahmed et al., 2014)	−0.81 ±0.16	−0.81 ±0.16	CSR 05	None	None	None	01/2003 – 09/2012
			(Ramillien et al., 2014)	−4.48	−4.48	Regional	None	None	None	06/2003 – 12/2012
			(Richey et al., 2015)	2.69 ± 0.8	−2.69 ±0.8	CSR 05	GLDAS	CLM 0.4	None	01/2003 – 12/2013
Nubian Sandstone	2.2	Chad, Egypt,	(Ahmed et al., 2014)	−3.72 ±0.27	−8.18 ±0.59	CSR 05	None	None	None	01/2003 – 09/2012

`

Aquifer System		Lybia, Sudan	(Richey et al., 2015)	−2.76 ±0.86	−6.08 ±1.9	CSR 05	GLDAS	CLM 0.4	None	01/2003 – 12/2013
Tigris and Euphrates River Basin	0.75	Turkey, Syria, Iraq, Iran	(Voss et al., 2013)	−27.2 ±0.6	−20.4 ±0.45	CSR 05	GLDAS	Altimetry	None	01/2003 – 12/2009
Middle East	NA	Iraq, Iran, Saudi Arabia, Turkey	(Joodaki et al., 2014)	NA	−43± 3	CSR 05	CLM 4.5	CLM 4.5 + Altimetry	None	02/2003 – 12/2012
Northwest India	0.56	India	(Rodell et al., 2009)	−40± 10	−17.7 ±4.5	CSR 04	GLDAS	None	GLDAS	08/2002 – 10/2008
			(J. Chen et al., 2014)	−47.7 ±12	−20.4 ±7.1	CSR 05	GLDAS	None	GLDAS	01/2003 – 12/2012
Northern India	2.7	India	(V. M. Tiwari et al., 2009)	−20± 3	−54± 9	CSR 04	CLM	CLM	GLDAS	04/2002 – 06/2008
North China	0.37	China	(Feng et al., 2013)	−22± 3	−8.3± 1.1	CSR 05	GLDAS	None	None	01/2003 – 12/2010
Hai River		China	(Shen et al., 2015)	−17.0 ±4.3	−5.5± 1.4	GRGS 2	In situ	In situ	None	01/2003 – 12/2012
Piedmont Plain	0.054	China	(Z. Huang et al., 2015)	−46.5 ±6.8	−2.5± 0.4	CSR 05	GLDAS	None	None	01/2003 – 07/2013
East Central Plain	0.086	China	(Z. Huang et al., 2015)	−16.9 ±1.9	−1.5± 0.2	CSR 05	GLDAS	None	None	01/2003 – 07/2013
Canning	0.43	Australia	(Munier et al., 2012)	−25.6	−11	GRGS 2	NOAH	None	None	01/2003 – 12/2009
Murray Darling Basin	1	Australia	(Leblanc et al., 2009)	−17± 7	17±7	GRGS 1	NOAH	In situ	None	01/2003 – 12/2007
			(J. L. Chen et al., 2016)	−17.2 ±4.7	17.2± 4.7	CSR 05	WGHM	WGHM	None	01/2003 – 12/2012
High Plains Aquifer	0.45	USA	(Breña et al., 2014)	−25.1 ±2.1	−11.4 ±0.4	CSR 05	NOAH	In situ	None	03/2003 – 02/2013

`

Sacramento and San Joaquin River Basins	0.154	USA	(Famiglietti et al., 2011)	−20.4 ±3.9	−3.1± 0.6	CSR 04	GLDAS	In situ	NORHSC	10/2002 – 03/2010
			(Scanlon et al., 2012)	−55.9 ±5.3	−8.6± 0.8	GRGS 2	GLDAS	In situ	SNODAS	04/2006 – 03/2010
			(Scanlon et al., 2012)	−44.9 ±8.5	−6.9± 1.3	CSR 04	GLDAS	In situ	SNODAS	04/2006 – 03/2010
Colorado River Basin	0.64	USA	(Castle et al., 2014)	8.75± 0.63	−5.6± 0.4	CSR 05	GLDAS	In situ	SNODAS	12/2004 – 11/2013

2.4 Groundwater quality

The rising water demand to satisfy human needs and the changing climate leads to significant pressure on groundwater. Anthropogenic factors are putting the quality of groundwater stored in aquifers under the earth's surface in jeopardy (Foster, 2020; Jha et al., 2020; Lall et al., 2020; Lerner & Barrett, 1996; Pérez et al., 2019; Qian et al., 2020; Talabi et al., 2019; Tiwari & Pal, 2021). Human activities such as over-extraction of groundwater, infiltration of dirty water, mixing of chemicals, pesticides, or fertilisers, and landfill, directly and indirectly, affect groundwater chemistry. Groundwater contamination from agricultural, industrial, and urban activities pose a severe danger to groundwater sustainability in the long run (Bearcock et al., 2019). Groundwater 'mining' can have detrimental consequences for meeting the long-term water demands of people. As the reliance on groundwater grows, water management bodies and policymakers must pay close attention to the quality of groundwater in addition to its quantity (Megdal, 2018).

Although groundwater has traditionally been a relatively pure natural resource within aquifers, human impacts increasingly threaten its integrity. Chemical quality changes occur because of direct anthropogenic substance inputs, groundwater withdrawal and the resulting shift in its flow regimes, and artificial recharge (Haritash et al., 2016). Groundwater quality is compromised, particularly in locations where surface water sources are few (arid and semi-arid regions) or contaminated (Jaiswal et al., 2003; Jha & Sinha, 2009).

Groundwater chemistry characterisation and monitoring are critical components of management and protection. These lay the groundwork for determining groundwater's appropriateness for its intended use, detecting contamination sources, and assessing any temporal changes. The European

`

Union legislation in the form of the Water Framework Directive, Groundwater Directive, EC drinking-water rules, and environmental-quality standards is the leading European impetus for characterising and monitoring groundwater quality. Anthropogenic compounds such as pesticides or chlorofluorocarbons (CFCs) in groundwater indicate contamination, but the distinction is less evident for compounds generated from pollution or natural sources, such as nitrate, phosphorus, or arsenic. Groundwater chemistry changes significantly due to numerous complicated geological, geochemical, hydrogeological, and climatic processes. Statistical methods, such as statistical summaries (medians, arithmetic means, percentiles), box plots, and cumulative probability diagrams, are among the most useful analytical tools for analysing chemical data.

The management of groundwater quality has gained regional and global consideration by humankind, especially after the industrial revolution (Arias et al., 2008). However, even today, several parameters for managing groundwater resources are complicated, and relevant knowledge remains elusive in many circumstances (Famiglietti, 2014). Besides the natural factors, anthropogenic activities significantly impact the natural water cycle and, as a result, affect groundwater quality. These alterations have the potential to have far-reaching consequences for ecosystem functioning and human health. Changes in surface roughness, surface sealing, topographic adjustments, river canalisation, and the development of artificial water bodies are all examples of physical changes to the landscape that might enhance risk (Bhaskar et al., 2016; Han et al., 2017). Anthropogenic activities include the widespread use of natural and artificial chemical compounds and modifying land cover. High crop yields, enhanced human and animal health, adequate energy, material production, and effective infrastructure have all resulted from the use of such items. However, many commonly used compounds are soluble, mobile, and persistent in groundwater, as well as harmful to the environment and human health (Wakida & Lerner, 2005).

When an aquifer is contaminated with hazardous chemicals, it might become unusable for decades. Depending on the physicochemical properties of the chemicals and the environmental conditions, the residence duration of pollutants in groundwater bodies can range from weeks to decades (Chapman & Parker, 2005; Freitas et al., 2015; Moeck et al., 2018). Furthermore, the consequences of groundwater contamination do not end with the loss of access to well water, but as groundwater flows through the hydrologic cycle, contaminants migrate from dumping or spill sites to surrounding aquifers, and ultimately to lakes and rivers (Conant Jr et al., 2004). The scientific community is aware of these challenges, and regulatory organisations in various parts of the world

`

have set concentration limits for various pollutants in drinking water sources, with nitrate being the most noteworthy example. Nonetheless, groundwater contamination caused by anthropogenic activity is a constant and growing hazard (Lapworth et al., 2017; Wakida & Lerner, 2005). The current expansion of human activities frequently runs counter to what is required to safeguard groundwater resources for future usage (Howard, 2015; Khan et al., 2016).

It is critical to establish a detailed understanding of groundwater flow, drought, recharge, and contaminant transport to address groundwater contamination and shortages (Sahoo & Sahoo, 2019). Advanced technologies such as GIS and remote sensing (Gemitzi et al., 2017), numerical and analytical models (Michael & Voss, 2009; Zhang et al., 2019), and the combination of models and GIS-remote sensing (Diepenbroek et al., 2002) can provide a holistic analysis saving time and money when surveying large areas. To observe, manage and protect groundwater quality are important economic and environmental concerns. Temporal and spatial changes in groundwater quality may arise because of various atmospheric stimulations, varied geology, variation in subsurface mineralogy and factors controlling residence times (Aldiss, 2014). Keeping track of groundwater quality fluctuation over time can assist decision-makers to better comprehend the long-term viability of an aquifer as a source of water and make appropriate policy decisions (Alley, 2007).

2.5 Suitability of study area

The goal of the thesis is to apply a combination of remote sensing techniques (SAR, GRACE) and geospatial analysis (water quality) to assess urban influences to groundwater. For that purpose, London and Delhi were selected. These locations are deemed suitable because with the increasing population of these two cities, there is a lot of pressure on groundwater resources. Thus, monitoring of groundwater variation of both these cities is essential for its sustainable development.

London and NCT-Delhi are perfect for studying groundwater induced land subsidence using PSInSAR for several reasons. Firstly, there is a consistent archive of microwave RADAR acquisition from several sensors starting from 1992 till the present day over both these cities. These enable us to monitor land deformation of different scales and types using various sensors. Secondly, a high density of permanent scatterers can be obtained over London and NCT-Delhi due to their urban fabric, allowing for a high density of reliable measurements points. Thirdly, a large amount of ground-based data is recorded and distributed over London and Delhi such as borewell

`

data, GPS data, GNSS data, site inspection data for surface and underground constructions and others. This data can be used for validating the remotely sensed observations. These nearly ideal conditions reveal the lower limits of deformation detection that are achievable with PSInSAR.

The excellent quality of PSInSAR ground deformation measurements also delivers practical and valuable information for a large number of civil engineering projects in both these cities. In turn, these projects provide data from a wealth of conventional ground-based monitoring, such as total stations, which validate the PSInSAR measurements. While the urban fabric of both these cities is ideal for PSInSAR, it also restricts conventional geological surveying techniques like GPS, GNSS or laser surveys. Hence, PSInSAR data offer the only feasible way to detect millimetre scale regional ground movements originating from anomalies in the geology of these cities. Identifying and constraining these anomalies is a promising approach to an improved understanding of aquifer behaviour and adding detail to the geological model of both these cities. Also, the groundwater chemistry of London is given in chapter 6. The data for various boreholes across London is provided in the open domain by the EA, which can be directly used to analyse the quality of groundwater for London.

2.6 Research Gap

Many studies have attempted to link InSAR measurements, land subsidence and groundwater levels (Section 2.2). Also, many studies have tried to link GRACE anomalies and groundwater variations (Section 2.3). The notable difference between the two technologies is their spatial resolution. However, exciting results about spatial and temporal groundwater variations could be obtained by using the two technologies in conjunction. While GRACE can give basin level variation, InSAR can read variations in any particular city. According to available literature, very few attempts have been made to combine PSInSAR derived land subsidence and GRACE gravity derived groundwater together (Castellazzi et al., 2016; Du et al., 2016; Guo et al., 2016). In this research work, an attempt has been made to explore the two technologies and their application to study variation in groundwater resources in conjunction, for London (Chapter 4). The results from our study can prove to be a new source of information for hydrologists and government agencies to deal with problems of land subsidence and over-extraction of groundwater. Identifying if InSAR and GRACE can be used as a predictive tool to indicate where groundwater levels are rising or

`

depleting would provide a cost-effective solution to survey vast areas as an alternative to traditional labour-intensive methods.

The capital cities in the UK (London) and India (Delhi) are witnessing an ever-increasing population growth that has exerted excess pressure on groundwater resources. Despite their different sub-surface geology, this increasing pressure on groundwater poses a significant threat of land movement in these cities. No previous study has attempted to examine the groundwater behaviour and resulting land-subsidence for both these cities simultaneously. By studying them together, it is interesting to see how urban cities respond to groundwater changes in developed and developing nations. By applying the methodology developed in Chapter 4, the groundwater induced subsidence for London and Delhi was studied (Chapter 5).

The monitoring of spatiotemporal variation of groundwater quality is essential for its efficient safeguarding and management. For London, there has been no comprehensive work in the last two decades that studies and compares spatiotemporal variation of groundwater quality parameters. A comprehensive assessment of groundwater quality focused on London was required to help allocate resources to maintain potable-quality groundwater. Chapter 6 of this study primarily aimed at describing temporal and spatial trends in groundwater quality parameters used for drinking water supplies in London between 2000-2020. The secondary aim was to examine an integrated dataset of concentrations of groundwater quality parameters, available in the open domain, for London, as a foundation for a comprehensive assessment. Chapter 6 highlights chemical status and key pressure on groundwater quality, which should be valuable information to government bodies, water regulators and environmental scientists.

`

Chapter 3 Overview of SAR Sensors and Software

Preface

Chapter 1 highlights that the objective of this research, among others, is to better understand the potential applications and limitations of the use of InSAR data over urban area (London and Delhi). Ideally, the information gained from InSAR should lead to a better understanding of the hydrogeology underneath these cities. But to achieve that, it is vital to understand the source of error in InSAR measurements, the nature of deformation that can be detected, and the ideal SAR sensor-software combination for SAR processing. During the early stages of the research, different approaches were evaluated in an attempt to identify the optimum tools and methodology for achieving these objectives.

The first year of this PhD was used to study the basic principles of SAR and interferometry. A good understanding of different SAR processing techniques was learnt specifically DInSAR and PSInSAR. Also, aims and objectives for the final work were pointed out, and attempts were made to start achieving those. The processing of SAR data to study land movement induced by groundwater was a primary task to start the PhD work. So, different options were explored to process the SAR data, especially as the Punnet software which was earlier used in our lab at Nottingham Geospatial Institute (NGI) had been commercialised with the formation of Geomatic Ventures Limited (GVL), and only limited access was available for new PhD students. This motivated the study of different open-source software and the merits and limitations of each were determined.

At the beginning of the study in 2017, ESA's SNAP software toolbox was the only available open-source, freely available, user-friendly graphical user interface (GUI) software package. This software was used to generate differential interferograms for London using two SAR images, to check if surface motions can be traced for short time intervals. The interpretation of these interferograms seemed a bit challenging with several limitations. Firstly, displacements were in the order of centimetres (Ferretti, 2014), but expected deformation in London is less than 1 cm for small time frames of a few years. Secondly, SNAP did not have any indigenous phase unwrapping principle, and Snaphu unwrapping package was used to do unwrapping, which brings all the limitations associated with Snaphu to the final results. Thirdly, SNAP gives an encapsulated GUI environment to generate interferogram and to investigate and update the principle used behind each

`

step was difficult. Fourthly, SNAP could only provide DInSAR with two images, and times series analysis with multiple SAR images was not supported. The DInSAR maps created using SNAP could be used as an interferometric input for further processing by external open-source software packages, such as StaMPS (A. Hooper et al., 2010) which is mainly dedicated to the Persistent Scatterer (PS) technique. However, in 2017 when this PhD was started, stamps could not process Sentinel-1 images, as merging the burst from Sentinel-1 TOPSAR acquisitions was a problem, and only recently solved (Foumelis et al., 2018).

Also, attempts were made to access funding for commercial software with different agencies. Thus, an application was made for funding with ESA, through their Eohops programme, for access to SARscape software for InSAR time series analysis. An access to the software ws granted initially for six months from January 2019 to June 2019 and then got that extended for another twelve months from July 2019 to June 2019. SARscape is available for Linux and Windows, as part of the ENVI software suite (distributed by Harris Geospatial), but the windows version is more widely used and better tested.

A comparative study was done on London using both these software packages (SNAP and SARscape) to understand the merits and limitations of each, so that the best available suitable software package can be used for further study. This comparison also highlighted that open source pacakages could give comparable results to expensive commercial results, and could be used for processing SAR datasets especially for novice users who maynot have access to commercial software. This study help us setup methodology for InSAR processing, that will be used to study land movement and related hydrogeology in futher chapters of this thesis. This comparative study, along with an overview of SAR sensors and softwares, was submitted as a research review paper to the 'Asian Conference of Remote Sensing – 2020, November 9-11 online, hosted at Deqing city, China', entitled '*An Overview of Sar Sensors And Software And A Comparative Study Of Open Source (Snap) And Commercial (Sarscape) Software For DInSAR Analysis Using C-Band Radar Images'*. The published paper is presented here in this thesis as Chapter 3.

ABSTRACT: Synthetic Aperture Radar (SAR) Interferometry has several proven applications in seismology, volcanology, land movement, glaciology, hydrology, forestry sciences and numerous other fields. SAR techniques can solely be handled by experts in RADAR image processing. In addition, commercial software and high-quality radar data can be expensive and out of reach for

`

most early researchers in this field. While many new SAR sensors are being launched, a look at their compatibility with different SAR processing software packages is also important. Thus an overview of past, present and future SAR sensors and software packages is discussed in this work. To understand the strength and limitations of open source and commercial SAR processing software, DInSAR land displacement maps were created. The open-source software SNAP and commercial software SARscape were used to generate the land displacement maps. Sentinel-1A data over London between April 2015 and April 2018 was used. The land movement results obtained, shows that SNAP results are in good agreement to SARscape results. To compare the results, all attempts were made to keep the user input parameters consistent in both the experiments like multilooking factor, phase unwrapping principle, and filtering methods. However, some differences are unavoidable because of the Ground Control Points (GCPs) selection, co-registration, or spectral shift filtering steps. A difference of 1 mm/year in subsidence was observed in the results obtained from the two software packages. This is the first study that compares SNAP and SARscape software using Sentinel-1A data for London. It can be concluded that open source and free of cost SAR software can be handy tools for DInSAR processing, especially for beginners who do not have access to expensive commercial software. It is recommended that more open source, free of cost datasets and software packages, will attract a larger number of early stage researchers in this field. It will enable an expansion of the use of DInSAR principle for different applications.

3.1 Introduction

Monitoring of surface movement is very important for city planners and managers, as it can be very dangerous for infrastructures such as canals, roads, railways, bridges, pipelines, and buildings. Even though accurate monitoring methods for surface displacement are present in geotechnical engineering, conventional geotechnical instruments are limited within a small area. For example, precise continuous monitoring over an extensive area can be achieved using GPS but still monitored area is limited to few square kilometers. Also, surface displacement monitoring on dangerous area or on disaster area is difficult using conventional methods as these require installation of monitoring devices on the site. These limitations can be mitigated using DInSAR.

DInSAR refers to interferograms, which has phase related to surface deformation only, and from which phase related to the topographic contribution has been deleted (Ferretti et al., 2000a). It can

`

monitor ground deformation for vast areas without requirement of any devices on the ground. Also, DInSAR can be useful in case of disasters like landslides and earthquakes, where conventionally installed measurement devices might be difficult to operate. It also provides weather independency, sunlight independency (active sensor) and high (basin-level or greater) spatial coverage (Refice et al., 2001; Smith, 2002).

The primary aim of this work is to improve the understanding of existing SAR software and products. For over three decades, various publications have highlighted the capability of differential interferometry to monitor ground movement in vertical direction with millimeter level accuracy (Colesanti & Wasowski, 2006; Crosetto & Crippa, 2005; Gabriel et al., 1989). But this technique can be mainly used by specialists in InSAR processing as data and software availability for processing can be a major limitation, especially for novice users. Also, most SAR tools and software packages are often hard to work by a new user, and expert skills of InSAR imagery may be needed. Thus, an attempt is made to overview most widely used datasets and software packages. Some work has been done for InSAR software comparison (Simonetto, 2008; Simonetto & Follin, 2012) using same data by different users, but SARscape and SNAP has not been studied together before. The strength, weakness and output of each processing step has been compared in this work. More open source, free of cost datasets and software packages will attract a larger number of early-stage researchers in this field and will enable an expansion of the use of DInSAR techniques for different applications.

3.2 SAR Sensors And Software Packages

3.2.1 SAR Sensors

SAR sensors can be mounted on airplanes, shuttles or satellites but discussion will be limited to satellite sensors only. SAR satellite orbits in low earth, polar, sun-synchronous orbit. The data acquisition can be made independent of cloud coverage, at any time of day and night, and has both amplitude and phase components (Unavco, 2020). The radar satellites work at specific wavelengths and L, C, and X-bands are the predominate ones. First radar satellite sensor was Seasat, set in motion in June 1978 by National Aeronautics and Space Administration, Jet Propulsion Laboratory (NASA/JPL), but its lifetime was less than 4 months (Seasat, 2020). Though Seasat itself was operational for a very short duration, but it led foundation for world

`

scientists to explore the new area of SAR satellite sensors. It led to the launching of numerous SAR sensors which provided valuable information about earth surface and space geodesy.

The first commercially successful SAR sensor mission was European Remote Sensing Satellite (ERS-1) launched on 17 July 1991 by ESA. It was launched at an altitude of approximately 785 km, which was operational for almost one decade (ERS, 2020). ERS-1 operated in C band of the MW radiations and comprised many instruments with different principles which gained and disseminated information about Earth's land, water, ice and atmosphere. ERS-1 was followed by many SAR sensors (Table 3.1) and the latest proposed SAR satellite sensor is NASA-ISRO Synthetic Aperture Radar (NISAR). It is a joint venture between NASA and ISRO and the first ever dual frequency radar imaging satellite (NISAR, 2020). NASA will contribute L band SAR, while ISRO will contribute S band SAR. The NISAR mission life is planned to be 3 years and will provide vital information about Earth's crust, ecosystem, climate change, coastal waters and hazard management. Table 3.1 summarises important past, present, and future projected SAR satellite missions. The list is not exhaustive, but it promises that a consistent SAR data is available.

Table 3.1: SAR Sensors

Sensor	Time Period	Repeat cycle (days)	Wavelength (cm), band	Polarisation	Supporting Agency
Seasat	June 1978 to October 1978 (110 days life time)	3	23.44, L band	HH	National Aeronautics and Space Administration/Jet Propulsion Laboratory (NASA/JPL)
ERS-1	1991-2000	35	5.66, C band	VV	European Space Agency (ESA)
JERS-1	1992-1998	44	33.53, L band	HH	Japan Aerospace Exploration Agency (JAXA)
SIR-C/X-SAR	April 1994 – October 1994	10	23.5, L band 5.8, C band 3.1, X band	L&C (Quad) X (VV)	NASA/JLP, Deutsches Zentrum für Luft- und Raumfahrt DLR (Germany), Italian Space Agency (ASI)
RADARSAT-1	1995 - 2013	24	5.66, C band	HH	Canadian Space Agency (CSA)
ERS-2	1995 - 2011	35	5.66, C band	VV	ESA
Envisat/ASAR	2002-2012	35	5.63, C band	Dual	ESA

`

ALOS-1	2006-2011	46	23.62, L band	Quad	JAXA
RADARSAT-2	2007-Present	24	5.55, C band	Quad	CSA
COSMO/SkyMed	2007-Present	16	3.125, X band	Dual	ASI
TerraSAR-X	2007 – present	11	3.125, X band	Quad	DLR
TanDEM-X	2010 - present	11	3.125, X band	Quad	DLR
RISAT-1	2012 - 2017	25	5.60, C band	Quad	Indian Space Research Organisation (ISRO)
KOMPSat-5	August 2013 - present	28	X band	Dual	Korea Areospace Research Institute (KARI)
ALOS-2	2013 – present	14	23.62, L band	Quad	JAXA
Sentinel – 1	2014-present	12	C Band	Dual	ESA
PAZ	Feb 2018 - Present	11	X band	Quad	Instituto National de Técnica Aeroespacial (INTA), Spain
SAOCOM	June 2018 - present	16	L band	Quad	Comision Nacional de Actividades Espaciales, Argentina
NISAR	Planned (2021)	12	24, L Band (NASA) 9.3, S band (ISRO)	Quad	ISRO and NASA

3.2.2 SAR Software Pacakages

DInSAR is gaining popularity as a deformation monitoring technique, and the availability of new processing software is also increasing. For selecting the software for SAR data analysis, important considerations are the cost of the license (either commercial or free of charge), the cost of service and maintenance (like hotline or mailing list), the oftenness of update, and compatibility with different platforms (Linux, Unix, Windows, MacOSX). It also depends on the software abilities like data handling capacity, multiple image processing and time series analysis. It further depends on processing capabilities like SAR focusing, unwrapping, geocoding and resampling, supported sensors and access to source code (Simonetto & Follin, 2012). These factors directly control the quality of the output and ability to enhanced understanding of groundwater resources.

`

Here a list of important and widely used commercial and free of charge open-source software have been provided. The open-source means that the source code is available, while free of charge might have restricted use and may be completely free. Our list is not comprehensive, as research institutes often develop their software tools and packages and do not share them for public use, for example, Altamira information in Barcelona (Altamira, 2020). Also, it is worth noting that the provided information about different software has been reported from documents available in the open domain. The authors have not tested all the software. The readers can also refer to (Crosetto & Crippa, 2005; Gens, 1999; Simonetto & Follin, 2012) for more details about different SAR processing software tools and packages available.

The open-source, free software included are SNAP, StaMPS, DORIS, ROI_PAC, ISCE, and GMTSAR. SNAP has a user-friendly graphical user interface. It is a common architecture for all Sentinel toolboxes, which is ideal for exploiting earth observation data. SNAP is excellent for DInSAR analysis, but the most significant limitation with SNAP at present is that it does not support multiple images time series analysis. However, it can alternatively prepare the interferometric inputs for further processing by external open-source software packages, such as StaMPS. The software StaMPS is mainly dedicated to the Persistent Scatterer (PS) technique. Details and strengths of all the software have been tabulated in Table 3.2.

Table 3.2: SAR Open Source Software

SNAP	StaMPS	DORIS	ROI_PAC	ISCE	GMTSAR
Developed by European Space Agency (ESA)	Developed by Stanford University	Developed by TU DELFT	Developed by JPL/Caltech	Developed by Stanford/Caltech /JPL	Developed by Scripps Institution of Oceanography and San Diego State University
Strengths: InSAR, DInSAR, geocoding, Unwrapping	Strengths: PSInSAR	Strengths: InSAR, DInSAR, no unwrapping	Strengths: SAR focusing, InSAR, DInSAR	Strengths: SAR focusing, InSAR, DInSAR, provides precise geolocation	Strengths: SAR focusing, InSAR, DInSAR
Supports: Radarsat1&2, ENIVISAT, ERS1&2, ALOS,Sentinel-1, TerraSAR-X	Supports: Radarsat1&2, ENIVISAT, ERS1&2, ALOS,	Supports: Radarsat1&2, ENIVISAT, ERS1&2, ALOS,	Supports: Radarsat1&2, ENIVISAT, ERS1&2, ALOS,	Supports: Radarsat1&2,ENIVISAT, ERS1&2, ALOS, Sentinel-1, TerraSAR-X	Supports: Radarsat1&2,ENIVISAT, ERS1&2, ALOS, Sentinel-1, TerraSAR-X

`

	Sentinel-1, TerraSAR-X	Sentinel-1, TerraSAR-X	Sentinel-1, TerraSAR-X	Latest	
Latest Release SNAP 7.0.0 (2019)	Latest Release 4.1b1 (2018)	Latest Release: V5.0.3 Beta (2017)	Latest Release:V3.0.1 (2017)	Release: V2.2.0 (2018)	Latest Release: V6.0 (2020)
Unix/Linux/Windows/MacOSX	Unix/Linux/MacOSX	Unix/Linux/MacOSX	Unix/Linux/MacOSX	Unix/Linux/Mac OSX	Unix/Linux/Mac OSX

The commercial software included are ENVI SARscape, SARPROZ, GAMMA, DIAPASON, and Imagine Radar Mapping Suite. These are user-friendly, semi-automated, and powerful software. These implements a wide range of Radar techniques including SAR, InSAR, DInSAR and time series techniques like Persistent Scatterer (PS) InSAR and Small BAseline Subset (SBAS) InSAR. All these software supports most satellites/data formats like ERS1&2, Radarsat1&2, ENIVISAT, ERS1&2, ALOS, Sentinel-1, TerraSAR-X, Alos, Cosmo SkyMed, and Kompsat-5. The major advantage of these software is continuous maintenance and updates, which supports the latest launched SAR sensors. Details and strengths of all the software have been tabulated in Table 3.3.

Table 3.3: SAR commercial Software

ENVI SARScape	**SARPROZ**	**Gamma**	**DIAPASON**	**IMAGINE Radar Mapping Suite**
Developed by Exelis/Sarmap	Developed by Daniele Perissin Italy	Developed by Gamma Remote Sensing	Developed by French Space Agency (CNES), but now managed by Altamira	Erdas developed by Leica Geosystems Geospatial Imaging
Strengths: SAR focusing, InSAR, DInSAR, PS, SBAS	Strengths: SAR focusing, InSAR, DInSAR, PS, SBAS	Strengths: SAR focusing, InSAR, DInSAR	Strengths: DInSAR	Strengths: SAR focusing, InSAR, DInSAR, PS, SBAS
Supports: ERS1&2, Radarsat1&2, ENIVISAT, ALOS, Sentinel-1, TerraSAR X, Alos, Cosmo SkyMed, Kompsat-5, Geofen-3	Supports: ERS1&2, Radarsat1&2, ENIVISAT, ALOS, Sentinel-1, TerraSAR X, Alos, Cosmo SkyMed, Kompsat-5,	Supports: ERS1&2, Radarsat1&2, ENIVISAT, ALOS, Sentinel-1, TerraSAR X, Alos, Cosmo SkyMed, SIR-C Kompsat-5, Geofen-3	Supports: ERS1&2, Radarsat1&2, ENIVISAT, ALOS, Sentinel-1	Supports: ERS1&2, Radarsat1&2, ENIVISAT, ALOS, Sentinel-1, TerraSAR X, Alos, Cosmo SkyMed, Kompsat-5, Geofen-3

`

Latest Release: V5.5.3 (2020)	Latest Release: 2019.0	Latest Release: V1.8 (2020)		Latest Release: V5.5.0 (2018)
Unix/Linux/Windows/ MacOSX	Unix/Linux/Windows/ MacOSX	Unix/Linux/ Windows/Mac OSX	Unix/Linux/ Windows/Mac OSX	Unix/Linux/Windows/ MacOSX

Several other software and tools exist for InSAR processing, each with its advantages and limitations. For example, POLSARPRO focuses on SAR data acquired in the quad polarimetric mode and allows their Pol-InSAR processing. Geospatial Data Abstraction Library (GDAL) is an open-source translator library for raster geospatial data formats. It offers readers for certain SAR data, for instance, CEOS SAR image files (Simonetto & Follin, 2012).

This study has compared open source SNAP and commercial SARscape software. SNAP is selected because it has a user-friendly GUI. The other open-source software are primarily command-line based packages, which complicates their use especially for novice users. Also, SNAP is compatible with all operating systems (32 and 64 bit Windows, Mac OS X and Linux). Its latest version of 7.0.0 is only around 0.5 GB in size for windows 64 bit. The hardware system requirements to run the software are also relatively minimal (4 GB ram is sufficient). SARscape is selected as access to the software could be obtained via the ESA Eohops programme. The SARscape is expensive and requires a high-end hardware machine to run efficiently. However, it is highly efficient in SAR processing, DInSAR, PSInSAR, and SBAS InSAR; and supports all the latest SAR sensors. Also, processing using SARscape is semi-automated and can be efficiently used for validating SNAP results.

Both the SARscape and the SNAP software support X-band and C-band band analysis, which are ideal for land deformation analysis, which can be future related to groundwater level change and local hydrogeology (which will be done in subsequent chapters of this thesis). Also, both these softwares support L and P band sensors which are capable of ground penetration and can be futher used for hydrogeology for a particular area (Pratesi et al., 2016; Strozzi et al., 2005; Wdowinski et al., 2008).

`

3.3 Materials And Methods

3.3.1 Data Used and Study Area

The following Sentinel -1A, Interferometric Wide (IW), Single Look Complex (SLC) data acquired on 12th April 2015 and 8th April 2018 has been used in the study:

S1A_IW_SLC__1SDV_20150412T174854_20150412T174921_005454_006F45_BEBD

S1A_IW_SLC__1SDV_20180408T174913_20180408T174943_021379_024CDB_9173

The above dataset has been acquired free from Copernicus open access hub (Copernicus, 2020). The data specifications are spatial resolution (range by azimuth): 5m, and wavelength: C band - 5.6 cm. The software used are SNAP 7.0. and ENVI SARscape 5.5.2.

The IW swath is Sentinel's primary operational mode over land and acquires 3 sub-swaths using Terrain observation with Progressive Scans SAR (TOPSAR). For Interferometry SLC data is used exploiting the complex imagery of both amplitude and phase. Each sub-swath image consists of a series of bursts and the input product contains 3 IW bands, and 9 bursts (SLC, 2020).

In the study, the area chosen is the administrative area of Greater London. The area is bounded by 0º30'W and 0º20'E longitudes and 51º42'N and 51º17'N latitudes covering an area of approximately 1600 km^2 in the southern part of England. According to the Copernicus EEA European urban atlas (UA), the land use within the London area is dominated by dense to medium density urban fabric. It has multiple industrial units and stretched port areas along the river Thames (EC, 2011). Also, according to the 2011 population census of the UK, the total population of London is around 9.5 million and has been continuously increasing since the 1980s. The ever-increasing population is exerting a pressure on groundwater to meet the increasing demand and thus can cause the problem of land subsidence.

3.3.2 Methodology

Here, the SNAP user environment is explored to generate DInSAR land displacement map using two S-1A images and a DEM. The same experiment is repeated using SARSCAPE environment. Figure 3.1 shows the overall methodology used in the study.

`

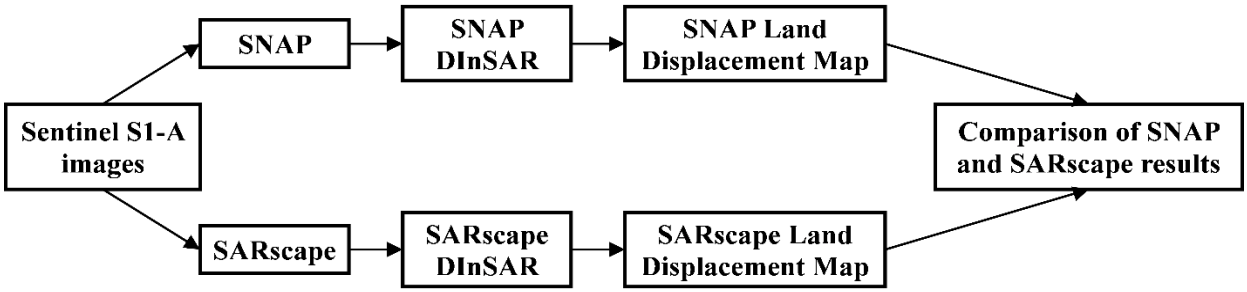

Figure 3.1: Methodology used in the experiment

For SNAP processing, the first step is to apply the orbit files in Sentinel-1A products, to provide accurate satellite position and velocity information. Then Sentinel-1 back-geocoding operator is used to co-register the two S-1 split products of the same sub-swath using a DEM and the orbits of the two products. Enhanced Spectral Diversity (ESD) operator is used for azimuth and range correction of the co-registered product, and interferogram is generated along with a coherence image. Re-sampling is done in azimuth and range direction to produce a debursted interferogram, which contains interferometric phase band and the coherence band. TopoPhaseRemoval operator is used to remove topographic phase from the debursted interferogram. Multilooking factor (8 in azimuth, 2 in range direction) is applied to minimize the speckle and to enhance the readability of the image. Phase filtering is performed for decreasing the phase noise from the mutilooked product. The output obtained after these steps is multi-looked and filtered differential interferogram. This product is free of topography component but the phase component has fringes only between –pi to +pi and thus a phase unwrapping (Ghiglia & Pritt, 1998) is required to get the absolute phase differences. After phase unwrapping, the final displacement map is generated from the interferometric phase.

For SARSCAPE the processing steps are rather simpler and semi-automatic in a user friendly environment (Sahraoui et al., 2006). It involves importing generic SAR data to make data in SARscape readable format. Primary image, secondary image and a DEM file are given as input to generate interferogram. Then it performs adaptive filtering and coherence, phase unwrapping, manual GCP selection, refinement and reflattening, and phase to displacement conversion.

3.4 Results and Discussion

The results obtained from both the software are discussed and compared in this section. Figure 3.2a and Figure 3.2b shows coherence map from SNAP and SARscape, respectively. A coherence

`

map is an indirect measure of quality of the interferogram. The values on coherence map vary from 0 to 1 and represents the similarity between each pixel on two images. The patches with greater coherence appear as brighter, and the patches of lower coherence appear as darker. The black areas, which are closer to zero, represents the vegetative areas (marked as A1 and B1 in Figure 3.2). The white areas which are closer to 1 represent buildings and urban areas (marked as A2 and B2 in Figure 3.2). It can be seen that both the images give consistent results, though coherence level in SARSCAPE is better than SNAP. The coherence has maximum value of 0.996, and statistical mean of 0.59 for SARscape, as compared to maximum value of 0.989, and statistical mean of 0.55 for SNAP. This discrepancy might arise because of results from co-registration or spectral shift filtering steps.

In SNAP, debrusting was required separately to get a spatially continuous interferogram, which represents the phase difference between the two images. For SARscape, debrusting is not required separately, as this process is done during the data import section only. In SNAP, the interferogram obtained from first processing contains both topography and deformation, so topophaseremoval operator is applied to obtain an interferogram that contains only the deformation. A multi-looking factor of 8 in azimuth and 2 in range direction is used in both the software. The filtering method used in both the software is Goldstein method given by Goldstein & Werner in 1998 (Goldstein & Werner, 1998). In SARscape, manual selection of Ground Control Points (GCP's) is required before orbit refinement stage. Such a process is not required in SNAP. The orbit refinement stage removes orbital residual patterns in SAR fringes. The residual fringes in azimuth direction are compensated by the surface represented by Equation 3.1 (Colesanti & Wasowski, 2006):

$$S(i, j) = \text{complex}\,[\cos(2\pi\, tl\, i + 2\pi\, tc\, j), \sin(2\pi\, tl\, i + 2\pi\, tc\, j)] \qquad \text{Equation 3.1}$$

The phase component at this stage has fringes only between –pi to +pi and thus a phase unwrapping is required to quantify deformation maps. SNAP uses SNAPHU application while SARscape has inbuilt unwrapping application. Minimum cost flow method has been used for unwrapping in both the software. After unwrapping, the displacement maps could be obtained, which are geocoded to get the final results (Figure 3.3).

It can be seen that the displacement pattern obtained is consistent in both the Figure 3.3a and Figure 3.3b, though the exact value of displacement varies for place to place. The west, central and south

`

London is largely showing land uplift, while north and south-eastern London is mainly showing land subsidence. It can be seen that areas marked as A1-A4 and B1-B4 are showing land uplift, while the areas marked as A5-A8 and B5-B8 are showing land subsidence.

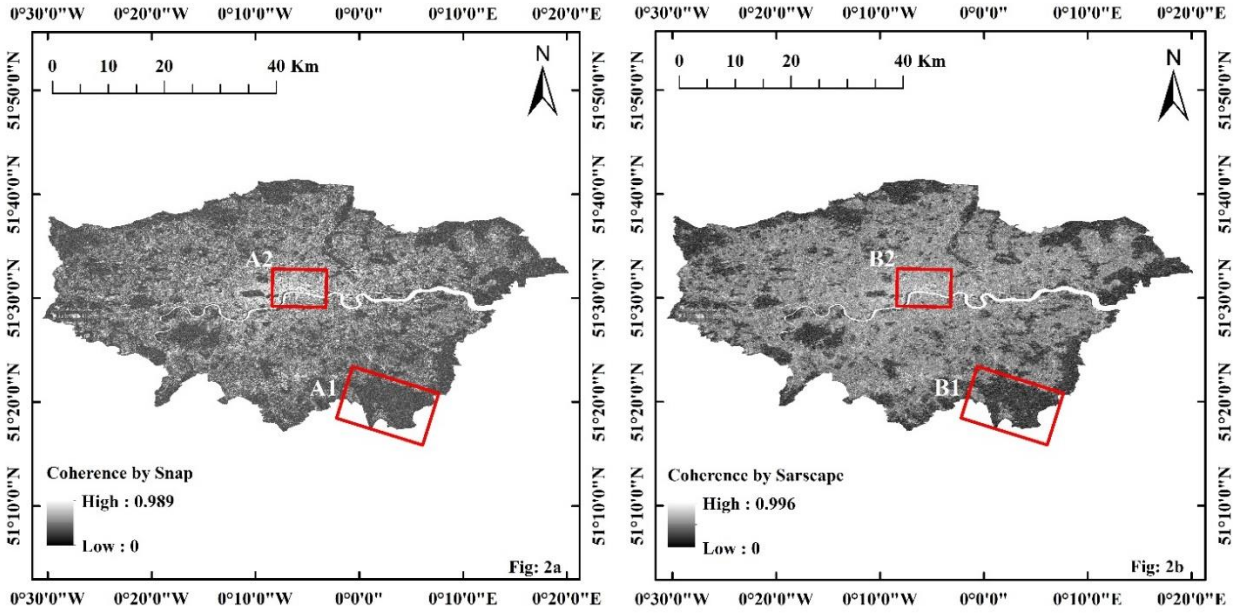

Figure 3.2: Coherence maps from (a) SNAP and (b) SARscape

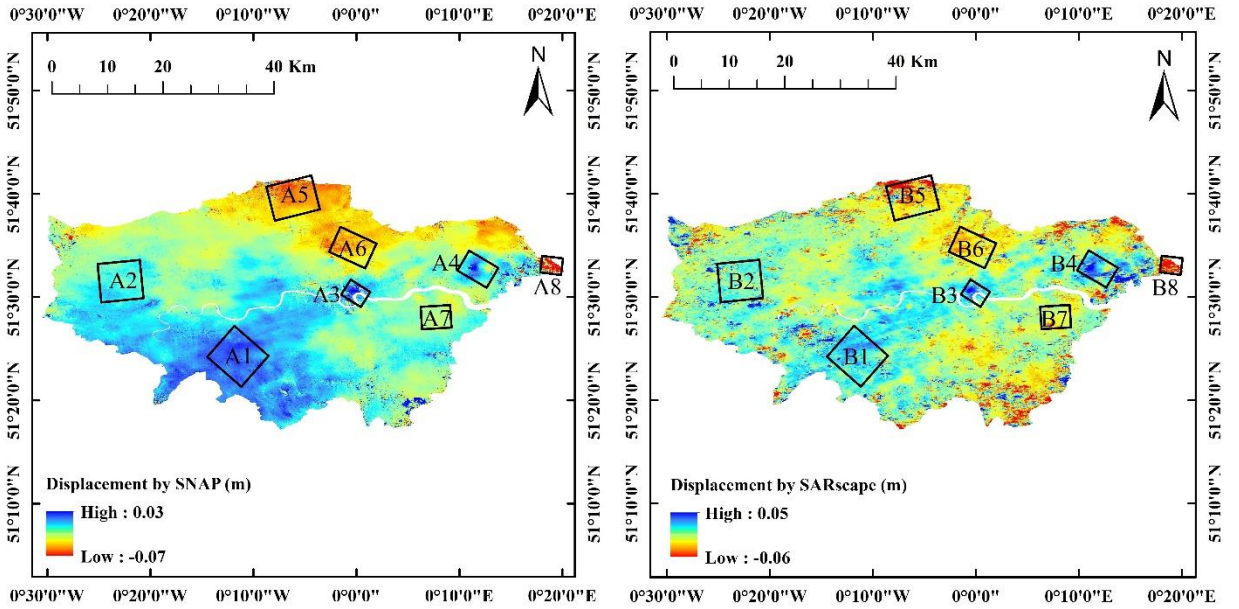

Figure 3.3: Land displacement maps from (a)SNAP and (b)SARscape

There are a variety of controlling factors which influences the rates of land level change. These range from near-surface to deep-seated mechanisms and from less than a decade to over 100,000

`

years' duration (Aldiss et al., 2014). The mean land movement over entire London between April 2015 and April 2018 obtained from SNAP is -5 mm/year, while that obtained from SARscape is -4 mm/year. The apparent difference of 1 mm/year in subsidence obtained from the two software's can be attributed to co-registration, spectral shift filtering, unwrapping or uncorrected orbital inaccuracies. The land movement values obtained in this study are in close agreement as suggested by the literature (Bischoff et al., 2019; Bonì et al., 2017). To validate the results, the difference between the two software should be less than the theoretical measurement potentiality of the data. This is given by (Simonetto, 2008):

$$\sigma_e = \frac{\lambda}{4\pi}\,\sigma_{phase} \qquad \text{Equation 3.2}$$

Considering appropriate number of looks, phase noise (σ_{phase}) can be given with reference to coherence level. Since our coherence level is nearly 0.6, a phase noise of 60^{O} is selected (Ferretti et al., 2007). Thus, for a wavelength of 5.6 cm, theoretical accuracy of our measurements should be less than 4.6 mm. Thus, our result from both software can be validated.

The land movement results obtained form these experiments set the basis for futher subsidence investigation in this thesis. InSAR land movement will be used and corelated to groundwater variations and hydrogeology of the London basin will be discussed in details. The methodology developed to map land movement using InSAR in this chapter will be used to investigate the relation between the hydrogeology, groundwater variations and land deformation of the London basin, and subsequently other cities like NCT-Delhi.

3.5 Conclusions

Working with SAR data is not simple and can be challenging specially for novice users with no expertise in SAR imagery. Open-source software and free datasets can motivate more people to work with SAR technology. The experiments here highlight that open source software can give excellent results, which are highly comparable to expensive commercial software. To compare the results, all attempts were made to keep the user input parameters consistent in both the experiments like multilooking factor, phase unwrapping principle, and filtering methods. But some differences are unavoidable because of GCP selection, co-registration or spectral shift filtering steps. The difference of 1 mm/year land displacement between two experiments can negatively affect the understanding of new users, as ideally same results is expected from same set of data. Only a little

`

work had been done using same data by different software, and more work on cross-verification will be helpful for the growth of DInSAR technique. Our study validates the use of SNAP for DINSAR and provides a good understanding of SARscape. Also, results have been verified with the published literature. The authors suggest that freely available software and datasets will encourage more researchers to work with InSAR technology.

Acknowledgements

The authors would like to thank the European Space Agency (ESA) for providing access to SARscape software for processing of InSAR data through Eohops programme. The authors would like to thank ESA RUS Copernicus, for providing webinars for SNAP and to Copernicus open access hub for providing the Sentinel-1 data. The research was funded by the University of Nottingham Faculty of Engineering Research Excellence PhD scholarship.

Authors Contributions: The authors who contributed to the paper presented in this chapter are Agarwal, Vivek* (V.A); Kumar, Amit (A.K); L. Gomes, Rachel (R.L.G); Marsh, Stuart (S.M). *Conceptualisation*, V.A., R.L.G. and S.M.; *data curation*, V.A., R.L.G. and S.M.; *formal analysis*, V.A. and A.K.; *funding acquisition*, V.A., R.L.G. and S.M.; *investigation*, V.A., R.L.G. and S.M.; *methodology*, V.A., A.K., R.L.G. and S.M.; *resources*, V.A.; *software*, V.A. and A.K.; *supervision*, R.L.G. and S.M.; *validation*, R.L.G. and S.M.; *visualisation*, V.A., A.K., R.L.G. and S.M.; *writing*—original draft, V.A.; *writing—review and editing*, V.A., R.L.G. and S.M.

`

Chapter 4 London InSAR-GRACE study

Preface

Chapter 3 concluded that, while open source freely available software packages will attract more new users, commercial software packages like SARscape can be a powerful semi-automated tool to carry out PSInSAR analysis. The ESA-Eohops sponsored ENVI-SARscape package was thus used for a detailed study of land movement using the PSInSAR module.

The SARscape module facilitates PSInSAR processing of SAR data in a multi-step but semi-automated process. Land movement was studied for London using C-band MW images, and various reasons responsible for causing this land movement were investigated. To check the accuracy and validation of InSAR results, in situ GNSS results were obtained and compared. This validation not only confirmed our analysis results in London but also faciliated our methodology to study land movement in other urban areas across the world, which could be used for further studies. The methodology used to study land movement in London using the PSInSAR module of ENVI SARscape is explained in this chapter, which presents both the spatial and temporal results.

The primary aim of the thesis is to study variation in groundwater and the resulting land subsidence. Thus, to examine change in groundwater, two methods are used: First, in situ measurements from various boreholes, and second, GRACE gravimetry anomalies. While the first method is accurate and highly reliable, the limited data availability in both spatial and temporal domains is a significant constraint. To obtain continuous, uninterrupted data over a large area spanning several years can be challenging, expensive and labour intensive. The second method, i.e. GRACE, is a remote sensing tool that can measure mass distribution around the planet and its variation over time. This mass change can be calibrated to calculate the quantitative change in groundwater. GRACE gravity anomaly data have emerged as a vital information source for hydrologists, as they can be used to provide optimal groundwater observations on a monthly basis. An attempt was made to study GRACE groundwater results and InSAR land subsidence results in conjunction, as no significant work has been done that combines these two technologies.

The spatial resolution for GRACE is low, while that of InSAR is high. The PSInSAR method is excellent for studying the spatial variation of groundwater, and GRACE is excellent for studying temporal variation of groundwater. The suitability of monitoring ground movement was explored

`

using PSInSAR subsidence and GNSS data for London between December 2002 and September 2010. Also groundwater variation was monitored using GRACE gravity anomalies and observed boreholes for London for the same time-period. A study was done over London using InSAR and GRACE to study groundwater induced land subsidence between 2002 to 2010 using ENVISAR-ASAR images. This study was submitted as a research paper to 'Applied Sciences', entitled '*Monitoring of Ground Movement and Groundwater Changes in London Using InSAR and GRACE'*. The published paper is presented here in this Thesis as Chapter 4.

Abstract: Groundwater-induced land movement can cause damage to property and resources, thus its monitoring is very important for the safety and economics of a city. London is a heavily built-up urban area and relies largely on its groundwater resource and thus poses the threat of land subsidence. Interferometric Synthetic Aperture Radar (InSAR) can facilitate monitoring of land movement and Gravity Recovery and Climate Experiment (GRACE) gravity anomalies can facilitate groundwater monitoring. For London, no previous study has investigated groundwater variations and related land movement using InSAR and GRACE together. In this paper, ENVISAT ASAR C-band SAR images were used to obtain land movement using PSInSAR technique and GRACE gravity anomalies to obtain groundwater variations between December 2002 and December 2010 for central London. Both experiments showed long-term, decreasing, complex, non-linear patterns in the spatial and temporal domain. The land movement values varied from -6 to +6 mm/year, and their reliability was validated with observed Global Navigation Satellite System (GNSS) data, by conducting a two-sample t-test. The average groundwater loss estimated from GRACE was found to be 9.003 MCM/year. The ground movement was compared to observed groundwater values obtained from various boreholes around central London. It was observed that when large volumes of groundwater is extracted then it leads to land subsidence, and when groundwater is recharged then surface uplift is witnessed. The results demonstrate that InSAR and GRACE complement each other and can be an excellent source of monitoring groundwater for hydrologists.

Keywords: PSInSAR; GRACE; surface subsidence; groundwater; London

4.1 Introduction

Groundwater contributes a significant proportion of the Earth's freshwater and a large part of the urban world is facing groundwater depletion and the problems related to it (V. M. Tiwari et al.,

`

2009). Over 40% of the public water supply comes from underground aquifers in most parts of Europe (Wolf et al., 2015). Thus, efficient management of groundwater is needed to ensure its sustainability. One of the major problems associated with over-abstraction of groundwater is land subsidence, resulting from the compression of the sub-surface aquifer system due to loss of pore pressure and/or land uplift, which is caused because of excessive groundwater recharge (Zheng et al., 2018). This land movement can cause major and recurrent harm to infrastructure, increase in floods, water contamination risks, and nonrecoverable losses in an aquifer's ability to store water. This is pertinent with globally increasing urbanisation.

The concept of an aquifer is explained in Terzaghi's theory of consolidation (Terzaghi, 1943), which states that if there is variation in pore pressure of a fluid, and total vertical stress is unchanged, then the effective stress modifies correspondingly within the aquifer and thus causes a change in volume. This volume change depends on the properties of the aquifer like compressibility, permeability and field capacity. Additionally, the ground movement in the vertical direction results from elastic or inelastic compression, which relies on variation in the hydraulic head and thickness of the unconsolidated deposits (Helm, 1975; Riley, 1969).

Chalk is the most vital aquifer in the United Kingdom (UK) as it provides approximately 60% of the groundwater consumed in the UK (BGS, 2013) and accounts for nearly 80% of water supply in River Thames catchment and 20% in London alone (Bonì et al., 2016). Chalk is one of the most supervised and controlled aquifer systems in the UK and has been providing water in London for domestic and industrial use since the 19th century (Jones et al., 2012; Royse et al., 2012). During the early and mid-twentieth century, a lot of groundwater abstraction took place because of anthropogenic development around central London. This abstraction led to a fall of water level to 88 m below sea level in the 1960s, which resulted in a depression in the water table. Due to the de-industrialisation since the 1980s, the abstraction was reduced, and the groundwater recovered by 3 m/year in the 1990s, which lead to the rise of groundwater level. This rise in groundwater level caused a threat to infrastructure in the London basin. To check this rise, the General Aquifer Research, Development and Investigation Team (GARDIT) strategy was implemented in 1992 (EA, 2017). The GARDIT strategy was implemented using groundwater withdrawal licensing and monitoring, which stabilised the groundwater around the year 2000. Subsequently, the study of groundwater and related subsidence during the period 2002 to 2010 has been carried out here using different geospatial tools.

`

To map the surface movement, traditional methods like levelling, Global Navigation Satellite System (GNSS), 3D laser scanning, and similar provide accurate information, but are tedious, expensive, have low spatial extent and; therefore, are unsuited to surveying large (basin level) areas (Huang et al., 2016; Zheng et al., 2018). A better alternative is to use the PSInSAR technique, which can identify coherent and stable scattering targets and use their phase history to measure land movement. Moreover, PSInSAR can carry out independent Phase Unwrapping for each permanent scatterer and provide weather independency, sunlight independency (active sensor) and high (basin-level or greater) spatial coverage. Therefore, PSInSAR provides better accuracy and spatial coverage as compared to other traditional methods of land surveying. It has also been used by many researchers to study land movement resulting from earthquakes (Fialko et al., 2001), glacial movements (Yong et al., 2015) and subsidence (Dai et al., 2015; Fan et al., 2015; Fan et al., 2015; Huang et al., 2016).

It is not convenient to directly estimate regional-scale water storage as it is labour intensive and expensive work. Many researchers have shown that Gravity Recovery and Climate Experiment (GRACE) gravimetry offers an alternative remote sensing tool (Ramillien et al., 2016; Rodell et al., 2009; Tiwari et al., 2009; Wang et al., 2011; Zaitchik et al., 2008), which is capable of monitoring water storage. This water may include surface water, groundwater, soil moisture, snow and ice. GRACE has emerged as a vital information source to hydrologists, as it can be used for optimal groundwater observations at a regional scale. When there is a large change in groundwater storage volume in a small area, GRACE can then detect the corresponding mass change because of its high signal-to-noise ratio (Guo et al., 2016; Longuevergne et al., 2013; Tourian et al., 2015). Therefore, GRACE data can be an excellent source of monitoring the variation in groundwater storage.

In this paper, the relationship between surface deformation and groundwater variation was comprehensively analysed. Also various natural and anthropogenic factors were discussed which affect both these phenomena. To the best of our knowledge, very few attempts have been made to study PSInSAR derived land subsidence and GRACE gravity derived groundwater together(Castellazzi et al., 2016; Du et al., 2016; Guo et al., 2016). For London, this is the first InSAR-GRACE study. The PSInSAR and GRACE are independent datasets and at different spatial resolution, hence the two datasets have not been directly correlated. The results are rather verified with observed borehole groundwater data and observed GNSS height values at various stations.

`

4.2 Study Area

In the study, the area chosen is the administrative area of Greater London (black boundary in the Figure 4.1). The area is bounded by 0°30′ W and 0°20′ E longitudes and 51°42′ N and 51°17′ N latitudes, covering an area of approximately 1600 km^2 in the southern part of England.

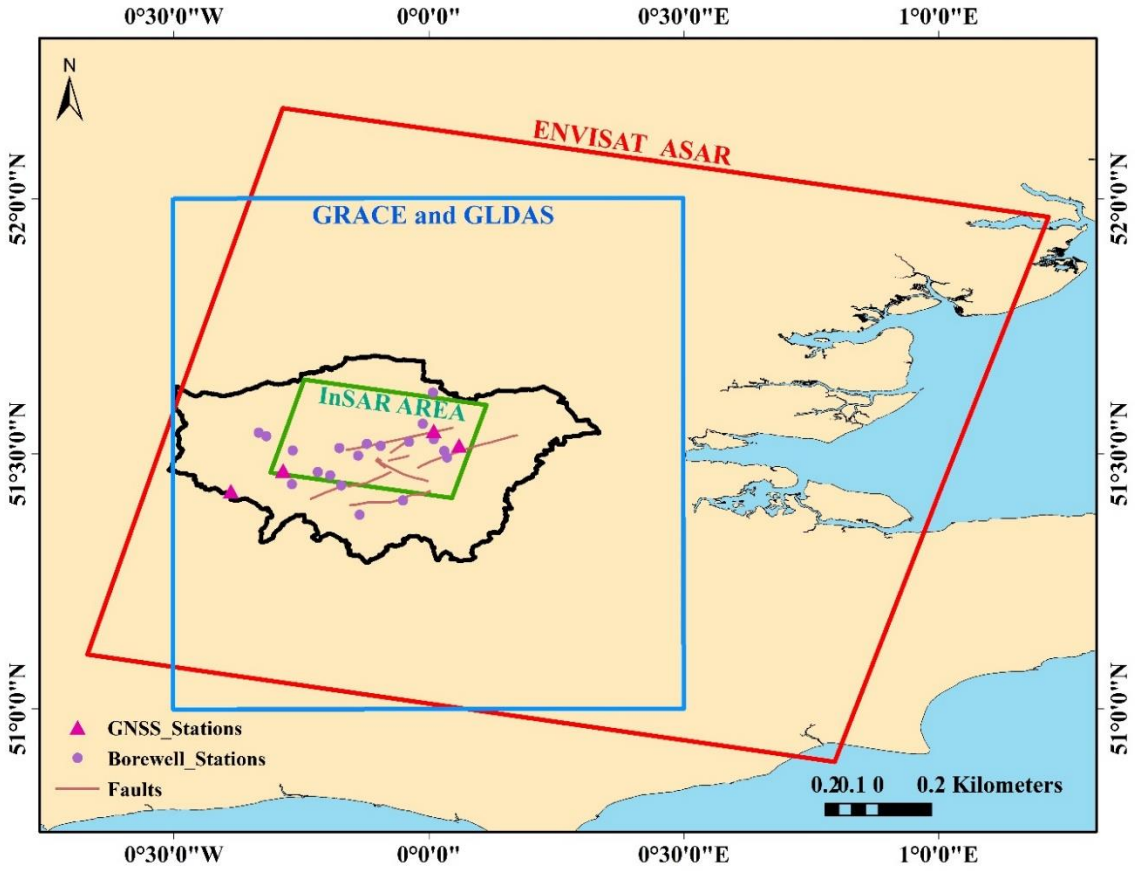

Figure 4.1: Study Area: Red box, blue box and green box show the extent of ENVISAT-ASAR (Environmental Satellite - Advanced Synthetic Aperture Radar) image, the extent of GRACE (Gravity Recovery and Climate Experiment) data used and InSAR (Interferometric Synthetic Aperture Radar) study area, respectively. Black boundary shows the administrative area of London. Purple dots, pink triangles and brown lines show the location of key boreholes, GNSS (Global Navigation Satellite System) stations and faults in the study area, respectively.

The London basin is infilled by younger Paleogene deposits and the chalk group forms a rim around it and has a depth exceeding 200 m in central London (Ford et al., 2010; Mathers et al., 2014). Table 4.1 and Figure 4.2 summarises the geology of the London Basin. Table 4.1 shows that the Bagshot formation and the Claygate member are present above the London clay. These are young deposits and form nearly 50% of the geology of the basin. London clay is densely

`

fissured and has a blue-grey texture, and beneath this is the Harwich formation which is mainly made of sand and gravels. Then comes the Lambeth group, which consists of sands, silts and clays. The Cretaceous era is mainly marked by chalk deposits, which forms one of the most important geological formations in the UK, as it accounts for the majority of the groundwater used in the country.

Table 4.1: Geology of the London Basin (adapted from EA (Environment Agency) status report 2010 (EA, 2010)).

Era	Group	Formation	Thickness (m)
Palaeogene	Thames	Bagshot Formation	10–25
		Claygate Member London Clay	30–90
		Harwich Formation	0–10
	Lambeth	Woolwich and Reading Beds	10–20
		Upnor Formation	5–7
		Thanet Sands	0–30
Cretaceous		Chalk	180–245

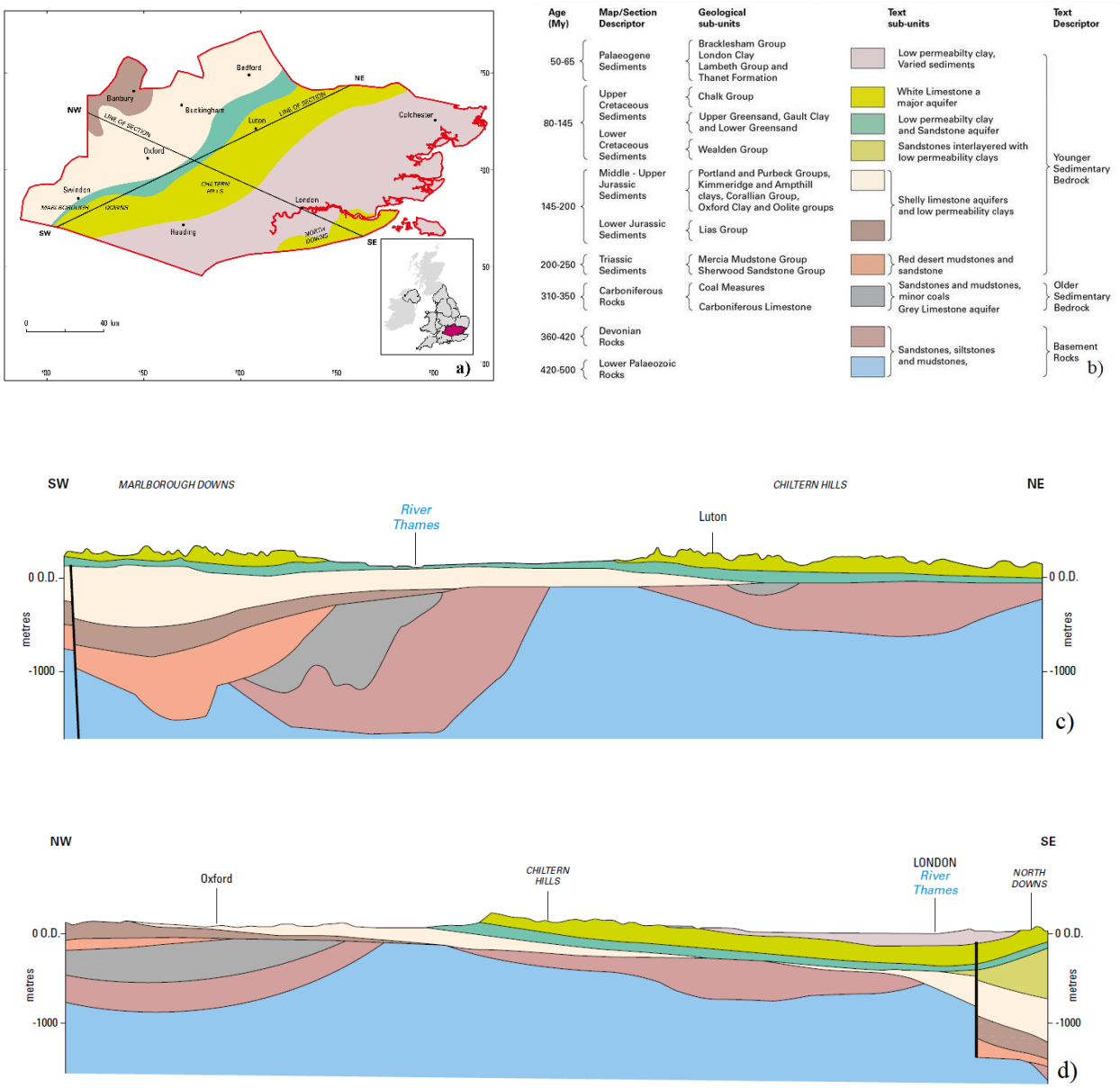

Figure 4.2: a) Generalised geological map showing the distribution of rock units in the London and the Thames Valley region. The inset shows the extent of the region in the UK. The bold black lines give the locations of the cross-sections shown in Figures 4.2c and 4.2d. Figure 4.2b shows the key to the rock types shown. Figure 4.2c shows schematic south-west to north-east cross-section through the Thames Valley from the Marlborough Downs to the Chiltern Hills. Figure 4.2d shows schematic north-west to south-east cross-section through the Thames Valley, passing through London. Note that the vertical scale is greatly exaggerated and actual dips of rock layers are much gentler than they appear here. Modified from (RWM, 2019).

`

Figure 4.2 shows the distribution of rock units in the London and the Thames Valley region. Figure 4.2c shows schematic south-west to north-east cross-section through the Thames Valley from the Marlborough Downs to the Chiltern Hills. Figure 4.2d shows schematic north-west to south-east cross-section through the Thames Valley, passing through London. The older sedimentary rocks such as limestone forms the base layers, while the younger sedimentary bedrock such as palaeogene and cretaceous sediments forms the upper layers. Table 4.1 and Figure 4.2 together gives a complete picture of subsurface geology for London basin. The chalk aquifer provides approximately 60% of the groundwater used in the country (UK Groundwater forum, 1998) and also is a source for nearly 80% of public water supply in the catchment area of the River Thames and approximately 20% in London (Thames Water, 2015).

The water supply in London for public and industrial use (Jones et al., 2012) is mainly provided by the chalk group aquifer and it also provides significant base flow to the Thames, with a base flow index of 0.63 at Kingston (NFRA, 2021). Even though the Paleogene group are not the main deposits, they confine the underlying chalk aquifer around central London. These provide a heterogeneous nature to the hydrogeology of the region and a good amount of groundwater can be present in sand-rich horizons. The study of the hydrogeology of central London and the response of the chalk aquifer to faulting by different researchers have highlighted that different permeability of faults results in irregular groundwater flow (Freitas, 2009; Royse et al., 2012). The infrastructure and lithology can cause ample pressure on the properties of the chalk aquifer in the Thames basin (Bloomfield et al., 2011), and chalk has a porosity of dual-medium with matrix and fracture (Gunn et al., 1995; Price, 1987). When the groundwater level declines then most flow occurs in fractures and storage occurs in a matrix. The chalk aquifer's primary porosity is between 0.25–0.40, which is due to the coccoliths found in the aquifer, which does not allow water to drain easily as the pore throats are tiny (Bloomfield et al., 1995; Price et al., 1976) and hence groundwater storage of the Thames aquifer is mainly secondary porosity along faults. According to the Copernicus EEA European urban atlas (UA), the land use within the London area is dominated by dense to medium density urban fabric with multiple industrial units and stretched port areas along the river Thames (EC, 2011). Additionally, according to the 2011 population census of the UK, the total population of London is around 9.5 million and has been continuously increasing since the 1980s. The ever-

`

increasing population is exerting a pressure on groundwater to meet the increasing demand and thus can cause the problem of land subsidence.

4.3 Materials and Methods

This study used InSAR, boreholes, GNSS, GRACE and Global Land Data Assimilation System (GLDAS) data obtained from various sources. The specifications of data used is summarised in Table 4.2 and the overall methodology used in this study is shown in Figure 4.3

Table 4.2: Data and software used.

InSAR Data	Borehole and GNSS Data	GRACE Data	GLDAS*Data
1. 47 Envisat-Asar Images 2. VV polarisation, Track 51, Descending, Left looking, Swath Id: IS2, Incidence Angle: 22.78° 3. Resolution: Azimuth: 4.05 m byRange: 7.80 m 4. Repeat Cycle: 35 days 5. Wavelength: 0.056 m, C-band 6. Primary Image: 20 July 2007 7. Time period: Dec-2002 to Dec-2010 **8.** Software Used: ENVI SARscape, ArcGIS (ArcMap 10.2.2)	1. Borehole groundwater data from The Environment Agency (EA) 2. GNSS data from The British Isles continuous GNSS Facility (BIGF)	1. COST-G RL01 Level 3 Data product 2. Source: Gravity Recovery and Climate Experiment (GRACE) 3. Spatial Resolution: 1° × 1° 4. Temporal Resolution: 1 month 5. Time period: Dec-2002 to Dec-2010 6. Software Used: RStudio V 1.2.5, ArcGIS (ArcMap 10.2.2)	1. NOAH, CLM, MOSAIC and VIC models from GLDAS framework 2. Land Surface model L4 monthly 1.0 by 1.0 degree V2.1 3. Time period: Dec-2002 to Dec-2010

*GLDAS - Global Land Data Assimilation System

The methodology mainly involved processing of InSAR data to calculate land subsidence/uplift using PSInSAR principle and validating the InSAR results using GNSS data. The PSInSAR principle was used as London has a dense urban fabric, and thus it can provide multiple permanent scatterers. The methodology also involved calculating change in groundwater level using GRACE anomalies and GLDAS framework. Finally, land subsidence/uplift and groundwater variation were correlated and studied in conjunction. The study was carried out for the time period between December 2002 to December 2010 in London, as the ENVISAT and GRACE data overlapped for this time-peroid for London.

`

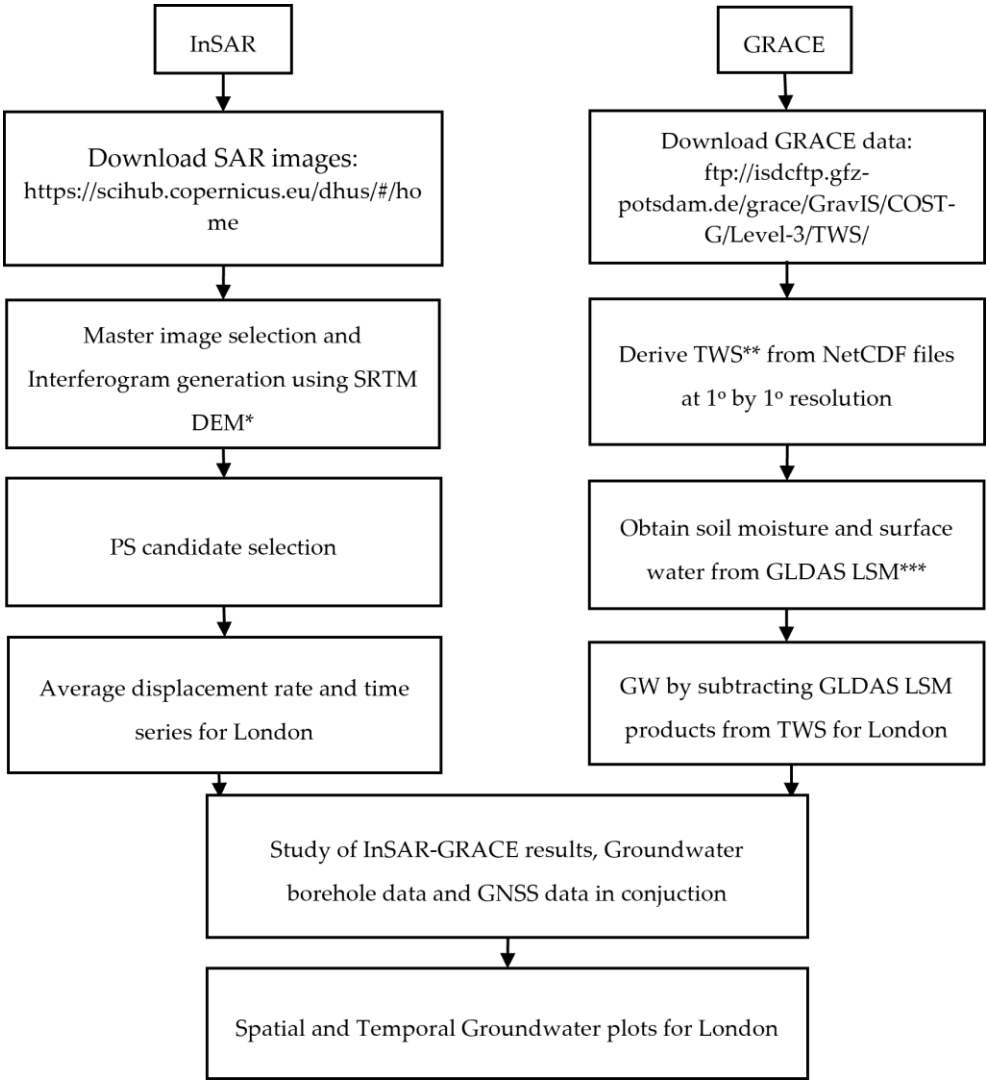

*Figure 4.3: Methodology used for the research. (*SRTM DEM - Shuttle Radar Topography Mission Digital Elevation Model, **TWS - Terrestrial Water Storage, ***LSM -Land surface Model)*

4.3.1 Subsidence from PSInSAR

The Interferometry Synthetic Aperture Radar (InSAR) provides the possibility to map the movement of the Earth surface with high accuracy. SAR data pairs with good coherence are required for informative interferogram generation. InSAR calculates the phase difference between various SAR acquisitions taken from the same orbital track. PSInSAR differs from conventional interferometry as it only uses pixels that show stability in phase for several interferograms. These stable pixels can be termed as Persistent Scatterers (PSs) or permanent scatterers (Hooper, 2008). The PSInSAR time series analysis allows us to do the following:

`

1. Allow better selection of coherent pixels;
2. Atmosphere/orbit errors can be reduced by filtering in space and time;
3. Make DEM (Digital Elevation Model) error estimation possible;
4. Make the most reliable phase unwrapping possible (3D);
5. Make sub-pixel resolution possible.

The inclination of ENVISAT-ASAR satellite ground tracks at the SAR scene centre was 14° in the south-north axis at the latitude of London, and the incidence angle of the employed sensor modes was 23° measured from the vertical direction. This means that the employed LOS could estimate purely vertical motions as approximately 92% of their actual amount, E–W motions as approximately 38% and N–S as only approximately 9% (Cigna et al., 2015).

The PSInSAR analysis in ENVI SARscape (Sarmap, 2014a) is a semi-automated process and involves multiple steps. The first step is to select a primary image, with reference to which all other secondary images are co-registered. The primary image is selected based on the minimum mean baseline of the stack, which means that the image should have an ideal temporal and spatial position with respect to the other ones. This simplifies data co-registration and provides higher coherence, as small baselines are less sensitive to volume de-correlation (Sarmap, 2014b).

To select the reference point, the PS algorithm in SARscape follows one of the two following principles: (a) If the area is larger than a given surface threshold, the whole image is divided in more subsets (considering an overlap) and each one will be processed separately with an own reference point, otherwise too many parameters should be estimated and the atmosphere estimation would become less accurate. So, in the final step, all single areas will be mosaiced. (b) On the other hand, if the area is smaller than this surface threshold, one reference point is sufficient, and the image will not be divided. This surface threshold is called “Area for Single Reference Point (sqkm)”. In our case this value was 25 km^2 and the first principle was followed. In total there were 63 ground control points.

After co-registration, interferograms were generated for each secondary image using the same primary image. Then interferogram flattening was performed using a reference DEM SRTM V4. The better the reference DEM accuracy (or resolution) the better the result in terms of topography removal. The flattening was followed by first step inversion to derive the coherence, displacement

`

velocity and residual topography, which were used to flatten the complex interferograms. The outputs from first inversion were addressed for the atmospheric phase components of the linear model products in the second inversion. Finally, the PS products were geocoded to display the velocity maps in both raster and vector formats.

4.3.2 Groundwater from GRACE

GRACE (Gravity Recovery And Climate Experiment) is a combined venture of the National Aeronautics and Space Administration (NASA), USA and the German Aerospace Center (DLR) (Tapley et al., 2004). It was launched on a rocket launch vehicle from the Plesetsk cosmodrome in Russia on 17 March 2002. The mission was operated by the German Space Operations Center (GSOC) and it consisted of two identical satellites named GRACE-A and GRACE-B. With over 15 years of operation, the predicted mission lifetime of 5 years was exceeded by more than 3 times and ended on October 2017. The GRACE Follow-On (GRACE-FO) is a sequel of the mission on almost similar hardware and was launched in May 2018.

A change in the mass of the Earth surface causes a change in gravity. This mass change can be assumed to be mainly concentrated near the earth surface in a shallow layer of a thickness of water. The monthly gravity changes mainly result from changes in water content in hydrologic reservoirs, atmospheric and land ice masses and by mass exchanges between the Earth system's compartments (Wahr et al., 1998). Thus, after postprocessing and applying corrections for non-water mass changes, GRACE gravity anomalies can provide the Terrestrial Water Storage (TWS) variation.

TWS was obtained using COST-G, RL01, level-3 data (Dahle & Murböck, 2020) filtered with VDK5 and VDK3 anisotropic filters (Horvath et al., 2018). The deterministic components from VDK5 were combined with residual monthly variations from VDK3, to account for noise level of seasonal components. To calculate TWS, stokes coefficients were used to invert mass anomalies by applying thin layer approximation (Wahr et al., 1998). To reduce the effect of atmospheric mass variability, the non-tidal de-aliasing product AOD1B RL06 (Dobslaw et al., 2017) was used for processing of level-2 monthly gravity fields. The signal estimates were accompanied by TWS standard deviations, which represents associated uncertainties that take into account the varying noise level from month-to-month. The uncertainty was simulated using the empirical covariance model, which considers non-stationarity, non-homogenous and anisotropic structures of spatial correlations.

`

The final Groundwater Storage Change (ΔGWS) could then be calculated by subtracting surface water storage, soil moisture and snow, and ice water storage from TWS.

$$\Delta GWS = \Delta TWS - (\Delta SWS + \Delta SMS + \Delta SIS) \quad \text{Equation 4.1}$$

where ΔTWS is the change in terrestrial water storage, ΔSWS is the change in surface water storage, ΔSMS is the change in soil moisture storage, and ΔSIS is the change in snow and ice water storage.

The surface water and soil moisture were obtained from a monthly GLDAS Land Surface Model (LSM). GLDAS drives four LSMs, namely NOAH (Ek et al., 2003), Community Land Model (CLM) (Dai et al., 2003), MOSAIC (Koster & Suarez, 1996), and Variable Infiltration Capacity (VIC) (Liang et al., 1994). To minimize any inherent deficiency in any model, an average of four LSM hydrological outputs from NOAH, CLM, MOSAIC and VIC were adopted for our study time period. The change in snow and ice cover was considered negligible given the climatic scenario of London city. To ascertain that spatial resolution of TWS (1º by 1º) provided by GRACE is consistent with SWS (0.5º by 0.5º) and SMS (0.5º by 0.5º) provided by GLDAS, the kriging interpolation was adopted to resample the GLDAS data with the same resolution as the GRACE data.

4.4 Results

4.4.1 InSAR Results

Figure 4.4 shows the Line of Sight (LOS) average land deformation map for central London acquired from 47 ENVISAT-ASAR images from December 2002 to September 2010, where positive values suggest that the surface is moving towards the sensor (uplift) and the negative values suggest that the surface is moving away from the sensor (subsidence). To analyse the multi-temporal InSAR monitoring results, the statistical deformation results of the entire area could be looked through the number of persistent scatterer points (PSNs), mean rate of deformation (MRD), and standard deviation (SD) of deformation (Table 4.3).

`

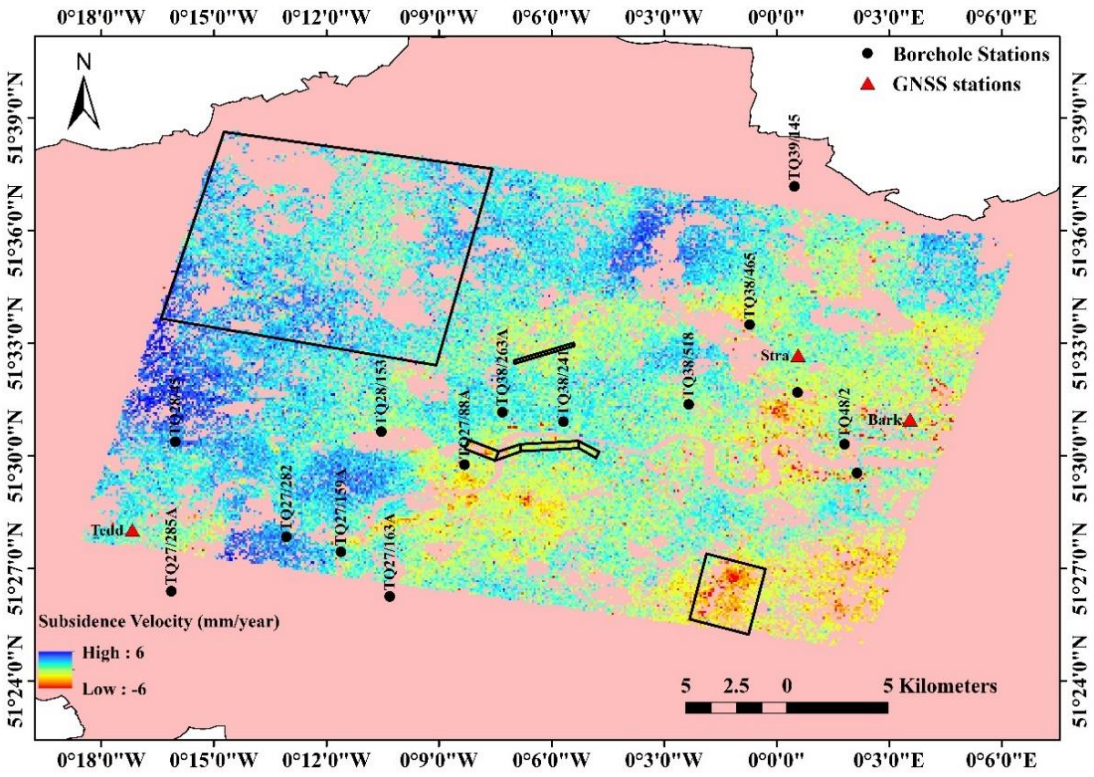

Figure 4.4: Line of Sight (LOS) average land deformation map for central London (blue areas depict uplift, while the red areas depict subsidence) with the location of observed boreholes (black dots), observed GNSS stations (red triangle) and four land movement sites (black boxes, detailed in Figure 8a–d).

Table 4.3: Statics of PSInSAR (Persistent Scatterer InSAR) subsidence.

Time period	PS Number	Area (km^2)	PS Density (PS/km^2)	PS Coherence Threshold	MRD (mm/year)	SD (mm/year)
December 2002 to September 2010	4,90,969	987	497	0.75	−0.18	0.665

London has mostly urban areas, which makes it highly suitable to study land movement using PSInSAR data, but open areas such as land, parks, etc., are not captured by PSInSAR properly. This is because for Persisitent Scatterers stable points are needed, which are found in abundance in urban areas, like poles, bridges, buildings, etc. The PS density depends on the coherence threshold, and the selection of optimum coherence threshold depends on the desired quality and number of persistent points in the resulting subsidence velocity map. A coherence threshold of 0.75 was chosen, which resulted in PS density of 497 PS/km^2. Locally, the displacement velocities and directions (towards or away from the satellite) obtained at PS points can differ because of

`

construction, road resurfacing, localised settlement, etc., but small-scale regional patterns are discernible geographically regardless of these high magnitude changes.

When land subsidence or uplift of an area is less than or equal to ±10 mm/year, the area can be termed as stable according to the theory of mining subsidence (Zheng et al., 2018). From Figure 4.4, it can be seen that the surface deformation varies from −6 to +6 mm/year, hence the study area can be considered stable during the observed time period. Additionally, it can be observed that uneven subsidence is prominent but that there are contiguous blocks of movement in a consistent direction (either uplift or subsidence). The area to the south of River Thames is mainly subsiding, while the area to the north is mainly rising. The main reason for this pattern can be attributed to the groundwater changes, sub-surface excavations for various construction activities and the subsurface geology. For example, there is uplift across the London clay adjacent to the south of River Thames, where white to grey chalk is present at the surface. Clays, some sands and gravels of the Lambeth Group and silts and sands of the Thanet Sand formation are present at the surface between the areas of London clay and chalk (Ellison et al., 2004). The subsidence near the Thames can be mainly attributed to compressible ground material such as alluvium.

The average temporal land movement for the entire study area (Figure 4.5) is showing continuous negative movement, so the area is subsiding slowly for our study period. It can also be verified by the fact that the average mean rate of deformation is −0.18 mm/year (Table 4.3). However, it can also be seen that there is an imperfect cyclic rise and fall of the land surface with a negative trend. This behaviour is probably because of seasonal and annual variations, which might be attributed to groundwater changes and the presence of compressible materials. This overall subsidence pattern can be attributed to the fact that the area has Holocene deposits of alluvium in the flood plains of the River Thames and the River Lea. These overlay deposits are of the London clay formation, Lambeth group, Thanet sand formation, Seaford chalk formation and Newhaven chalk formation. These Holocene alluviums are prone to slowly compact, dry and compress, if there is removal of groundwater, and thus can lead to subsidence.

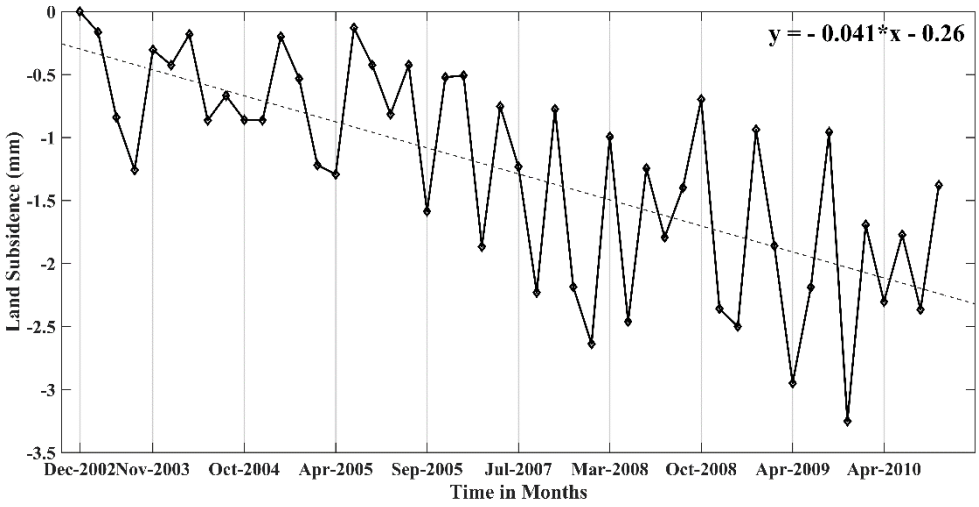

Figure 4.5: Time series of average subsidence for central London.

The standard deviation of average velocity for all the Persistent Scatterers (PSs) obtained from PSInSAR range from 0.45 to 10.5 mm/year. The statistical analysis suggests that the standard deviation is less than 3 mm/year for 75.34% of the monitoring points and less than 5 mm/year for 98.22% of the monitoring points (Figure 4.6), which suggests that the land displacement monitoring accuracy using the Envisat-ASAR PSInSAR is high. The accuracy of PSInSAR results is further validated using observed GNSS data by two sample t-test and discussed in Section 4.5.1.

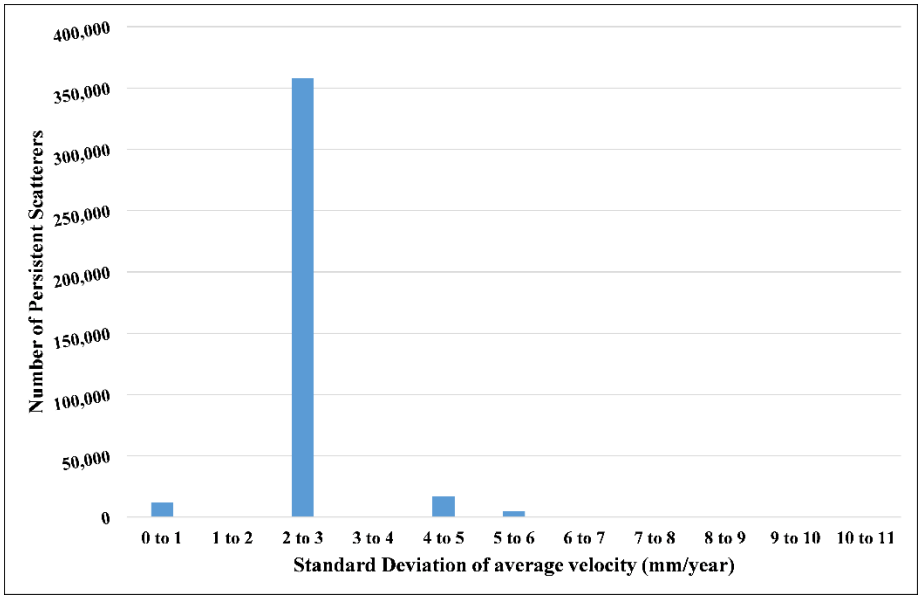

Figure 4.6: Standard deviation distribution of average subsidence velocity (mm/year).

`

4.4.2 GRACE Results

The primary aim of the GRACE mission was to map gravity variations and infer corresponding hydrological redistributions. The small timeframe mass variations occurring at or near the Earth's surface are much greater than those taking place deep inside the Earth (Kusche & Schrama, 2005), and hence GRACE anomalies can be related to hydrology after removing the contribution of atmospheric masses from air pressure data. The spatial and temporal groundwater variations from GRACE results are shown in Figure 4.7a, and Figure 4.7b, respectively. Only four representative points could be observed for our study area, owing to the poor spatial resolution of GRACE. The spatial variations map (Figure 4.7a) was made by IDW interpolation of the representative points. The temporal series (Figure 4.7b) was made by averaging all the points in Figure 4.7a.

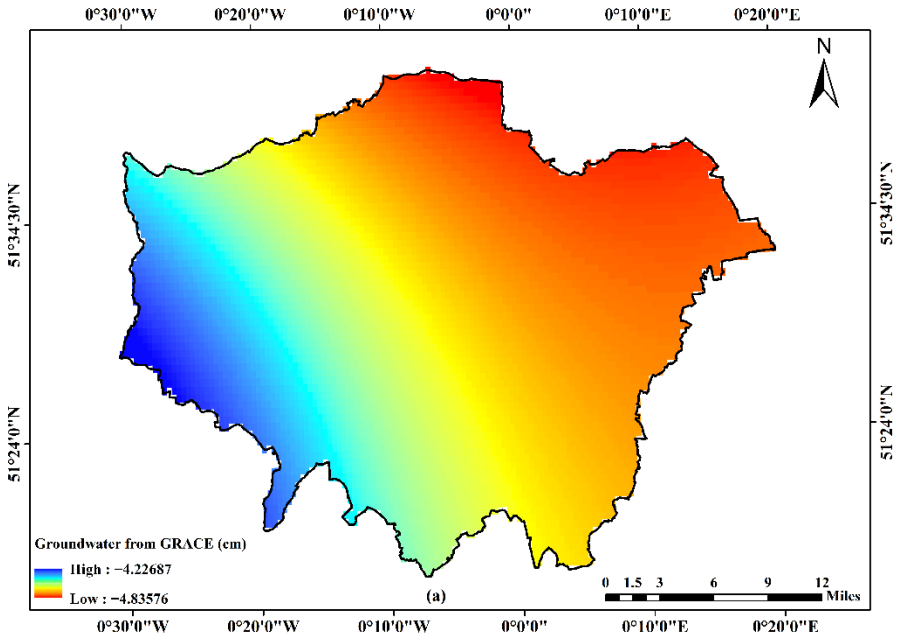

`

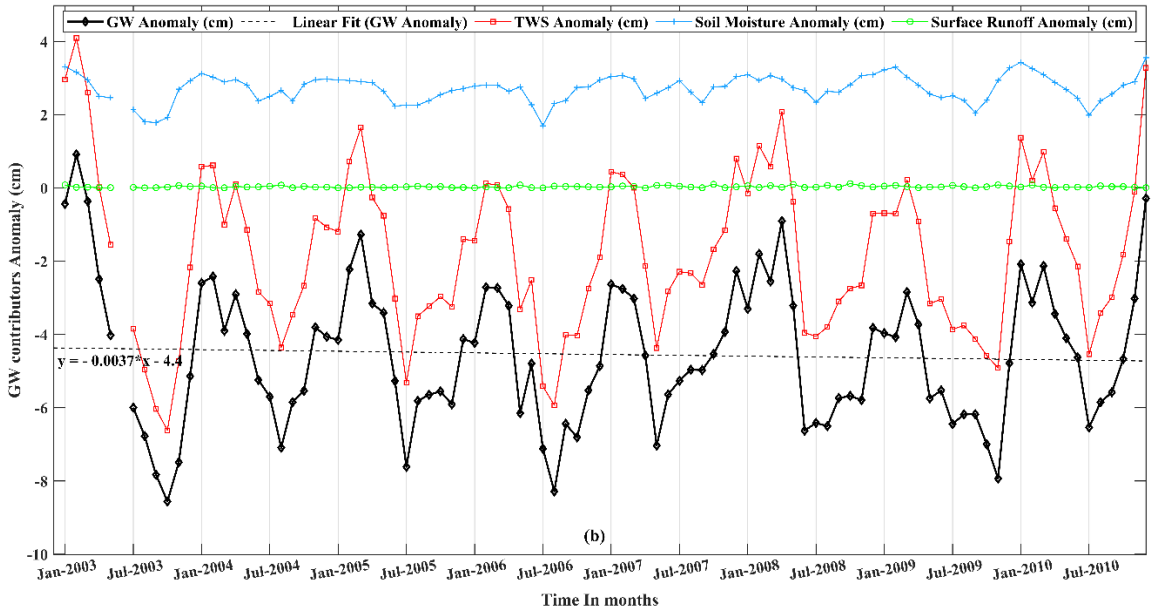

*Figure 4.7: (a) Spatial variation of groundwater from GRACE (the red zones signifies larger groundwater depletion as compared to the blue zones). **(b)** Temporal variation of Terrestrial Water Storage (TWS) from GRACE (red line), soil moisture (blue line) and surface runoff (green line) from GLDAS, resulting in groundwater (black line) and linear fit for groundwater (black dotted line).*

From the spatial variations map (Figure 4.7a), the total average groundwater over the observed time period seems to be decreasing from the north-western region to the south-eastern region. In Figure 4.7a, the red zones signifies more groundwater depletion as compared to the blue zones. From the temporal series (Figure 4.7b), it can be observed that the major contribution to Terrestrial water Storage (TWS) is from groundwater and the contribution from soil moisture and surface runoff is relatively small, thus TWS can be taken as a good representation of groundwater. The slope of best-fit line for the groundwater variation is negative, which indicates that, overall, there is groundwater depletion with time. This overall groundwater is reducing mainly due to the urban fabric of London city. The ever-increasing population exerts pressure on groundwater resource, which leads to its depletion. However, temporal rise and fall in groundwater can be seen, which can be attributed to seasonal and annual changes. A general trend which can be observed is rise in groundwater in winter months around January–February, and fall in groundwater in summer months around June–August.

Table 4.4 summarises the results from spatial groundwater variations from GRACE. On averaging groundwater change over Figure 4.7a, a value of −4.547 cm over London for an area of 1584 km^2

`

observed. The uncertainties associated with this was calculated from accompanied TWS standard deviations and showed an average value of ±2.1 cm. Thus, a total of 72.024 million cubic meter (MCM) groundwater deficit is estimated from January 2003 to December 2010, which gives an average value of 9.003 MCM/year. This is approximately 17 times less than the groundwater mass loss for Mexico around the same time period (Castellazzi et al., 2016).

Table 4.4: Groundwater variations from GRACE.

Study Area Extent	Average (Spatial) GW Change	Average Volumetric (Spatial) GW Change	Average Yearly GW Change
1584 km^2	−4.5471 cm	−72.024 MCM	−9.003 MCM

In the early 1990s, the Environment Agency (EA) implemented the General Aquifer Research, Development and Investigation Team (GARDIT) strategy to control the groundwater level rise in the chalk aquifer under central London resulting from the previous relocation of industries from central London. GARDIT strategy issued licenses to abstract groundwater from London and by the early 2000′s the rise in groundwater had been stabilized. The yearly data for groundwater abstraction and recharge for north London and groundwater abstraction data for the whole chalk aquifer of the London area is provided by EA (EA, 2017).

The EA report suggests total groundwater abstraction of 30.480 MCM and a total recharge of 15.520 MCM between 2003 and 2010, which amounts to 50.91% recharge as compared to abstraction. The report also suggests an overall abstraction of 245.311 MCM groundwater from London chalk aquifer for our study period and, assuming the same recharge rate of 50.91% as north London, the total recharge for London chalk aquifer is estimated as 124.887 MCM, which results in a groundwater deficit of 120.423 MCM. The groundwater deficit as suggested by GRACE is 72.024 MCM, which is only ~60% of the same as suggested by the groundwater monitoring estimated by EA. Thus, around 40% of the deficit estimated by EA is not sensed by GRACE. This could be because of the signal loss in averaging, interpolation and downscaling the GRACE resolution. This shows that even though GRACE data is freely available, and it proves to be a suitable alternative to costly, spatially restricted microgravity surveys, it may not precisely quantify water variations for typical aquifer scales. Despite this, it gives a clear “big picture” indication of spatial variation for total groundwater induced mass variations, which is an

`

appropriate input for setting broad regional or national policies (Famiglietti & Rodell, 2013), a view for which our study provides further evidence.

4.5 Discussions

4.5.1 Validation of InSAR Subsidence with GNSS Data

To validate the reliability of results obtained from PSInSAR, they were compared with GNSS data obtained from The British Isles continuous GNSS Facility (BIGF). The BIGF Level-2 products are a time series of the station-specific daily coordinate estimates obtained from the processing of continuous GNSS data, which have been subject to time series analysis to represent them as Cartesian differences or north, east, up differences (from an assumed reference coordinate at the central epoch) such that the "up" differences can be compared with PSInSAR-derived subsidence results. To verify PSInSAR subsidence results with the GNSS data, several steps were performed:

- The average monthly data sets were obtained by averaging the daily data for a particular month.
- The overlapping period for GNSS and InSAR image data were selected for each GNSS station.
- To get the subsidence at the location of the GNSS station, the average of all the persistent scatterers that are present within 300 m of the GNSS station was used. This was done as getting PS point and GNSS station at the exact same location may not always be possible, and also GNSS up values will be affected by its nearby areas, and hence it is suitable to take the contribution of nearby points for a particular GNSS station.
- Two-sample paired t-test (at 95% confidence limit) was done on each station to test the null hypothesis that the mean difference between the two sets is zero.

The location of GNSS stations is shown in Figure 4.1 and Figure 4.4. Thr subsidence patterns were discussed for three GNSS stations, namely Bark, Stra and Tedd, because data available from these stations overlap with our InSAR data both spatially and temporally. Figure 4.8a–c highlights that both the InSAR-derived subsidence and GNSS up values exhibit a non-linear pattern.

In Figure 4.4, the region surrounding Bark station has a red-yellow patch and exhibits average subsidence of approximately 5 mm/year. The time variation of InSAR subsidence and GNSS up values from December 2002 to September 2010 at Bark station are shown in Figure 4.8a. Both the

`

series exhibit similar patterns with negative subsidence, which means that the bark station is subsiding with some seasonal variations. To check whether the differences between the two series are within the acceptable range, the two-sample *t*-test was carried out. Table 4.5 shows the results of two-sample *t*-test for Bark, Tedd and Stra stations. For each of the stations, the mean difference is not the same, but it is important to check if this difference is statistically significant to conclude whether our PSInSAR results are in agreement with observed GNSS results or not. For two-sample paired *t*-test, the null hypothesis and alternate hypothesis were taken as: Null Hypothesis (H_0): $\mu = 0$, the mean difference is zero and alternate Hypothesis (H_A): $\mu \neq 0$, the mean difference is not zero.

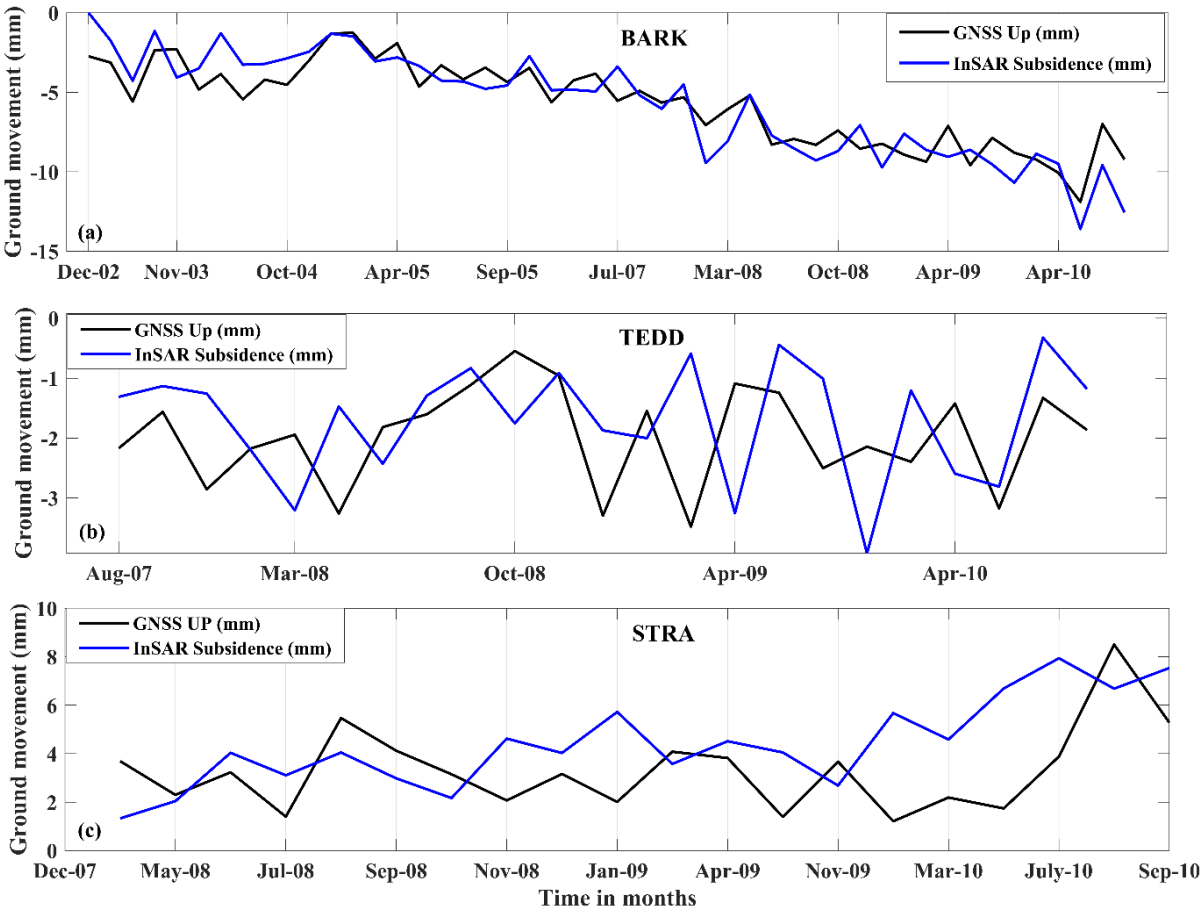

Figure 4.8: Time series comparison for InSAR subsidence and GNSS up values at (a) Bark (b) Tedd and (c) Stra stations.

`

Table 4.5: Two-paired t-test for GNSS and InSAR land movement.

Parameter	BARK	TEDD	STRA	Parameter	BARK	TEDD	STRA
Mean (UP)	−5.707	−1.978	3.318	***p* (T <= t) two-tail**	0.825	0.290	0.043
Mean (INSAR Sub)	−5.753	−1.696	4.400	**t Critical two-tail**	2.011	−0.281	2.093
Variance (Up)	6.788	0.673	3.018	**Mean difference**	0.046	−0.281	−1.082
Variance (InSAR Sub)	10.687	0.933	3.372	**St. Deviation of difference**	1.444	1.246	2.234
Observations	48	23	20	**Standard error of difference**	0.208	0.259	0.499
Pearson Correlation	0.903	0.033	0.218	**T alpha half 95% CI**	2.011	−1.083	0.111
Hypothesized Mean Difference	0	0	0	**Lower confidence limit**	−0.373	−0.563	−1.138
Df (degree of freedom)	47	22	19	**Upper confidence limit**	0.465	0	−1.026
t Stat	0.221	−1.083	−1.287				

From the observed results, the *t*-value at Bark it is 0.221. This signifies that these results are occurring about 0.22 standard deviations away from the mean. To accept the null hypothesis, *t*-value less than critical *t*-value (2.011 for Bark) is required. The *t*-value for Bark is less than the critical *t*-value, signifying acceptance of null hypothesis, showing no significant difference between the average monthly up and InSAR subsidence. Another way is to look at *p*-value (0.825 for Bark) and alpha (0.05 for 95% confidence limit). For the stations, a *p*-value greater than alpha null hypothesis is accepted. Thus, acceptance of null hypothesis shows that subsidence indicated by InSAR and GNSS is consistent at Bark. Similarly, *t*-value for Tedd and Stra are −1.08 and −1.28, respectively, while critical *t*-values for Tedd and Stra are −0.28 and 2.09, respectively. Additionally, the *p*-value for Tedd and Stra are 0.0337 and 0.2188, respectively, which are both higher than alpha (0.05). Therefore, this provides enough evidence that subsidence indicated by PSInSAR are consistent and agree very well with observed GNSS up values for all the three observed stations.

4.5.2 Site-Specific Ground Movement and Its Possible Reasons

The analysis of site-specific monthly subsidence velocity revealed a complex pattern of movements. Multiple sites show abrupt changes and indicate distinct land movement which might be induced by changes in groundwater, fault-controlled or dominated by various other controlling

`

factors. The tributaries of the River Thames form a dense drainage network which directly affects the topography, geomorphology and geology of the study area. Additionally, the study area has flood plains containing alluvium, clay areas, open sandy layers, landslide gradients and deep-seated underground tectonic constructions, making the land surface prone to displacements. In Figure 4.9a–d, land movement patterns for different sites were identified and reasons for such movements are discussed below. These sites were selected based on distinct land movement pattern and available literature.

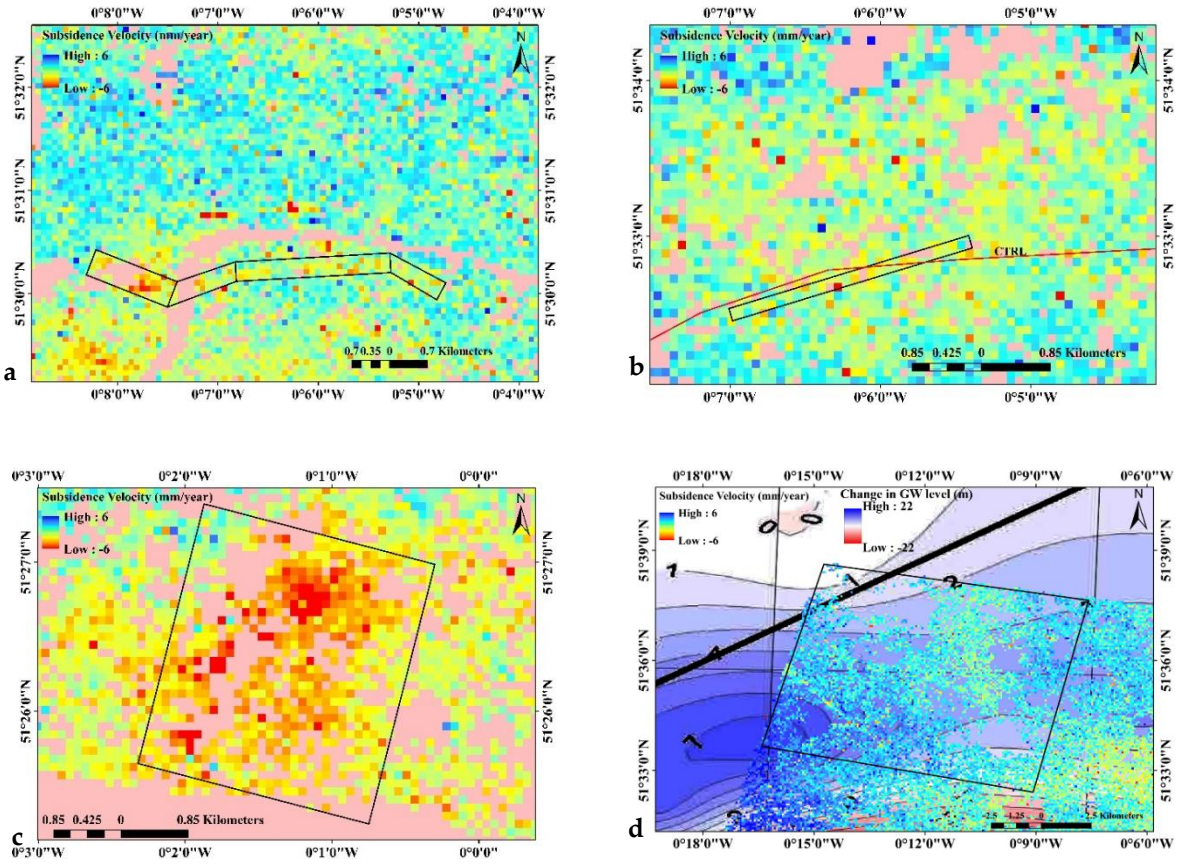

*Figure 4.9: PSInSAR site specific subsidence maps for London. (**a**)area crossing Thames river; (**b**)area on the north of Thames river and passing through CTRL (Channel Tunnel Rail Link); (**c**)area on the south of Thames river showing distinct subsidence; (**d**)area on the north of Thames river overlaid on groundwater contour provided by EA.*

In the Figure 4.9a, the area marked covers 1.63 km^2 and crosses multiple important anthropogenic structures like Westminster Bridge above the River Thames, the Commonwealth Secretariat, Supreme Court and Parliament Square, Waterloo train station, Nelson square, London Bridge

`

station, Buckingham Palace, London Eye, and sections of the British rail network. This area is a low-lying river flood plain with elevations between 5 to 10 m above Ordnance Datum (mOD), and the bedrock geology is dominated by the London clay formation. Superficial deposits in the area include alluvium, peat, Kempton Park gravel formation, Langley silt member and Taplow gravel formation. This area also coincides with the location of the Jubilee Line extension, which was constructed between 1993 and 1999 (Standing & Selman, 2001). The total number of PS points obtained within the area marked are 3131, and the average land movement for all the PS points is −0.87 mm/year, where the negative sign shows land movement away from the sensor, therefore subsiding. This subsidence in Figure 4.9a, can be attributed to the continuous effect of subsurface construction works, which were carried out for the Jubilee Line extension and compression of alluvium because of groundwater abstraction.

The area marked in the Figure 4.9b spans over 0.29 km^2 and crosses multiple important anthropogenic structures like Highbury and Islington station, Canonbury station, Alwyne Castle and, St. Andrew church. It also lies along the path of Channel Tunnel Rail Link (CTRL), which is a high speed 1 (HS1) railway, joining the Channel Tunnel and London (operational since 2007). The total number of PS points obtained within the area marked are 323 and the average land movement for all the PS points is −0.83 mm/year. The part of CTRL track between Caledonian Road and Canonbury (area marked) was constructed during our study period. The land movement of the area marked can be attributed to the construction of CTRL and to the possible compaction of subsurface particles around the tunnel along its track. Our results are in close agreement with the results obtained by PanGeo Project (Cigna et al., 2015), as the authors obtained subsidence rates of −1.09 mm/year around the same area, marked as PGGH_London_015.

The area marked in Figure 4.9c is a heavily built-up area and contains buildings, roads and other man-made structures. It contains the train-line between Beckenham Hill, Bellingham and Catford. It contains other important structures like Kings church, schools, hospitals and large residential areas. Additionally, the area contains around 38 boreholes, from which groundwater is directly pumped out to meet the local requirements. Groundwater is abstracted from these boreholes through the chalk aquifer at depths in excess of 70 m. The area marked has an extent of 6.25 km^2 and contains 4319 PS points. The average subsidence for the region is −1.95 mm/year and, since no other explanation for this subsidence could be identified, it appears groundwater abstraction has caused the area to subside due to compaction of the subsurface aquifer. Our results are close

`

to results obtained by PanGeo Project (Cigna et al., 2015), as the authors obtained subsidence rate of −1.21 mm/year around the same area, marked as PGGH_london_12.

In the Figure 4.9d, the north-western region exhibits distinct areas of uplift. The area marked has an extent of 82.6 km^2 and 53,503 PS points. The mean uplift for this area is 0.21 mm/year. When the area on geo-referenced groundwater contour map obtained from EA (EA, 2017) is overlapped, then it can be observed that the uplift area largely coincides with the area of the rise in groundwater levels. Additionally, the area has many lakes and ponds, like Brent reservoir and Viaduct pond, which helps with groundwater recharge. Thus, it can be concluded that the general uplift trend in the area marked is mainly because of groundwater rebound. However, an uplift of 0.21 mm/year is less and it cannot be said with certainty that for an area of nearly 83 km^2, this value is significant. Additionally, it is not as certain that groundwater rebound is the only reason for uplift, and there may be various factors which determine the land movement, ranging from near-surface to deep-seated mechanisms and from less than a decade to over 100,000 years duration.

Also there may be obvious correlation between geology in Figure 4.2 and settlement profiles in Figure 4.9, as the local geology may influence the amount of settlement/uplift observed at the surface over different profiles in Figure 4.9. However, the influence of local geology is combined with the impact of many other factors such as tunnel depth, dewatering, etc. To establish how influential each of these factors is, including local geology, it would be necessary to compare smaller sections of the profile in more detail and to include data on water abstraction rates (if there was dewatering), local boreholes, and more detailed information on the geology encountered during tunnelling.

4.5.3 Relationship between Ground Movement and Groundwater Change

The ground movement obtained from PSInSAR largely depicts uplift in northern London and subsidence in southern London. Additionally, GRACE highlights that there is more groundwater loss from southern London as compared to northern London during our study period. The two results compliments each other as they represent the same water variations through compaction (InSAR) and mass variation (GRACE). However, there are some anomalies while comparing GRACE results with observed groundwater values for aquifer scale regions and it is difficult to derive a direct relationship between them. The main restriction of GRACE to manage groundwater has been described by (Alley & Konikow, 2015) and it specifies that it requires great modesty to

`

view GRACE as a water management tool at aquifer scale. Nevertheless it provides a "big picture" view that is appropriate input for setting broad regional or national policies (Famiglietti & Rodell, 2013), a view for which our study provides further evidence.

Hence, to further study the relationship between ground movement and groundwater change observed groundwater data is taken from boreholes provided by the EA. The EA publishes a "management of the London basin chalk aquifer" status report each year and the data is extracted for key boreholes from graphs provided in the report for the year 2010.

The contour map for change in groundwater levels for London between the years 2000 and 2010 provided by the EA is consistent, and agrees well with the PSInSAR subsidence map of London obtained using Envisat data (Figure 4.10). The overall land movement pattern suggests an uplift in north London and subsidence in south London. This is consistent with the EA contour map for groundwater, which shows that there is an overall increase in groundwater level for the northern part and decrease in the southern part of the study area. The average water level rise is in the order of 7 m in north-west London and 4 m in central London, which corresponds to an average uplift of 31 and 20 mm, respectively.

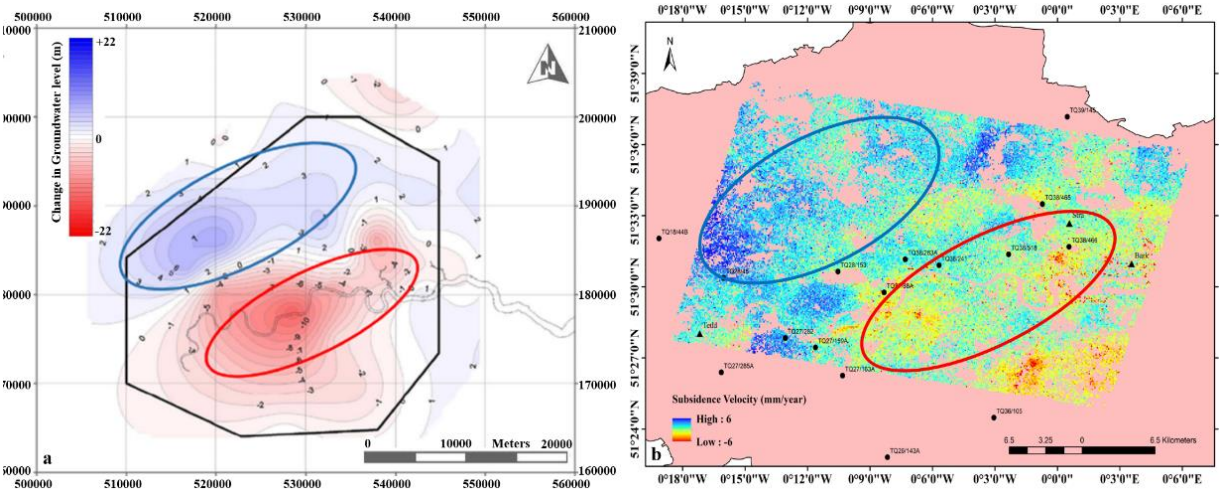

*Figure 4.10: (**a**) Contour map for groundwater level change for London between 2002 and 2010, obtained from "management of the London basin chalk aquifer" status report, EA, 2010 (EA, 2017). (**b**) PSInSAR ground movement map for London between 2002 and 2010. The area marked with a blue oval in (**a**,**b**) highlights an increase in groundwater and land uplift, respectively, for north London; while the area marked with a red oval highlights a decrease in groundwater and land subsidence for south London.*

`

It can be seen from Figure 4.10a that water level is decreasing to form a zone of water level fall crossing from south to east London, and there is prominent land subsidence in the corresponding area. Therefore, it cen be concluded that extraction or recharge of groundwater for a particular area directly contributes to the land subsidence or uplift of the corresponding area. Additionally, there might be a threat of saline intrusion in east London, in the area where the chalk outcrops around the River Thames from Greenwich to Woolwich. It can be observed from the contour map that groundwater flow is in a north-westerly direction, and thus water extraction could capture saline water if it enters the aquifer. Thus, there were restrictions applied to water abstraction licenses in this area (EA, 2017).

Figure 4.10 validates that groundwater level directly influences the ground movement pattern. To further study both the phenomena, individual boreholes have been analysed (location marked in Figure 4.1 and Figure 4.4). The time-series of groundwater variation for boreholes are compared to time-series of subsidence patterns at the corresponding location.

The land movement is an indirect effect of groundwater change, and hence it is smaller in magnitude than groundwater change. In addition, a time lag is expected in land movement when compared to the groundwater change. To obtain the subsidence at the location of a particular borehole, the average of all the Persistent Scatterers (PSs) present within 300 m of the borehole station was used. This is to address the challenge of obtaining a PS point at the exact location of borehole. As the groundwater level of a borehole will affect its nearby areas, it is suitable to take the contribution of nearby PS points for a particular borehole station.

Figure 4.11a–d shows time-series variation for four key boreholes and their related subsidence. Three out of the four locations selected (i.e., TQ2788a (Ashley Gardens, Westminster), TQ27_159 (Ram Brewery, High street, Wandsworth), and TQ28_153 (Kensington Gardens)) show decreasing trends for both groundwater and ground movement (subsidence). Additionally, from Figure 4.4 it can seen that all three boreholes are surrounded by reddish-yellow patches, indicating subsidence in the corresponding area. On the contrary, a dark blue patch can be seen in Figure 4.4 surrounding borehole TQ27_282 (I Stratford Grove, Putney) suggesting overall uplift. Temporal groundwater variation and subsidence trends from Figure 4.11d suggest the same. This pattern of land movement for all the four borehole stations can be attributed to the change in groundwater, as no other major contributing factors for this behaviour can be found.

`

Figure 4.1 shows the location of major faults in the study area. The faults might interfere with the groundwater flow, such that it can hinder the flow if fault material has low permeability, or it can act as flow conduits to promote the flow. The northern boundary fault has boreholes TQ38_241 (45–47 Gresham Street) and TQ38_263a (Victoria House, Southampton Row) on its southern and northern sides, respectively. The hydrographs from both the boreholes (Figure 4.12) shows comparable water levels and variation trends. The average change in groundwater for TQ38_241 (45–47 Gresham Street) is −1.1233 m and that for TQ38_263a (Victoria House, Southampton Row) is −1.279 m. Similarly, the subsidence pattern for both the boreholes shows similar trends, with an average value of −0.70 and −0.65 mm/year respectively. This suggests that this fault does not act as a barrier in this area.

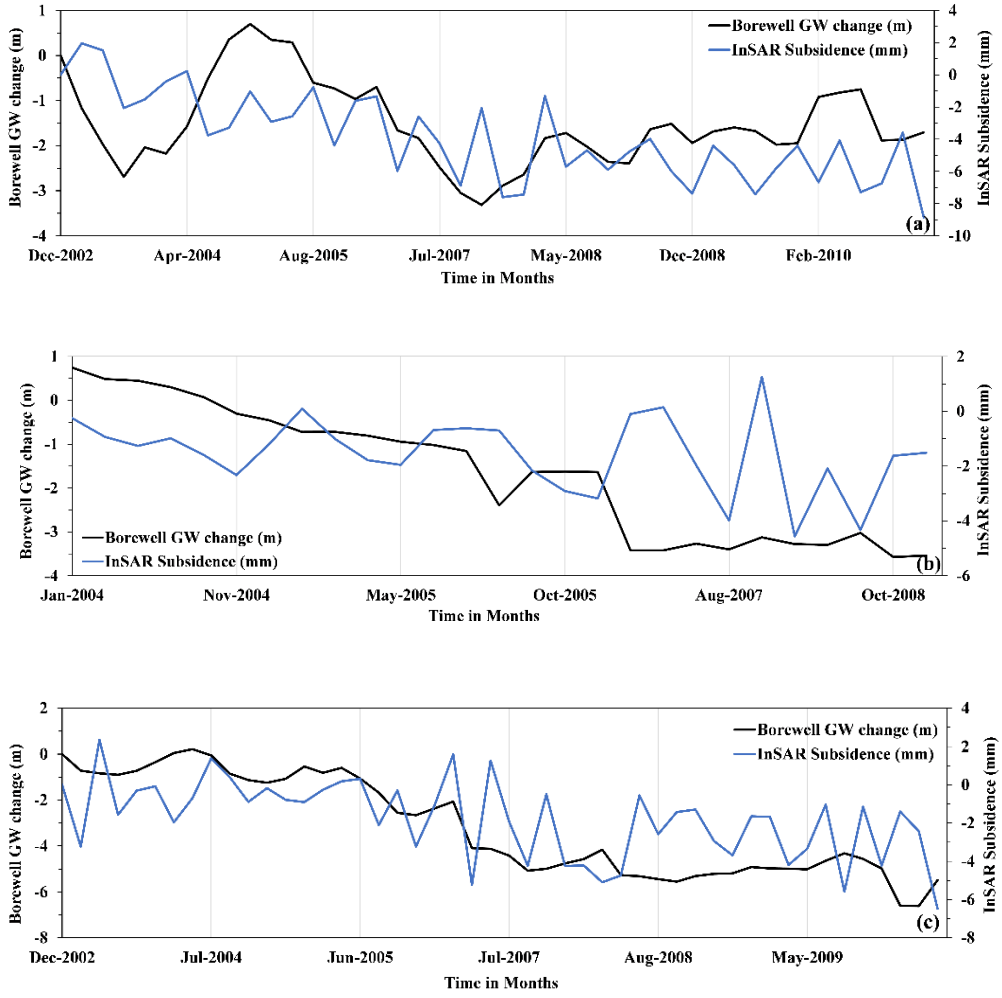

`

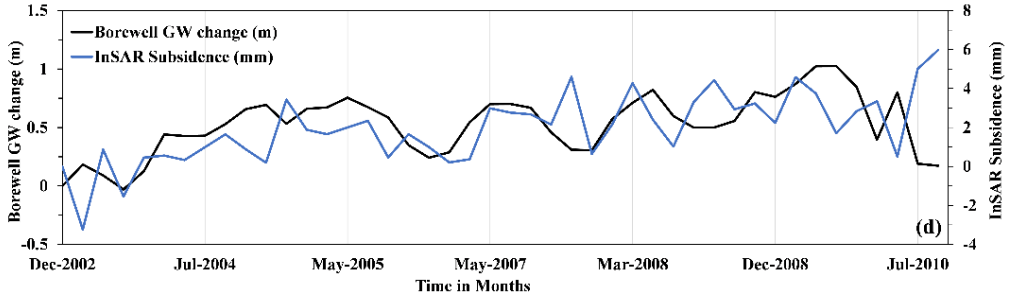

*Figure 4.11: (**a**–**d**): Time-series variation of groundwater change (from borehole) and subsidence (from InSAR) for (**a**) TQ2788a (Ashley Gardens, Westminster), (**b**) TQ27_159 (Ram Brewery, High street, Wandsworth), (**c**) TQ28_153 (Kensington Gardens) and (**d**) TQ27_282 (I Stratford Grove, Putney).*

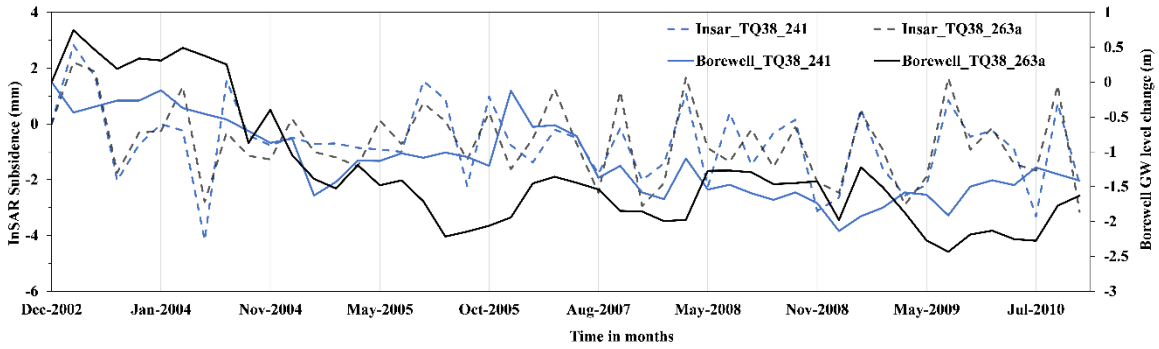

Figure 4.12: Subsidence and groundwater time-series for boreholes on either side of the northern boundary fault (i.e., TQ38_241 (45–47 Gresham Street) on the southern side and TQ38_263a (Victoria House, Southampton Row) on the northern side).

While looking at boreholes on either side of Greenwich fault (Figure 4.1), the two boreholes selected for this analysis were TQ48_2 (Victoria docks) and TQ47_90 (Charlton Obh). The average change in groundwater for TQ48_2 is −1.386 m and that for TQ47_90 is −0.197 m. Similarly, the subsidence pattern for both the boreholes varies significantly with an average value of −0.634 and −1.44 mm/year, respectively. This suggests that the Greenwich fault acts as a flow barrier. In addition, Rotherhithe Fault and Mitcham Fault at the centre of the basin are likely to act as flow barriers. However, there is no evidence for Wimbledon fault and Streatham fault to impede the groundwater flow (EA, 2017).

`

4.6 Conclusions

In this study, the suitability of monitoring ground movement using PSInSAR subsidence and GNSS data for London between December 2002 and September 2010 is explored. Also the groundwater variation using GRACE gravity anomalies and observed boreholes for London for the same time period is monitored.

It can be observed that the ground movement in London is distinctly uneven and non-linear. The ground movement in the north-western part of the study area is positive, implying land uplift. On the contrary, the ground movement in the south-eastern part of the study area is negative, implying land subsidence. The average subsidence in the study area is found to be −0.176 mm/year. By statistically analysing the average subsidence velocities, it is observed that the standard deviation of 98.22% of the PS points are less than 5 mm/year, and that for overall PSInSAR subsidence is 0.665 mm/year. The InSAR subsidence values were validated using GNSS data. The two-sample *t*-test provides enough evidence that GNSS up values are in close agreement with the obtained InSAR subsidence values, thus demonstrating that the PSInSAR is an efficient way to survey ground movement in London.

The groundwater changes obtained from GRACE demonstrates a decreasing tendency and the average groundwater loss from GRACE was found to be 9.003 MCM/year. The best-fit line for the temporal groundwater variation from GRACE has a negative slope, indicating groundwater depletion. The volumetric change of groundwater derived from GRACE data accounted for 60% of the total change in the report from the Environment Agency. In addition, the GRACE-derived temporal time-series showed seasonal and annual variations.

Different reasons for site-specific land movement patterns were discussed. The major factor which was consistent with spatial ground movement is the spatial change in the groundwater. In addition, ground movement was studied in conjunction with groundwater variation obtained from various boreholes. It is suggested that when a large volume of groundwater is extracted from an aquifer, it results in compaction of underlying aquifer material and, in turn, is responsible for land subsidence, and, in contrast, recharge or rebound of groundwater results in land upliftment.

The spatial resolution for GRACE is low, while that of InSAR is high. The PSInSAR method is excellent for studying spatial variation of groundwater, and GRACE is excellent for studying temporal variation of groundwater. With new processing algorithms and the GRACE follow-on

`

mission, the resolution is expected to improve. In addition, the increasing coverage and availability of SAR data should enhance the accuracy of subsidence mapping. With these updated data sets, it will be suitable to read InSAR and GRACE results at the same resolution and make a direct statistical comparison for future studies. Overall, the study of InSAR and GRACE in conjunction provides an interesting technology for spatial and temporal mapping of groundwater and ground movement.

Author Contributions: The authors who contributed to the paper presented in this chapter are Agarwal, Vivek* (V.A); Kumar, Amit (A.K); L. Gomes, Rachel (R.L.G); Marsh, Stuart (S.M). *Conceptualisation*, V.A., R.L.G. and S.M.; *data curation*, V.A., R.L.G. and S.M.; *formal analysis*, V.A. and A.K.; *funding acquisition*, V.A., R.L.G. and S.M.; *investigation*, V.A., R.L.G. and S.M.; *methodology*, W.A., A.K., R.L.G. and S.M.; *resources*, V.A.; *software*, V.A. and A.K.; *supervision*, R.L.G. and S.M.; *validation*, R.L.G. and S.M.; *visualisation*, V.A., A.K., R.L.G. and S.M.; *writing*—original draft, V.A.; *writing—review and editing*, V.A., R.L.G. and S.M.

Acknowledgments: The authors would like to thank the European Space Agency (ESA) for providing access to SARscape software for processing of InSAR data through Eohops programme. The authors would also like to thank the EA for providing "management of the London basin chalk aquifer" status report 2010. The services of the Natural Environment Research Council (NERC) British Isles continuous GNSS Facility (BIGF), www.bigf.ac.uk, in providing archived GNSS data (and/or products) to this study, are gratefully acknowledged.

`

Chapter 5 London-Delhi Subsidence Study

Preface

Chapter 4 studied groundwater induced subsidence for London using C-band Envisat-ASAR images between 2002-2010. The results were validated with in situ GNSS and borehole data. The methodology developed and validated in chapter 4 was then extended to study more recent trends in groundwater-induced land movement variation. The PSInSAR module of ENVI SARscape was used to study the latest land movement pattern in London between October 2016 to December 2020 using Sentinel-1 images. In addition, the land movement pattern in Delhi was obtained using the same methodology as for London. Both the cities have dense urban fabric, and hence and the methodology developed in the previous chapter is applicable in both areas.

One of the conclusions from the previous chapter was that GRACE gravity anomalies could provide very detailed groundwater variation on continental scales. Still, its poor spatial resolution cannot provide a detailed variation pattern for small areas and cities like London and Delhi (<2000 km^2). Thus, this chapter does not use the GRACE methodology, but groundwater variation is studied using in situ borehole data for both cities.

Rapid population growth has been reported in the last decade in London and Delhi because of the opportunities for economic growth and resources available in these capital cities. This increased population exerts extra pressure on groundwater resources to meet the local water demand. Thus, monitoring groundwater-induced land movement in both these cities is very important so that the associated risk to infrastructure can be measured and minimised. Both cities exhibit local patches of subsidence, uplift and differential land movement caused by various natural and anthropogenic factors. A consistent factor causing land movement across different areas in both cities is groundwater withdrawal and rebound. Spatial and temporal variation of groundwater and the related subsidence has been studied in this chapter and compared for the two cities.

Further, a model to relate groundwater quantity variation to subsidence has been made by modifying a model given by BGS. The 1-D model attempts to directly quantify the change in land movement (subsidence/uplift) resulting from the corresponding change in groundwater level.

The study performed on London and Delhi using InSAR and in situ groundwater levels between 2016 to 2020 has been submitted to the journal ‘Remote Sensing’, entitled ‘*Comparative study of*

`

groundwater-induced subsidence for London and Delhi using PSInSAR'. The proposed paper is presented here in this thesis as Chapter 5.

Abstract: Groundwater variation can cause land-surface movement, which in turn can cause significant and recurrent harm to infrastructure and the water storage capacity of aquifers. The capital cities in the England (London) and India (Delhi) are witnessing an ever-increasing population that has resulted in excess pressure on groundwater resources. Thus, monitoring groundwater-induced land movement in both these cities is very important in terms of understanding the risk posed to assets. Here, Sentinel-1 C-band radar images and the persistent scatterer interferometric synthetic aperture radar (PSIn-SAR) methodology are used to study land movement for London and National Capital Territory (NCT)-Delhi from October 2016 to December 2020. The land movement velocities were found to vary between −24 and +24 mm/year for London and between −18 and +30 mm/year for NCT-Delhi. This land movement was compared with observed groundwater levels, and spatio-temporal vari-ation of groundwater and land movement was studied in conjunction. It was broadly observed that the extraction of a large quantity of groundwater leads to land subsidence, whereas groundwater recharge leads to uplift. A mathematical model was used to quantify land subsidence/uplift which occurred due to groundwater depletion/rebound. This is the first study that compares C-band PSInSAR-derived land subsidence response to observed groundwater change for London and NCT-Delhi during this time-period. The results of this study could be helpful to examine the po-tential implications of ground-level movement on the resource management, safety, and economics of both these cities.

Keywords: PS-InSAR, Sentinel-1, surface subsidence, groundwater, London, NCT-Delhi.

5.1 Introduction

Water is essential to sustain life on earth; however, its availability is not uniform within the spatial and temporal domains. Groundwater meets a large part of the water demand, and ever-increasing dependence on this resource has led to groundwater depletion across various parts of the world (Dalin et al., 2017; Konikow & Kendy, 2005; Wada et al., 2010). Amidst the threat of global warming and climate change, groundwater acts as a lifeline for many parts of the world. Thus, adequate management of groundwater is essential to ensure its sustainability. Excessive abstraction and change in rainfall patterns make it necessary to regularly revise and monitor groundwater abstraction policies.

`

For decades, groundwater has been extensively exploited for domestic, agricultural, and industrial purposes; this has necessitated subsequent artificial recharge to balance the groundwater depletion and control land subsidence (Figueroa et al., 2018; Li et al., 2021). Long-term groundwater exploitation and recharge in confined aquifers alters the piezometric and pore pressures in aquifers (Zhang et al., 2018; Zheng et al., 2019). According to the effective-stress principle, aquifer systems consolidate owing to these changes in their properties, leading to land subsidence (Chai et al., 2004; Lyu et al., 2020). Therefore, it is necessary to understand land subsidence and the compaction process caused by groundwater exploitation and recharge.

Extraction or recharge of groundwater can cause land subsidence or uplift, respectively, and this can cause significant harm to buildings, infrastructure, and the water storage capacity of aquifers (Agarwal et al., 2020b; Bateson et al., 2009; Galloway & Burbey, 2011; Scoular et al., 2020; Yu et al., 2020). The conventional methods to study land movement, such as global positioning systems (GPS), global navigation satellite systems (GNSS), levelling, and others, can provide precise information but are labour intensive, costly over vast extents, and have a poor resolution, and thus, an alternative is needed. Satellite interferometric techniques, such as persistent scatterer interferometric synthetic aperture radar (PSInSAR), provides the means for less tedious, cost-effective, large spatial coverage (basin level) mapping of ground movement without compromising on accuracy and precision (Biswas et al., 2017; Karanam et al., 2021; Kim et al., 2007; Peltier et al., 2010). This technique was first introduced by Alessandro Ferretti in 2000 (Ferretti et al., 2000b) and has been developed and applied for mapping surface deformation associated with groundwater change (Agarwal et al., 2020b; Devleeschouwer et al., 2008; Khorrami et al., 2019, 2020; Mason et al., 2015). While PSInSAR can provide accurate land deformation information, it can only be calculated on permanent scatterers that maintain stable scattering with respect to time. This methodology is thus most effective in urban areas where multiple permanent scatters can be obtained (Ferretti et al., 2000b).

The chalk is the most important aquifer unit in the English capital city of London and has been supplying water for public consumption since the 19th century (Jones et al., 2012). London witnessed groundwater depletion during the first half of the 20th century, due to increased urban development and human activities. This depletion resulted in a decrease in groundwater level to 88 m below mean sea level (MSL) in the 1960s. The depletion was checked because of de-industrialisation in the 1980s, which led to groundwater rebound by 3 m/year in the 1990s. This

`

dramatic rebound posed potential harm to buildings and structures and, to counter this, the General Aquifer Research, Development, and Investigation Team (GARDIT) strategy was implemented in 1992 (EA, 2019). This enforced licensed groundwater withdrawal and regular monitoring and thus stabilised the groundwater around the year 2000, and since then, groundwater has been monitored regularly.

India is home to over 1.3 billion people, and its ever-increasing population, urbanisation and non-uniform abstraction have likewise increased the depletion rate of groundwater resources (Central Ground Water Board, 2018). The National Capital Territory (NCT) of Delhi lies in the heart of India and forms the capital city of the country. The subsurface geological features of NCT-Delhi determine its discrete landform units, which are directly related to groundwater availability. The primary source of irrigation in NCT-Delhi is groundwater, although surface water is also available from Trans Yamuna Canal Network. The Central Ground Water Board (CGWB) monitors and publishes groundwater records for India. It took on the aquifer mapping program during the 12th five-year plan for the entire country (including NCT-Delhi) for sustainable development and management of groundwater resources (Central Ground Water Board, 2016a). The groundwater level in NCT-Delhi is continuously declining and is at a critical stage (Gupte, 2019), and this decline in groundwater level poses a significant threat of land subsidence (Garg et al., 2020).

The population explosions in London and NCT-Delhi exert increased pressure on groundwater resources, thus posing a threat of land subsidence. However, the subsurface geology and infrastructure of the two cities are different, and yet the responses of groundwater to anthropogenic activities and its subsequent effect on land movement is not well understood. To the best of our knowledge, no previous attempts have been made to simultaneously examine the specific causes of groundwater-induced land subsidence for London alongside that of NCT-Delhi using PSInSAR. In this study, the groundwater-induced land subsidence for the two major cities is studied between October 2016 and October 2020 using a variety of geospatial techniques such as PSInSAR, GIS, spatio-temporal analysis, mathematical modelling, and statistical analysis. The objectives of this paper are (i) to describe spatio-temporal variation in land subsidence/uplift and investigate the natural and anthropogenic factors affecting land deformation; (ii) to analyse localised uplift, subsidence, and differential movement; (iii) to study temporal and spatial variation in groundwater and related subsidence at different locations for both the cities; and (iv) to construct a mathematical

`

model where a groundwater change input could be used to calculate the expected localised change in land deformation.

5.2 Study Area

The geographical areas selected in this study are the administrative area of Greater London (Figure 5.1a) and the administrative area of NCT-Delhi (Figure 5.1b). London extends over 0°30′ W to 0°20′ E longitudes and 51°42′ N to 51°17′ N latitudes, comprising nearly 1600 km^2 in the southern part of England. Meanwhile, the NCT-Delhi area is bounded by 76°50'24" E to 77°20'30" E longitudes and 28°24'15"N to 28°53'00"N latitudes, comprising a 1500 km^2 area in the central part of India.

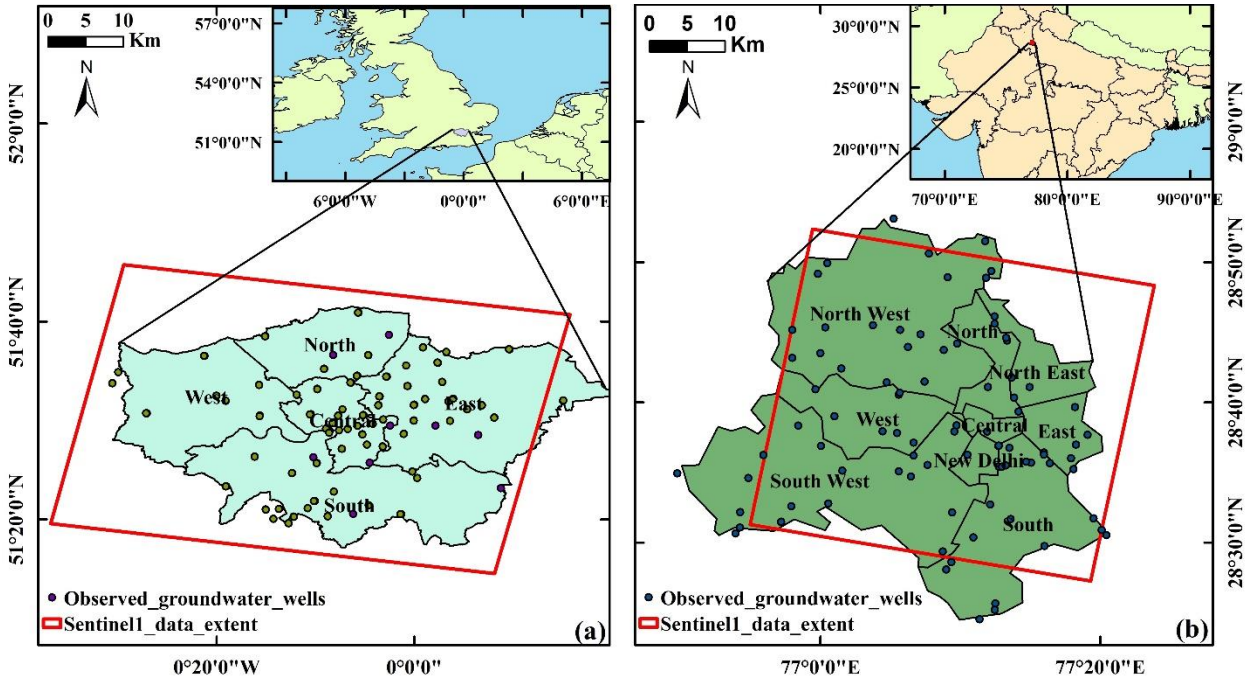

Figure 5.1: Study area showing administrative boundary of (a) London and (b) NCT-Delhi. The red boundary shows the extent of Sentinel data processed, and black dots show the location of observed groundwater wells.

The London basin is infilled by younger Paleogene deposits, and the chalk group forms a rim around it and has a depth exceeding 200 m in central London (Ford et al., 2010; Mathers et al., 2014). The NCT-Delhi is bounded by the Indo-Gangetic plains on the north-eastern side, Aravalli ranges on the southern side, and Indian Thar desert on the western side. It is drained by the Yamuna sub-basin, which flows in a north–south direction. The NCT-Delhi is dominated by three main

`

geomorphic units: rocky surface, older alluvium plain, and flood plains of Yamuna. The area has mainly calcareous soil and comprises clay, silt, and fine to medium sand (Gupte, 2019).

In the United Kingdom (UK), chalk aquifers account for about 60% of the groundwater used (BGS, 2013), and provide approximately 80% of the water supply in the River Thames catchment and 20% in London alone (Bonì et al., 2016). In NCT-Delhi, the groundwater level variation is quite extensive because of the wide range of topographic relief. The southern part of NCT-Delhi has deeper wells (~40 m below ground level) compared to those in the northern part (~10 m below ground level) (Central Ground Water Board, 2016b). In both cities, the local hydrogeological conditions mainly govern the groundwater conditions, and it is controlled by a mix of rainfall, river, canal water, and irrigation return flows.

The population of London had an increased rate of 1.4% per annum during the decade 2001–2011, while the rate for NCT-Delhi was 2.25%. The official projected population for London in 2025 is 9.31 million (GLA, 2021a), while that for NCT-Delhi is 22.1 million (ESD, 2021). These estimates represent the urban agglomeration of the city, which typically includes the city's population in addition to adjacent suburban areas.

London's climate is warm and temperate, and the average annual temperature and the average annual rainfall is 11.1 °C and 621 mm, respectively. At the same time, NCT-Delhi is characterised by extreme dry hot summer and extreme cold winter climatic conditions. The temperature varies from a minimum of 7.3° in winter to a maximum of 47° in summer and receives a mean annual rainfall of 611.8 mm. The land use within both cities is dominated by dense to medium density urban fabric with multiple industrial units.

The demography, geology, rainfall, and hydrology of London and NCT-Delhi are highly contrasting. The two cities represent densely populated urban cities of developed and developing nations, respectively, and land deformation problems have been reported in both these cities. This study will help to improve the knowledge of land deformation response to groundwater use, through seeking to establish whether the land deformation response to groundwater change is universal irrespective of the differences in the characteristics of the cities, or whether it is very much location specific. This outcome of the study could therefore contribute towards infrastructure planning of urban areas in developed and developing nations.

`

5.3 Materials and Methods

5.3.1 PSInSAR Processing

The data specifications and overall methodology used in this study are summarised in Table 5.1 and Figure 5.2, respectively. Land movement for each study area was calculated using the PSInSAR principle (Ferretti et al., 2000b) implemented in the ENVI SARscape software (Sarmap, 2014a). The software package is highly efficient at interferometric synthetic aperture radar (InSAR) processing using DInSAR, PSInSAR, and SBAS InSAR techniques, and supports all the latest synthetic aperture radar (SAR) sensors (Agarwal et al., 2020a; Sahraoui et al., 2006; Simonetto & Follin, 2012). The PSInSAR technique, in general, requires at least twenty or more SAR image pairs to generate reliable results (Kim et al., 2007). Specifically, stacks of 99 and 95 Sentinel-1 C-band images acquired between October 2016 and October 2020 over London and NCT-Delhi, respectively, were obtained and used to compute land movement. This time period was chosen as consistent SAR data was available for both these cities from Sentinel-1 between cotber 2016 to October 2020.

Table 5.1: Data and software used

Data	London	NCT-Delhi
InSAR Data	99 Sentinel-1 SLC images	95 Sentinel-1 SLC images
	VV polarisation, Frame 422, Descending, IW Beam mode	VV polarisation, Frame 496, Descending, IW Beam mode
	Resolution: Azimuth: 20 m by Range: 5 m	Resolution: Azimuth: 20 m by Range: 5 m
	Repeat Cycle: 12 days	Repeat Cycle: 12 days
	Wavelength: 5.6 cm, C-band	Wavelength: 5.6 cm, C-band
	Primary Image: 01 Nov 2018	Primary Image: 24 Sep 2018
	Time period: Oct-2016 to Oct-2020	Time period: Oct-2016 to Oct-2020
	Digital Elevation Model: SRTM V4	Digital Elevation Model: SRTM V4
	Software Used: ENVI SARscape, ArcGIS (ArcMap 10.2.2)	Software Used: ENVI SARscape, ArcGIS (ArcMap 10.2.2)
Ancillary data	Borehole groundwater data from the UK Environment Agency for 81 boreholes.	Groundwater Level data (Source: Central Ground Water Board, CGWB) for 98 boreholes. Geological data of Delhi (Source: CGWB)

`

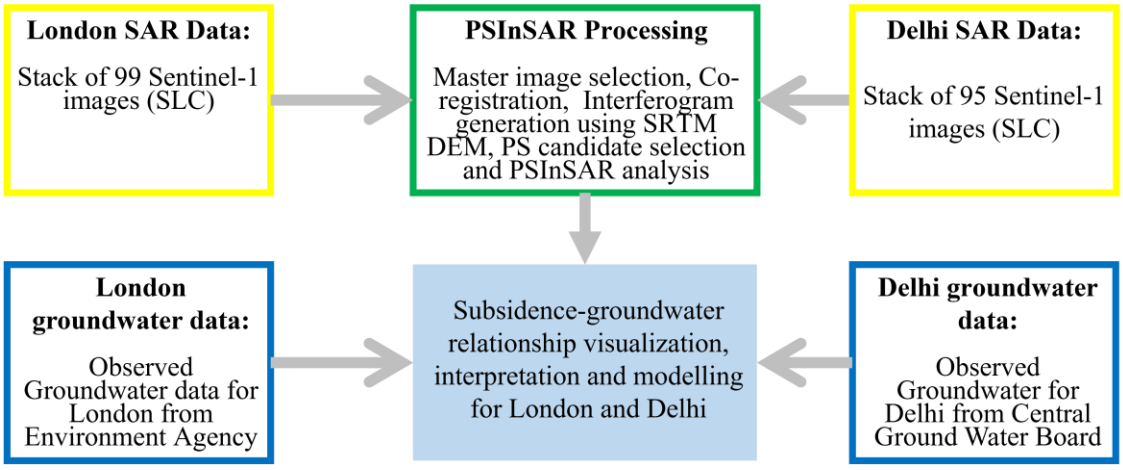

Figure 5.2: Methodology

The SARscape module facilitates PSInSAR processing of SAR data in a multi-step, semi-automated process (Sarmap, 2014b). To begin, a master image is chosen to which all slave images are co-registered. To select the master image, the least average baseline of the stack is considered so that an optimum spatio-temporal position of the master image is ensured with respect to the slave images. This ensures increased coherence and better data co-registration, as small baselines are less sensitive to volume de-correlation (Sarmap, 2014b, 2014a)

After co-registration, interferograms were generated using master–slave pairs and flattening was achieved by applying a reference digital elevation model (SRTM DEM V4). To select a reference point for PSInSAR analysis, SARscape breaks the whole area into subsets (accounting for an overlap) if the area under consideration is bigger than a chosen threshold area. Then, each subset was analysed independently, with each having its own reference point. This was performed in order to improve the accuracy of the atmosphere estimation, and finally all the independent areas were mosaicked. This chosen threshold area is known as "Area for Single Reference Point (sq km)" (Sarmap, 2014a). In this study, this threshold was set at 25 km^2 and in total there were 238 subsets for London and 143 subsets for NCT-Delhi.

The density of permanent scatterers (PS), used to derive land motion measurements, relies on the selected coherence threshold for the PSInSAR analysis. The greater the coherence threshold, the better the quality and smaller the number of PS obtained, and vice versa. Therefore, the coherence threshold should be selected such that an optimum trade-off is reached between the quality of PS points and the number of PS points selected. The first step inversion was carried out to obtain the

`

coherence, displacement velocity, and residual topography. These results were further employed for flattening the complex interferograms. Then, the second inversion step was performed to address the atmospheric phase components of the linear model products arising from the first inversion. Finally, geocoding was performed to display maps of the average (linear) velocity and displacement time-series for the observed time-period.

5.3.2 Groundwater Variation

To compare and validate the PSInSAR-derived land movements with groundwater variations, observed groundwater monitoring data were obtained from the UK Environment Agency for London (from 81 boreholes) and CGWB for NCT-Delhi (98 boreholes). The UK Environment Agency publishes an annual report on 'Management of the London Basin Chalk Aquifer' and the groundwater data was extracted from maps of the water table given in reports for January 2017 and January 2020 (EA, 2017, 2019). Additionally, the monthly groundwater level for the Battersea chalk borewell was obtained from the UK Environment Agency. For NCT-Delhi, the groundwater data provided by CGWB was obtained for November 2016 and November 2020. The groundwater levels from 2016 were subtracted from that of 2020 to find the find the change and then interpolated using the inverse distance weighting (IDW) interpolation method (Bartier & Keller, 1996) to produce a groundwater change map covering the whole area. The groundwater maps were then subsequently analysed in comparison to the subsidence maps.

5.3.3 Groundwater-Subsidence Mathematical Model

A simple mathematical model was used to calculate the amount of strata compaction resulting from a reduction in the piezometric head. The adopted model was a modified version of that applied in the Europe-led Terrafirma project (Bateson et al., 2009) and coalfields in Derbyshire and Nottinghamshire (Gee et al., 2020). It is used in order to analyse the relationship between groundwater level and observed subsidence for London and NCT-Delhi.

This model was based on the effective stress principle proposed by Terzaghi (Terzaghi, 1925), which calculates the land deformation (subsidence or uplift) with respect to groundwater change (decrease or increase). The model was treated as a homogeneous matrix, where the initial bed thickness (b_0) (m) was calculated as the depth from the surface to the groundwater level at the start of the modelling epoch. As a formation was laid down and subsequently overlain by more

`

material, the geostatic pressure (p_0) increases. The geostatic pressure is resisted by a combination of the fluid pressure of the pore water (p_{w0}) and the intergranular (effective) stress (p_{s0}) within the rock matrix (Shearer, 1998).

$$p_0 = p_{s0} + p_{w0} \quad \text{Equation 5.1}$$

For an unconfined aquifer, the geostatic pressure is divided as p_{s0} (60%) and p_{w0} (40%), and for a confined aquifer the geostatic pressure is divided as p_{s0} (75%) and p_{w0} (25%) (Gee et al., 2020). The stress transfer from the fluid to rock matrix per unit change in the piezometric head is calculated at 10 kPa/m (Poland, 1984). The geostatic pressure is calculated from the initial bed thickness (b_0) as:

$$p_0 = 10 * b_0 \quad \text{Equation 5.2}$$

The total difference in bed thickness (Δb), after an instantaneous change in effective stress (Δp_s), is calculated as a function of the coefficient of volume compressibility (m_v) and initial thickness (b_0) as:

$$\Delta b = m_v * \Delta p_s * b_0 \quad \text{Equation 5.3}$$

where (m_v) can be defined as a function of the coefficient of compressibility (a_v) and the initial void ratio (e_0).

$$m_v = \frac{a_v}{1 + e_0} \quad \text{Equation 5.4}$$

where (a_v) is the ratio of change in void ratio to effective stress

$$a_v = \frac{\Delta e}{\Delta p_s} \quad \text{Equation 5.5}$$

The initial void ratio and final void ratio (e_1) can be related as follows:

$$\Delta e = e_1 - e_0 = -c_c \log\left(\frac{p_{s1}}{p_{s0}}\right) \quad \text{Equation 5.6}$$

`

$$e_0 = \frac{n_o}{1 + n_o}$$ Equation 5.7

where (c_c) is compressibility index, and (n_o) in initial porosity.

The model was constructed in R programming, where the compaction of each layer (formation) was calculated using the above parameters and equations. The total amount of compaction is the combined total of each formation compaction. Each of the formations was assumed to contain a homogeneous matrix, and each assigned an average density and initial porosity based upon sediment type and depth of burial (Zimmerman, 1990). For London, the initial thickness of each formation was estimated using the London Basin 3D model constructed using GSI3D (Zimmerman, 1990). For NCT-Delhi, it was obtained from the hydrogeological framework and groundwater management plan of NCT-Delhi (Sarkar et al., 2016). It is a layer-cake model which assumes that each layer is uninform; thus, thickness and physical properties for each subsurface layer are considered the same for all the locations of London, and for NCT-Delhi (Table 5.2).

Table 5.2: Physical properties of sub-surface layers

Location	Formation	Thickness (m)	Void ratio	Porosity	Compression Index
Delhi	Clay and Kankar	160	0.65	-	0.045
	Silt and Kankar	45	0.55	-	0.0924
	Sand	20	0.45	-	0.00525
London	Lambeth Group	11.98	-	0.35	0.0025
	Thanet Sands	10.20	-	0.3	0.0015
	Chalk Group	201.09	-	0.55	0.001

5.4 Results

Figure 5.3a,b displays the land displacement velocity map for London and NCT-Delhi obtained using 95 and 99 Sentinel-1 SAR images, respectively. The movement of land in the direction of sensor (uplift) and away from the sensor (subsidence) is represented by positive (green colour) and negative values (red colour), respectively. Table 5.3 summarises the statistics of the deformation results obtained.

`

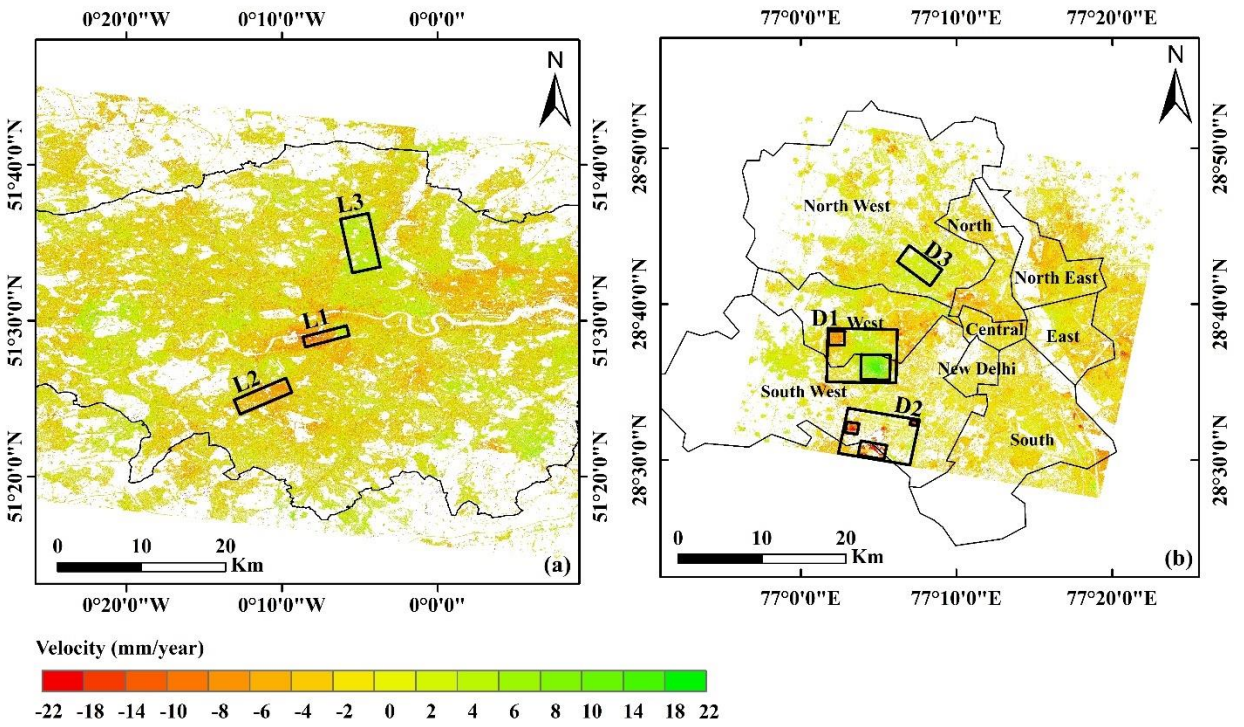

Figure 5.3: Land movement map obtained using Sentinel-1 data for (a) London and (b) NCT-Delhi. The green areas depict uplift, while the red areas depict subsidence. The black rectangular boxes show the selected sites for case studies.

Table 5.3: Statistics of PSInSAR-derived subsidence

Area	Time-period	Area (km^2)	PS coherence threshold used	Number of Permanent Scatterers obtained (PS)	PS density (PS/km^2)	Mean rate of Deformation (mm/year)	Standard Deviation (mm/year)
London	Oct 2016 to Oct 2020	2607	0.5	14,327,370	5496	-0.08	1.34
NCT-Delhi	Oct 2016 to Oct 2020	1611	0.5	7,764,180	4819	-0.04	1.70

Both London and NCT-Delhi are heavily built-up urban areas and therefore prove to be ideal sites for PSInSAR analysis. A coherence threshold of 0.50 was used for this experiment, resulting in a PS density of 2607 PS/km^2 for London and 1611 PS/km^2 for NCT-Delhi. For London, the land movement ranges between −24 and +24 mm/year, while for NCT-Delhi, it ranges from −18 to +30 mm/year. An area can typically be considered unstable if land movement is greater than ±10

`

mm/year (Zheng et al., 2018). For both these cities, even though the land movement is stable on the whole (in terms of the mean deformation rate shown in Table 5.3), it is predominantly spatially variable with distinct chunks of displacement in the form of either uplift or subsidence. Even though the land movement is small (mm-level), it is identifiable from the Sentinel data. These motions can likely be attributed to groundwater variations, underground construction activities, or subsurface geology, as discussed in Section 5.5.

For London, the groundwater data obtained from the Environment Agency report represents groundwater level in meters above ordnance datum (mAOD). For NCT-Delhi, groundwater measurements provided by the CGWB represent the depth to water level from the surface. In groundwater maps for both the cities, depletion is represented by red (negative values) and recharge by blue (positive values) (shown in Figure 5.4–5.9, explained in section 5.5). The change in groundwater levels varies between −35 and +20 m for London and between −16 and +12 m for NCT-Delhi for the observed time-period (Table 5.5-5.7, explained in section 5.5)

Several interesting features are identified from the Sentinel PSInSAR measurements for both cities. These land movement features are discussed as case studies, the locations of which are marked with black rectangular boxes in Figure 5.3. These include:

- Differential land motion areas: Northern Line Extension, London (L1-a,b in Figure 5.4) and Magenta-Blue Metro Line, NCT-Delhi (D1-a,b in Figure 5.5).
- Subsidence areas: Wimbledon to Tooting, London (L2 in Figure 5.6) and Haryana-Delhi Border, NCT-Delhi (D2-a,b,c in Figure 5.7).
- Uplift areas: Bruce Castle to Abney Park, London (L3 in Figure 5.8) and Rohini, NCT-Delhi (D3 in Figure 5.9).

The results from the mathematical model used to compute the expected land movement from an observed change in groundwater level for all the case studies (L1, D1, L2, D2, and L3 and D3) are presented in Table 5.4. The 4-year average monthly change in the piezometric head is given for each case study. The average land movement at each location was calculated with this constant groundwater change rate. The land movement calculated at each location using the model and that calculated using PSInSAR is shown in Table 5.4. The difference in land deformation rate between the InSAR and modelled output is also shown. The mean of this difference in deformation for

`

London is −0.63 mm/year with a standard deviation of 1.58, while that for NCT-Delhi is −0.55 mm/year with a standard deviation of 3.10 mm/year. The maximum and minimum difference in rate is 4.83 mm/year at D3 and 0.26 mm/year at L1-a, respectively.

Table 5.4: Comparison of land deformation from land subsidence and PSInSAR

Area		Groundwater monthly change (m/month)	Model Change (mm/year)	PSInSAR change (mm/year)	Difference in rate (model-PSInSAR)
L1	L1-a	-0.339	-3.18	-3.44	0.26
	L1-b	0.313	2.94	4.55	-1.61
D1	D1-a	-0.029	-7.79	-5.09	-2.7
	D1-b	0.038	10.14	11.06	-0.92
L2		-0.401	-3.75	-4.87	1.12
D2	D2-a	-8.770	-8.77	-5.28	-3.49
	D2-b	-0.012	-3.19	-4.37	1.18
	D2-c	-0.022	-5.97	-3.74	-2.23
L3		0.145	1.36	3.64	-2.28
D3		0.041	11.13	6.30	4.83

5.5 Discussion

5.5.1 Differential Land Motion Areas

There are areas in London and NCT-Delhi where notable differential motion in the form of subsidence observed in close proximity to uplift occurs. In the London area, this is associated with the Northern Line extension (NLE) (Figure 5.4), while in the NCT-Delhi area, this is near the Janakpuri-Dwarka Magenta-Blue Line metro stations (Figure 5.5). Table 5.5 summarises the statistics of land movement and groundwater change for both areas.

Table 5.5: Statistics of land uplift and groundwater augmentation for Northern Line Extension (London) and Magenta-Blue Metro Line (NCT-Delhi)

Location ID	Location Name	Area (km^2)	No. of PS	PS Density (PS/km^2)	Land Deformation (mm/year)				Groundwater change (m)		
					Max	Min	Mean	St. Dev.	Max	Min	Mean
L1-a	NLE: Battersea	0.68	7831	11516	17.04	-22.71	-6.05	2.42	-9.40	-5.70	-8.15

`

L1-b	NLE: Kennington	0.54	6360	11778	9.93	-10.26	4.55	1.37	10.61	6.20	7.52
D1-a	Magenta-Blue metro line: a	2.86	36930	12912	30.15	-18.49	-5.09	3.31	-2.32	-0.52	-1.38
D1-b	Magenta-Blue metro line: b	8.96	107198	11964	30.21	-18.69	11.06	4.61	+4.80	-1.16	+1.84

The NLE between Kennington and Battersea was proposed to help regenerate the Vauxhall, Nine Elms, and Battersea areas and is scheduled to be completed by the end of year 2021 (Transport for London, 2021). Figure 5.4a shows the displacement velocity map obtained from Sentinel-1 images between October 2016 and October 2020. It highlights distinct subsidence and uplift pattern near Battersea Power Station and Kennington, respectively. To help analyse these patterns, the time series of surface deformation for both the uplifting and subsiding areas were also extracted (Figure 5.4c,d).

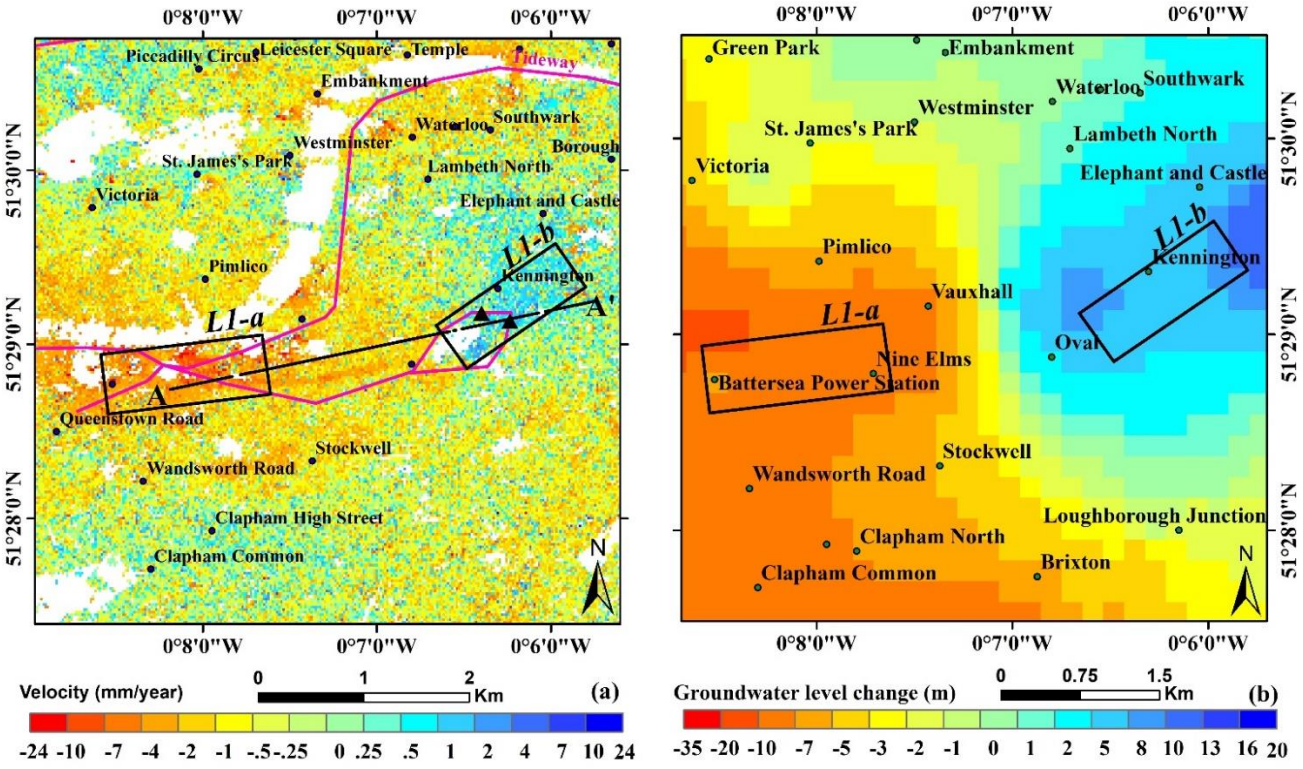

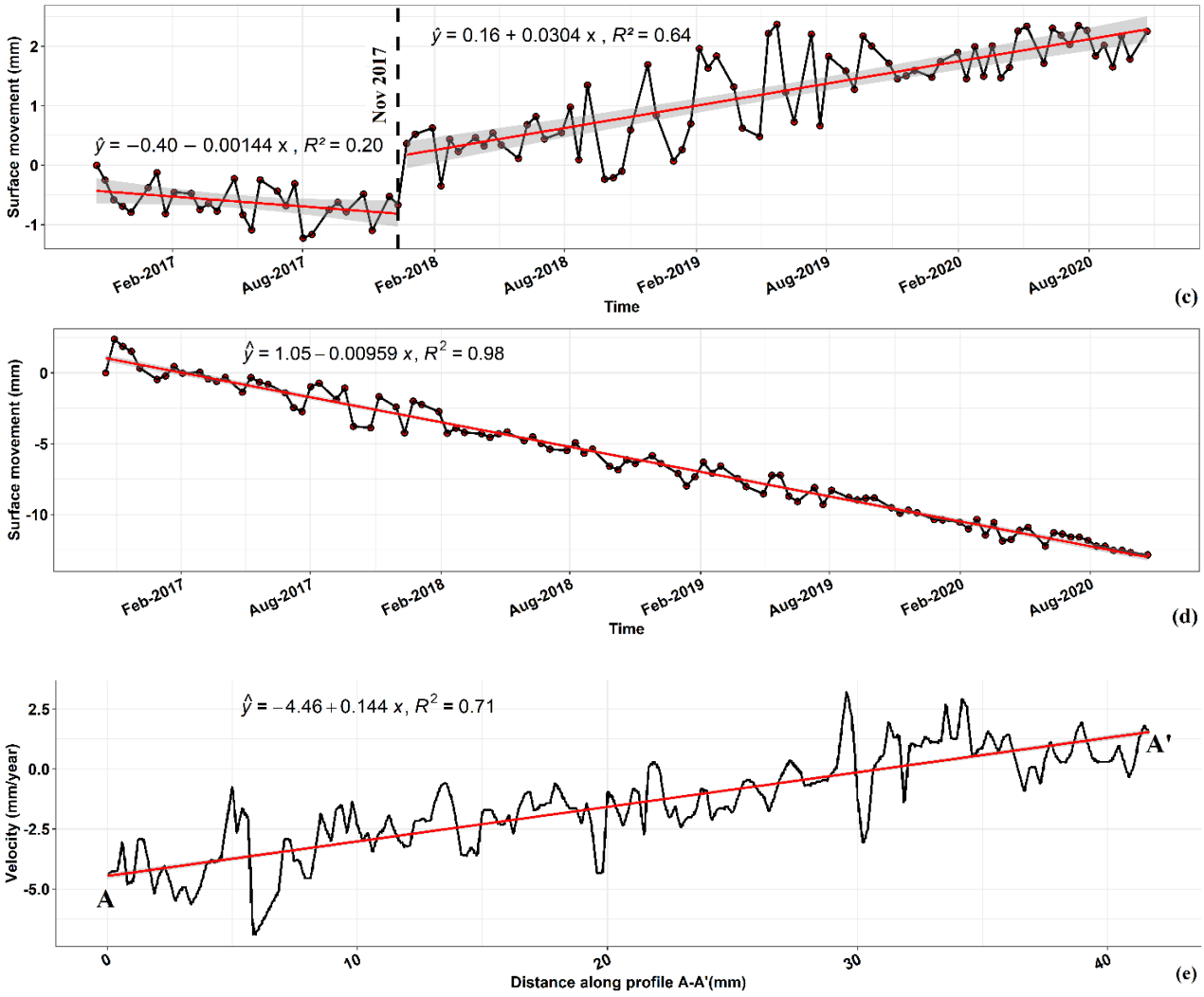

Figure 5.4: For Northern Line Extension: (a) PSInSAR land movement map, (b) groundwater change map, (c) time-series of land uplift (L1-b), (d) time-series of land subsidence (L1-a), and (e) profile across A-A' marked on Figure 5.4a. The black triangles in Figure 5.4a, represents the location of the two main dewatering shafts required for placing the tunnel boring machine.

The main tunnelling work of the NLE consisted of creating two tunnels between Battersea and Kennington Park. The construction for the NLE began in July 2016 (Transport for London, 2021) and required dewatering of the 'deep' aquifer, which includes the lower part of the Lambeth group. The dewatering shafts for the NLE are located on the northern edge of Kennington Park, and the location of the two main shafts required for placing the tunnel boring machines are shown in Figure 5.4a (black triangles). The geology of the area is relatively complex, with several faults, buried hollows and laterally discontinuous superficial strata (Transport for London, 2021).

`

The underground construction work, tunnelling shafts, and groundwater extraction contributed to the land motion pattern observed in this area. In Kennington, the average land motion trend during the observed time-period is that of uplift (Figure 5.4a), which is concurrent with the change in groundwater level (Figure 5.4b). However, the deformation time series exhibits phases of both subsidence and uplift during this period (Figure 5.4c). Specifically, the ground subsided during 2016–2017, before continuously uplifting since November 2017. This motion corresponds to subsidence due to dewatering during the construction of the tunnels, following by groundwater rebound (heave) once the dewatering ceased in November 2017. Around Battersea Power Station, the time series (Figure 5.4d) shows a linear trend of land subsidence between 2016 and 2020. The surface displacement here is consistent with the decrease in the groundwater level during this period (Figure 5.4b) and is most likely due to the groundwater abstraction that was undertaken to dewater the locality for the NLE tunnelling (Transport for London, 2021). The construction activities around Battersea Power Station are still ongoing; hence, the groundwater extraction and associated ground deformation can be seen to continue beyond the observed time-period.

A strong displacement gradient between Battersea Power Station and Kennington Park can also be seen in the displacement profile A-A' (Figure 5.4e). It reveals that the area near the Battersea Power Station is experiencing subsidence of up to 6 mm (near A), which gradually decreases in magnitude along the profile. The motion is reversed, close to Kennington Park, with an uplift of >2 mm at point A'. There are numerous faults in this area within the chalks (EA, 2019), which could potentially compartmentalise the aquifer and subsequently constrain the differential land movement within these segments.

Similar differential land movement can also be seen in NCT-Delhi in the area encompassing the Magenta-Blue Line metros (Figure 5.5a). The Blue Line metro is the longest metro line running on the Delhi metro network and was built in 2006 (DMRC, 2021). In Figure 5.5a, the area marked shows clear strong uplift sandwiched between Blue Line's (phase 1) Janakpuri East to Dwarka Mor stations on the north-eastern side, and Dwarka sector 14 to Dwarka sector 10 stations on the south-western side. Moreover, the Magenta Line (line 8, phase 3), a rapid transit system, passes through the intense part of the uplift area, where the underground metro stations of Dabri Mor (South Janakpuri), Dashrathpuri, and Palam stations are located. Most of the underground construction for these stations was completed by September 2016, and these then became

`

operational in May 2018 (DMRC, 2018). Dewatering in the area ceased at the end of 2016, and so the consistent uplift observed here most likely represents groundwater rebound.

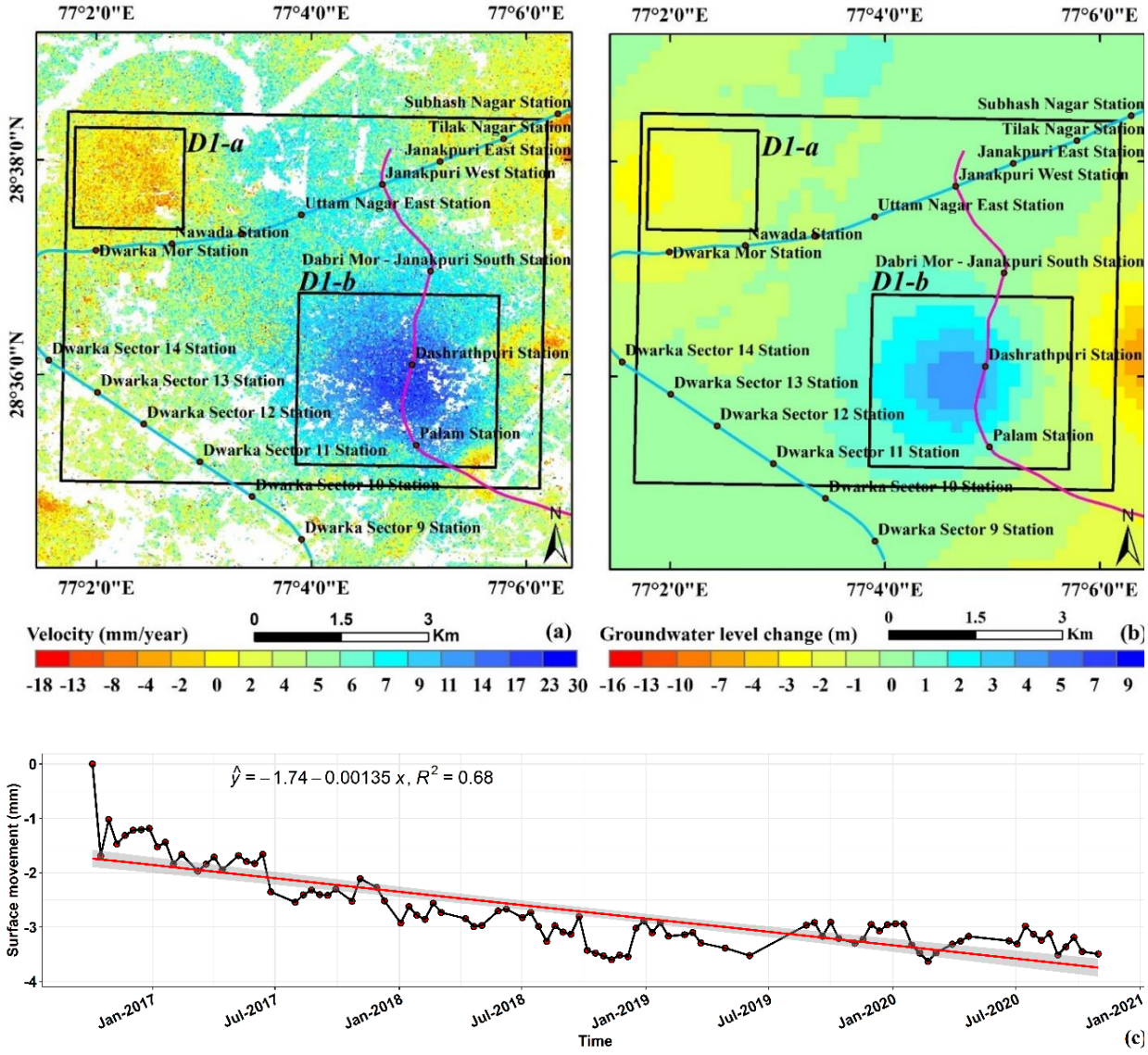

`

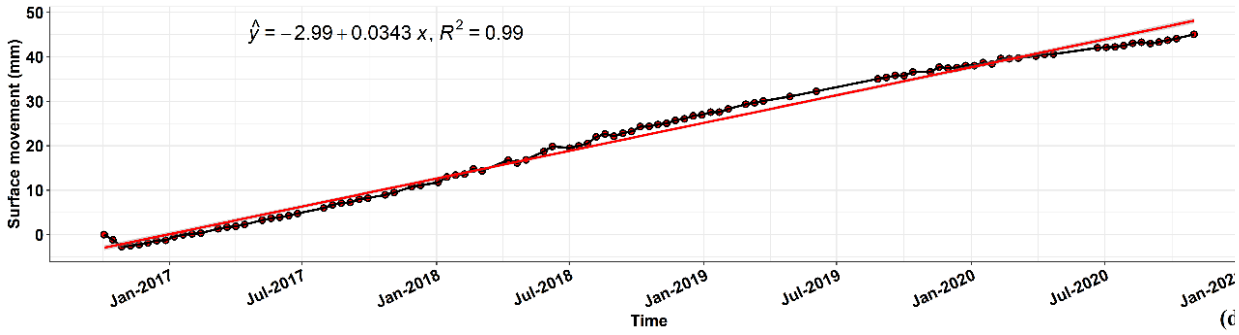

Figure 5.5: For Magenta-Blue metro line: (a) PSInSAR land movement map, (b) groundwater change map, (c) time-series of land subsidence (D1-a), and (d) time-series of land uplift (D1-b).

In Figure 5.5a, the area marked on the northwest (D1-a) is a heavily built-up area and contains buildings, roads, metro, temples, and other man-made structures. The area has an extent of 2.86 km^2 and contains 36,930 PS points. The average subsidence rate for the region is −5.09 mm/year. It includes the built-up urban areas of Laxmi Vihar, Ranjan Vihar, Shakti Vihar, Mahavir enclave, and important political buildings. The area also contains a densely packed residential complex, and consequently groundwater is extracted to meet the demands of the population, which could lead to subsidence (Central Ground Water Board, 2018). The groundwater variation agrees with the observed subsidence pattern on visual inspection (Figure 5.5a,b). From Table 5.5, it can be seen that at L1-a, the average decrease in groundwater is 8.15 m, causing a resulting average subsidence of 6.05 mm/year. On the contrary at L1-b, the average increase in groundwater is 7.52 m, causing a resulting average subsidence of 4.55 mm/year

Clearly, both cities have a complex pattern of land movement, which depends on several factors, including natural processes such as compaction of deposits on the river floodplain and anthropogenic instability due to water abstraction and recent engineering works. The main cause of local land uplift was found to be groundwater rebound after completion of underground activities, whilst that for land subsidence was groundwater extraction. The relationship between ground motion rates and groundwater pumping showed good agreement for both cities, in a qualitative sense based on visual comparison of the maps (Figure 5.4, 5.5), and in a quantitative sense based on the results in the Table 5.5.

`

5.5.2 Subsidence Areas

Areas where subsidence is dominant can also be seen in both London and NCT-Delhi. The London area extends from Wimbledon to Tooting (Figure 5.6), while NCT-Delhi area lies in the vicinity of Delhi-Haryana border (Figure 5.7). Table 5.6 summarises the statistics of land subsidence and groundwater depletion for both of these areas.

Table 5.6: Statics of land subsidence and groundwater depletion for Wimbledon to Tooting (London) and Delhi-Haryana border (NCT-Delhi)

Location ID	Location name	Area (km^2)	Number of PS	PS Density (PS/km^2)	Land Deformation (mm/year)				Groundwater change (m)		
					Max	Min	Mean	St. Dev.	Max	Min	Mean
L2	Wimbledon to Tooting	7.71	86822	11,261	22.89	-14.61	-4.87	1.19	-5.95	-13.79	-9.6
D2-a	Delhi-Haryana Border: a	1.65	13444	8148	28.43	-18.71	-5.28	5.26	-9.46	-5.97	-7.77
D2-b	Delhi-Haryana Border: b	4.70	26368	5610	30.19	-18.71	-4.37	7.71	-7.72	-4.87	-5.64
D2-c	Delhi-Haryana Border: c	0.40	4653	11632	28.01	-18.71	-3.74	6.63	-1.46	-0.73	-1.06

In Figure 5.6a, the area marked (L2) is located in south London and mainly contains urban built-up areas, which comprise construction, roads, metros, residential complexes, and other man-made structures. The PSInSAR analysis of this area achieved a PS density of 11,261 PS/km^2, with an average subsidence rate of −4.87 mm/year. The linear regression of the time series for average land movement of the area (Figure 5.6c) has a negative slope (i.e., subsidence), with an R2 value of 0.8. The area contains the urban centres of Tooting, Colliers, Dundonald Road, Wimbledon, and others. The London Clay Formation is predominant in the area, and clays, silt, and sand of the Lambeth group are also present in small deposits. More than 250 working borewells are present in the area (BGS, 2021), and the observed deformation pattern is mainly related to increased groundwater abstraction at these locations. Figure 5.6b shows groundwater change between 2017 and 2020, which shows groundwater level changes in the range of −5.97 to −13.7 m. In this area, water is abstracted from chalk up to depth greater than 70 m, and the groundwater level was lowered by an average of 9.6 m during the observed time-period.

`

The northwest edge of the area is bounded by the Wimbledon Fault. In this area, it appears that faults parallel to the Wimbledon Fault are controlling the local subsidence patterns, and groundwater movement (Bateson et al., 2009). It is also noteworthy that the width of the Thames floodplain increases markedly downstream of the Wimbledon Fault, due to the outcrop of the Holocene deposits. The author in (Aldiss, 2014) found that ground motions in this area were attributed to groundwater abstraction from the Merton Abbey public water supply well (green triangle in Figure 5.6a,b) during 1995–2005. This was further analysed in the framework of the BGS Terrafirma project, via the production of the Terrafirma, London H3 Modelled Product (Bateson et al., 2009). The study found striking correlation between variation in land movement and groundwater change at the Merton Abbey public water supply well, where the groundwater level dropped by 30 m enforcing subsidence of 0.5 mm/year.

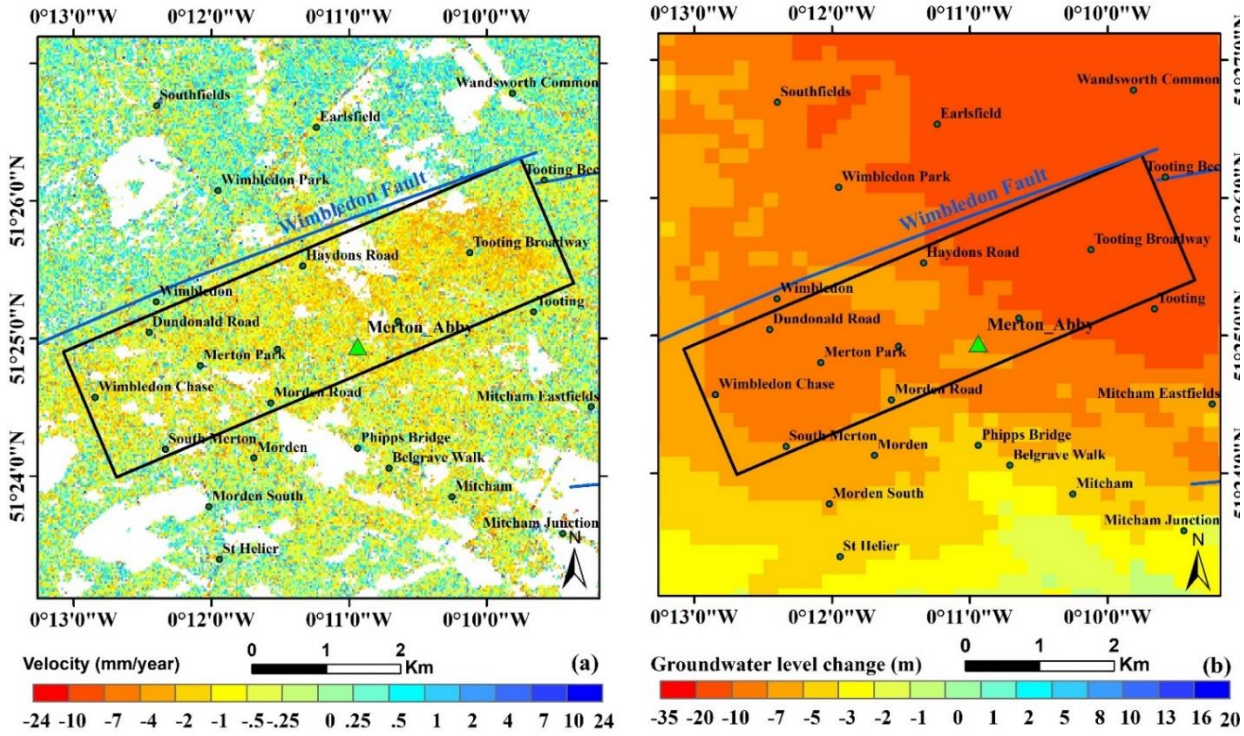

`

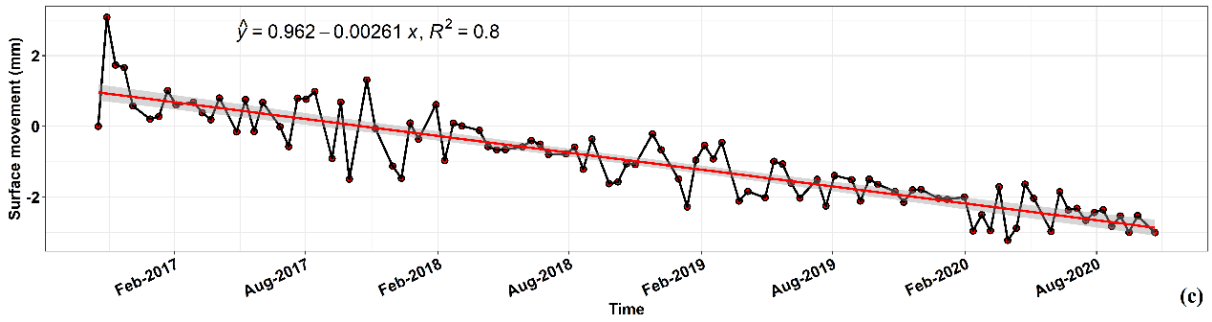

Figure 5.6: For Wimbledon to Tooting: (a) PSInSAR land subsidence map, (b) groundwater depletion map, and (c) time-series of land subsidence (L2). The green triangle in Figure 5.6a,b shows the location of Merton Abbey public water supply well.

The Wimbledon-Tooting area contains numerous underground metro stations where groundwater extraction and construction activities are carried out for repair and maintenance work. In addition, the area extends over only 7.7 km^2 and has more than 250 active boreholes clearly indicating that groundwater depletion is evident in this area. These are the driving force for the subsidence pattern obtained, and groundwater depletion map is consistent with the subsidence map.

A similar subsidence pattern can be seen in the vicinity of Delhi-Haryana border marked in Figure 5.7a. The area, as a whole, lies to the south of Airport Express metro line joining New Delhi to Dwarka sector 21. All three metro stations shown on Figure 5.7a (Delhi Aerocity, IGI Airport, and Dwarka sector 21) are underground stations and opened in 2011 (DMRC, 2021).

`

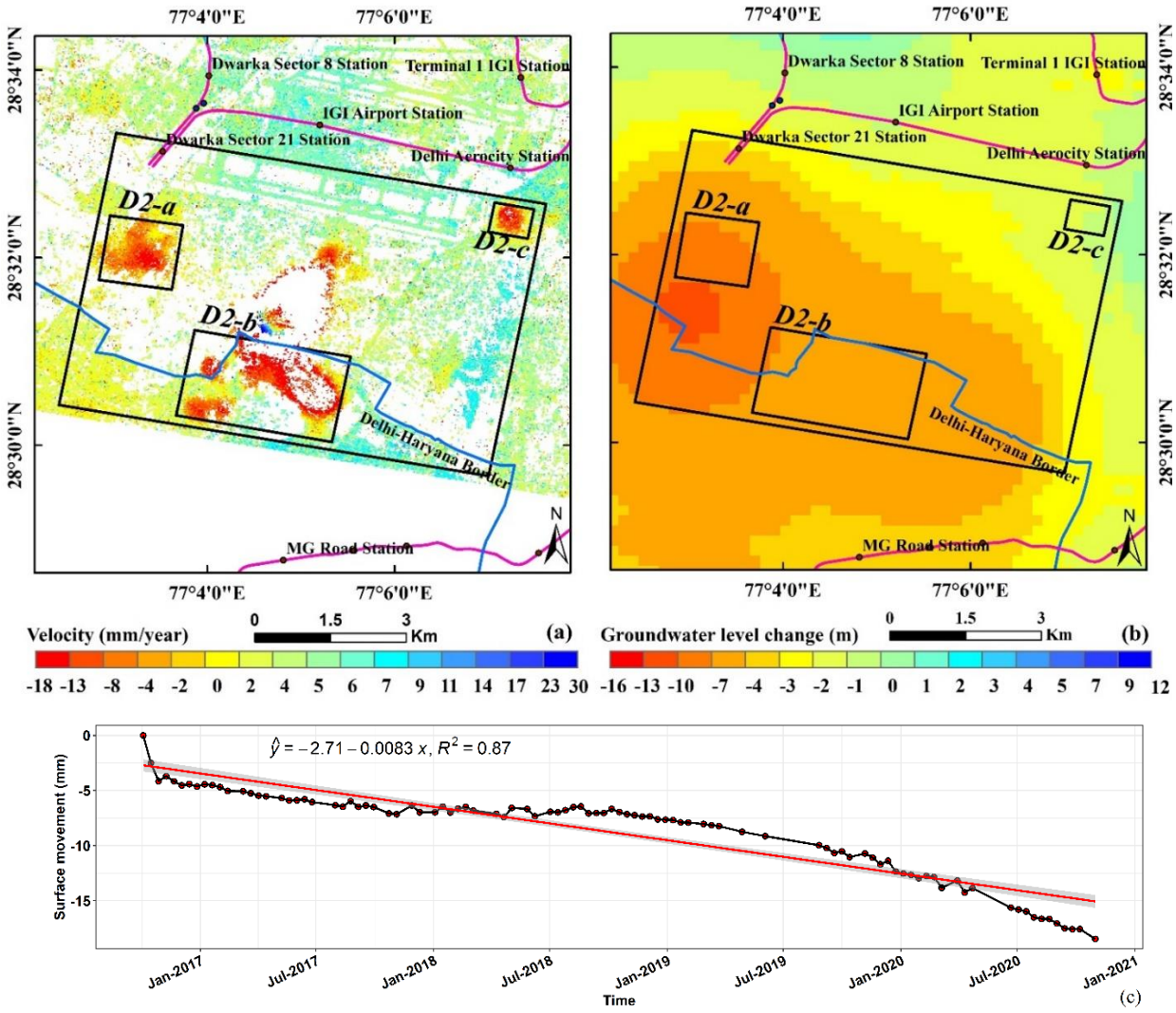

Figure 5.7: For Delhi-Haryana: (a) PSInSAR land subsidence map, (b) groundwater depletion map, and (c) time-series of land subsidence for the area (D2-b).

Additionally, the area under the three black boxes (D2-a, D2-b, and D2-c) in Figure 5.7a, are heavily populated areas with a high population density of 20,000 person/km^2 (Geoiq, 2021). The area D2-b, has a large population living on the borders of Delhi-Haryana, as these people can use the benefits of a capital city without paying the heavy living expenses (Google, 2021a). This increased population exerts heavy pressure on the groundwater resources and leads to groundwater depletion. The linear regression of the time series (Figure 5.7c) for average land movement of the study area (D2-b, in Figure 5.7a) has a negative slope (thus subsidence), with an R^2 value of 0.87. Moreover, continuous underground construction work is being carried out for extension of the metro lines (DMRC, 2018). The map of groundwater depletion (Figure 5.7b) is consistent with

`

that of subsidence maps, and so it can be reasonably concluded that the two are directly interdependent. Overall, the subsidence pattern for both cities (London and NCT-Delhi) is similar and interestingly controlled by the same factors, despite differences in their bedrock geology.

5.5.3 Uplift Areas

The The areas that experience notable uplift in London and NCT-Delhi are also evident. The London area stretches from Bruce Castle to Abney Park (Figure 5.8), while the NCT-Delhi area is across the Rohini metro line (Figure 5.9). Table 5.7 summarises the statistics of land uplift and groundwater change for both these areas.

Table 5.7: Statics of land uplift and groundwater augmentation for Bruce Castle to Clissold Park (London) and Rohini (NCT-Delhi)

Location ID:	Location	Area (km^2)	Number of PS	PS Density (PS/km^2)	Land Deformation (mm/year)				Groundwater change (m)		
					Max	Min	Mean	St. Dev.	Max	Min	Avg
L3	Bruce Castle to Clissold Park	13.8	150,354	10,895	23.09	-20.54	3.64	1.21	8.28	-0.04	3.48
D3	Rohini	10.1	99,665	9867	29.49	-18.14	6.30	2.17	1.50	2.58	1.97

The area marked in Figure 5.8 contains Holocene alluvium, and the uplift is observed due to groundwater rebound arising from aquifer recharge for an area of 13.8 km^2. The InSAR results show an uplift of 3.64 mm/year based on a PS density of 10,895 PS/km^2. The linear regression line for the time series (Figure 5.8c) shows a positive slope (i.e., uplift), with an R^2 value of 0.6. Visually, the groundwater change map is consistent with the land subsidence map. This area is a low-lying river flood plain with elevations between 2 and 14 mAOD. The bedrock geology is dominated by the London Clay formation, silt, and sand of the Lambeth Group, whereas superficial deposits in the area consist mostly of alluvium of the River Thames and River Lee. The area has several water reservoirs and recreation parks, which assists with the recharge of groundwater. The recreation parks include Clissold park, Abney park, Downhills park, Lordship recreation ground, and Bruce Castle park; and the reservoirs include East and West Reservoirs with Warwick and Lockwood reservoir in the area's vicinity (Google, 2021b). Seepage from the various water reservoirs and artificial watering of the various recreation parks are the important contributing

`

factors for the increase in groundwater level, which is likely attributable for the land uplift observed.

The area marked in Figure 5.9 shows the Rohini area, with the Red Line metro stations, which consists of the first stretch of the Delhi Metro. These stations were built in phase 1 Red Line and opened in 2004 (DMRC, 2021). Figure 5.9a shows the displacement velocity map obtained from Sentinel-1 PSInSAR analysis between October 2016 and October 2020 and reveals distinct uplift with an average rate of 6.30 mm/year. The groundwater variation map is visibly consistent with the pattern shown in the land deformation map, and the time series also confirms continuous uplift. This is one of the wealthiest areas of Delhi city and is subject to managed groundwater abstraction and recharge (Mammen, 2021). This has led to a rise in groundwater level and the subsequent continuous uplift.

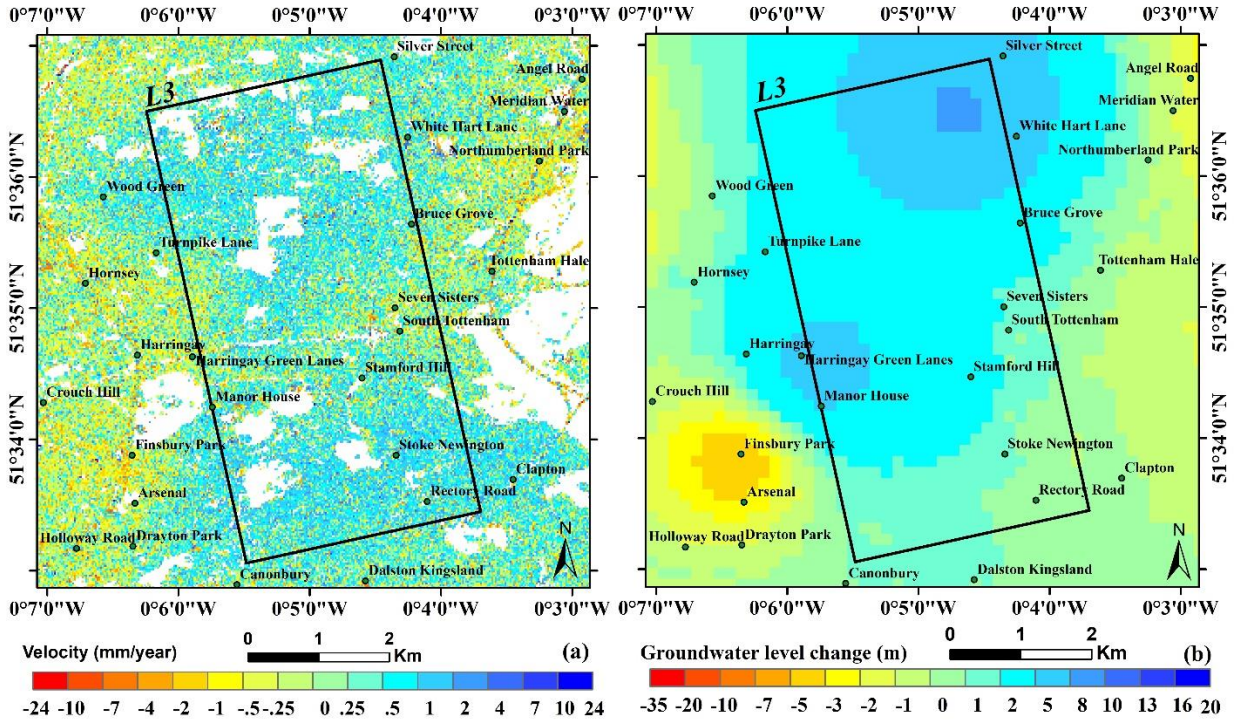

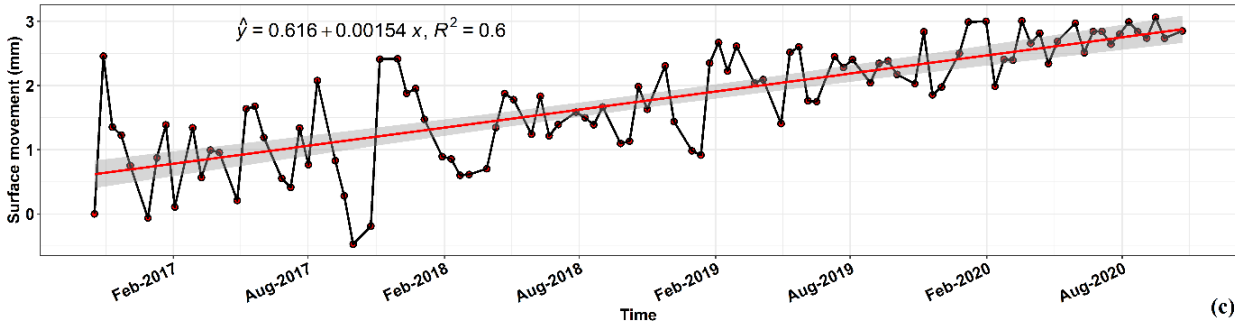

Figure 5.8: For Bruce Castle to Abney Park: (a) PSInSAR land uplift map, (b) groundwater augmentation map, and (c) time-series of land uplift for the whole area marked in box.

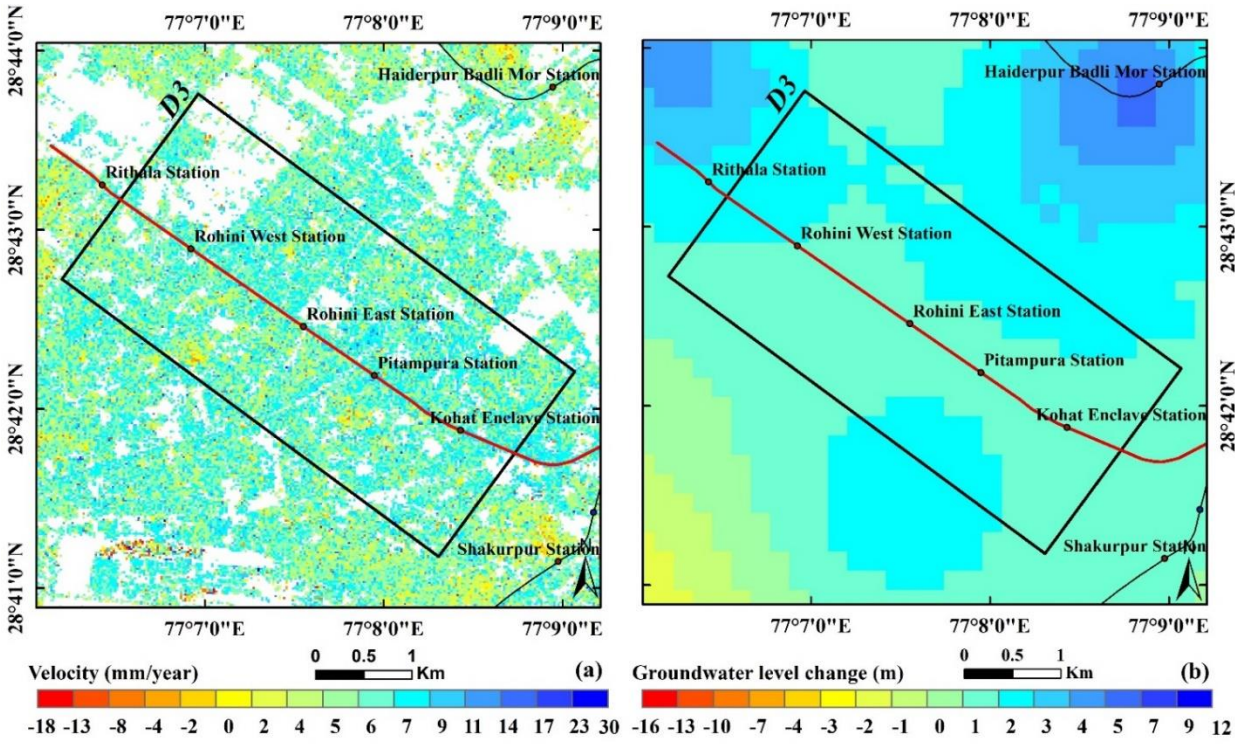

`

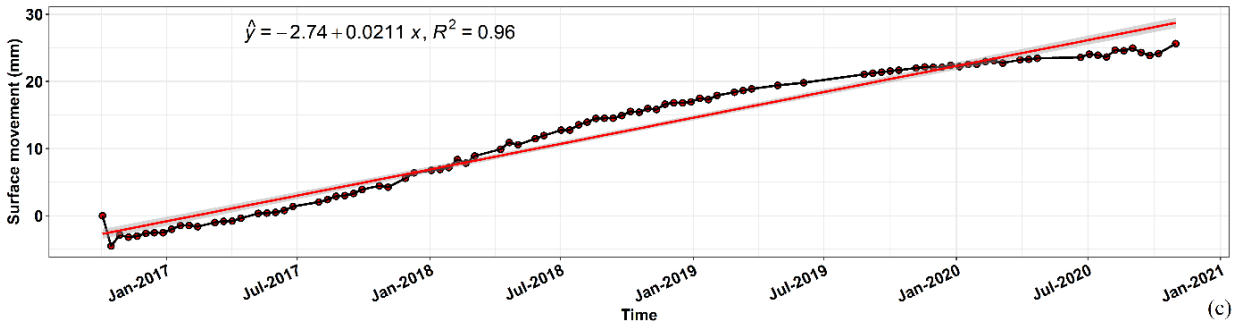

Figure 5.9: For Rohini PSInSAR: (a) land uplift map, (b) groundwater augmentation map, and (c) time-series of land uplift for the whole area marked in box.

5.5.4 Modelling of Land Deformation due to Groundwater Change

The results discussed in Sections 5.1–5.3 establish that a reduction in groundwater level can result in the compaction of strata and subsequent subsidence of the overlaying terrain. Due to a change in hydrostatic pressure, the amount of compaction depends on the rock matrix's physical properties and the strata's geological setting. A mathematical model was constructed to calculate the expected land deformation owing to a given change in the groundwater level.

The model requires input parameters of the change in groundwater level, the thickness of underlying geological units, and geological characteristics (Table 5.2). The model is set to run for any number of time steps, the size of which are defined by the rate of piezometric head reduction. As the model time-step is advanced, it recalculates the new formation thickness, void ratio, and compaction. A monthly rate was found to be the best compromise between time and resolution. For our study, two test cases were conducted using differing temporal resolutions for the groundwater level fluctuation:

Case 1 required the model to be run using a 4-year average change in groundwater for all the locations studied above in London and NCT-Delhi. The 4-year average was divided into monthly rates for each location, and the model was run for the 4-year (48 months) duration.

Case 2 focused on a single location at Battersea Power Station, London. Here, monthly rates of head fluctuation were used, based upon levels measured at a groundwater pumping station. The model was tested only for one location in London since continuous monthly groundwater variations for other locations could not be obtained.

`

The results obtained from case 1 are summarised in Table 5.4. The difference in land-surface deformation rate calculated using the model and measured using PSInSAR varied between 0.26 and 4.83 mm/year. The correlation between both methods is shown in Figure 5.10. The deformation rates from both the methods have R^2 value of 0.881, indicating a very high rate of correlation, thus validating the model and PSInSAR results. It also confirms confirm quantitatively that the observed deformation is directly associated with changes in the groundwater level.

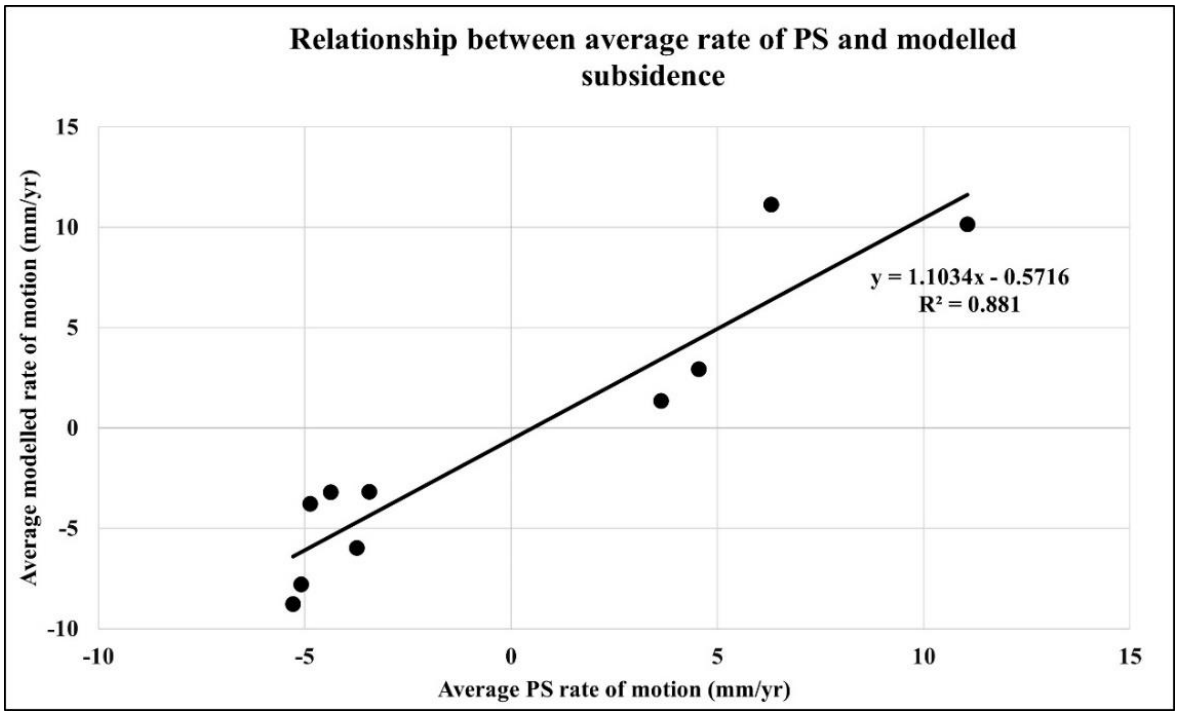

Figure 5.10: Correlation between the modelled and PSInSAR measured land-surface deformation.

For the Battersea case, the monthly groundwater fluctuation was obtained for 4-year period between October 2016 and November 2020. The piezometric head exhibited a constant decrease in groundwater levels. The compaction predicted by the model over the 4-year pumping period for Battersea is given in Figure 5.11. As no time-lag constant was used, the modelled variation in compaction rate varies considerably on a monthly scale, in-line with the groundwater levels that were input. August 2016 was used as the datum for the groundwater change and compaction rates. The land movement from two different datasets is interestingly very similar. Direct comparison of the motion rates is not possible since the dates when groundwater levels were measured and the radar scenes were acquired are not coincident. Statistically, the two datasets are very similar; the average rate of motion for the PSInSAR is −6.05 mm/year and for the modelled motions it is −5.51

`

mm/year, which is a difference of just 0.54 mm/year. The small difference between the modelled deformation for a given groundwater level (using either case 1 or 2) and the actual measured deformation (from PSInSAR) adds confidence to the argument that the observed motion is indeed primarily associated with the groundwater change.

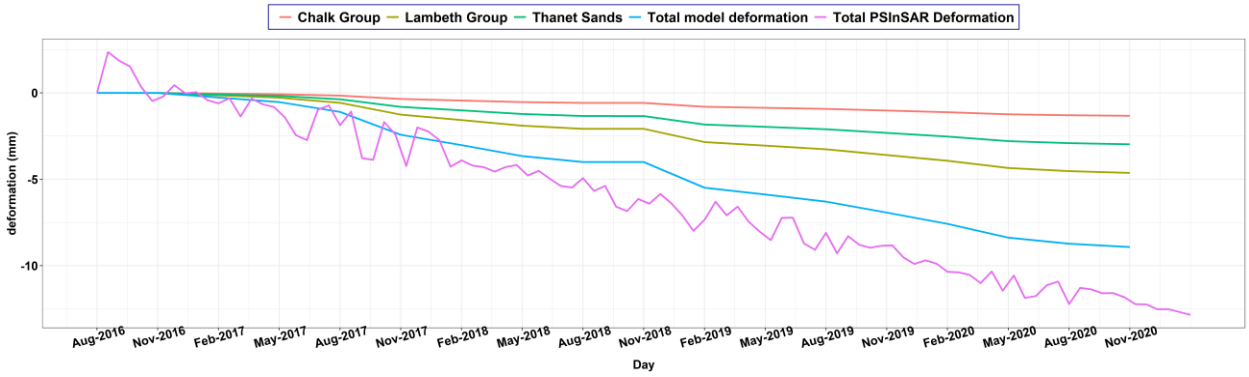

Figure 5.11: Time series for modelled and PSInSAR measured land-surface deformation for Battersea, London.

The validation of PSInSAR with ground-based measurements may need a more systematic approach, beyond comparing individual time series. Further analysis of the different settlement areas should focus on different stretches to properly understand the influence of local geology, using more detailed numerical modelling of the predicted settlement trough to compare with PSInSAR data. Investigation of the relationship between reported structural damage and observed deformation patterns measured would also be very useful, for example, is there a critical rate of settlement or slope.

Further geological investigations—using borehole logs, piezometer readings, and other data—should be undertaken of anomalous features to determine whether they do indeed relate to geological structures, particularly faults and buried hollows, which are a significant hazard in Civil Engineering. An improved understanding of the Chalk-Basal Sands aquifer through a more detailed analysis of settlement and subsequent rebound might reveal whether the behaviour is partly non-elastic and whether previous dewatering affects the ground response. PSI monitoring could be of real benefit to groundwater management in London and Delhi if the regional surface response can reliably be related to aquifer changes—a relationship which may differ across London and Delhi—using long time series piezometer and PSI observations.

`

5.6 Conclusions

In this study, the land movement pattern for London and NCT-Delhi during 2016–2020 was examined using the PSInSAR methodology, and sought to establish the factors governing this land movement. Both cities were found to have experienced long-term, complex, non-uniform patterns of land motion in the spatial and temporal domains. Different types of site-specific movement of uplift, subsidence, and differential motion, along with the corresponding groundwater variations were analysed. Across both the cities and all types of movement, the most common factor controlling the spatial patterns of land motion was the change in groundwater level. It can be concluded that when groundwater is extracted from an aquifer, it decreases pore pressure, and thus leads to land subsidence. Conversely, a rebound or recharge of groundwater leads to land uplift. NCT-Delhi has been declared as a groundwater critical zone by the government of India. It is one of the most exploited cities with regards to groundwater owing to its urban fabric and ever-increasing population, and these results offer confirmation of that. London is not recognised by a critical status, but its ever-increasing population and government's aquifer recharge policy exerts local pressure and this is borne out by results shown for areas L1-a and L2. Along with the groundwater extraction and recharge, sub-surface geology, underground construction, and metro extensions all contribute to form a complex land movement pattern.

The results obtained from the mathematical model agree well with our PSInSAR results. The formations are considered homogeneous, and the water removal is considered as a rate of piezometric head reduction (m/time) and not a quantity removed (m^3), and the time-lag constant was not considered in the model. It is however possible to apply the time-lag constant to the output after the model if an approximation of the time-lag is required. The accuracy of the model relies on the accuracy of the groundwater level input, and with actual observed groundwater data, the model could be verified for other locations as well. Since, the model is able to estimate the land-surface deformation rate and pattern for a known groundwater level change, it could be useful for assessing and mitigating risks associated with ground deformation.

Whilst the two cities are superficially different in terms of civil engineering, the response of their groundwater to engineering decisions (such as underground metro construction) and how that is reflected in change in surface-level tells a similar story. This suggests that it may be a universal effect, which might be anticipated by observing in other major cities worldwide, which are

`

subjected to similar engineering decisions. Some InSAR deformation relating to groundwater results have been presented before for London, but not in NCT-Delhi. The purpose of the paper was to demonstrate that a groundwater and subsidence inter-relationship generally holds true. This study can serve as a guideline to government agencies in identifying the areas and extent of groundwater-induced land subsidence, and to take proper steps to mitigate them.

Author Contributions: Conceptualisation, Vivek Agarwal, Rachel L. Gomes and Stuart Marsh; Data curation, Vivek Agarwal, Amit Kumar and Stuart Marsh; Formal analysis, Vivek Agarwal, Amit Kumar, David Gee, Stephen Grebby, Rachel L. Gomes and Stuart Marsh; Funding acquisition, Vivek Agarwal; Investigation, Vivek Agarwal, Amit Kumar, Stephen Grebby, Rachel L. Gomes and Stuart Marsh; Methodology, Vivek Agarwal, Amit Kumar, David Gee, Stephen Grebby, Rachel L. Gomes and Stuart Marsh; Resources, Vivek Agarwal; Software, Vivek Agarwal and Stuart Marsh; Supervision, Rachel L. Gomes and Stuart Marsh; Validation, Vivek Agarwal, Stephen Grebby and Stuart Marsh; Visualisation, Vivek Agarwal and Stuart Marsh; Writing – original draft, Vivek Agarwal; Writing – review & editing, Amit Kumar, David Gee, Stephen Grebby, Rachel L. Gomes and Stuart Marsh.

Acknowledgments: The authors would like to thank the European Space Agency (ESA) for providing access to SARscape software for processing of InSAR data through Eohops programme. The authors would also like to thank the Environment Agency for providing the "management of the London basin chalk aquifer" status reports.

`

Chapter 6 Groundwater quality of London

Preface

Chapters 3, 4, and 5 present the study of change in groundwater quantity and its associated land movement. To understand the overall behaviour of groundwater, the study of its quality is equally important as its quantity. The availability of groundwater in ample amounts does not guarantee that the water is potable and can be used safely. Water quality inspection is essential before sending it to the treatment process. Knowledge of the quality status of raw groundwater can significantly help to reduce the cost of the treatment process, and sometimes when the groundwater quality is good enough for drinking, it can be used directly without any treatment process.

Groundwater quality monitoring is an essential element in any environmental information system. Based upon validated groundwater monitoring data, information is derived on which decisions can be made. Constant monitoring provides the necessary data input for our smart environment and forms the basis of the decision making process concerning spatio-temporal planning and climate change adaptation.

The groundwater quality of London for the last two decades have not been studied comprehensively in the literature. Thus, the variation of groundwater quality and various physicochemical parameters for groundwater in the London basin between the years 2000 and 2020 is investigated in this chapter. The EA provided the data for the study in open domain. The spatial and temporal variation of different water quality parameters is studied, and their interdependence on each other is studied using Pearson correlation analysis. GIS and statistical tools have been used to derive readable and valuable data from the EA data, which is highly inconsistent in both spatial and temporal domains.

The study helps to monitor the sustainability of the London aquifer as a safe and stable water supply and adjust appropriate policies accordingly. It contributes to identifying subsurface contaminants and points to a need to narrow down the contamination sources. This study provides the data and methodology based upon which water boards and municipalities can take appropriate mitigation measures to protect the groundwater quality of London. This study was submitted as a research paper at ‘Journal of Hydrology: Regional Studies’, entitled ‘*Evaluating spatio-temporal*

`

decadal-scale changes in groundwater quality for London, 2000-2020. The published paper is presented here in this Thesis as Chapter 6.

Abstract: The groundwater is relatively a pure natural resource as compared to the surface water, but anthropogenic activities pose a threat to its quality and suitability for drinking. Thus, monitoring of spatio-temporal variation of groundwater quality is very important for its management and protection. Geographical Information System (GIS) and statistics can be useful to monitor and evaluate the groundwater quality. For London, there is no comprehensive work in the last two decades for studying the spatio-temporal variation for monitoring groundwater quality and its parameters. The data samples have been used from 500 wells in London basin and the data is provided in free access open domain by Environment Agency. The Trilinear-Piper plot highlighted overall groundwater as dominant magnesium bicarbonate type and spatio-temporal variation of hardness, sodium, and dissolved oxygen (DO) was studied. Large variations in the range of each constituent were found, which was attributed to variation in geology of the London Palaeogene aquifers and anthropogenic activities. This research can be used to determine whether groundwater is suitable for its intended purpose, discover pollutant inputs, and examine any temporal variations.

6.1 Introduction

Groundwater is a substantial resource to meet the water demand on earth. In England, approximately 35% of public water demand is fulfilled using groundwater, and for south and east England, this contribution rises to around 70% (Bonì et al., 2016). It also contributes to maintain baseflows to rivers and wetlands during dry seasons and thus ensures a sustainable water-cycle (Royse et al., 2012). The quality of groundwater stored in aquifers below earth's surface is under an ever-increasing danger from anthropogenic factors (Foster, 2020; Jha et al., 2020; Lall et al., 2020; Lerner & Barrett, 1996; Pérez et al., 2019; Qian et al., 2020; Talabi et al., 2019; Tiwari & Pal, 2021). The groundwater chemistry changes through direct and indirect effects of anthropogenic activities such as over extraction of groundwater, infiltration of polluted water, mixing of chemicals, pesticides or fertilizers and landfill. The contamination of groundwater by agricultural, industrial, and urban activities is a serious threat to long-term groundwater sustainability (Bearcock et al., 2019).

`

The groundwater ideally must abide by the water cycle, which primarily consists of groundwater recharge through rain water, which flows through subsurface voids in unsaturated areas; and abstraction from boreholes or springs. Thus the constituent aspects of urban growth that interfere in the natural water cycle, consequently affecting the groundwater quality and quantity, must be taken into account. Changes in groundwater tables because of its overuse, dewatering for domestic and industry uses, and loss during urban water transport are all aspects of urban areas that have an effect on groundwater boundary conditions. Groundwater level is maintained by governmental and water supplying agencies, such as Thames Water Utilities Limited (TWUL, 2020) in London, to track these effects when they are quantifiable at a regional scale.

A variety of anthropogenic activities influence the physical features of urban groundwater systems. The building of on-surface and underground layers that obstruct water flow has the greatest impact. The infrastructure and related facilities, such as buildings, pavements, parking, swimming pools, and the range of underground constructions that facilitates conveyance, are all examples of anthropogenic hard surface material construction in urban environments. The building of "impermeable hard surfacing" not only inhibits water seepage to the subsurface due to the less permeability of the construction materials, but it is also frequently coupled with surface stress and compression, which seals near-surface voids, thus reducing infiltration.

To observe, manage and protect groundwater quality are important economic and environmental concerns. Temporal and spatial changes in groundwater quality may arise because of various atmospheric stimulations, varied geology, variation in subsurface mineralogy and factors controlling residence times (Aldiss, 2014). Keeping track of groundwater quality fluctuation over time can assist decision-makers to better comprehend the long-term viability of an aquifer as a source of water and make appropriate policy decisions (Alley, 2007).

Half of the world's megacities are believed to be groundwater dependent, while aquifers beneath metropolitan areas provide over 40% of water supply in parts of Europe (Wolf et al., 2007). Furthermore, in metropolitan locations, groundwater resources include not just water for home and industrial use, but also ground source heating. For example, in London, it is anticipated that ground heat sources could meet 19% of the city's entire heat demand (Greater London Authority, 2013).

Historically, the groundwater quality of London shows large variations at spatial and temporal scales both between and within aquifers (Bearcock & Smedley, 2010). Also, the anthropogenic

`

activities are continuously changing the natural groundwater chemistry in London. The groundwater chemistry for London basin and its variability is discussed in (Ineson & Downing, 1963), which summarised that the carbonate and non-carbonate hardness decreased while sulphate and chloride concentration increased towards the center of the London basin. (Flavin & Joseph, 1983) noticed abnormally high values of sulphate, calcium, magnesium, iron, and manganese. They also found a high concentration of sulphate in Lee catchment where London clay was thin or absent. In the late 20th century, high concentration of iron, sulphate, and manganese have raised concern for the groundwater aquifers in London (Flavin & Hawn, 1979; Flavin & Joseph, 1983). Some other studies on groundwater quality focused on London basin are on lee valley (Kinniburgh et al., 1994) and on the western end of the basin in Berkshire (Edmunds et al., 1987). Rae and Parker (1992) found that areas with very less or no London clay witness pyrite oxidation as during dewatering oxygen can actively enter these areas. Pyrite oxidation releases iron into pore waters, as well as other key mineral changes such as carbonate dissolution and the synthesis of iron oxides and hydroxides. The British Geological Survey (BGS) published a report on 'Baseline groundwater chemistry: the Palaeogene of the Thames Basin' in 2010 (Bearcock & Smedley, 2010), and found that London groundwater witnessed problems related to pyrite oxidation, which occurred irregularly in Palaeogene deposits, and can cause acidic, hard, metal-rich waters. The accountability for groundwater management of London is discussed in Bricker et al. (2017).

The concentration of groundwater quality parameters varies significantly on a local scale, and thus drawing basin-wide predictions becomes difficult (Shand et al., 2007). The UK Government Office for Science has conducted a city foresight exercise with the goal of gathering scientific data to support policy decisions and to inform the measures to be taken required to create the UK's urban future (Go-Science, 2021). While investigating groundwater use for domestic and industrial water supply in London is critical, the baseflow index (BFI) for the River Thames at Kingston is 0.63 (NFRA, 2021) indicating that groundwater accounts for 63% of river flow. This shows how groundwater from the larger river watershed helps to support London's surface water abstraction.

For London, there is no comprehensive work in the last two decades for studying the spatio-temporal variation for monitoring groundwater quality and its parameters. This maybe because insitu water quality monitoring over large temporal and spatial scales is difficult, and remote sensing water quality monitoring is still a developing science. and A comprehensive assessment of groundwater quality focused on London is required in order to allocate resources to maintain

`

potable-quality groundwater. The main objectives of this study are to (1) describe temporal and spatial trends in groundwater quality parameters potentially used for drinking water supplies in London between 2000-2020, (2) Determine the hardness, sodium, and dissolved oxygen concentration and potential sources in the groundwater in the London basin, and (3) To examine an integrated dataset of concentrations of groundwater quality parameters, available in open domain, for London, as a foundation for a comprehensive assessment. This study highlights baseline information, chemical status and key pressure on groundwater quality, which should be valuable information to government bodies, water regulators and environment scientists.

6.2 Study area

This study is focused on the administrative boundary of the London city (Figure 6.1) and extends over 0°30′ W to 0°20′ E longitudes and 51°42′ N to 51°17′ N latitudes, with around 1600 km^2 area in the southern part of England. Table 6.1 and Figure 6.2 shows the geological age and thickness of the bedrock geological formations found within the London Basin.

London is a good representative for examining groundwater in urban areas since it is a megacity with a strong historical legacy and has gone through many eras of development. It is situated in the River Thames catchment's estuary and the Chalk aquifer, which is the UK's most important aquifer (MacDonald & Allen, 2001), lies beneath the city. Clays with interbedded sand and gravel deposits cover and confine the aquifer. The chalk group forms a rim surrounding the London basin, which comprises younger Paleogene layers. The chalk group is over 200 m deep in central London (Ford et al., 2010; Mathers et al., 2014). The hydrogeology of the London basin is heterogenous in nature as Paleogene deposits confine the underlying chalk aquifer around central London, and thus sand-rich strata can contain huge amounts of groundwater. The Chalk aquifer is protected by these overlaying deposits, which also provide a limited amount of additional resource from the more permeable granular deposits. Figure 6.2 shows the distribution of rock units in the London and the Thames Valley region. Figure 6.2c shows schematic south-west to north-east cross-section through the Thames Valley from the Marlborough Downs to the Chiltern Hills. Figure 6.2d shows schematic north-west to south-east cross-section through the Thames Valley, passing through London. The older sedimentary rocks such as limestone forms the base layers, while the younger sedimentary bedrock such as palaeogene and cretaceous sediments forms the upper layers. Table 6.1 and Figure 6.2 together gives a complete picture of subsurface geology for London basin.

`

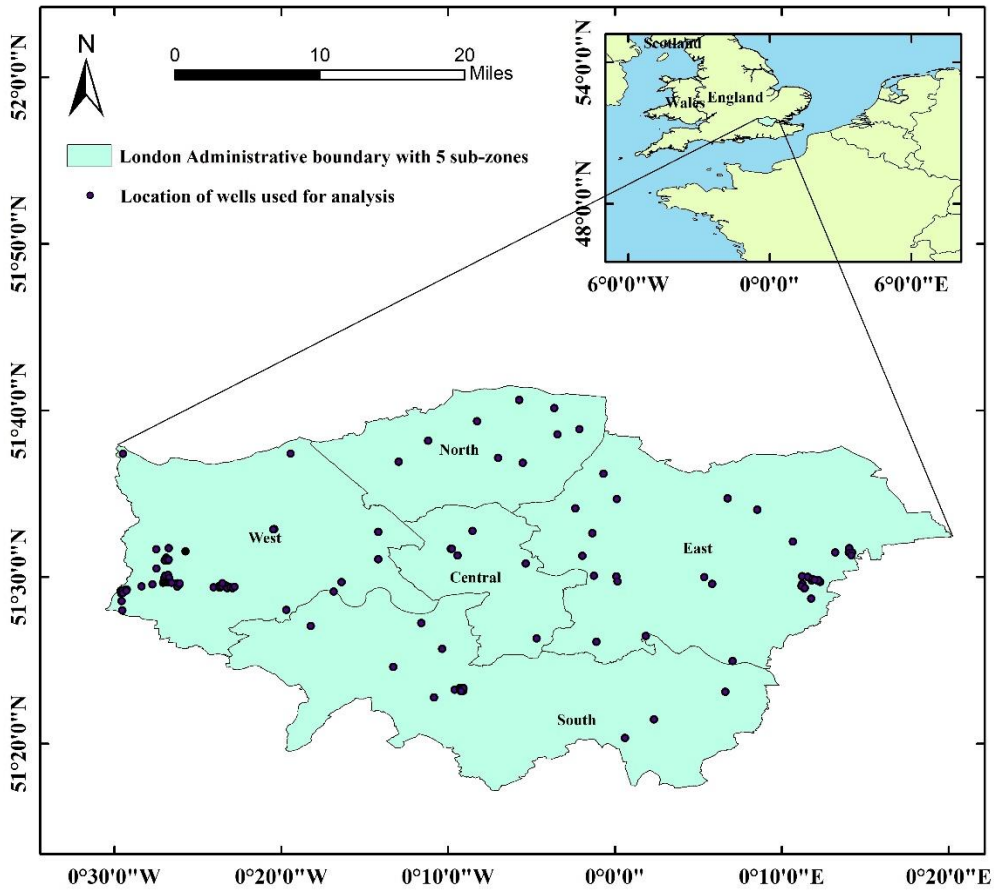

Figure 6.1: Study area showing London in 5 subzones as per Great London Authority, 2011 (GLA, 2011)

Table 6.1: Geology of the London Basin (adapted from EA status report 2010)

Era	Group	Formation	Thickness (m)
Palaeogene	Thames	Bagshot Formation	10-25
		Claygate Member	30-90
		London Clay	
		Harwich Formation	0-10
	Lambeth	Woolwich and Reading Beds	10-20
		Upnor Formation	5-7
		Thanet Sands	0-30
Cretaceous		Chalk	180-245

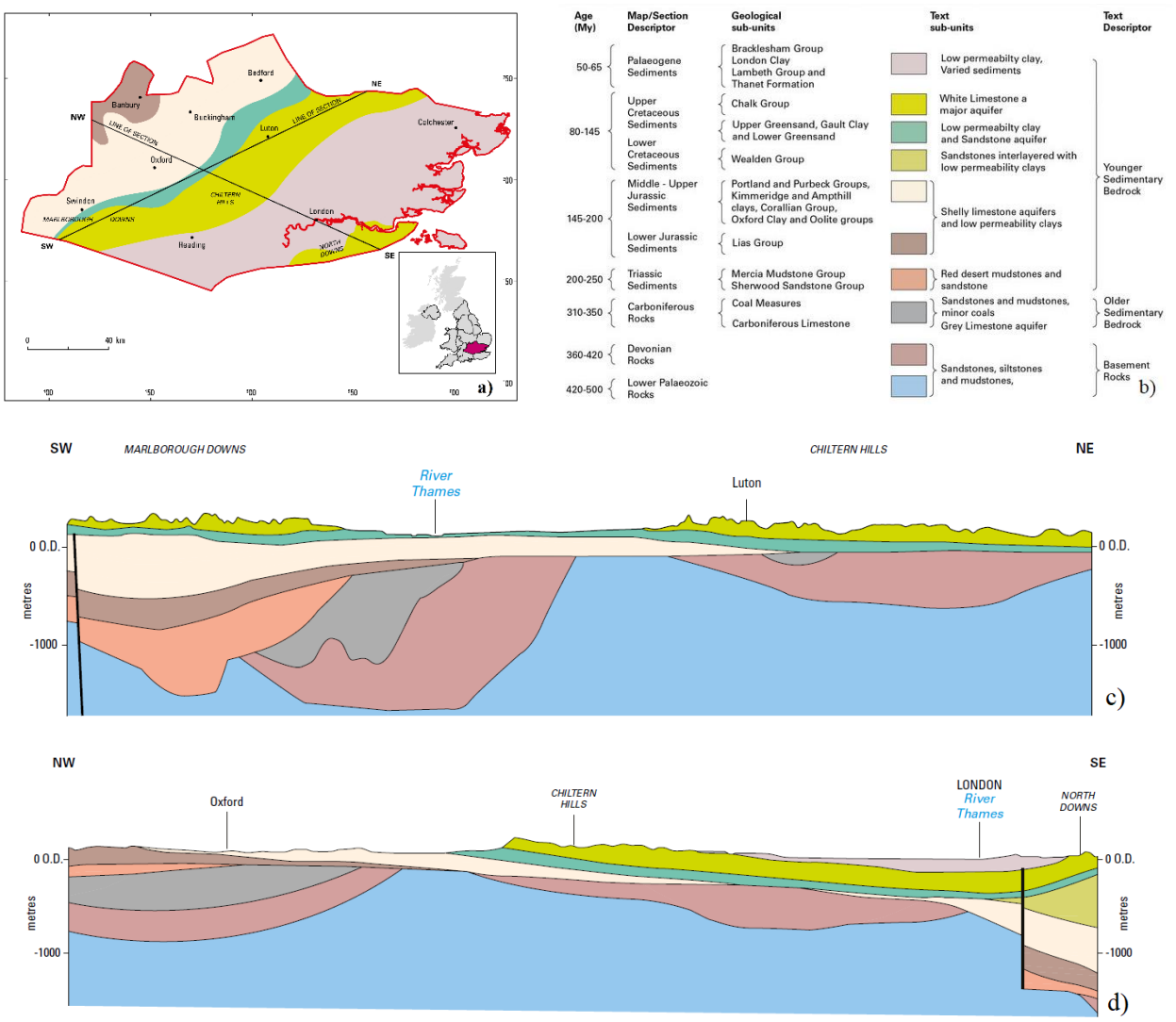

Figure 6.2: a) Generalised geological map showing the distribution of rock units in the London and the Thames Valley region. The inset shows the extent of the region in the UK. The bold black lines give the locations of the cross-sections shown in Figures 6.2c and 6.2d. Figure 6.2b shows the key to the rock types shown. Figure 6.2c shows schematic south-west to north-east cross-section through the Thames Valley from the Marlborough Downs to the Chiltern Hills. Figure 6.2d shows schematic north-west to south-east cross-section through the Thames Valley, passing through London. Note that the vertical scale is greatly exaggerated and actual dips of rock layers are much gentler than they appear here. Modified from (RWM, 2019)

The Chalk aquifer in the United Kingdom (UK) accounts for roughly 60% of all groundwater used (BGS, 2013), providing approximately 80% of water supply in the Thames basin and 20% in London alone (Bonì et al., 2016). The Chalk aquifer in London meets the water demand of humans

`

since the 1850s and is one of the most supervised groundwater resource in the UK (Royse et al., 2012). The sufficient availability of groundwater in London in terms of quality and quantity, have played significant part of its industrial development (Wilkinson & others, 1985); similarly changes in industry are reflected in fluctuations in water demand and water resilience (groundwater resource, energy, hazard and ecosystem services).

The London basin is an asymmetric syncline that plunges gradually to the east along an ENE-WSW fold axis. There is also a sequence of smaller, parallel folds that run beside it. Gentle folds with a significant NW-SE axial direction emerged from the deformation. Dome formations have resulted from the axial intersection of the two sets of smaller folds, which have experienced significant erosion (Rae & Parker, 1992). Also, the study area is demarcated by faults and distinct permeability of each fault leads to irregular groundwater flow (Agarwal et al., 2020b; Freitas, 2009).

London is one of the world's greatest urban economies, with a population of about 8.5 million people. London's job market is predicted to increase to 5.8 million jobs by 2036, up from 4.9 million in 2011, and an additional 1 million households will be accommodated during that time (GLA, 2021b). Simultaneously, considerable infrastructure investment of the order of £1.3 trillion is expected by 2050. While majority of this money goes to transportation and housing, there is also money for water infrastructure (4%) and green infrastructure (2%) with plans for a 10% increase in urban green space (MOL, 2021). The climate of London is warm and temperate, with an average annual temperature of 11.1°C and 621 millimetres of rainfall, respectively.

With a rising population that uses an increasing volume of water per head, in conjunction with climate change projections, London is forecasted a growing deficit, increasing from 125 Ml/d in 2020 to 367 Ml/d by 2040, which is equivalent to the water used by over 2.2 million household customers (TWUL, 2020). Trading with other water firms including Essex and Suffolk Water and RWE N-Power, as well as discovering new resource choices, is helping to address the water shortage. New wastewater re-use systems are also being considered, such as two wastewater reverse osmosis re-use plants: Deephams recycling 60 Ml/d in 2027 and Beckton recycling 100 Ml/d in 2032 (WRMP, 2021). However, emerging pollutants, such as pharmaceuticals must be taken into account when evaluating these approaches (Stuart et al., 2012).

`

6.3 Data and methods used

The data used for the study was obtained from water quality archive from the Environment Agency (EA) (EAWQA, 2021) for over 500 wells at different locations across London, between the years 2000 to 2020. The data provided by the EA is highly inconsistent in both temporal and spatial domains. It was collected for physiochemical groundwater quality parameters such as hardness, dissolved oxygen (DO), nitrates, nitrites, temperature, major anions (bicarbonates, carbonates, chloride and sulphate) and major cations (calcium, magnesium, sodium and potassium).

Data preprocessing was performed to remove the data inconsistency limitations and transform it into a consistent dataset suitable for analysis. In the temporal domain, data was averaged over three months, to get quarters based on seasons (MO, 2021), as shown in Table 6.2. This was done as when yearly observations were tried then very few samples were available to downscale the resolution, and when monthly samples were tried, the data distributin was highly inconsistent. In the spatial domain, all the observations stations were studied over 5 subzones defined as per the London plan consultation, great London authority, 2011 (GLA, 2011): Central, East, North, South, and West (Figure 6.1).

Table 6.2: Temporal quarters defined based on seasons (MO, 2021)

Quarter	Season	Months
Quarter 1 (Q1)	Winter	December, January, February
Quarter 2 (Q2)	Spring	March, April, May
Quarter 3 (Q3)	Summer	June, July, August
Quarter 4 (Q4)	Autumn	September, October, November

The processing of observed data was done using R programming using libraries such as dplyr, rgdal, raster, rgeos and ggpolt2, and NADA package (RPackages, 2021) and following steps were taken:

- All the observation stations laying outside the administrative boundary of London were removed.
- At each station, all the observations other than groundwater were removed (For example, surface water, sweage flow, and others were available and removed as the study is mainly focused on groundwater).

`

- All the observation data for north London and south London were joined in a single file.
- The observation stations were spatially divided into 5 subzones i.e. Central, East, North, South, and West London.
- All the observations within a quarter (based on the seasons) were averaged to get quarterly temporal series.
- Individual parameter-wise quarters temporal plots were created to study the temporal variation of all the parameters.
- Individual parameter-wise spatial plots were created for the years 2000, 2010 and 2020 to study the decadal spatial variation of all the parameters.

Since the area of each subzone was small (~ 300km^2), hence all the observation stations laying in a particular subzone, was considered as a representative point for the whole subzone, so aggregate of all the points in a subzone was taken to study time series of that particular subzone. Statistical parameters, such as arithmetic means, standard deviation, and kurtosis; and boxplots were used for the investigation of individual groundwater quality parameters in this study. Also, Piper-Trilinear plots was used to indicate the overall quality of the groundwater (Morris et al., 1983). The Piper diagram is widely adopted to study hydrochemistry of a water sample. It has three parts: a triangle diagram for cations in the lower left, a triangular diagram for anions in the lower right, and a diamond diagram in the middle top that shows matrix transformation of the two triangular diagrams. The equivalents per mole (epm) percentage values of groundwater quality parameters are used for making the plot (Morris et al., 1983). Grapher-13 software was used for the plotting of Piper-Trilinear diagrams.

To study the spatial distribution, thematic maps were created at a decadal interval for each water quality parameter. A geodatabase file was created for each parameter with all observation stations in a point attribute table. This file was used to create thematic maps using Inverse distance weighted (IDW) raster interpolation method in ArcMap 10.5 GIS software. Zonal mean over each London ‘ward’ was used to study changes spatially at ward level for the selected groundwater quality parameters.

6.4 Results and discussions

To judge the groundwater quality, samples can be categorised in three main divisions based on chemical compounds i.e bicarbonate, sulphate and chloride (Chebotarev, 1955). For

`

interpretability, the analytical data was presented in Piper-Trilinear plots (Figure 6.3), which indicates that the hydro-chemical facies of groundwater in the study area were magnesium bicarbonate types. The groundwater of central, east, south, and north London could be classified as dominant magnesium bicarbonate types, while that of west London could be classified as a mix of sodium chloride and sodium bicarbonate type. Also, it can be directly concluded that all the subzones (except west London) had alkaline earths exceeding alkalies, and weak acids (HCO_3+CO_3) exceeding strong acids (Cl+SO_4). Thus, the bicarbonate anion dominated the concentration of sulphate and chloride in central, east, south, and north London.

The HCO_3^-, $SO4_2^-$, Cl^- sequence in groundwater is developed from recharge towards the discharge area, and depends on proximity to the sea and contact time (Chebotarev, 1955). Besides this, saltwater intrusion should be inspected as a reason for the obtained groundwater quality of London owing to its proximity to North Sea. The bicarbonate-chloride ratio can indicate saltwater intrusion in groundwater (Jamshidzadeh & Mirbagheri, 2011). Chloride is heavily present in seawater and in small amount in groundwater, while bicarbonate is usually heavily present in groundwater and in a small amount in seawater. The average ratio of HCO_3/Cl in all 5 sub-zones of London is shown in Table 6.3. The Simpson ratio, first described by Todd in 1959 (Todd, 1959) is the ratio of HCO_3/Cl, rates water sample as the good quality (no salt water intrusion) if the ratio value is 2 and above (Korfali & Jurdi, 2010; Moujabber et al., 2006; Todd, 1959). Except for west London, bicarbonate-chloride ratio was greater than 2 for all the subzones and hence salt-water intrusion is not a major problem for London groundwater.

`

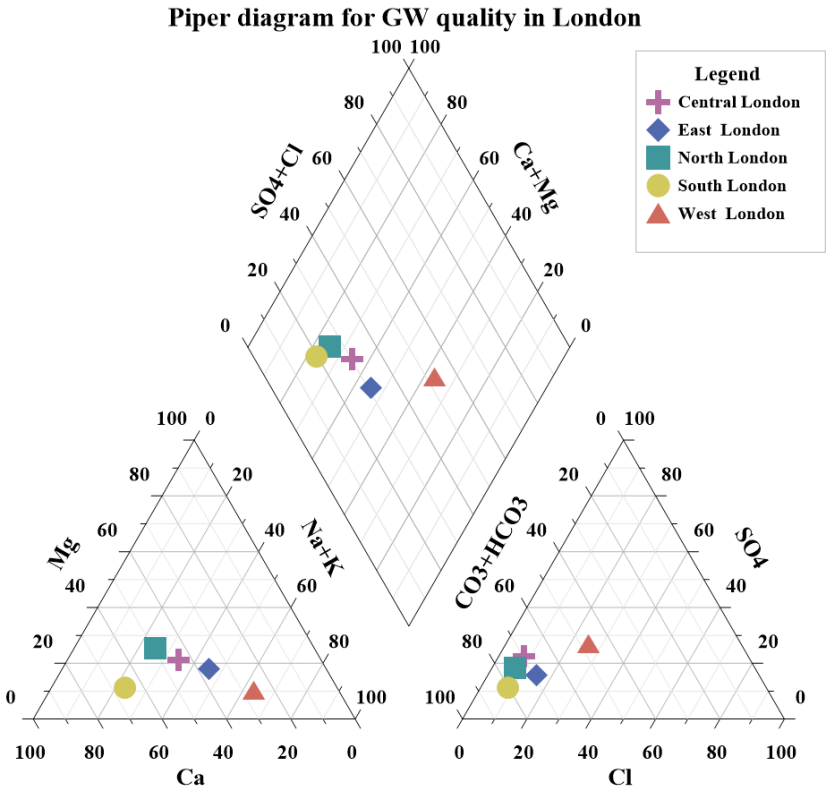

Figure 6.3: Piper trilinear plot representing groundwater quality for 5 sub-zones in London

Table 6.3: Average ratio of Bicarbonate-Chloride ions in groundwater for all the 5 subzones of London

Ratio	Central London	East London	North London	South London	West London
HCO_3/Cl	8.93	4.51	10.29	9.55	1.85

The density of infrastructure such as transit tunnels in London's subsurface is expanding, necessitating dewatering techniques to control groundwater during construction (Royse et al., 2012). Construction in the subsurface has a variety of effects on groundwater, including: (i) partitioning of groundwater, which alters natural flow paths and complicates groundwater modelling; (ii) increased vulnerability due to penetration of the confining layer, which impedes protection of groundwater quality; (iii) the networks of transportation, energy, and fluids all have the potential to leak contaminants; and (iv) as development progresses deeper into the subsurface, groundwater mixing becomes more likely, posing a risk of groundwater quality degradation. Such implications necessitate increasingly technological and strong solutions to suit the city's growing population's resilience needs. To this end, new technologies are being developed, such as the

`

employment of robots to repair subterranean pipes (Hollingum, 1998) and geophysics to identify pipe leaks (Kuras et al., 2016). The induced ground level change visible in remotely sensed radar interferometry can be used to monitor the extent of groundwater abstraction (Agarwal et al., 2021; Bonì et al., 2016).

To study spatio-temporal variation in London's groundwater quality, each individual parameter can be studied. Several water quality parameters were considered, for example, temperature, nitrates, nitrites, fluorides, hardness, sodium, Dissolved Oxygen (DO) and others. Groundwater serves a variety of purposes, including providing drinkable water, diluting and attenuating toxins, and functioning as a medium for capturing subsurface heat. The proper assessment and management of ecosystem services given by the groundwater, on the other hand, are less well known. In central London, there are more than 40 operational ground source heating and cooling systems, including those used by London Underground to cool the platform using groundwater pumped from Victoria Station as part of the station's dewatering system. It is projected that geothermal heat sources might provide up to 19% of London's total heat demand (GLA, 2021b). Despite the opportunity, rising groundwater temperatures are already a worry, with sections of London experiencing a 2°C spike in temperature between 2005 and 2019 (EA, 2019).

Nitrate pollution is a serious concern, in groundwater beneath agricultural areas with high-permeable soils and oxic geochemical conditions (Chen et al., 2016). High nitrate levels in groundwater have been frequently observed because of increased anthropogenic nitrogen inputs (Fabro et al., 2015; Suthar et al., 2009). Although methemoglobinemia (blue-baby syndrome) is the most significant thrteat of nitrate exposure (particularly for infants), additional serious effects have been identified, including different types of cancer and birth abnormalities (Gulis et al., 2002). Fluoride is found mostly as a free ion in natural waters. The most prevalent source of fluoride in groundwater is the dissolution of fluoride-bearing rocks (fluorite CaF_2). At concentrations of less than 1 mg/L, fluoride in drinking water is effective in preventing dental cavities (Gulis et al., 2002). However, the World Health Organization (WHO) undertook a thorough investigation and discovered that fluoride levels in drinking water over 1.5 mg/L were occasionally linked to dental fluorosis. The literature suggests that both these parameters (Nitrate and Fluoride) are found in excess to Drinking Water Inspectorate (DWI) allowable limits, in those areas of England which are dominated by vegetation and agricultural activities (Aldiss, 2014; BGS, 2013; Shand et al., 2007). But London being an urban area, the concentration of nitrates, nitrites

`

and fluorides in groundwater were less than 10 mg/l, 0.02 mg/l and 1.5 mg/l respectively, at all times during our observation period, for all the 5 subzones of London. So, the groundwater represented by observed samples in this research is safe for nitrates, nitrites and fluorides.

This study is focused and limited to London, where agricultural activities are in sparse and hence parameters like nitrates, nitrites and fluorides are within acceptable limits in groundwater. The case studies presented in this paper are for hardness, sodium, and DO. These case studies are chosen as hardness and sodium exceeded the prescribed allowable limits of portable water by DWI on numerous occasions, and for DO, even though no limits have been prescribed, but its overall concentration plays a vital function in groundwater quality maintenance. Table 6.4 summarises the statistics of different water quality parameters for each of the 5 subzones in London.

Table 6.4: Statistical summary of observed data for different groundwater quality parameters zones between the year 2000-2020

WQ Parameter		**Hardness (mg/l)**	**Sodium (mg/l)**	**Dissolved Oxygen (mg/l)**
Drinking Water Inspectorate (DWI) Limits		100 (min)-200 (max)	200 (max)	-
Central London	Mean	282.85	123.06	3.80
	Standard Deviation	92.93	139.83	2.33
	Kurtosis	5.42	1.18	0.45
	Skewness	1.62	0.41	0.33
	Min - Max	146 - 570	11.50 - 308	0.00001-9.51
	Count	23	15	23
	% Samples exceeding DWI limits	91.30	40.00	-
East London	Mean	410.20	329.73	5.01
	Standard Deviation	394.32	684.88	2.54
	Kurtosis	18.04	7.48	-0.55
	Skewness	3.78	2.45	0.16
	Min - Max	57.9 - 2362.2	17.4 - 2533.04	0.00001-10.7
	Count	50	43	117
	% Samples exceeding DWI limits	86	16.27	
North London	Mean	315.7	41.31	5.14
	Standard Deviation	83.02	12.55	2.31

`

	Kurtosis	2.72	3.49	-0.65
	Skewness	0.66	0.74	0.18
	Min - Max	201 - 530	18.4 - 71.95	0.60-10.1
	Count	39	29	97
	% Samples exceeding DWI limits	100	0.0	
South London	Mean	228.53	29.44	5.75
	Standard Deviation	73.50	15.24	3.21
	Kurtosis	1.96	2.75	-1.08
	Skewness	0.013	0.82	-0.17
	Min - Max	96.9 - 359	11.2 - 67.0	0.00001-10.5
	Count	53	41	117
	% Samples exceeding DWI limits	58.49	0.0	
West London	Mean	160.18	121.13	5.83
	Standard Deviation	96.49	88.46	2.67
	Kurtosis	5.02	1.75	-1.04
	Skewness	1.27	0.47	-0.06
	Min - Max	61 - 500	17.33 - 274.00	0.74-10.74
	Count	42	35	71
	% Samples exceeding DWI limits	26.19	22.85	

6.4.1 Hardness

Hardness in water is caused by minerals like calcium and magnesium, and when rainwater permeates through rocks, it dissolves these minerals (Mosavi et al., 2020). It can be either temporary (carbonate) or permanent (non-carbonate), and expressed in terms of the equivalent of $CaCO_3$ mg/l. The groundwater hardness varies based on local scale geology. Hardness in water greater than 200 mg/l can cause scale and lower than 100 mg/l can be erosive to pipes (Drinking Water Inspectorate, 2017). There is no health based standard for the hardness of drinking water but extremely low values (less than 80 mg/l) can lead to inadequate uptake of essential nutrients, principally calcium and magnesium (Hudak, 2001).

Table 6.4 shows that average value of hardness for central, east, north and south London is above, while that for west London is within DWI prescribed limits for drinking water of 200 mg/l. For

`

central London, as high as 91.3% of samples exceeds the DWI limit, thus groundwater must be treated for hardness, before using it for potable purposes. The standard deviation for east London is quite high (~394 mg/lit). For west London, only 26.19% of samples exceed 200 mg/l, thus major treatment for hardness of groundwater coming from west London is not required. The skewness is positive for all the 5-subzones (varies between 0.01 to 1.6), which indicates that bulk of the values lie to the right of the mean. This pattern is expected for water quality data, as negative concentrations do not exist. Kurtosis identifies whether the tails of a distribution contain extreme values. For east London, a kurtosis value of 18.04, shows that observed data differs heavily from normal distribution.

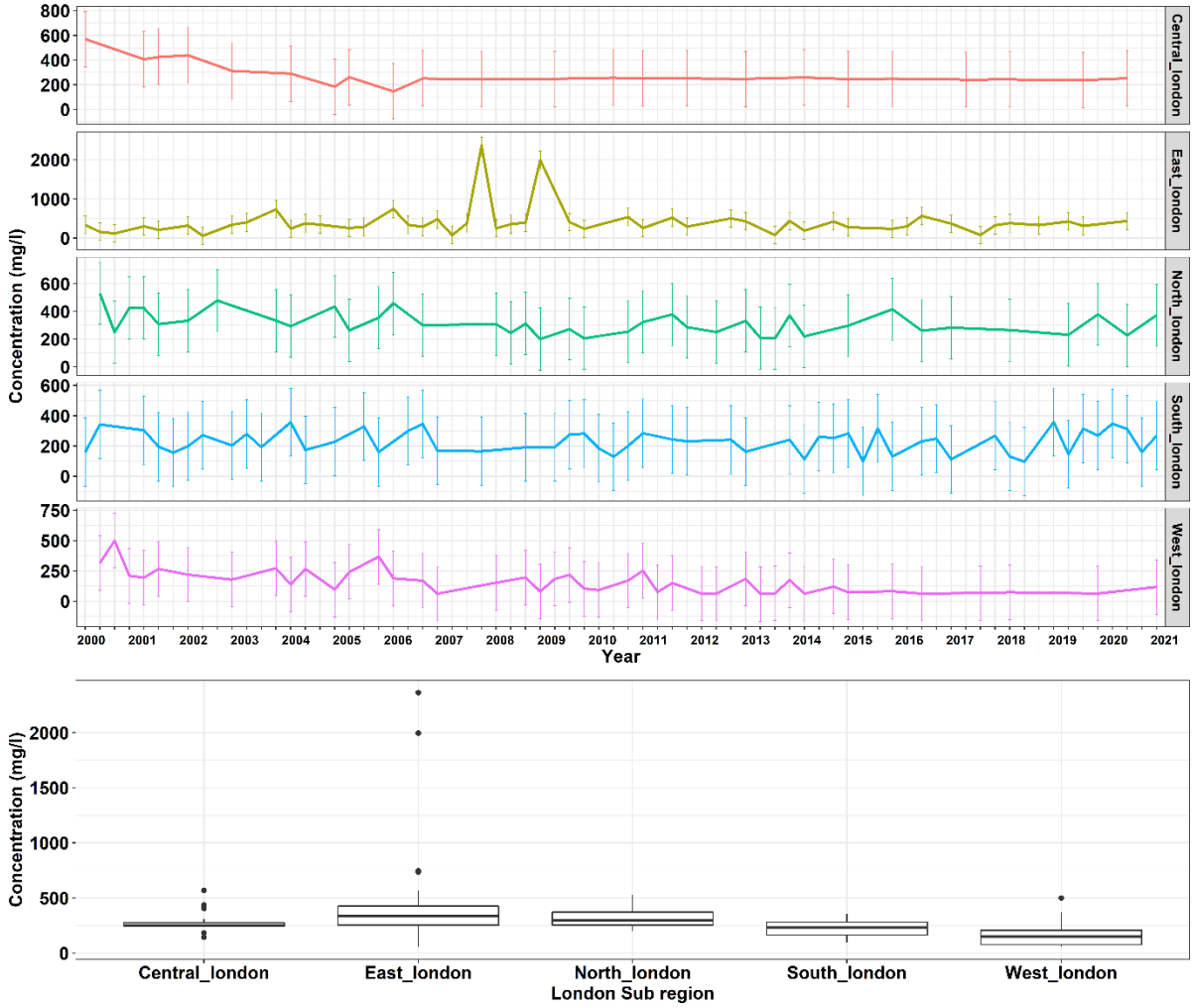

Figure 6.4: (a) Time-series and (b) boxplot for hardness variation in groundwater across the 5 sub-zones between the year 2000-2020 quarterly. In Figure 6.4a, red, yellow, green, blue, and pink colour represents central, east, north, south, and west London respectively.

`

The temporal series and boxplots (Figure 6.4) show that for most values of east London, the hardness of groundwater is above 200 mg/l, and thus groundwater taken from boreholes in east London must be softened before supplying for potable use. Some abnormal rise in hardness values can be observed between 2007 and 2009, these values are outliers and should be neglected as no reason could justify such a sharp rise. In north London the time series and boxplots also suggest that hardness in greater than 200 mg/l for all the 20 years. A similar trend can be observed in central and south London. In west London, the hardness is less than 200 mg/l between the years 2011 and 2020, and thus groundwater can be used directly with respect to hardness.

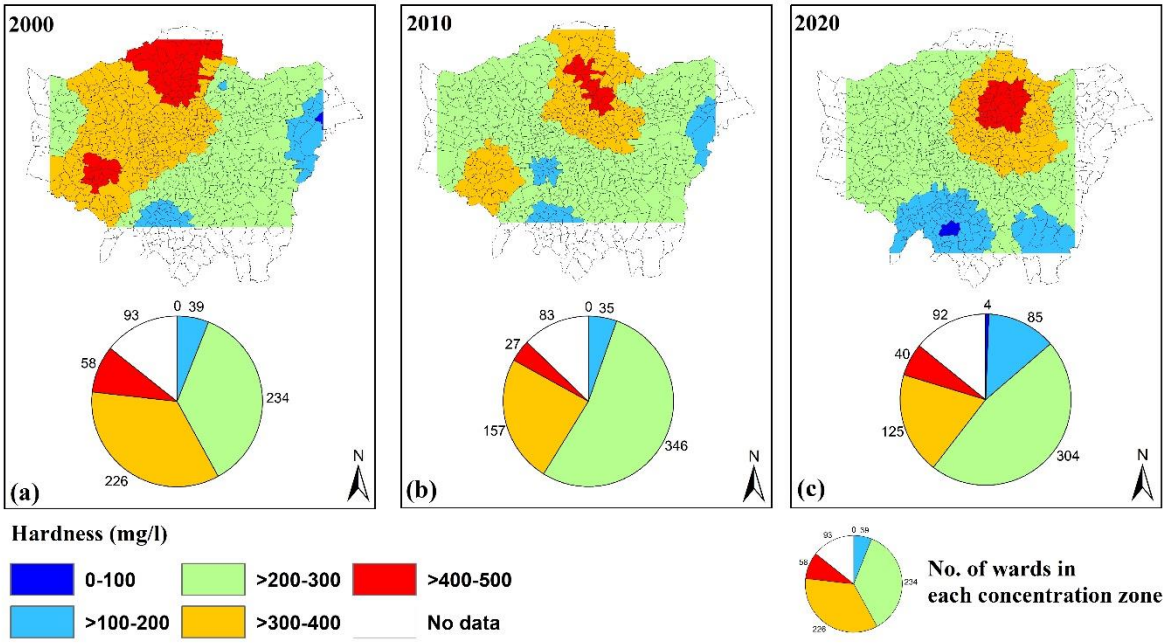

Figure 6.5: Spatial variation of hardness on ward level for second quarter (March, April and May) of the year (a) 2000 (b) 2010 and (c) 2020.

The spatial distribution of hardness over London is shown in Figure 6.5. A comparison of mean concentrations of hardness by ward for second quarters of the year 2000, 2010 and 2020 shows that maximum number of wards has hardness between 200-300 mg/l for all the three years. Only 39 wards in 2000, 35 wards in 2010 and 89 wards in 2018 have hardness within the acceptable limits of less than 200 mg/l. Also, the extreme hardness of 400-500 mg/l is found mostly in north London for all the three years. Total number of wards with hardness concentration between 200 to 500 mg/l is 518, 430 and 469 in 2000, 2010 and 2020 respectively, thus covering a major portion of London city. A general trend across the London is that groundwater is softer in south and

`

becomes harder moving north. The wards shown in the maps with white polygons have no data, only wards with coloured polygons should be compared across the decades.

The BGS groundwater report for Thames basin in 2010 (Bearcock & Smedley, 2010), also found hardness over 200 mg/l in north London, and reported that increased hardness in strata below the constraining London Clay is due to pyrite oxidation, which occurs periodically across the Palaeogene beds as a result of anthropogenic groundwater extraction from the chalk below. DWI recommends water supply companies to ensure a hardness of 150 mg/l, as there is some evidence of it being helpful for cardiovascular health (DWI, 2011). Few people suffering from skin sickness like eczema, have claimed that soft water for washing have proved beneficial for them, but Softened Water Eczema Trial (SWET) trial run by the University of Nottingham reported no significant difference in houses with or without water softeners (Thomas et al., 2011).

6.4.2 Sodium

Sodium concentration in drinking water in optimum amount is important for human health. It influences muscular contraction and the synthesis of adrenaline and amino acids, as well as provides nutrition (Weast & Astle, 1983), and contributes to electrolyte regulation by the kidneys (Howard & Schrier, 1990). High sodium concentrations, on the other hand, can cause cell or blood chemistry to be disrupted (Dahl & Love, 1957; Hoffman, 1988).

The DWI limit for sodium in drinking water is 200 mg/l, as greater than this amount can give unacceptable taste and cause cardiovascular illness (Drinking Water Inspectorate, 2017). From Table 6.4, it can be seen that sodium has a range of 61-750 mg/l across the London, which is a typical range for sandstone aquifers in England (Drinking Water Inspectorate, 2017). The main source of sodium in groundwater is mixing with rainwater (Shand et al., 2007), although higher concentration of 750 mg/l is unusual.

`

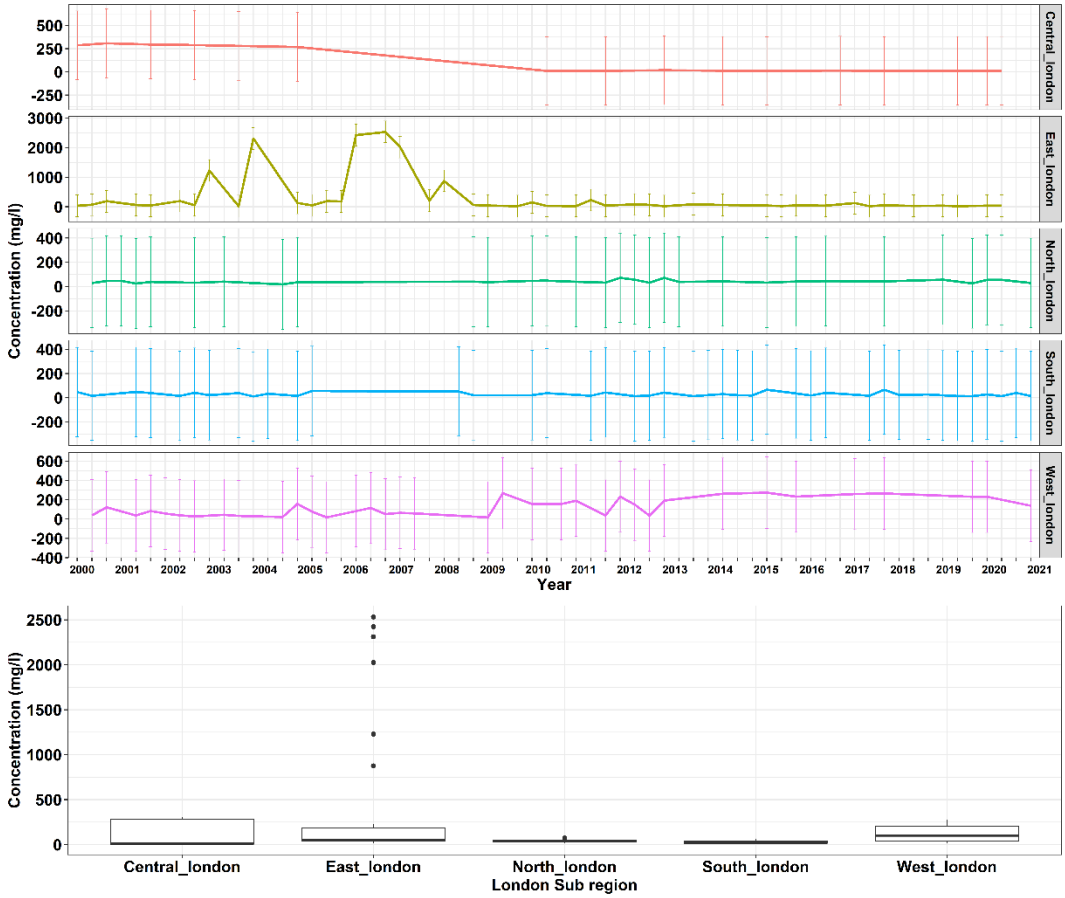

Figure 6.6: (a) Time-series and (b) boxplot for sodium variation in groundwater across the 5 sub-zones between the year 2000-2020 quarterly. In Figure 6.6a, red, yellow, green, blue, and pink colour represents central, east, north, south and west London respectively.

From Table 6.4, it can be seen that average sodium concentration for east London is above DWI prescribed limits, while that for other four subzones of London is within the prescribed limit (less than 200 mg/l). Also, for central London, about 40% of samples exceed the prescribed limit, and none of the samples in east and north London exceeded the required limits. Kurtosis values vary from 1 to 3 except for east London, thus signifying that observed data does not differ heavily from normal distribution. The time series for north and south London, shows the sodium concentration is always less than 70 mg/l during our observation period. There is a sharp decrease in sodium concentration between 2004 to 2011, and thereafter the concentration is within acceptable limits. For west London, there is a rise in sodium concentration after 2013. For east London, between 2002 to 2007, there is unusual and alarming rise in the concentration values. The boxplot suggests that this higher concentration in east London could be treated as an outlier.

`

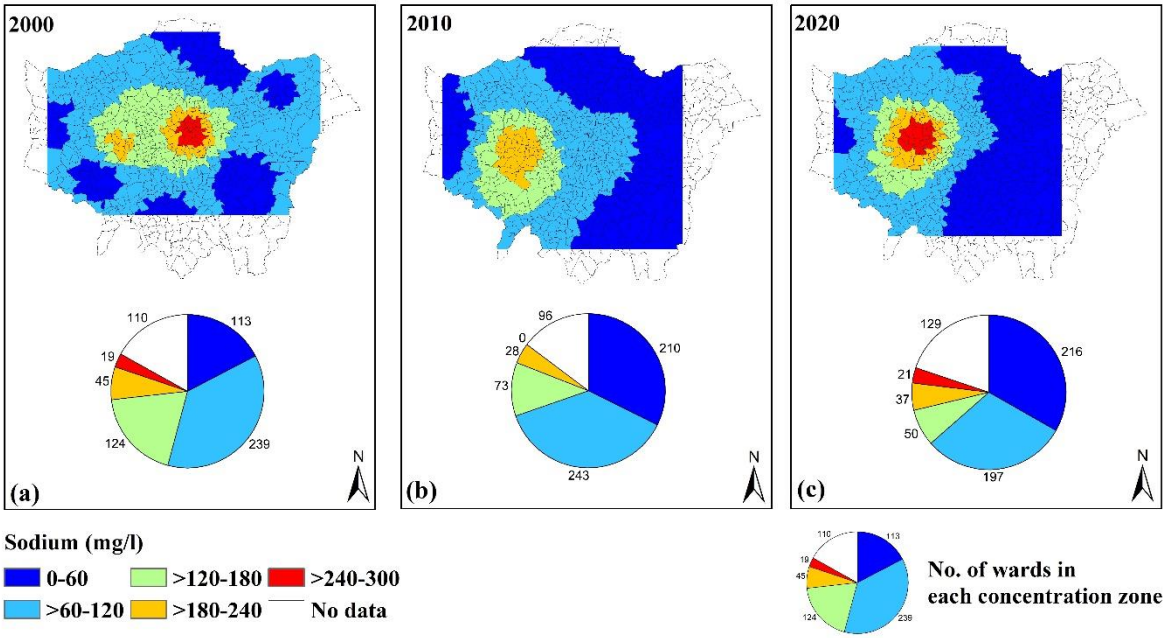

Figure 6.7: Spatial variation of sodium on ward level for second quarter (March, April and May) of the year (a) 2000 (b) 2010 and (c) 2020.

The spatial distribution of sodium over London is shown in Figure 6.7. A comparison of mean concentrations of sodium for the second quarter of the year 2000, 2010 and 2020 by ward shows that highest number of wards has sodium concentration between 60-120 mg/l for 2000 and 2010, while for 2020 maximum number of wards has concentration between 0-60 mg/l. Only 64, 28 and 58 wards in London had sodium concentration over 180 mg/l, thus for most of the London area the groundwater is safe for drinking purpose, with respect to sodium. A general spatial trend is that the concentration of sodium increases radially inwards towards the centre of the city. Clays and plagioclase (Na-Ca) feldspars are the most common sodium-containing mineral phases in aquifers, however, halite (NaCl) may be present in evaporite sediments (Bearcock & Smedley, 2010). Although pollution (e.g., septic tank leaks, road salt application) may increase sodium levels in groundwaters, mineral-water reactions involving Na-bearing minerals could be another reason for increased concentration.

6.4.3 Dissolved Oxygen

Ideally, Dissolved Oxygen (DO) is considered as absent below the water table, and if present, it is considered harmless to human beings, and thus the measurement of oxygen concentration is not mandatory by drinking water standards (Winograd & Robertson, 1982). However, DO

`

concentration influences the valence state of trace metals and restricts the bacterial metabolism of dissolved organic molecules, which affects water quality (Rose & Long, 1988). As a result, DO monitoring should be a must in any water quality investigation. DO is a geochemically active oxidant that regulates the solubility of a variety of naturally occurring polyvalent elements in groundwater. For example, iron concentrations are usually below maximum drinking water standards in oxic water because of the precipitation of iron oxyhydroxides. The oxyhydroxides, in turn, are important adsorbents of heavy metals (Stumm & Morgan, 1981).

Table 6.4, shows that DO measured has a wide range of 0.0 mg/l to 10.74 mg/L. The mean DO in groundwater for central London is 3.84 mg/l, while that for other parts of London is over 5 mg/l. This is a complete range from anoxic to fully saturated and the appreciable amount is mainly because either or both of the two reasons. Firstly, the microbial reduction of oxygen is limited in many aquifers, or secondly, oxygen can be effectively transported to the phreatic zone from the overlying vadose zone. DO can prove to be an important parameter for estimating groundwater quality, especially involving migration of landfill leachate or mining waste. DO frequently regulates the types and numbers of microbes present in an aquifer, hence controlling the destiny of dissolved organic pollutants. Most alkyl benzene and chlorobenzene groups, for example, are likely to biodegrade in aerobic water while remaining stable in anaerobic water (Wilson & McNabb, 1983).

`

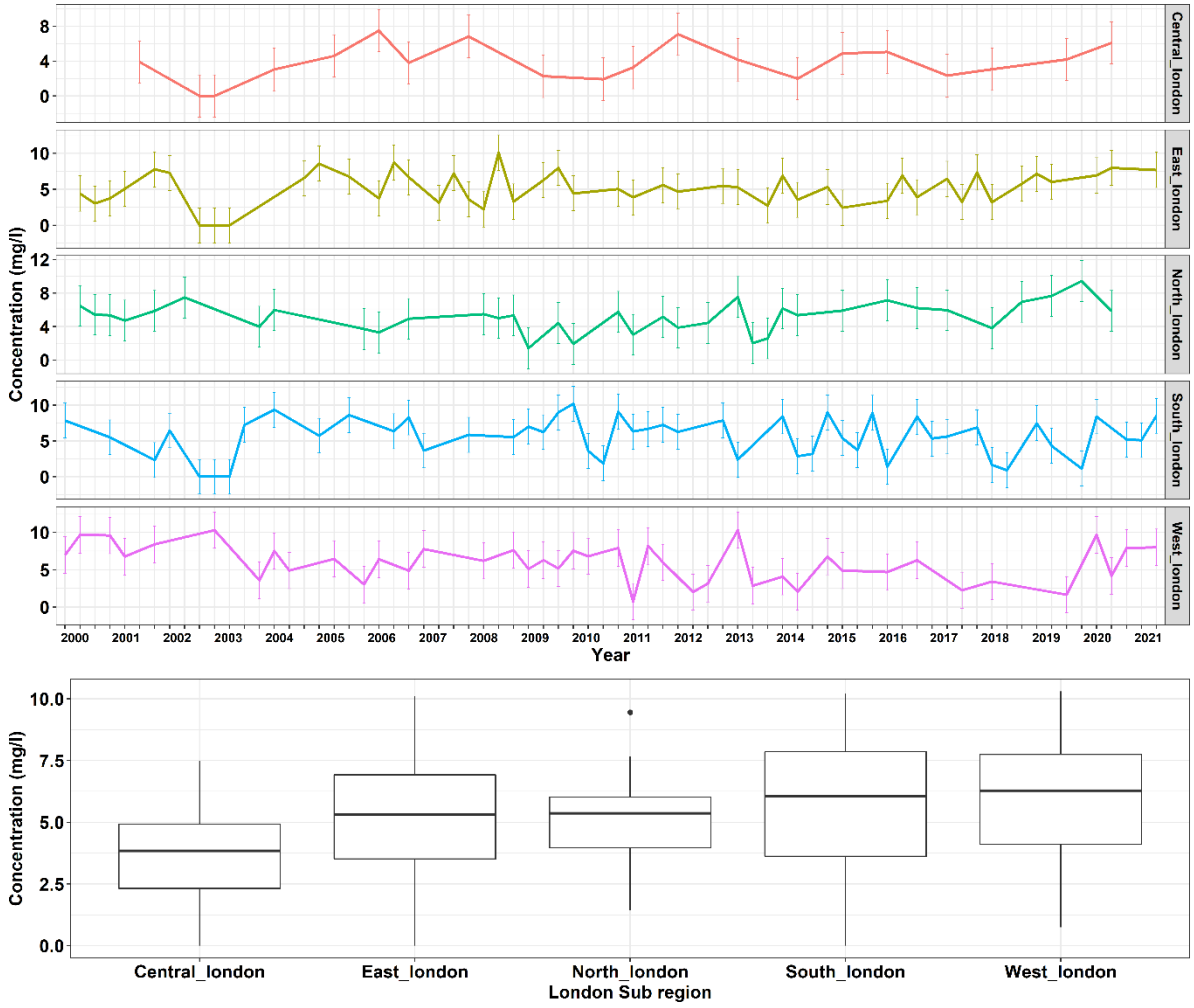

Figure 6.8: (a) Time-series and (b) boxplot for Dissolved Oxygen (DO) variation in groundwater across the 5 sub-zones between the year 2000-2020 quarterly. In Figure 6.8a, red, yellow, green, blue, and pink colour represents central, east, north, south and west London respectively.

In the Figure 6.8a, the time series shows that for central, east and south London the DO is nearly 0 mg/l for Q1 of the year 2003. This could be because of groundwater pollution due to anthropogenic avtivities, where dissolved organic carbon is several times more than in uncontaminated groundwater, and DO is likely absent from such contaminated groundwater. However, this assumption always requires site-specific verification. Furthermore, the variation across all the 5 subzones is inconsistent, but maintaining variation between 0 to 10 mg/l.

`

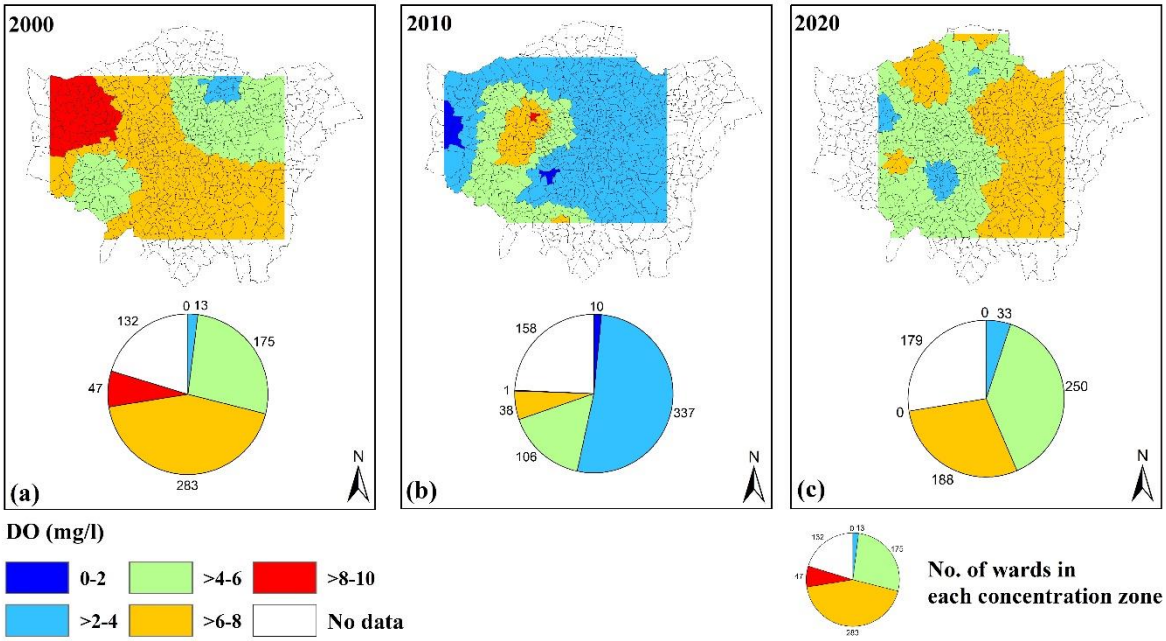

Figure 6.9: Spatial variation of Dissolved Oxygen (DO) on ward level for second quarter (June, July and August) of the year (a) 2000 (b) 2010 and (c) 2020.

The spatial distribution of DO over London is shown in Figure 6.9. A comparison of mean concentrations of DO for third quarters of the year 2000, 2010 and 2020 by ward shows a decrease in mean highest concentration (>8 to 10 mg/l) during the first decade and second decade. The pie charts show that the number of towns with mean concentrations of DO greater than 8 mg/L was 47 in 2000, 1 in 2010, and 0 in 2019. Between 2000 and 2010, the number of wards with a mean concentration of DO between 2-4 mg/L increased by nearly 26 times, and then decreased 10 times between 2010 and 2020. For the year 2000 highest number of wards (283) had DO values between 6-8 mg/l, while that for the year 2010 was between 2-4 mg/l with a count of 337, and finally for 2020, highest number of wards (250) had DO values between 4-6 mg/l. The spatial variation of DO across two decades for London, thus shows inconsistent rise and fall in DO level mostly varying between 2 to 8 mg/l. Although there are no guidelines for DO limits based on health issues, yet high level of DO (>5mg/l) may lead to copper erosion and corrode metal pipes. Also, decrease in DO in water supplies can encourage microbial reduction of nitrate to nitrite and sulphate to sulphide (Huo et al., 2021).

`

6.4.4 Inter-relationship between the observed parameters

The three groundwater quality parameters observed showed spatial and temporal variation across the London. The presence or absence of one parameter may influence the presence and absence of other. The Pearson's correlation coefficient (r) (Benesty et al., 2009; Stigler, 1989) between two variables gives an indication of the strength of the relationship between them. It is thus useful to determine the degree of corelation between groundwater quality parameters for 5 sub-zones. The closer the value of 'r' is to ±1, the stronger the correlation between the two variables (Stigler, 1989). A negative 'r' shows that if first parameter increases then second parameter decreases, while a positive 'r' shows that first parameter increases with the second and a value of '0' means that there is no association between the two parameters (Benesty et al., 2009). The correlation between the parameters is characterised as strong, when 'r' is between +0.7 to +1.0 and -0.7 to -1.0, moderate when it is having a value between +0.3 to +0.7 and -0.3 to -0.7, weak when it is between 0.0 to +0.3 and 0.0 to -0.3 (Ratner, 2009). The Pearson coefficient (r) for all the three parameters across all 5 subzones is shown in Figure 6.10.

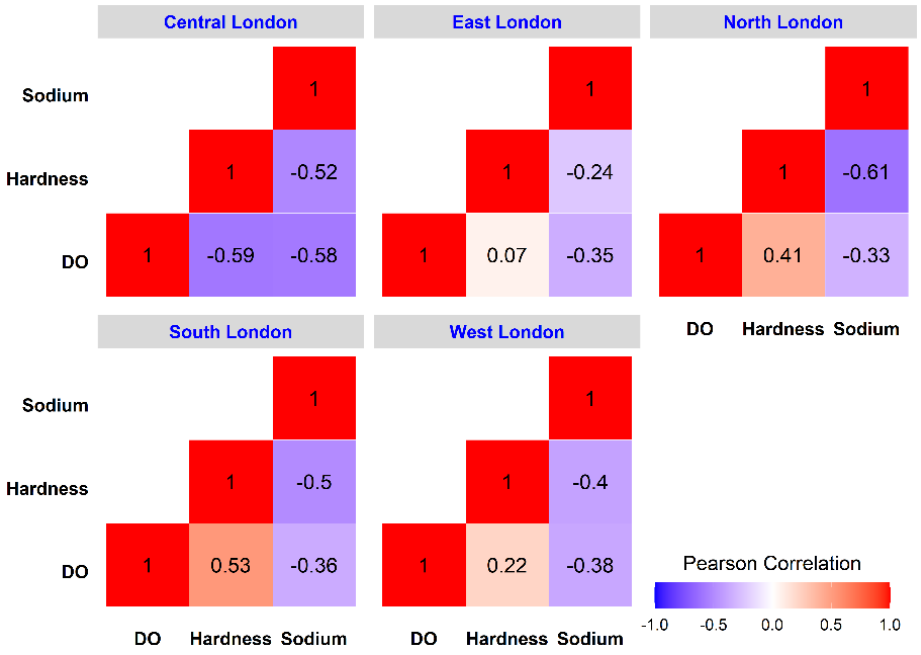

Figure 6.10: Pearson corelation parameters

The Pearson coefficient for sodium and hardness is negative for all the 5 subzones, which shows that with an increase in sodium, the hardness decreases in water. The highest 'r' value between sodium and hardness is for north London (-0.61), and least for east London (-0.24), showing

`

variability from moderate to weak relationship. Some water softeners employ an ion exchange mechanism to replace the calcium and magnesium that produce hardness with an equal quantity of sodium using this feature (Kusrini et al., 2020; Lakshmanan & Gokhale, 2020). Similarly, sodium and DO are negatively correlated in all the 5 subzones, which shows that the DO in water decreases with increase in sodium content. The nature of relationship is consistent and in the moderate range for all the five subzones of central London. The relation between hardness and DO is negative for central London, positive for north, south and west London, and almost zero for east London. Also, the relationship is moderate for central, north and south London, and weak for other two subzones. Thus, a mixed interdependence between DO and hardness can be seen across whole London.

Variability in 'r' can be observed over the 5 sub-areas, which is expected given the variability in our observed data. Also, several factors contribute to groundwater quality variations in London, including rock/sediment composition, groundwater chemical evolution, seepage from nearby formations, and probable human controls.

6.5 Conclusions

While London is an excellent case study for cities that have gone through numerous stages of development, it also symbolises one of the world's most historic urban developments. As a result, a unique set of circumstances exist that make urban planning particularly challenging in terms of land use changes and transitions through secondary and tertiary industries, resulting in competition for subsurface space, legacy contaminants, and heavily exploited natural resources in an area with heterogeneous ground conditions. Thus, the monitoring and assessment of groundwater quality parameters for multiple years is helpful in developing new strategies.

This study shows that statistics and Geographical Information Systems (GIS) can prove useful tools for groundwater quality evaluation. The study categorised the groundwater of London based on its physiochemical parameters and analyse spatio-temporal variation of hardness, sodium and Dissolved Oxygen (DO). Between the years 2000 and 2020, the groundwater hardness varied between 50 mg/l to 2363 mg/l, sodium varied between 11 to 308 mg/l and DO varied between 0 to 10.7 mg/l. The varied range in these constituents can be attributed to variation in geology of the London Palaeogene aquifers and anthropogenic activities. Trilinear Piper plots highlighted the overall groundwater of London can be summarised as dominant magnesium bicarbonate type. The spatial variation maps showed that there are localised patches of groundwater below Drinking

`

Water Inspectorate (DWI) acceptable limits, but overall London's groundwater is of potable status. The Pearson corelation coefficients showed that hardness and sodium are negatively corelated, and also DO and sodium are negatively correlated. The study can act as a guide for decision making and to identify hazardous contaminants. It has potential for prioritisation of management efforts and funds, assess overall effects of water quality interventions, monitor water resource and health.

Authors Contributions: The authors who contributed to the paper presented in this chapter are Agarwal, Vivek* (V.A); Kumar, Amit (A.K); L. Gomes, Rachel (R.L.G); Marsh, Stuart (S.M). *Conceptualisation*, V.A., R.L.G. and S.M.; *data curation*, V.A., R.L.G. and S.M.; *formal analysis*, V.A. and A.K.; *funding acquisition*, V.A., R.L.G. and S.M.; *investigation*, V.A., R.L.G. and S.M.; *methodology*, W.A., A.K., R.L.G. and S.M.; *resources*, V.A.; *software*, V.A. and A.K.; *supervision*, R.L.G. and S.M.; *validation*, R.L.G. and S.M.; *visualisation*, V.A., A.K., R.L.G. and S.M.; *writing*—original draft, V.A.; *writing—review and editing*, V.A., R.L.G. and S.M.

Acknowledgments: The authors would like to thank the Department for Environment Food & Rural Affairs, Environment Agency for providing water quality archive datasets in open domain.

`

Chapter 7 Discussion

The discussions for each case study are given in chapters 3 to 6 in detail. In this chapter, broader aspects of this research work are discussed. It sets out to establish whether all the objectives mentioned in section 1.2.1 have been achieved. The rationale of all case studies and optimum strategy for monitoring ground is discussed. It also explores how monitoring strategies could be affected in developed countries (such as England) and developing countries (such as India). Groundwater quantity-quality interdependence is discussed in brief. The InSAR-GRACE applications, limitations and their future scope are discussed. Finally, the chapter is summarised.

7.1 Overview of objectives achieved

The overarching goal of the thesis is to identify the optimal combination of different, modern geospatial techniques like InSAR, GRACE, GIS, observed in-situ data, data analysis and data visualisation to study the spatio-temporal variation in quantity-quality of groundwater and related subsidence. The aim is supported by various specific objectives mentioned in section 1.2.1, which are discussed below:

i. Study the sensors and software available for InSAR data processing and identify the optimum sensor–software combination for analysis, based on availability, requirements, and performance.

SAR data were first used in groundwater science in the late 1990s. The development of ground displacement data generated from InSAR processing was their most significant contribution to groundwater science. However, working with SAR data is not simple and can be challenging, especially for novice users with no expertise in SAR imagery. Thus, different approaches were evaluated during the early stages of this research to identify the optimum tools and methodology for InSAR processing. This has been addressed in chapter 3 of this thesis.

Both open-source and commercial software and datasets have their strengths and limitations. Thus, the most commonly used software and datasets were reviewed in brief in chapter 3.Open-source SNAP and commercial SARscape were compared to generate DInSAR land displacement maps using two S-1A images and a DEM for London. To compare the results, all attempts were made to keep the user input parameters consistent in both the experiments, like multilooking factor,

`

phase unwrapping principle, and filtering methods. However, some differences are unavoidable because of GCP selection, co-registration or spectral shift filtering steps. A difference of 1 mm/year land displacement between the two experiments was observed, which can negatively affect the understanding of new users, as ideally, the same results are expected from the same set of input data.

The experiments highlighted that open-source software could give excellent results, which are highly comparable to expensive commercial software. However, the interpretation of interferograms from SNAP had a few limitations. SNAP uses the Snaphu unwrapping package, which brings all the limitations associated with Snaphu to the results. SNAP gives an encapsulated GUI environment to generate interferograms, and investigating and updating the principle used behind each step is tricky. SNAP could only support DInSAR with two images, and times series analysis with multiple SAR images is not supported. Nevertheless, the DInSAR maps created using SNAP could be used as an interferometric input for further processing by external open-source software packages, such as StaMPS (Hooper et al., 2010), which is mainly dedicated to the PSInAR technique.

Only a little work has been done using the same data with different software, and more work on cross-verification will be helpful for the growth of the InSAR technique. Our study validates the use of SNAP for DInSAR and provides a good understanding of SARscape. Also, results have been verified with the published literature. It concluded that while commercial software packages like SARscape are powerful tools for InSAR processing, they might be difficult to access. Thus, freely available software and datasets will encourage more researchers to work with InSAR technology. With regular updates on packages like SNAP, Stamps and ISCE, the open-access route will become steadily more user-friendly for InSAR processing.

ii. Identify the potential applications and limitations of using InSAR data over an urban area

Ground displacement data enables the detection of groundwater depletion zones, the mapping of lithological boundaries, the inference of limited aquifer storage qualities, and the calibration of groundwater models. InSAR's integration into groundwater science was aided by the development of interferometry time-series algorithms in the early 2000s (Ferretti et al., 2001), which allowed the reduction of atmospheric artefacts and the monitoring of finer displacements such as aquifer

`

reaction to pumping and recharge over time. Since then, processing techniques have progressed in tandem with increased imaging capabilities and data availability (including open access choices) from orbital SAR systems (Crosetto et al., 2016).

The literature presented in this thesis highlights applications of InSAR over an urban area to various challenges, like the study of earthquakes, landslides, groundwater extraction, coal mining and others. This research explores the potential application of InSAR for studying groundwater induced subsidence in urban areas. The average subsidence in London was found to be −0.176 mm/year between the years 2002 and 2010. For later periods of October 2016 to December 2020, the land movement velocities were found to vary between -24 mm/year to +24 mm/year for London. For NCT-Delhi the land movement velocities were found to vary between -18 mm/year to +30 mm/year between October 2016 and December 2020. The rise in availability of SAR stacks and the development of InSAR processing techniques enabled routine monitoring of ground displacements with millimetre scale accuracy for these periods.

The InSAR data processing has certain limitations and challenges which were encountered and overcome during this research work. The loss of coherence in natural systems is one of the critical issues of applying InSAR to water science. The SAR wavelength is usually inversely related to the loss of interferometric coherence. Although areas of trees in urban contexts are typically smoothed by downsampling or compensated by interpolating the final data, lack of coherence is a concern when heavy vegetation dominates the land cover. For urban areas like London and NCT-Delhi, since forest and vegetation are not dense, coherence loss was not a severe issue in this study. Atmospheric effects also impact InSAR data on a scale of a few mm/year, but they can be eliminated using new sensors and methodological advances. The displacement recorded by InSAR is frequently thought to be due to aquifer compaction in hydrogeology. Although extracting ground displacements at the mm/year scale has crucial applications, interpreting them remains difficult when many reasons for displacements overlap at the same site. Between acquisitions, the SAR phase should be comparable. If the difference in movement between two acquisitions of a SAR time-series is more significant than the length of a SAR wave phase and is not spatially progressive, phase "jumps" occur, compromising the inversion of the phase into displacement. As a result, the temporal density of an InSAR stack, or the time gap between acquisitions, should be sufficient to match the expected displacement rates. Other factors such as the SAR data's noise

`

level, the phase unwrapping approach, and the ground displacements' temporal variability should also be considered.

iii. Study the groundwater quantity variation in London and resulting land subsidence using InSAR and GRACE.

Geodesy opens up new possibilities for developing worldwide and independent groundwater monitoring techniques. Geodetic methods have the advantage of being politically agnostic, having a worldwide scope, and being freely available. SAR imaging and time-variable gravity monitoring (GRACE satellites), for example, are two technologies that can be used to examine groundwater in order of historical appearance. The GRACE (Tapley, Bettadpur, Ries, et al., 2004) gravity field variation time-series also provides a new view into groundwater systems. GRACE provides a direct and quantitative insight into groundwater storage changes since it is sensitive to mass variations. The methodology to use InSAR and GRACE together for studying groundwater variations and resulting land deformation is used over London in this thesis in chapter 4.

The InSAR subsidence values were validated using GNSS data. The two-sample *t*-test provides enough evidence that GNSS up values are in close agreement with the obtained InSAR subsidence values, thus demonstrating that the PSInSAR is an efficient way to survey ground movement in London. GRACE derived temporal groundwater variations were compared with Environment Agency observed values, and GRACE data accounted for 60% of the total observed groundwater change.

While the immense value of a completely geodetic, quantitative, and high-resolution mapping of groundwater storage change was emphasised, the critical importance of creating GRACE and InSAR results with similar resolutions for any research area and application was equally stressed. GRACE gravity variation groundwater recovery and InSAR-derived ground displacement data promise to assist and help evaluate groundwater management practices. However, the GRACE system's resolution is poor, and inverting InSAR data into groundwater storage loss volume necessitates the use of substantial and frequently unavailable lithological data. InSAR may be used to spatially target GRACE-derived groundwater mass loss to depletion zones, narrowing the gap between GRACE and regular water management scales.

iv. Compare groundwater induced subsidence for London and Delhi using PSInSAR

`

Subsurface movement of earth materials causes land subsidence, which is a gradual to rapid sinking of the earth's surface (Galloway et al., 1998). It is linked to various human activities, including groundwater withdrawal, oil and gas extraction, and the associated generation of brackish and saline waters. It may also be linked to water application to unconsolidated moisture-deficient deposits, loads imposed by engineering structures causing foundation settlement, and others.

The population explosions in London and NCT-Delhi exert increased pressure on groundwater resources, thus posing a threat of land subsidence. Since the subsurface geology and infrastructure of the two cities are different, it is interesting to study the response of groundwater to anthropogenic activities and its effect on land movement. Thus, this thesis has addressed groundwater-induced land subsidence for London, alongside NCT-Delhi using PSInSAR in chapters 4 and 5. Both cities were found to have experienced long-term, complex, non-uniform patterns of land motion in the spatial and temporal domains. Different types of site-specific movement were analysed for uplift, subsidence and differential motion, along with the corresponding groundwater variations causing that motion. Across both the cities and all types of movement, the most common factor controlling the spatial patterns of land motion was the change in groundwater level. It can be concluded that significant groundwater extraction from an aquifer leads to land subsidence. Conversely, a rebound or recharge of groundwater leads to land uplift.

The majority of the detected subsidence is due to groundwater depletion due to human activities. The increasing use of land and water resources worsens existing land subsidence issues while also introducing new ones. Groups and institutions involved in the planning and management of groundwater reservoirs, as well as the day-to-day mechanics of operating a groundwater reservoir, should be familiar with subsidence, its causes, spatio-temporal effects, and the assessment of damage associated with it.

Several other countries across the world, including China, Japan, Mexico, United States, and others, experience land-surface deformation due to heavy and extended groundwater pumping. It could potentially happen in other places where groundwater is pumped. Its detection necessitates implementing an effective vertical control monitoring programme to prevent damage to engineering structures.

`

v. Suggest and use a mathematical model to quantify subsidence for a given change in groundwater.

This thesis establishes that a reduction in groundwater level can result in the compaction of strata and subsidence of the overlaying terrain; in contrast, an increase in groundwater level can cause land uplift. While monitoring using remote sensing, GIS and observed data gives a qualitative idea of the groundwater and land deformation relationship, a mathematical model is required to define the quantitative relationship. The complex nature and required level of data needed to run complicated numerical subsidence models make them costly in terms of time and required resources. Thus, a simplified 1-D model is used in this thesis to quantify the relationship between groundwater level change and land deformation and has been presented in chapter 5.

The model assumes a homogenous matrix, average density, and starting porosity based on the sediment type and burial depth. While these assumptions approximate the unit as a whole, they fail to account for local differences that could affect the predicted behaviour. Furthermore, the water removal is modelled as a rate of piezometric head reduction (m/time) rather than an amount removed (m^3), and the time-lag constant is not taken into account. If an approximation of the time-lag is necessary, the time-lag constant can be applied to the output after the model.

The model calculates the amount of compaction caused by a change in hydrostatic pressure using Terzaghi's effective stress theory. It is influenced by the rock matrix's physical qualities, the strata's geological location, and its hydrological history. For a given change in groundwater level, the modelled land deformation was compared with the land deformation using PSInSAR, and a linear regression R^2 value of 0.881 was obtained. This validation of the InSAR and modelled results further verifies that a direct relation exists between groundwater and land subsidence.

vi. Evaluate spatio-temporal decadal-scale changes in groundwater quality for London, 2000-2020

Since the dawn of time, groundwater has been considered a pristine and sacred resource. Because rocks act as a natural filter, it is often of excellent quality in its natural state. The chemical composition is mainly generated from mineral dissolution in the soil and rocks it is or has been in contact with. Although rocks contain purifying capacities that improve groundwater quality, aquifers do not have an endless capacity for filtering contaminated water; therefore, dilution is not

`

a reliable pollution treatment. The natural quality of groundwater in aquifers is constantly being influenced by human activity. Groundwater abstraction and the resulting shift in groundwater flow, artificial recharge, and direct anthropogenic material inputs contribute to this. For efficient management of this vital resource, a complete understanding of groundwater quality in our aquifers is required.

As defined by the Guidelines, safe drinking water poses no significant danger to health throughout a lifetime of use, including varying sensitivities that may develop as people age. However, infants and small children, the elderly, persons with disabilities and even the general population are all in danger of contracting a waterborne disease if they live in polluted surroundings. Those at risk of waterborne sickness, in general, may need to take extra precautions, such as boiling their drinking water, to protect themselves. All common residential purposes, such as drinking, food preparation, and personal cleanliness, necessitate safe drinking water. Thus, it is essential to monitor that the groundwater available in its natural form has a chemical composition within the allowable limits recommended by official bodies like World Health Organisation (WHO) and Drinking Water Inspectorate (DWI).

The spatio-temporal variation in groundwater quality for London for the last two decades have been studied using observed data and addressed in chapter 6 of this thesis. The geology of the London palaeogene aquifer varies, and therefore so does the natural character of the groundwater it contains. Investigation of statistical distributions, regional mapping variability, assessing temporal changes, and interpretation of the primary geochemical processes have all been used to characterise the chemical compositions of groundwaters. Several water quality parameters were considered: nitrates, nitrites, hardness, sodium, Dissolved Oxygen (DO), and others. The case studies are presented in detail for hardness, sodium, and DO. A great range of variations of these parameters could be found and was attributed to variation in the geology of the London Palaeogene aquifers and anthropogenic activities. The spatial variation maps showed that there are localised patches of groundwater below Drinking Water Inspectorate (DWI) acceptable limits, but overall, London's groundwater is of potable status. The Pearson correlation coefficients showed that hardness and sodium are negatively correlated, and DO and sodium are negatively correlated.

The groundwater quality status in London is explored in this thesis. However, the type and form of drinking water standards may differ between countries and areas. There is not a single strategy

`

that works for everyone. The present or planned legislation relating to water, health, and local government, as well as the capability of regulators, must be considered in the creation and implementation of standards. Approaches that work in one country or region may or may not work in another country or location. In order to build a regulatory framework, each country must assess its own needs and capabilities.

7.2 Challenges faced and overcome in the study

Groundwater variation, in terms of quantity and quality, and land deformation are active fields of research with developments focused on refined algorithms, optimisation of data processing, and adaptation to different satellite sensors. This research shows that expertise in SAR image processing, and experience in data interpretation are both crucial to understanding PSInSAR data. While commercial software packages like SARscape can successfully produce PSInSAR results, it is essential to understand the limitations of the data and their dependence on the parameters chosen for an individual data set.

For remote sensing and GIS related research, data availability is always a significant limitation. Even if the data is available, it could be very expensive and difficult to get access to such data. Thus, in this research mostly open access freely available data was used. For example, the InSAR data used was from ENVISAT-ASAR and Sentinel sensors, gravity data used was from GRACE satellites. For groundwater quality observations, open-source data provided by the Environment Agency was used. To get access to GNSS data and observed groundwater data for validation of InSAR and GRACE results was really challenging. The thesis work became possible with active help from institutions and agencies like the Environment Agency, British Isles Continuous GNSS Facility (BIGF), and Central Ground Water Board (CGWB) – India who provided groundtruth data on our request for research purposes. Another challenge that was overcome, was to secure funding with ESA, through their Eohops programme, for access to the SARscape software for InSAR time series analysis.

The biggest challenge that was faced during this research work was the outbreak of COVID-19 and the resulting work from home conditions. I shared the flat with 3 other people, and there was always a fear of getting infected, since we are using common kitchen facilities. During the lockdown I had not been able to go out or travel at all and staying at home was sometimes very

`

frustrating. The COVID-19 disease was spreading very fast in my home country, India, and I was always worried about the health and safety of my family. But with constant support and motivation from both my supervisors, I managed the stress and finished the research work on time.

This thesis presents results from only a small fraction of the vast amount of information contained in the PSInSAR data sets revealing groundwater induced surface deformation across London and NCT-Delhi, and groundwater quality analysis of London. There are plenty of opportunities to improve and extend the research discussed already. The various spatial and temporal plots relating to groundwater and related phenomenon presented in this thesis could be very useful in groundwater management of urban areas.

7.3 Optimum strategy for groundwater monitoring

According to the International Groundwater Resources Assessment Centre (IGRAC) global inventory of groundwater monitoring and systematic monitoring of groundwater quantity or quality, even at a regional scale, is minimal or non-existent in many countries (Jousma and Roelofsen, 2004). Due to a lack of monitoring, undiscovered degradation of water resources may occur, either due to over-abstraction or pollution, resulting in the following scenarios: groundwater levels decline and groundwater reserves are depleted; reduced base flows occur in streams and springs, as well as reduced flows to sensitive ecosystems like wetlands; reduced access to groundwater for drinking and irrigation purposes; increased expenditures for pumping and treatment; and damage to foundations due to subsidence.

Various aspects must be considered for drafting an optimum strategy for monitoring and assessing groundwater. This may include defining the area to be monitored, defining information needs, defining monitoring objectives, data source types involved, using existing data, prioritising monitoring efforts, and presenting results.

All the above aspects have been addressed in this thesis for groundwater monitoring. The study is focused on urban areas, since the large population in cities exerts pressure on groundwater leading to its depletion in quantity and quality. The areas selected for monitoring in the thesis are London and NCT-Delhi, and the methodology used could be extended to any other urban area across the globe. The information provided in this thesis broadly covers change in groundwater levels,

`

groundwater induced subsidence and groundwater quality status and these are used to study spatio-temporal variations in groundwater.

The data source availability is usually a significant limitation especially on large spatial and temporal scales. While terrestrial in situ measurements are expensive and time-consuming, satellite measurements are consistent in the temporal domain and can cover large spatial extents. However, satellite measurements need validation, which needs ground truth data. Most countries have different government agencies that monitor groundwater data, but these are limited in temporal and spatial domains and can be highly inconsistent. Thus, a hybrid approach towards data sources is used in this thesis. The satellite measurements like InSAR and GRACE have been used and observed ground measurements from different UK and India government agencies. The data has been presented via various spatial and temporal maps using GIS and data visualisation based on R programming.

Thus, this research suggests that the optimum strategy for monitoring groundwater properties and behaviour is using remote sensing principles like InSAR and GRACE in conjunction with observed in situ data either recorded by reliable agencies or acquired by conducting field experiments. The data analysis, visualisation and presentation are then needed and should be based on the required outputs and the questions to be answered.

7.4 Groundwater subsidence in developed and developing nations

According to recent studies by WHO, planet earth is soon approaching a threat of diminishing freshwater because of increasing demand (exceeding supply), resulting in freshwater inaccessibility for significant portions of the world population (WHO, 2017). Each person on the planet is believed to require a minimum of 1,000 m^3 of water per year for domestic uses. Currently, 1.6 billion people live in river basins where water availability is inadequate (Fraiture et al., 2007). According to projections, more than half of the world's freshwater supplies will be stressed or in short supply by 2025 (Rogers, 2008). According to models that analyse the sensitivity of water supplies to future climate behaviour, population expansion and relocation, and urbanisation, water depletion trends can be related to climate variation and population increase. Climate change can cause good and negative responses that will vary by region. However, population growth to over

`

8 billion combined with climate variations is anticipated to result in a worldwide increment in the unavailability of freshwater (Vörösmarty et al., 2000).

The use of groundwater to meet overall water requirements is highly significant, and the increment in its demand in future will pose a considerable groundwater management challenge. Indeed, as groundwater supersedes surface water to meet human needs, the stress on the groundwater is likely to increase in the future. The natural positive characteristics of groundwater (quality and quantity wise) and economic availability via improved and less expensive pumping methods will drive this transformation (Villholth et al., 2007).

Groundwater withdrawals are expected to increase quickly in developing nations like India, Pakistan, and China, whereas its exploitation in the United States, the United Kingdom and Europe are expected to remain relatively stable (Shah, 2005). Global outlook also shows that focusing on agricultural groundwater usage is critical, because the amount of water required for agriculture far outstrips the amount necessary for industrial and domestic uses (Burke, 2002). According to the FAO (2003), managing groundwater requirements for agricultural services is restricted, especially in developing countries where poor farmers do not have alternatives. It further suggests that the overuse of groundwater can enforce socioeconomic transformation like relocations, transfer of resources, and transfer of rights to rich and influential people.

According to Villholth et al. (2007), survival and profit are two crucial factors influencing groundwater management in any country. A poor farmer on a small field in a developing country may symbolise one extreme, while the large-scale commercial farmer growing thousands of acres in a developed nation may represent the other. Large-scale users put the most stress on the groundwater per capita, yet when multiple small-scale users are grouped in big economies, such as China and India, the cumulative impact may be equivalent. In both scenarios, groundwater depletion will take place and result in negative consequences. The primary distinction between the two scenarios is that there are regulations to check overuse and enforce sustainable water development methods in developed nations. In contrast, in developing nations, the regulations are neither adequate nor enforced, which hinders the management of groundwater.

The above-predicted groundwater usage shows that government bodies and researchers will contribute a crucial part in discovering answers to the complicated groundwater management challenges faced today and anticipated in the future. The socioeconomic and sociopolitical

`

condition of society using groundwater and the physiochemical and biological aspects of groundwater will need to be considered while developing management solutions. The purpose of this study is to help develop such solutions.

7.5 Groundwater quantity and quality interactions

Anthropogenic impacts on groundwater aquifers are not limited to groundwater removal and forced discharge but can also impact their quality. This is especially true for groundwater contamination, which is a result of human activity in which the vast majority of people have no intention of interfering with groundwater. It is also worth noting that those who contaminate groundwater are not always the same as others who consume and gain from the same resource. As a result, most people may not receive direct feedback from their polluting activities, which does not help motivate them to improve their practices or consider sustainable use of the resource.

Variations in groundwater volume may have an impact on groundwater quality, either directly or indirectly. Changes in the groundwater regime generated by withdrawal can cause the migration of water masses of varying quality, resulting in groundwater quality degradation. These domains are not characterised by the entrance of new compounds but by the migration of substances already present in the water masses or the subsurface. The most typical example is a local rise in groundwater salinity caused by either seawater intrusion or the upconing of saline water beneath fresh groundwater, both of which are triggered by groundwater exploitation. The injection of contaminants into the aquifer or the transport of contaminants via the soil into the groundwater domain can both cause groundwater quality degradation. The addition of chemicals to water volumes characterises this type of groundwater quality degradation.

Some examples of groundwater quality and interactions are as follows: The increase in salinity in aquifers receiving irrigation return flows. The latter not only returns water with more concentrated minerals, but also flushes out some of the fertilisers and pesticides that have been applied. Another example is the induced rise in arsenic levels in shallow groundwater in Bangladesh, which was caused by intense groundwater exploitation. Another example is, parts of the London basin aquifer in the United Kingdom that were dewatered due to over-abstraction from 1820 to 1940. Because of pyrites (iron sulphide) oxidation in some of the dewatered zones, groundwater quality

`

deteriorated at some sites. The oxidation posed operating challenges for extraction because of the high iron and sulphate content.

The most prevalent induced groundwater quality degradation type is seawater intrusion and saline water upconing in coastal zones. This has been observed in various countries throughout the twentieth century, including China, along the Mediterranean Sea and the North Sea, and the United States (Atlantic Coast, Florida and California). Reduced groundwater abstraction rates, artificial recharge, and pumping impediments are all possible ways to control it. Faulty drilling operations, insufficient well construction, and well casing corrosion can all cause induced groundwater quality degradation, resulting in hydraulic short-cuts across aquifers with varying groundwater quality. While investigating groundwater quantity exploitation and quality deterioration independently is essential, studying their interaction would be advantageous for effective monitoring.

7.6 SAR-GRACE applications other than groundwater

GRACE and SAR have great potential as a source of information for researchers and scientists. The two technologies together can make a special contribution to research in oceanography, glaciology, and hydrology, where the necessary information includes a static field and changes in that field with time. In oceanography, SAR-GRACE studies will allow more detailed research of mass and heat transport by ocean currents between different regions of the earth. Combining geoid information retrieved from GRACE data; ocean level, oil spills and ship detection from SAR data; satellite altimetry data; and temperature and salinity values directly measured by sea vessels, it will be feasible to map reasonably accurate directions and speeds of different currents. In glaciology, the SAR-GRACE data can facilitate calculation and control of ice mass changes in glaciers in different world regions and estimate glacial-isostatic adjustment of uplift of the earth's crust. In most hydrological problems, this combined approach can provide reliable data for estimating the total water budget, which is extremely challenging using in situ data. The study of lithosphere reactions to large earthquakes, which occurred within the operational period of the SAR and GRACE satellites, could be explored in detail. By lithosphere reactions, changes in the density distribution near the earthquake epicentre could be understood, which induce temporal variations in the gravity field, and phase changes in InSAR signals, as registered by the GRACE and SAR satellites.

`

The potential for combining GRACE and SAR measurements is promising, but methodological difficulties are now limiting it. GRACE has a limited spatial resolution, but SAR has a high spatial resolution. The SAR approach is ideal for examining spatial fluctuations, while GRACE is ideal for studying geophysical processes across time. The resolution is projected to improve with improved processing methods and the GRACE follow-on mission. Furthermore, as the coverage and availability of SAR data expand, the accuracy of subsidence mapping should improve. It will be possible to read SAR and GRACE results at the similar resolution and make a direct statistical comparison for future investigations using these revised data sets. Overall, the combination of SAR with GRACE provides an intriguing method for tracking groundwater and ground movement in both space and time. There is both hope and anticipation for a viable solution for remote geophysical process evaluation employing SAR-GRACE concepts in the future.

7.7 The future of InSAR and GRACE

The future is SAR technology is promising. With multiple sensors being launched and various data processing algorithms, the accuracy of InSAR is expected to improve. Microwave radar images with higher wavelengths (such as the L-band PALSAR onboard the ALOS) are now accessible, allowing InSAR deformation imaging at global scales where C-band InSAR is prone to signal loss due to vegetation. The use of fully polarised SAR sensors (such as ALOS, Radarsat-2, TerraSAR-X, TanDEM-X, and others) allows for a better characterisation of crops, forests and infrastructure. Landscape mapping and deformation monitoring is more prominent because of the combination of polarimetric and interferometric analysis (Pol-InSAR). The atmospheric delays that reduce InSAR accuracy will be decreased by routinely estimating water vapour content using a high-resolution weather model, continuous global positioning system (CGPS) network, or other satellite sensors such as the Moderate Resolution Imaging Spectroradiometer (MODIS), Advanced Spaceborne Thermal Emission and Reflection Radiometer (ASTER), and European Medium Resolution Imaging Spectrometer (MERIS) to improve InSAR deformation measurements. Automated SAR and InSAR processing systems will become more widely available, enhancing SAR/InSAR processing and laying the groundwork for routine monitoring of natural hazards and natural resources. The automated SAR/InSAR processing system is critical for near-real-time decision support as more satellite radar sensors and radar satellite constellations become available over the next decade.

`

GRACE gravimetry, like InSAR, offers a lot of potential in the future. GRACE-FO is the follow-on mission to the original GRACE mission, which orbited the earth from 2002 to 2017. GRACE-FO is planned to continue the highly successful work of its predecessor while also putting to the test a new technology that will significantly improve the measurement system. GRACE-FO, launched on May 22, 2018, will keep watch on changes in subsurface water storage, the amount of water in big lakes and rivers, soil moisture, ice sheets and glaciers, and sea level caused by the addition of water to the ocean. These findings offer a unique perspective on earth's climate and have far-reaching implications for society and the global population.

7.8 Summary of the chapter

This chapter evaluates if all the objectives drawn are addressed. Then a broader perspective of the research work is discussed. Issues and topics not directly addressed in our case studies have been briefly discussed, for example, the importance of groundwater quality-quantity interdependence. The groundwater monitoring approach in developed and developing nations has been discussed, and a feasible optimum monitoring approach in urban areas has also been discussed. The strengths, limitations and future of InSAR and GRACE technologies have been discussed as well.

`

Chapter 8 Conclusions And Recommendations for Future Research

This research highlights a range of remotely sensed methods and tools to monitor groundwater quantity changes and subsequent land movement in London (and NCT-Delhi), most of which can generally be extended to other urban environments. In this thesis, a fresh endeavour is made to investigate InSAR and GRACE technologies, as well as their application to studying variance in groundwater resources in London. Land subsidence in the London and Delhi has also been investigated, as both cities are experiencing rapid population development, putting undue strain on groundwater resources. Despite their differences in subsurface geology, these cities face a serious threat of land shift as a result of rising groundwater pressure. There has never been a research that looked at the groundwater behaviour and the associated land subsidence for both of these cities at the same time. Furthermore, no systematic work on the spatiotemporal variation of groundwater quality measures has been done in London in the recent two decades. To help allocate resources to preserve potable-quality groundwater, a detailed assessment of spatio-temporal changes in groundwater quality of London in terms of various physio-chemical parameters using inferential statistics and GIS tools was done. The major conclusions from each of the case studies are summarized below:

8.1 Selection of SAR processing Sensor and Software

The ability of differential interferometry to monitor ground movement in the vertical direction with millimetre level accuracy has been noted in several papers for over three decades. However, because data and software availability for processing can be a substantial limitation, especially for beginner users, this technique is best suited for InSAR experts. In addition, most SAR tools and software packages are difficult to understand for a novice user, and specialist knowledge of InSAR imaging may be required. Thus, a comprehensive review of all past, present, and future SAR sensors was provided in chapter 3. The strengths and limitations of each sensor were presented. Since 2014, Sentinel-1 provides open access, continuous data in C-band, and was used to study land subsidence in this thesis. For data before 2014, ENVISAT-ASAR, another C-band open access sensor, was used to study land subsidence. The most important reasons for selecting datasets from these two sensors were: (i) C-band data is capable of measuring millimetre level deformation, (ii) the repeat cycle of 35 days and 12 days for ASAR and Sentinel-1 respectively ensures

`

continuous monthly monitoring, (iii) the free open access availability, (iv) availability of continuous images over our study area.

After deciding on the sensors, the best software package to process InSAR data was needed. Most available open-source and commercial software packages were studied and explored. Snap (open-access) and SARscape (commercial) were then tried, and experiments were performed on London using the DInSAR methodology. It was concluded that open-source software and free datasets can give excellent results, which are highly comparable to expensive commercial software, and can motivate more people to work with SAR technology. However, extensive coding requirements to work with packages like Stamps and ISCE can be very challenging for novel users.

On the other hand, commercial software like SARscape is more user-friendly with a graphical user interface, semi-automated, saves computing time, and is capable of reducing errors like surface decorrelations, atmospheric effects, atmospheric noise, baseline errors (spatial and temporal), DEM error, orbit error and others. The funding was obtained for ENVI-SARscape distributed by Harris Geospatial via the ESA-Eohops programme. Thus, for this thesis, Envisat ASAR and Sentinel-1 data were used for London (and Delhi) for different time intervals, which were processed to get land movement in SARscape software.

8.2 InSAR-GRACE Study for London

London is a heavily built-up area with a dense urban fabric and witnessing a continuous increase in population. This population increase can put extra pressure on groundwater resources, further triggering the problem of land subsidence. Thus, changes were monitored in groundwater and subsidence for London using different geospatial tools like PSInSAR, GRACE gravity anomalies, GNSS and observed boreholes between December 2002 and September 2010. The following conclusions were obtained from the study:

1) The ground movement in London was found to be noticeably irregular and non-linear. The ground movement in the north-western corner of the research area (Central London) was positive, indicating land uplift; while the ground movement in the south-eastern half of the research region was negative, signifying land subsidence.

2) The average deformation in the study area was found to be −0.176 mm/year, indicating overall subsidence. By statistically analysing the average subsidence velocities, it was

`

observed that the standard deviation of 98.22% of the PS points was less than 5 mm/year, and that for overall PSInSAR subsidence was 0.665 mm/year.

3) The InSAR subsidence values were validated using GNSS data. The two-sample *t*-test provides enough evidence that GNSS up values were in close agreement with the obtained InSAR subsidence values, thus demonstrating that the PSInSAR is an efficient way to survey ground movement in London.

4) The groundwater changes obtained from GRACE demonstrated a decreasing tendency, and the average groundwater loss from GRACE was found to be 9.003 MCM/year. The best-fit line for the temporal groundwater variation from GRACE had a negative slope, indicating groundwater depletion.

5) The volumetric change of groundwater derived from GRACE data accounted for 60% of the total change in the report from the Environment Agency. In addition, the GRACE-derived temporal time-series showed seasonal and annual variations.

6) The ground movement was studied in conjunction with groundwater variation obtained from various boreholes. The spatial change in ground movement and the spatial change in the groundwater were found to be consistent.

7) Our results confirm that, when a large volume of groundwater is extracted from an aquifer, it results in compaction of underlying aquifer material and, in turn, this is responsible for land subsidence, and, in contrast, recharge or rebound of groundwater results in land upliftment.

8.3 London-Delhi Subsidence study

The land movement due to groundwater withdrawal and recharge was studied for London and Delhi between 2016 and 2020. Different factors resulting in anthropogenic groundwater withdrawal and recharge like construction of underground tunnels, pressure on boreholes, and others were studied in conjunction with associated land movement. Different types of site-specific land movement like uplift, subsidence, and differential deformations, and corresponding groundwater variations were analysed for both cities.

1) Across both the cities and in all cases, the most common factor controlling the spatial patterns of land motion was the change in groundwater level. It was again concluded that

`

when groundwater is extracted from an aquifer in large quantities, it leads to land subsidence. Conversely, a rebound or recharge of groundwater leads to land uplift.

2) The differential deformation area was found near the Northern Line extension (NLE) in London. The Battersea area near NLE had mean subsidence of -3.44 ± 2.4 mm/year, while the Kennington area nearby had mean uplift of 4.55 ± 1.37 mm/year. In Kennington, the ground subsided during 2016-2017, before continuously uplifting since November 2017. This motion corresponds to subsidence due to dewatering during the tunnel's construction, followed by groundwater rebound (heave) once the dewatering ceased in November 2017.

   In NCT-Delhi, the differential land deformation was observed near the Magenta-Blue metro line, with mean subsidence of -5.09 ± 3.31 mm/year and mean uplift of 11.06 ± 4.61 mm/year. This land movement was mainly attributed to the extraction and rebound of groundwater to construct underground metros.

3) The subsidence area studied in London extended from Wimbledon to Tooting. The area suffered mean subsidence of -4.87 ± 1.19 mm/year. The Wimbledon Fault bounds the northwest edge of the area, and also it contains Merton Abbey public water supply well, which is one of the most heavily exploited groundwater wells in London. Both these factors largely controlled the land deformation pattern in this region.

   The subsidence area in NCT-Delhi lies in the vicinity of the Delhi-Haryana border, which had average subsidence of -4.37 ± 1.71 mm/year. A large population reside on the border of Delhi-Haryana, as these people can use the benefits of a capital city without paying the heavy living expenses. This increased population exerts serious pressure on the groundwater resources and leads to groundwater depletion and induced subsidence.

4) The uplift area in London stretches from Bruce Castle to Abney Park with a mean uplift of 3.64 ± 1.21 mm/year. The area has several water reservoirs and recreation parks, which assists in the recharge of groundwater. Seepage from the various water reservoirs and artificial watering of the various recreation parks are the important contributing factors for the increase in groundwater level, which is why land uplift is witnessed.

   For NCT-Delhi, the uplift area is across the Rohini metro line with mean uplift of 6.30 ± 2.17 mm/year. This area is one of the wealthiest regions of Delhi city and is subjected to

`

managed groundwater abstraction and recharge. This led to a rise in groundwater level and thus showing continuous uplift.

5) A 1-D mathematical model was used to calculate groundwater depletion from a given change in groundwater level. The results obtained from the mathematical model agrees well with our PSInSAR results.

6) NCT-Delhi has been declared as a groundwater critical zone by the government of India. It is one of the most exploited cities with regards to groundwater, owing to its urban fabric and ever-increasing population, and these results reflect that. London is not recognised as having a critical status, but its ever-increasing population and the government's aquifer recharge policy exerts local pressure and is borne out by these results.

8.4 Groundwater quality for London

1) The monitoring of spatio-temporal variation of groundwater quality for London is done using Geographical Information System (GIS) and inferential statistics between 2000-2020. Data samples from 500 wells have been used in the London basin, and the data is provided in the open access domain by Environment Agency.

2) The Piper-Trilinear plots indicated the hydro-chemical facies of groundwater in the study area were magnesium bicarbonate types. The groundwater of central, east, south, and north London could be classified as dominant magnesium bicarbonate types, while that of west London could be classified as a mix of sodium chloride and sodium bicarbonate type.

3) Except for west London, the bicarbonate-chloride ratio was greater than 2 for all the subzones, and hence salt-water intrusion is not a significant problem for London groundwater.

4) The concentration of nitrates and nitrites in groundwater were less than 10 mg/l and 0.02 mg/l respectively, during our observation period, for all the 5 subzones.

5) For central London, as high as 91.3% of samples exceeded the DWI limit, and thus groundwater must be treated for hardness before using it for potable purposes. For west London, only 26.19% of samples exceed 200 mg/l, thus major treatment for the hardness of groundwater coming from west London is not required. A comparison of mean concentrations of hardness by wards for the second quarter of the year 2000, 2010 and 2019

shows that the maximum number of wards has hardness between 200-300 mg/l for all three years. Only 39 wards in 2000, 35 wards in 2010 and 89 wards in 2018 have hardness within the acceptable limits of less than 200 mg/l. Also, the extreme hardness of 400-500 mg/l is found mainly in north London for all three years. A general trend across London is that groundwater is softer in the south and becomes harder moving north.

6) Sodium had a range of 61-750 mg/l across London, which is a typical range for sandstone aquifers in England. The average value of sodium for east London was above DWI prescribed limits, while that for the other four subzones of London was within the prescribed limit (less than 200 mg/l). A comparison of mean concentrations of sodium for the second quarter of the year 2000, 2010 and 2019 by ward showed that the highest number of wards had sodium concentration between 60-120 mg/l for 2000 and 2010, while for 2019 maximum number of wards had a concentration between 0-60 mg/l. Only 64, 28 and 58 wards for those three dates in London had sodium concentration over 180 mg/l, thus for most of the London area, the groundwater is safe for drinking purposes, with respect to sodium. A general spatial trend is that the concentration of sodium increases radially inwards towards the centre of the city.

7) DO measured has a wide range of 0.0 mg/l to 10.74 mg/L. The mean DO in groundwater for central London was 3.84 mg/l, while that for other parts of London was over 5 mg/l. DO frequently regulates the types and numbers of microbes present in an aquifer, hence controlling the destiny of dissolved organic pollutants. A comparison of mean concentrations of DO for the third quarter of the year 2000, 2010 and 2019 by ward showed a decrease in the mean highest concentration (>8 to 10 mg/l) during the first decade and second decade. The pie charts showed that the number of wards with mean DO concentrations greater than 8 mg/L was 47 in 2000, 1 in 2010, and 0 in 2019. Between 2000 and 2010, the number of wards with a mean concentration of DO between 2-4 mg/L increased by nearly 26 times, and then decreased 10 times between 2010 and 2019. For the year 2000 highest number of wards (283) had DO values between 6-8 mg/l, while that for the year 2010 was between 2-4 mg/l with a count of 337, and finally, for 2019, the highest number of wards (250) had DO values between 4-6 mg/l.

`

8) The Pearson coefficient for sodium and hardness was negative for all the 5 subzones, which shows that with an increase in sodium, the hardness decreases in water. Similarly, sodium and DO are negatively correlated in all 5 subzones, which showed that the DO in water decreases with an increase in sodium content. Variability in 'r' was observed over the 5 sub-areas, which is expected given the variability in our observed data. Also, several factors contributed to groundwater quality variations in London, including rock/sediment composition, groundwater chemical evolution, seepage from nearby formations, and probable human controls.

9) The study can act as a guide for decision making and to identify hazardous contaminants. It has the potential to prioritise management efforts and funds, assess the overall effects of water quality interventions, and monitor water resources and health.

8.5 Future scope and Recommendations

This thesis has considered open-sourced SNAP and commercial SARscape for processing the InSAR data. There are several others software packages available, as discussed in chapter 3, that could be tried. For example, with the latest release and updates on ICSE and its support by UNAVCO, it could be a really powerful open-source processing software. By considering the output required, available resources, and analysing the strengths and limitations of each software package, it could be helpful to try other software packages to process InSAR data. The SAR processing was done using Sentinel-1 and ENVISAT-ASAR, C band data, but other MW sensors with different wavelengths could be tried. For example, the density of PS obtained will be much higher if X-band sensors are used, but the X-band data is not accessible in the open domain and getting access could be very expensive.

The spatial resolution for GRACE is low, while that of InSAR is high. The PSInSAR method is excellent for studying the spatial variation of groundwater, and GRACE is excellent for studying the temporal variation of groundwater. With new processing algorithms and the GRACE follow-on mission, the resolution is expected to improve. In addition, the increasing coverage and availability of SAR data should enhance the accuracy of subsidence mapping. With these updated data sets, it will be suitable to read InSAR and GRACE results at the same resolution and make a direct statistical comparison for future studies. Overall, the study of InSAR and GRACE in

`

conjunction provides an interesting technology for spatial and temporal mapping of groundwater and ground movement.

London and Delhi are both urban cities, but they are superficially different in terms of civil engineering and city planning. Their response to the groundwater extraction and recharge and how that is reflected in the change of surface level tells a similar story. This suggests that it may be a universal effect, which is anticipated observing in other major urban cities worldwide, subjected to similar engineering decisions. Thus, the methodology developed in chapter 5 could be tried in other cities across the world, to test the efficiency and validity of the results. Also, the mathematical model used to corelate groundwater and land deformation did not consider time-lag constant. It is however possible to apply the time-lag constant to the output after the model if an approximation of the time-lag is required.

The overall groundwater quality for London has been studied for the last two decades. The study analysed several water quality parameters but Hardeness, Sodium and DO have been discussed in detail owing to their behavior in the study area. The methodology developed could be used to further study various other parameters in detail, for London as well Delhi. The groundwater quality variation and quantity variation has been studied separately as different case studies. Further modelling and applying the data and methodologies developed in this thesis, a link between groundwater quantity and quality variation could also be studied in future. For example, parts of the London basin aquifer in the United Kingdom were dewatered because of over-abstraction from 1820 to 1940. At some sites, this caused deterioration in groundwater quality because of pyrites (iron sulphide) oxidation in some of the dewatered zones. The oxidation caused operational difficulties for abstractions because of the high iron and sulphate content. Thus, the effect of over-extraction or recharge of groundwater on its quality could be interesting to explore.

`

References

Abelson, P. H. (1984). Groundwater contamination. *Science*, *224*(4650), 673.

Abidin, H. Z., Djaja, R., Darmawan, D., Hadi, S., Akbar, A., Rajiyowiryono, H., Sudibyo, Y., Meilano, I., Kasuma, M. A., Kahar, J., & others. (2001). Land subsidence of Jakarta (Indonesia) and its geodetic monitoring system. *Natural Hazards*, *23*(2), 365–387.

Aeschbach, H. W., & Gleeson, T. (2012). Regional strategies for the accelerating global problem of groundwater depletion. *Nature Geoscience*, *5*(12), 853–861.

Agarwal, V., Kumar, A., Gomes, R. L., & Marsh, S. (2020a). An overview of SAR sensors and software and a comparative study of poen source (Snap) and commercial (SARscape) software for DInSAR analysis using C-band Radar images. *41st Asian Conference on Remote Sensing - ACRS*. https://www.researchgate.net/publication/345335178

Agarwal, V., Kumar, A., Gomes, R. L., & Marsh, S. (2020b). Monitoring of ground movement and groundwater changes in London using InSAR and GRACE. *Applied Sciences (Switzerland)*, *10*(23), 1–21. https://doi.org/10.3390/app10238599

Agarwal, V., Kumar, A., Gomes, R. L., & Marsh, S. (2021). *Comparison of groundwater induced Land subsidence in London and Delhi using PSInSAR*.

Ahmed, M., Sultan, M., Wahr, J., & Yan, E. (2014). The use of GRACE data to monitor natural and anthropogenic induced variations in water availability across Africa. *Earth-Science Reviews*, *136*, 289–300.

Albino, F., Biggs, J., Yu, C., & Li, Z. (2020). Automated Methods for Detecting Volcanic Deformation Using Sentinel-1 InSAR Time Series Illustrated by the 2017--2018 Unrest at Agung, Indonesia. *Journal of Geophysical Research: Solid Earth*, *125*(2), e2019JB017908.

Aldiss, D. (2014). The stratigraphical framework for the Palaeogene successions of the London Basin, UK. In *Open Report OR/14/008*.

Aldiss, D., Burke, H., Chacksfield, B., Bingley, R., Teferle, N., Williams, S., Blackman, D., Burren, R., & Press, N. (2014). Geological interpretation of current subsidence and uplift in the London area, UK, as shown by high precision satellite-based surveying. *Proceedings of the Geologists' Association*. https://doi.org/10.1016/j.pgeola.2013.07.003

`

Alley, W. M. (2007). The Importance of Monitoring To Groundwater Management. *US Geological Survey*.

Alley, W. M., & Konikow, L. F. (2015). Bringing GRACE Down to Earth. In *Groundwater*. https://doi.org/10.1111/gwat.12379

Alsdorf, D. E., Melack, J. M., Dunne, T., Mertes, L. A. K., Hess, L. L., & Smith, L. C. (2000). Interferometric radar measurements of water level changes on the Amazon flood plain. *Nature*, *404*(6774), 174–177.

Altamira. (2020). *Altamira*. https://site.tre-altamira.com/ Last Accessed: 2020-10-03

Amelung, F., Jonsson, S., Zebker, H., & Segall, P. (2000). Widespread uplift and 'trapdoor'faulting on Galapagos volcanoes observed with radar interferometry. *Nature*, *407*(6807), 993–996.

An, D., Xi, B., Wang, Y., Xu, D., Tang, J., Dong, L., Ren, J., & Pang, C. (2016). A sustainability assessment methodology for prioritizing the technologies of groundwater contamination remediation. *Journal of Cleaner Production*, *112*, 4647–4656.

Andersen, O. B., Seneviratne, S. I., Hinderer, J., & Viterbo, P. (2005). GRACE-derived terrestrial water storage depletion associated with the 2003 European heat wave. *Geophysical Research Letters*, *32*(18).

Andrew, G., & Richard, G. (1988). Crossed orbit interferometry: theory and experimental results from SIR-B. *International Journal of Remote Sensing*, *9*(5), 857–872.

Arias, E.-M., López-Periago, E., Mart\'\inez-Carballo, E., Simal-Gándara, J., Mejuto, J.-C., & Garc\'\ia-R\'\io, L. (2008). The mobility and degradation of pesticides in soils and the pollution of groundwater resources. *Agriculture, Ecosystems \& Environment*, *123*(4), 247–260.

Bandikova, T. (2015). *The role of attitude determination for inter-satellite ranging*. Fachrichtung Geodäsie und Geoinformatik der Leibniz-Universität.

Bank, W. (2012). *India groundwater: A valuable but diminishing resource*. World Bank Washington, DC, USA.

Barlow, J. R. B., & Clark, B. R. (2011). *Simulation of water-use conservation scenarios for the*

`

Mississippi Delta using an existing regional groundwater flow model. US Department of the Interior, US Geological Survey.

Bartier, P. M., & Keller, C. P. (1996). Multivariate interpolation to incorporate thematic surface data using inverse distance weighting (IDW). *Computers and Geosciences*. https://doi.org/10.1016/0098-3004(96)00021-0

Bateson, L., Barkwith, A., Hughes, A., & Aldiss, D. (2009). Terrafirma: London H-3 Modelled Product: comparison of PS data with the results of a groundwater abstraction related subsidence model. *British Geological Survey Commissioned Report*, *OR/09/032*, 47.

Baum, R. L., Galloway, D. L., & Harp, E. L. (2008). *Landslide and land subsidence hazards to pipelines*.

Bawden, G. W., Thatcher, W., Stein, R. S., Hudnut, K. W., & Peltzer, G. (2001). Tectonic contraction across Los Angeles after removal of groundwater pumping effects. *Nature*, *412*(6849), 812–815.

Bearcock, J. M., & Smedley, P. L. (2010). *Baseline groundwater chemistry: the Palaeogene of the Thames Basin*.

Bearcock, J. M., Smedley, P. L., Fordyce, F. M., Everett, P. A., & Ander, E. L. (2019). Controls on surface water quality in the River Clyde catchment, Scotland, UK, with particular reference to chromium and lead. *Earth and Environmental Science Transactions of the Royal Society of Edinburgh*. https://doi.org/10.1017/S1755691018000397

Benesty, J., Chen, J., Huang, Y., & Cohen, I. (2009). Pearson correlation coefficient. In *Noise reduction in speech processing* (pp. 1–4). Springer.

Berardino, P., Fornaro, G., Lanari, R., & Sansosti, E. (2002). A new algorithm for surface deformation monitoring based on small baseline differential SAR interferograms. *IEEE Transactions on Geoscience and Remote Sensing*. https://doi.org/10.1109/TGRS.2002.803792

Berry, P. A. M., Garlick, J. D., Freeman, J. A., & Mathers, E. L. (2005). Global inland water monitoring from multi-mission altimetry. *Geophysical Research Letters*, *32*(16).

Berthold, S., Bentley, L. R., & Hayashi, M. (2004). Integrated hydrogeological and geophysical

`

study of depression-focused groundwater recharge in the Canadian prairies. *Water Resources Research*, *40*(6).

BGS. (2013). Industrial and urban pollution of groundwater. *UK Groundwater Forum*.

BGS. (2021). *Geoindex Onshore for boreholes provided by British Geological Surevy*. http://mapapps2.bgs.ac.uk/geoindex/home.html?layer=BGSBoreholes

Bhaskar, A. S., Beesley, L., Burns, M. J., Fletcher, T. D., Hamel, P., Oldham, C. E., & Roy, A. H. (2016). Will it rise or will it fall? Managing the complex effects of urbanization on base flow. *Freshwater Science*, *35*(1), 293–310.

Bischoff, C. A., Ghail, R. C., Mason, P. J., Ferretti, A., & Davis, J. A. (2019). Revealing millimetre-scale ground movements in London using squeeSAR^{TM}. *Quarterly Journal of Engineering Geology and Hydrogeology*. https://doi.org/10.1144/qjegh2018-075

Biswas, K., Chakravarty, D., Mitra, P., & Misra, A. (2017). Spatial-Correlation Based Persistent Scatterer Interferometric Study for Ground Deformation. *Journal of the Indian Society of Remote Sensing*. https://doi.org/10.1007/s12524-016-0647-5

Bjerklie, D. M., Dingman, S. L., Vorosmarty, C. J., Bolster, C. H., & Congalton, R. G. (2003). Evaluating the potential for measuring river discharge from space. *Journal of Hydrology*, *278*(1–4), 17–38.

Bjerklie, D. M., Moller, D., Smith, L. C., & Dingman, S. L. (2005). Estimating discharge in rivers using remotely sensed hydraulic information. *Journal of Hydrology*, *309*(1–4), 191–209.

Blanco-Sanchez, P., Mallorqu\'\i, J. J., Duque, S., & Monells, D. (2008). The coherent pixels technique (CPT): An advanced DInSAR technique for nonlinear deformation monitoring. In *Earth sciences and mathematics* (pp. 1167–1193). Springer.

Bloomfield, J. P., Brewerton, L. J., & Allen, D. J. (1995). Regional trends in matrix porosity and dry density of the Chalk of England. *Quarterly Journal of Engineering Geology*, *28*(Suppl. 2). https://doi.org/10.1144/gsl.qjegh.1995.028.s2.04

Bloomfield, J. P., Bricker, S. H., & Newell, A. J. (2011). Some relationships between lithology, basin form and hydrology: A case study from the Thames basin, UK. *Hydrological Processes*. https://doi.org/10.1002/hyp.8024

`

Bonì, R., Cigna, F., Bricker, S., Meisina, C., & McCormack, H. (2016). Characterisation of hydraulic head changes and aquifer properties in the London Basin using Persistent Scatterer Interferometry ground motion data. *Journal of Hydrology*. https://doi.org/10.1016/j.jhydrol.2016.06.068

Bonì, R., Meisina, C., Cigna, F., Herrera, G., Notti, D., Bricker, S., McCormack, H., Tomás, R., Béjar-Pizarro, M., Mulas, J., & Ezquerro, P. (2017). Exploitation of satellite A-DInSAR time series for detection, characterization and modelling of land subsidence. *Geosciences (Switzerland)*. https://doi.org/10.3390/geosciences7020025

Breña, N. J. A., Kendall, A. D., & Hyndman, D. W. (2014). Improved methods for satellite-based groundwater storage estimates: A decade of monitoring the high plains aquifer from space and ground observations. *Geophysical Research Letters*, *41*(17), 6167–6173.

Bricker, S. H., Banks, V. J., Galik, G., Tapete, D., & Jones, R. (2017). Accounting for groundwater in future city visions. *Land Use Policy*, *69*, 618–630.

Buckley, S. M., Rosen, P. A., Hensley, S., & Tapley, B. D. (2003). Land subsidence in Houston, Texas, measured by radar interferometry and constrained by extensometers. *Journal of Geophysical Research: Solid Earth*, *108*(B11).

Budhu, M., & Adiyaman, I. B. (2010). Mechanics of land subsidence due to groundwater pumping. *International Journal for Numerical and Analytical Methods in Geomechanics*, *34*(14), 1459–1478.

Bulut, O. F., Duru, B., Çakmak, Ö., Günhan, Ö., Dilek, F. B., & Yetis, U. (2020). Determination of groundwater threshold values: A methodological approach. *Journal of Cleaner Production*, *253*, 120001.

Burke, J. J. (2002). Groundwater for irrigation: productivity gains and the need to manage hydro-environmental risk. *Intensive Use of Groundwater Challenges and Opportunities*, *478*.

Cai, B., Liu, B., & Zhang, B. (2019). Evolution of Chinese urban household's water footprint. *Journal of Cleaner Production*, *208*, 1–10.

Carbognin, L., Teatini, P., & Tosi, L. (2004). Eustacy and land subsidence in the Venice Lagoon at the beginning of the new millennium. *Journal of Marine Systems*, *51*(1–4), 345–353.

`

Carnec, C., & Fabriol, H. (1999). Monitoring and modeling land subsidence at the Cerro Prieto geothermal field, Baja California, Mexico, using SAR interferometry. *Geophysical Research Letters*, *26*(9), 1211–1214.

Castellazzi, P., Martel, R., Rivera, A., Huang, J., Pavlic, G., Calderhead, A. I., Chaussard, E., Garfias, J., & Salas, J. (2016). Groundwater depletion in Central Mexico: Use of GRACE and InSAR to support water resources management. *Water Resources Research*. https://doi.org/10.1002/2015WR018211

Castle, S. L., Thomas, B. F., Reager, J. T., Rodell, M., Swenson, S. C., & Famiglietti, J. S. (2014). Groundwater depletion during drought threatens future water security of the Colorado River Basin. *Geophysical Research Letters*, *41*(16), 5904–5911.

Central Ground Water Board. (2016a). *Ground Water Year Book, NCT Delhi, 2015-16*.

Central Ground Water Board. (2016b). *Groundwater scenario in India, November 2016*.

Central Ground Water Board. (2018). Ground water year book-India 2017-18. *Ministry of Water Resources, Government of India*.

Chai, J.-C., Shen, S.-L., Zhu, H.-H., & Zhang, X.-L. (2004). Land subsidence due to groundwater drawdown in Shanghai. *Geotechnique*, *54*(2), 143–147.

Chang, W. L., Smith, R. B., Farrell, J., & Puskas, C. M. (2010). An extraordinary episode of Yellowstone caldera uplift, 2004-2010, from GPS and InSAR observations. *Geophysical Research Letters*. https://doi.org/10.1029/2010GL045451

Changming, L., Jingjie, Y., & Kendy, E. (2001). Groundwater exploitation and its impact on the environment in the North China Plain. *Water International*, *26*(2), 265–272. https://doi.org/10.1080/02508060108686913

Chapman, S. W., & Parker, B. L. (2005). Plume persistence due to aquitard back diffusion following dense nonaqueous phase liquid source removal or isolation. *Water Resources Research*, *41*(12).

Chatterjee, R. S., Fruneau, B., Rudant, J. P., Roy, P. S., Frison, P. L., Lakhera, R. C., Dadhwal, V. K., & Saha, R. (2006). Subsidence of Kolkata (Calcutta) City, India during the 1990s as observed from space by Differential Synthetic Aperture Radar Interferometry (D-InSAR)

technique. *Remote Sensing of Environment*. https://doi.org/10.1016/j.rse.2006.02.006

Chebotarev, I. I. (1955). Metamorphism of natural waters in the crust of weathering. *Geochimica et Cosmochimica Acta*, *8: 22-48*(198–212), 137–170. https://doi.org/10.1016/0016-7037(55)90015-6

Chen, J. L., Wilson, C. R., Tapley, B. D., Scanlon, B., & Güntner, A. (2016). Long-term groundwater storage change in Victoria, Australia from satellite gravity and in situ observations. *Global and Planetary Change*, *139*, 56–65.

Chen, J., Li, J., Zhang, Z., & Ni, S. (2014). Long-term groundwater variations in Northwest India from satellite gravity measurements. *Global and Planetary Change*, *116*, 130–138.

Chen, J., Wu, H., & Qian, H. (2016). Groundwater nitrate contamination and associated health risk for the rural communities in an agricultural area of Ningxia, northwest China. *Exposure and Health*, *8*(3), 349–359.

Chen, L., Wilson, C. R., Tapley, B. D., Yang, Z. L., & Niu, G.-Y. (2009). 2005 drought event in the Amazon River basin as measured by GRACE and estimated by climate models. *Journal of Geophysical Research: Solid Earth*, *114*(B5).

Chen, X., Wang, P., Muhammad, T., Xu, Z., & Li, Y. (2020). Subsystem-level groundwater footprint assessment in North China Plain--The world's largest groundwater depression cone. *Ecological Indicators*, *117*, 106662.

Cheng, X., Chen, L., Sun, R., & Jing, Y. (2019). Identification of regional water resource stress based on water quantity and quality: A case study in a rapid urbanization region of China. *Journal of Cleaner Production*, *209*, 216–223.

Chinnasamy, P., Hubbart, J. A., & Agoramoorthy, G. (2013). Using remote sensing data to improve groundwater supply estimations in Gujarat, India. *Earth Interactions*, *17*(1), 1–17.

Chow, V. T. (1959). Open-channel hydraulics. *McGraw-Hill Civil Engineering Series*.

Cigna, F., Jordan, H., Bateson, L., McCormack, H., & Roberts, C. (2015). Natural and Anthropogenic Geohazards in Greater London Observed from Geological and ERS-1/2 and ENVISAT Persistent Scatterers Ground Motion Data: Results from the EC FP7-SPACE PanGeo Project. *Pure and Applied Geophysics*. https://doi.org/10.1007/s00024-014-0927-3

`

Cigna, F., & Tapete, D. (2021). Satellite InSAR survey of structurally-controlled land subsidence due to groundwater exploitation in the Aguascalientes Valley, Mexico. *Remote Sensing of Environment*, *254*, 112254.

Colesanti, C., & Wasowski, J. (2006). Investigating landslides with space-borne Synthetic Aperture Radar (SAR) interferometry. *Engineering Geology*. https://doi.org/10.1016/j.enggeo.2006.09.013

Conant Jr, B., Cherry, J. A., & Gillham, R. W. (2004). A PCE groundwater plume discharging to a river: influence of the streambed and near-river zone on contaminant distributions. *Journal of Contaminant Hydrology*, *73*(1–4), 249–279.

Copernicus. (2020). *Scihub*. https://scihub.copernicus.eu/ Last Accessed: 2020-09-03

Costantini, M., Falco, S., Malvarosa, F., & Minati, F. (2008). A new method for identification and analysis of persistent scatterers in series of SAR images. *IGARSS 2008-2008 IEEE International Geoscience and Remote Sensing Symposium*, *2*, II--449.

Crosetto, Biescas, E., Dura, J., Closa, J., & Arnaud, A. (2008). Generation of advanced ERS and envisat interferometric SAR products using the stable point network technique. *Photogrammetric Engineering and Remote Sensing*. https://doi.org/10.14358/PERS.74.4.443

Crosetto, M., & Crippa, B. (2005). State of the art of land deformation monitoring using differential SAR interferometry. *ISPRS Hannover …*.

Crosetto, M., Monserrat, O., Cuevas-González, M., Devanthéry, N., & Crippa, B. (2016). Persistent Scatterer Interferometry: A review. In *ISPRS Journal of Photogrammetry and Remote Sensing*. https://doi.org/10.1016/j.isprsjprs.2015.10.011

Curtis, C., & Howard, Z. (2001). Two-dimensional phase unwrapping with use of statistical models for cost functions in nonlinear optimization. *JOSA A*, *18*(2), 338–351.

Dahl, L. K., & Love, R. A. (1957). Etiological role of sodium chloride intake in essential hypertension in humans. *Journal of the American Medical Association*, *164*(4), 397–400.

Dahle, C., & Murböck, M. (2020). Post-processed GRACE/GRACE-FO Geopotential GSM Coefficients COST-G RL01 (Level-2B Product). *GFZ Data Services*.

Dai, K., Liu, G., Li, Z., Li, T., Yu, B., Wang, X., & Singleton, A. (2015). Extracting vertical

`

displacement rates in Shanghai (China) with multi-platform SAR images. *Remote Sensing*. https://doi.org/10.3390/rs70809542

Dai, Y., Zeng, X., Dickinson, R. E., Baker, I., Bonan, G. B., Bosilovich, M. G., Denning, A. S., Dirmeyer, P. A., Houser, P. R., Niu, G., Oleson, K. W., Schlosser, C. A., & Yang, Z. L. (2003). The common land model. *Bulletin of the American Meteorological Society*. https://doi.org/10.1175/BAMS-84-8-1013

Dalin, C., Wada, Y., Kastner, T., & Puma, M. J. (2017). Groundwater depletion embedded in international food trade. *Nature*, *543*(7647), 700–704.

Das, R., Laishram, B., & Jawed, M. (2019). Perception of groundwater quality and health effects on willingness to procure: The case of upcoming water supply scheme in Guwahati, India. *Journal of Cleaner Production*, *226*, 615–627.

de Fraiture, C., Wichelns, D., Rockstrom, J., Kemp-Benedict, E., Eriyagama, N., Gordon, L. J., Hanjra, M. A., Hoogeveen, J., Huber-Lee, A., & Karlberg, L. (2007). *Looking ahead to 2050: scenarios of alternative investment approaches*.

Devleeschouwer, X., Declercq, P.-Y., Flamion, B., Brixko, J., Timmermans, A., & Vanneste, J. (2008). Uplift revealed by radar interferometry around Liège (Belgium): a relation with rising mining groundwater. *Proceedings of the Post-Mining Symposium*, 6–8.

Diepenbroek, M., Grobe, H., Reinke, M., Schindler, U., Schlitzer, R., Sieger, R., & Wefer, G. (2002). PANGAEA—an information system for environmental sciences. *Computers \& Geosciences*, *28*(10), 1201–1210.

DMRC. (2018). *Annual Report of DMRC 2017-2018*. http://www.delhimetrorail.com/annual_report.aspx/

DMRC. (2021). *Delhi Metro Present Projects (DMRC)*. DMRC Official Website. http://www.delhimetrorail.com/projectpresent.aspx

Dobslaw, H., Bergmann-Wolf, I., Dill, R., Poropat, L., Thomas, M., Dahle, C., Esselborn, S., König, R., & Flechtner, F. (2017). A new high-resolution model of non-tidal atmosphere and ocean mass variability for de-aliasing of satellite gravity observations: AOD1B RL06. *Geophysical Journal International*. https://doi.org/10.1093/GJI/GGX302

`

Döll, P., Mueller Schmied, H., Schuh, C., Portmann, F. T., & Eicker, A. (2014). Global-scale assessment of groundwater depletion and related groundwater abstractions: Combining hydrological modeling with information from well observations and GRACE satellites. *Water Resources Research*, *50*(7), 5698–5720.

Donoso, G., Lictevout, E., Rinaudo, J.-D., & others. (2020). *Groundwater management lessons from Chile*.

Drinking Water Inspectorate. (2017). What are the Drinking Water Standards? *DWI Advice Leaflets*.

Du, Z., Ge, L., Ng, A. H. M., & Li, X. (2016). Time series interferometry integrated with groundwater depletion measurement from grace. *International Geoscience and Remote Sensing Symposium (IGARSS)*. https://doi.org/10.1109/IGARSS.2016.7729295

DWI. (2011). *Water hardness -DRINKING WATER INSPECTORATE*. https://cdn.dwi.gov.uk/wp-content/uploads/2020/09/23151702/hardness.pdf

EA. (2017). Management of the London Basin Chalk Aquifer. Status Report 2017. *Environment Agency of England and Wales, Thames Region Report.* https://www.gov.uk/government/publications/london-basin-chalk-aquifer-annual-status-report

EA. (2019). Management of the London BAsin Chalk Aquifer. Status Report 2019. *Environment Agency of England and Wales, Thames Region Report.*

EAWQA. (2021). *Environment Agency water quality archieve*. https://environment.data.gov.uk/water-quality/view/download/new

EC. (2011). *Mapping Guide for a European Urban Atlas.*

Edmunds, W. M., Cook, J. M., Darling, W. G., Kinniburgh, D. G., Miles, D. L., Bath, A. H., Morgan-Jones, M., & Andrews, J. N. (1987). Baseline geochemical conditions in the Chalk aquifer, Berkshire, U.K.: a basis for groundwater quality management. *Applied Geochemistry*. https://doi.org/10.1016/0883-2927(87)90042-4

Edmunds, W. M., Shand, P., Hart, P., & Ward, R. S. (2003). The natural (baseline) quality of groundwater: a UK pilot study. *Science of the Total Environment*, *310*(1–3), 25–35.

`

Ek, M. B., Mitchell, K. E., Lin, Y., Rogers, E., Grunmann, P., Koren, V., Gayno, G., & Tarpley, J. D. (2003). Implementation of Noah land surface model advances in the National Centers for Environmental Prediction operational mesoscale Eta model. *Journal of Geophysical Research D: Atmospheres*. https://doi.org/10.1029/2002jd003296

Ellison, R. a, Woods, M. A., Allen, D. J., Forster, A., Pharaoh, T. C., & King, C. (2004). Geology of London. Special Memoir for 1:50 000 Geological sheets 256 (North London), 257 (Romford), 270 (South London) and 271 (Dartford) (England and Wales). *Geological Magazine*. https://doi.org/sheets 256

ERS. (2020). *ERS*. https://earth.esa.int/web/guest/missions/esa-operational-eo-missions/ers Last accessed: 2020-10-03

ESD. (2021). *Demographic profile of delhi, Economic Survey of Delhi*. http://delhiplanning.nic.in/sites/default/files/19. Demography.pdf

Ezquerro, P., Guardiola-Albert, C., Herrera, G., Fernández-Merodo, J. A., Béjar-Pizarro, M., & Bon\`\i, R. (2017). Groundwater and subsidence modeling combining geological and multi-satellite SAR data over the alto guadalent{\'\i}n aquifer (SE Spain). *Geofluids*, *2017*.

Fabro, A. Y. R., Ávila, J. G. P., Alberich, M. V. E., Sansores, S. A. C., & Camargo-Valero, M. A. (2015). Spatial distribution of nitrate health risk associated with groundwater use as drinking water in Merida, Mexico. *Applied Geography*, *65*, 49–57.

Famiglietti, J. S. (2014). The global groundwater crisis. *Nature Climate Change*, *4*(11), 945–948.

Famiglietti, J. S., Lo, M., Ho, S. L., Bethune, J., Anderson, K. J., Syed, T. H., Swenson, S. C., de Linage, C. R., & Rodell, M. (2011). Satellites measure recent rates of groundwater depletion in California's Central Valley. *Geophysical Research Letters*, *38*(3).

Famiglietti, J. S., & Rodell, M. (2013). Water in the balance. In *Science*. https://doi.org/10.1126/science.1236460

Fan, H. D., Cheng, D., Deng, K. Z., Chen, B. Q., & Zhu, C. G. (2015). Subsidence monitoring using D-InSAR and robability integral prediction modelling in eep mining areas. *Survey Review*. https://doi.org/10.1179/1752270614Y.0000000153

Fan, H., Gao, X., Yang, J., Deng, K., & Yu, Y. (2015). Monitoring mining subsidence using a

combination of phase-stacking and offset-tracking methods. *Remote Sensing*. https://doi.org/10.3390/rs70709166

FAO. (2003). *Groundwater Management: The Search for Practical Approaches* (Vol. 25). Food and Agriculture Organization of the United Nations.

Farr, T. G., Rosen, P. A., Caro, E., Crippen, R., Duren, R., Hensley, S., Kobrick, M., Paller, M., Rodriguez, E., Roth, L., & others. (2007). The shuttle radar topography mission. *Reviews of Geophysics*, *45*(2).

Fatland, D. R., & Lingle, C. S. (1998). Analysis of the 1993-95 Bering Glacier (Alaska) surge using differential SAR interferometry. *Journal of Glaciology*, *44*(148), 532–546.

Feng, W., Lemoine, J.-M., Zhong, M., & Hsu, T.-T. (2012). Terrestrial water storage changes in the Amazon basin measured by GRACE during 2002—2010. *Chinese Journal of Geophysics*, *55*(3), 814–821.

Feng, W., Shum, C. K., Zhong, M., & Pan, Y. (2018). Groundwater storage changes in China from satellite gravity: An overview. *Remote Sensing*, *10*(5), 674.

Feng, W., Zhong, M., Lemoine, J.-M., Biancale, R., Hsu, H.-T., & Xia, J. (2013). Evaluation of groundwater depletion in North China using the Gravity Recovery and Climate Experiment (GRACE) data and ground-based measurements. *Water Resources Research*, *49*(4), 2110–2118.

Ferretti, A. (2014). *Satellite InSAR data: reservoir monitoring from space*. EAGE publications.

Ferretti, A., Fumagalli, A., Novali, F., Prati, C., Rocca, F., & Rucci, A. (2011). A new algorithm for processing interferometric data-stacks: SqueeSAR. *IEEE Transactions on Geoscience and Remote Sensing*. https://doi.org/10.1109/TGRS.2011.2124465

Ferretti, A., Monti-guarnieri, A., Prati, C., Rocca, F., & Massonnet, D. (2007). InSAR Principles: Guidelines for SAR Interferometry Processing and Interpretation. In *ESA Publications*.

Ferretti, A., Novali, F., Fumagalli, A., Prati, C., Rocca, F., & Rucci, A. (2009). Beyond PSInSAR: the SqueeSAR approach. *AGU Fall Meeting Abstracts*, *2009*, G31A--02.

Ferretti, A., Prati, C., & Rocca, F. (2000a). Analysis of Permanent Scatterers in SAR interferometry. *International Geoscience and Remote Sensing Symposium (IGARSS)*.

https://doi.org/10.1109/igarss.2000.861695

Ferretti, A., Prati, C., & Rocca, F. (2000b). Nonlinear subsidence rate estimation using permanent scatterers in differential SAR interferometry. *IEEE Transactions on Geoscience and Remote Sensing*. https://doi.org/10.1109/36.868878

Ferretti, A., Prati, C., & Rocca, F. (2001). Permanent scatterers in SAR interferometry. *IEEE Transactions on Geoscience and Remote Sensing*. https://doi.org/10.1109/36.898661

Fialko, Y., & Simons, M. (2000). Deformation and seismicity in the Coso geothermal area, Inyo County, California: Observations and modeling using satellite radar interferometry. *Journal of Geophysical Research: Solid Earth*, *105*(B9), 21781–21793.

Fialko, Y., Simons, M., & Agnew, D. (2001). The complete (3-D) surface displacement field in the epicentral area of the 1999 Mw 7.1 Hector Mine earthquake, California, from space geodetic observations. *Geophysical Research Letters*. https://doi.org/10.1029/2001GL013174

Fielding, E. J., Blom, R. G., & Goldstein, R. M. (1998). Rapid subsidence over oil fields measured by SAR interferometry. *Geophysical Research Letters*, *25*(17), 3215–3218.

Figueroa, M. S., Tuxpan-Vargas, J., Ramos-Leal, J. A., Hernández-Madrigal, V. M., & Villaseñor-Reyes, C. I. (2018). Land subsidence by groundwater over-exploitation from aquifers in tectonic valleys of Central Mexico: A review. *Engineering Geology*, *246*, 91–106.

Flavin, R. J., & Hawn, R. J. E. (1979). Artificial Recharge by the Thames Water Authority in the Lee Valley, North London, England Title. *Proc. of Int. Symp. on Artificial Groundwater Recharge, Dortmund, FDR.*

Flavin, R. J., & Joseph, J. B. (1983). The hydrogeology of the Lee Valley and some effects of artificial recharge (London, UK). *Quarterly Journal of Engineering Geology*. https://doi.org/10.1144/GSL.QJEG.1983.016.01.06

Ford, J. R., Mathers, S. J., Royse, K. R., Aldiss, D. T., & Morgan, D. J. R. (2010). Geological 3D modelling: scientific discovery and enhanced understanding of the subsurface, with examples from the UK. *Zeitschrift Der Deutschen Gesellschaft Für Geowissenschaften*. https://doi.org/10.1127/1860-1804/2010/0161-0205

`

Foster, J., Brooks, B., Cherubini, T., Shacat, C., Businger, S., & Werner, C. L. (2006). Mitigating atmospheric noise for InSAR using a high resolution weather model. *Geophysical Research Letters*, *33*(16).

Foster, S. (2020). Global Policy Overview of Groundwater in Urban Development—A Tale of 10 Cities! *Water*, *12*(2), 456.

Foumelis, M., Blasco, J. M. D., Desnos, Y.-L., Engdahl, M., Fernández, D., Veci, L., Lu, J., & Wong, C. (2018). ESA SNAP-StaMPS integrated processing for Sentinel-1 persistent scatterer interferometry. *IGARSS 2018-2018 IEEE International Geoscience and Remote Sensing Symposium*, 1364–1367.

Fournier, T. J., Pritchard, M. E., & Riddick, S. N. (2010). Duration, magnitude, and frequency of subaerial volcano deformation events: New results from Latin America using InSAR and a global synthesis. *Geochemistry, Geophysics, Geosystems*, *11*(1).

Frappart, F., & Ramillien, G. (2018). Monitoring groundwater storage changes using the Gravity Recovery and Climate Experiment (GRACE) satellite mission: A review. *Remote Sensing*, *10*(6), 829.

Frappart, F., Ramillien, G., & Famiglietti, J. S. (2011). Water balance of the Arctic drainage system using GRACE gravimetry products. *International Journal of Remote Sensing*, *32*(2), 431–453.

Frappart, F., Ramillien, G., & Seoane, L. (2016). Monitoring water mass redistributions on land and polar ice sheets using the grace gravimetry from space mission. In *Land Surface Remote Sensing in Continental Hydrology* (pp. 255–279). Elsevier.

Freitas, de. (2009). Geology; its principles, practice and potential for Geotechnics. In *Quarterly Journal of Engineering Geology and Hydrogeology*. https://doi.org/10.1144/1470-9236/09-014

Freitas, J. G., Rivett, M. O., Roche, R. S., Durrant, M., Walker, C., & Tellam, J. H. (2015). Heterogeneous hyporheic zone dechlorination of a TCE groundwater plume discharging to an urban river reach. *Science of the Total Environment*, *505*, 236–252.

Furuya, M., & Wahr, J. M. (2005). Water level changes at an ice-dammed lake in west Greenland inferred from InSAR data. *Geophysical Research Letters*, *32*(14).

`

Gabriel, A. K., Goldstein, R. M., & Zebker, H. A. (1989). Mapping small elevation changes over large areas: differential radar interferometry. *Journal of Geophysical Research*. https://doi.org/10.1029/JB094iB07p09183

Galloway, D. L., & Burbey, T. J. (2011). Regional land subsidence accompanying groundwater extraction. *Hydrogeology Journal*, *19*(8), 1459–1486.

Galloway, D. L., Hudnut, K. W., Ingebritsen, S. E., Phillips, S. P., Peltzer, G., Rogez, F., & Rosen, P. A. (1998). Detection of aquifer system compaction and land subsidence using interferometric synthetic aperture radar, Antelope Valley, Mojave Desert, California. *Water Resources Research*. https://doi.org/10.1029/98WR01285

Gambolati, G., & Teatini, P. (2015). Geomechanics of subsurface water withdrawal and injection. *Water Resources Research*, *51*(6), 3922–3955.

Gambolati, G., Teatini, P., & Ferronato, M. (2006). Anthropogenic land subsidence. *Encyclopedia of Hydrological Sciences*.

Garg, S., Mahdi, M., & Indu, J. (2020). *Land Subsidence in Delhi, India investigated using Sentinel-1 InSAR measurements*. https://doi.org/https://doi.org/10.5194/egusphere-egu2020-21138

Gee, D., Bateson, L., Grebby, S., Novellino, A., Sowter, A., Wyatt, L., Marsh, S., Morgenstern, R., & Athab, A. (2020). Modelling groundwater rebound in recently abandoned coalfields using DInSAR. *Remote Sensing of Environment*. https://doi.org/10.1016/j.rse.2020.112021

Gemitzi, A., Ajami, H., & Richnow, H.-H. (2017). Developing empirical monthly groundwater recharge equations based on modeling and remote sensing data--Modeling future groundwater recharge to predict potential climate change impacts. *Journal of Hydrology*, *546*, 1–13.

Gens, R. (1999). SAR interferometry: Software, data format, and data quality. In *Photogrammetric Engineering and Remote Sensing*.

Geoiq. (2021). *GeoIQ's spatial AI: India's comprehensive and granular location data stack*. Geoiq. https://geoiq.io/

Ghiglia, D. C., & Pritt, M. D. (1998). Two-dimensional phase unwrapping: theory, algorithms, and

software. In *J Investig Dermatol*.

GLA. (2011). *London Plan Consultation Greater London Authority (GLA)*. https://data.london.gov.uk/dataset/sub-regions-london-plan-consultation-2009

GLA. (2021a). *London datastore, Greater London Authority (GLA)*. https://data.london.gov.uk/dataset/trend-based-population-projections

GLA. (2021b). *The London plan, The Spatial Development Strategy for Greater London*. https://www.london.gov.uk/sites/default/files/the_london_plan_2021.pdf

Gleeson, T., Wada, Y., Bierkens, M. F. P., & Van Beek, L. P. H. (2012). Water balance of global aquifers revealed by groundwater footprint. *Nature*, *488*(7410), 197–200.

Go-Science. (2021). *Government Office for Science, Future of Cities: Foresight for Cities. A resource for policy-makers*. www.gov.uk/go-science

Goldstein, R. M., Engelhardt, H., Kamb, B., & Frolich, R. M. (1993). Satellite radar interferometry for monitoring ice sheet motion: application to an Antarctic ice stream. *Science*, *262*(5139), 1525–1530.

Goldstein, R. M., & Werner, C. L. (1998). Radar interferogram filtering for geophysical applications. *Geophysical Research Letters*. https://doi.org/10.1029/1998GL900033

Gonçalvès, J., Petersen, J., Deschamps, P., Hamelin, B., & Baba-Sy, O. (2013). Quantifying the modern recharge of the "fossil" Sahara aquifers. *Geophysical Research Letters*, *40*(11), 2673–2678.

Google, E. P. 7. 3. 3. 778. (2021a). *Delhi Haryana Border. 28°30'54.84"N, 77° 4'21.80"E, Eye alt 13.45 km. Borders and labels; places layers. . NOAA, DigitalGlobe 2021*. Google Earth; Gogle Earth. http://www.google.com/earth/index.html

Google, E. P. 7. 3. 3. 778. (2021b). *East Reservoir. 51°34'15.45"N, 0° 5'8.45"W, Eye alt 3.20 km. Borders and labels; places layers. . NOAA, DigitalGlobe 2021*. Google Earth. http://www.google.com/earth/index.html

Graham, L. C. (1974). Synthetic interferometer radar for topographic mapping. *Proceedings of the IEEE*, *62*(6), 763–768.

Gray, A. L., Short, N., Mattar, K. E., & Jezek, K. C. (2001). Velocities and flux of the Filchner Ice

Shelf and its tributaries determined from speckle tracking interferometry. *Canadian Journal of Remote Sensing*, *27*(3), 193–206.

Gray, L., Joughin, I., Tulaczyk, S., Spikes, V. B., Bindschadler, R., & Jezek, K. (2005). Evidence for subglacial water transport in the West Antarctic Ice Sheet through three-dimensional satellite radar interferometry. *Geophysical Research Letters*, *32*(3).

Greater London Authority. (2013). *London's Zero Carbon Energy Resource: Secondary Heat Report Phase 1*. *January*, 1–138. http://www.london.gov.uk/sites/default/files/031250 GLA Secondary Heat - Summary Report.pdf

Grimmeisen, F., Lehmann, M. F., Liesch, T., Goeppert, N., Klinger, J., Zopfi, J., & Goldscheider, N. (2017). Isotopic constraints on water source mixing, network leakage and contamination in an urban groundwater system. *Science of the Total Environment*, *583*, 202–213.

Gulis, G., Czompolyova, M., & Cerhan, J. R. (2002). An ecologic study of nitrate in municipal drinking water and cancer incidence in Trnava District, Slovakia. *Environmental Research*, *88*(3), 182–187.

Gunn, J., Downing, R. A., Price, M., & Jones, G. P. (1995). The Hydrogeology of the Chalk of North-West Europe. *Transactions of the Institute of British Geographers*. https://doi.org/10.2307/622666

Guo, J., Zhou, L., Yao, C., & Hu, J. (2016). Surface subsidence analysis by multi-temporal InSAR and GRACE: A case study in Beijing. *Sensors (Switzerland)*. https://doi.org/10.3390/s16091495

Guo, Q., Huang, J., Zhou, Z., & Wang, J. (2019). Experiment and numerical simulation of seawater intrusion under the influences of tidal fluctuation and groundwater exploitation in coastal multilayered aquifers. *Geofluids*, *2019*.

Guppy, L., Uyttendaele, P., Villholth, K. G., & Smakhtin, V. (2018). *Groundwater and sustainable development goals: Analysis of interlinkages*.

Gupte, P. R. (2019). *GROUNDWATER RESOURCES VS DOMESTIC WATER DEMAND AND SUPPLY-NCT DELHI*.

Han, D., Currell, M. J., Cao, G., & Hall, B. (2017). Alterations to groundwater recharge due to

anthropogenic landscape change. *Journal of Hydrology*, *554*, 545–557.

Hanssen, R. F. (2001). *Radar interferometry: data interpretation and error analysis* (Vol. 2). Springer Science \& Business Media.

Haritash, A. K., Gaur, S., & Garg, S. (2016). Assessment of water quality and suitability analysis of River Ganga in Rishikesh, India. *Applied Water Science*, *6*(4), 383–392.

Helm, D. C. (1975). One-dimensional simulation of aquifer system compaction near Pixley, California: 1. Constant parameters. *Water Resources Research*. https://doi.org/10.1029/WR011i003p00465

Hoffman, C. J. (1988). Does the sodium level in drinking water affect blood pressure levels? *Journal of the American Dietetic Association*, *88*(11), 1432–1435.

Hoffmann, J., Zebker, H. A., Galloway, D. L., & Amelung, F. (2001). Seasonal subsidence and rebound in Las Vegas Valley, Nevada, observed by synthetic aperture radar interferometry. *Water Resources Research*, *37*(6), 1551–1566.

Hole, J. K., Bromley, C. J., Stevens, N. F., & Wadge, G. (2007). Subsidence in the geothermal fields of the Taupo Volcanic Zone, New Zealand from 1996 to 2005 measured by InSAR. *Journal of Volcanology and Geothermal Research*, *166*(3–4), 125–146.

Hollingum, J. (1998). Robots explore underground pipes. *Industrial Robot: An International Journal*.

Hooper, A. J. (2008). A multi-temporal InSAR method incorporating both persistent scatterer and small baseline approaches. *Geophysical Research Letters*. https://doi.org/10.1029/2008GL034654

Hooper, A., Segall, P., & Zebker, H. (2007). Persistent scatterer interferometric synthetic aperture radar for crustal deformation analysis, with application to Volcán Alcedo, Galápagos. *Journal of Geophysical Research: Solid Earth*. https://doi.org/10.1029/2006JB004763

Hooper, A., Spaans, K., Bekaert, D., Cuenca, M. C., Ar\ikan, M., & Oyen, A. (2010). StaMPS/MTI manual. *Delft Institute of Earth Observation and Space Systems Delft University of Technology, Kluyverweg*, *1*, 2629.

Hooper, A., Zebker, H., Segall, P., & Kampes, B. (2004). A new method for measuring

deformation on volcanoes and other natural terrains using InSAR persistent scatterers. *Geophysical Research Letters*. https://doi.org/10.1029/2004GL021737

Horvath, A., Murböck, M., Pail, R., & Horwath, M. (2018). Decorrelation of GRACE time variable gravity field solutions using full covariance information. *Geosciences (Switzerland)*. https://doi.org/10.3390/geosciences8090323

Hosseini, M. S.-M., Araghinejad, S., Ebrahimi, K., Tang, Q., & AghaKouchak, A. (2020). Using GRACE satellite observations for separating meteorological variability from anthropogenic impacts on water availability. *Scientific Reports*, *10*(1), 1–12.

Hounsinou, S. P. (2020). Assessment of potential seawater intrusion in a coastal aquifer system at Abomey-Calavi, Benin. *Heliyon*, *6*(2), e03173.

Howard, K. W. F. (2015). Sustainable cities and the groundwater governance challenge. *Environmental Earth Sciences*, *73*(6), 2543–2554.

Howard, R. L., & Schrier, R. W. (1990). A unifying hypothesis of sodium and water regulation in health and disease. *Hormone Research in Paediatrics*, *34*(3–4), 118–123.

Huang, J., Deng, K., Fan, H., & Yan, S. (2016). An improved pixel-tracking method for monitoring mining subsidence. *Remote Sensing Letters*. https://doi.org/10.1080/2150704X.2016.1183177

Huang, Z., Pan, Y., Gong, H., Yeh, P. J.-F., Li, X., Zhou, D., & Zhao, W. (2015). Subregional-scale groundwater depletion detected by GRACE for both shallow and deep aquifers in North China Plain. *Geophysical Research Letters*, *42*(6), 1791–1799.

Hudak, P. F. (2001). Water hardness and sodium trends in Texas aquifers. *Environmental Monitoring and Assessment*, *68*(2), 177–185.

Humme, A. J. . (2007). Point density optimization for SAR interferometry: a study tested on salt mine areas. *Delft, University of Technology, Delft, The Netherlands*.

Humphrey, V., Gudmundsson, L., & Seneviratne, S. I. (2016). Assessing global water storage variability from GRACE: Trends, seasonal cycle, subseasonal anomalies and extremes. *Surveys in Geophysics*, *37*(2), 357–395.

Huo, C., Dar, A. A., Nawaz, A., Hameed, J., Pan, B., Wang, C., & others. (2021). Groundwater

contamination with the threat of COVID-19: insights into CSR theory of Carroll's pyramid. *Journal of King Saud University-Science*, *33*(2), 101295.

Hussain, D., Kao, H.-C., Khan, A. A., Lan, W.-H., Imani, M., Lee, C.-M., & Kuo, C.-Y. (2020). Spatial and temporal variations of terrestrial water storage in upper indus basin using GRACE and altimetry data. *IEEE Access*, *8*, 65327–65339.

Hussin, A. A., & Ghazal, K. A. (2020). The quality of groundwater in the Samawah desert (Iraq) and its impact on increasing the likelihood of severe desertification in the cultivated pasture lands. *International Journal of Psychosocial Rehabilitation*, *24*(09).

Inbev, A.-B., Worldwide, A., Auto, B., Chance, C., DHL, D. P., Embraer, S. A., & Mutual, O. (2013). *World economic forum*.

Ineson, J., & Downing, R. A. (1963). Changes in the chemistry of ground waters of the Chalk passing beneath argillaceous strata. *Bulletin of the Geological Survey of Great Britain*, *20*, 176–192.

Ishikawa, A., Amagasa, M., Shiga, T., Tomizawa, G., Tatsuta, R., & Mieno, H. (1993). The max-min Delphi method and fuzzy Delphi method via fuzzy integration. *Fuzzy Sets and Systems*, *55*(3), 241–253.

Jabbari, E., Fathi, M., & Moradi, M. (2020). Modeling groundwater quality and quantity to manage water resources in the Arak aquifer, Iran. *Arabian Journal of Geosciences*, *13*(14), 1–16.

Jaiswal, R. K., Mukherjee, S., Krishnamurthy, J., & Saxena, R. (2003). Role of remote sensing and GIS techniques for generation of groundwater prospect zones towards rural development--an approach. *International Journal of Remote Sensing*, *24*(5), 993–1008.

Jamshidzadeh, Z., & Mirbagheri, S. A. (2011). Evaluation of groundwater quantity and quality in the Kashan Basin, Central Iran. *Desalination*. https://doi.org/10.1016/j.desal.2010.10.067

Jasechko, S., Perrone, D., Befus, K. M., Cardenas, M. B., Ferguson, G., Gleeson, T., Luijendijk, E., McDonnell, J. J., Taylor, R. G., Wada, Y., & others. (2017). Global aquifers dominated by fossil groundwaters but wells vulnerable to modern contamination. *Nature Geoscience*, *10*(6), 425–429.

Jha, B. M., & Sinha, S. K. (2009). Towards better management of ground water resources in India.

`

QJ, *24*(4), 1–20.

Jha, M. K., Shekhar, A., & Jenifer, M. A. (2020). Assessing groundwater quality for drinking water supply using hybrid fuzzy-GIS-based water quality index. *Water Research*, *179*, 115867.

Jia, X., Hou, D., Wang, L., O'Connor, D., & Luo, J. (2020). The development of groundwater research in the past 40 years: A burgeoning trend in groundwater depletion and sustainable management. *Journal of Hydrology*, *587*, 125006.

Jia, Z., Qiao, J., Peng, J., Lu, Q., Xia, Y., Zang, M., Wang, F., & Zhao, J. (2021). Formation of ground fissures with synsedimentary characteristics: A case study in the Linfen Basin, northern China. *Journal of Asian Earth Sciences*, *214*, 104790.

Jin, Y.-F., Yin, Z.-Y., Shen, S.-L., & Hicher, P.-Y. (2016). Selection of sand models and identification of parameters using an enhanced genetic algorithm. *International Journal for Numerical and Analytical Methods in Geomechanics*, *40*(8), 1219–1240.

Jin, Y.-F., Yin, Z.-Y., Wu, Z.-X., & Zhou, W.-H. (2018). Identifying parameters of easily crushable sand and application to offshore pile driving. *Ocean Engineering*, *154*, 416–429.

Jones, M. A., Hughes, A. G., Jackson, C. R., & Van Wonderen, J. J. (2012). Groundwater resource modelling for public water supply management in London. *Geological Society Special Publication*. https://doi.org/10.1144/SP364.8

Jonsson, S. (2002). *Modeling volcano and earthquake deformation from satellite radar interferometric observations*. Stanford University.

Joodaki, G., Wahr, J., & Swenson, S. (2014). Estimating the human contribution to groundwater depletion in the Middle East, from GRACE data, land surface models, and well observations. *Water Resources Research*, *50*(3), 2679–2692.

Joughin, I. R., Kwok, R., & Fahnestock, M. A. (1998). Interferometric estimation of three-dimensional ice-flow using ascending and descending passes. *IEEE Transactions on Geoscience and Remote Sensing*, *36*(1), 25–37.

Ju, Y., Massoudieh, A., Green, C. T., Lee, K.-K., & Kaown, D. (2021). Complexity of groundwater age mixing near a seawater intrusion zone based on multiple tracers and Bayesian inference. *Science of The Total Environment*, *753*, 141994.

`

Junxiang, L., Conghe, S., Lu, C., Feige, Z., Xianlei, M., & Jianguo, W. (2011). Impacts of landscape structure on surface urban heat islands: A case study of Shanghai, China. *Remote Sensing of Environment*, *115*(12), 3249–3263.

Kampes, B. M. (2005). *Displacement parameter estimation using permanent scatterer interferometry*.

Kang, Y., Zhao, C., Zhang, Q., Lu, Z., & Li, B. (2017). Application of InSAR techniques to an analysis of the Guanling landslide. *Remote Sensing*, *9*(10), 1046.

Karanam, V., Motagh, M., Garg, S., & Jain, K. (2021). Multi-sensor remote sensing analysis of coal fire induced land subsidence in Jharia Coalfields, Jharkhand, India. *International Journal of Applied Earth Observation and Geoinformation*, *102*, 102439.

Kaur, H., & Garg, P. (2019). Urban sustainability assessment tools: A review. *Journal of Cleaner Production*, *210*, 146–158.

Kenny, J. F., Barber, N. L., Hutson, S. S., Linsey, K. S., Lovelace, J. K., & Maupin, M. A. (2009). *Estimated use of water in the United States in 2005*.

Kerrou, J., Renard, P., & Tarhouni, J. (2010). Status of the Korba groundwater resources (Tunisia): observations and three-dimensional modelling of seawater intrusion. *Hydrogeology Journal*, *18*(5), 1173–1190.

Ketelaar, G. (2009). Satellite radar interferometry: Subsidence Monitoring Techniques. In *Scientific American*. https://doi.org/10.1007/978-1-4020-9428-6

Khan, M. R., Koneshloo, M., Knappett, P. S. K., Ahmed, K. M., Bostick, B. C., Mailloux, B. J., Mozumder, R. H., Zahid, A., Harvey, C. F., Van Geen, A., & others. (2016). Megacity pumping and preferential flow threaten groundwater quality. *Nature Communications*, *7*(1), 1–8.

Khorrami, M., Abrishami, S., Maghsoudi, Y., Alizadeh, B., & Perissin, D. (2020). Extreme subsidence in a populated city (Mashhad) detected by PSInSAR considering groundwater withdrawal and geotechnical properties. *Scientific Reports*, *10*(1), 1–16.

Khorrami, M., Alizadeh, B., Ghasemi Tousi, E., Shakerian, M., Maghsoudi, Y., & Rahgozar, P. (2019). How groundwater level fluctuations and geotechnical properties lead to asymmetric

subsidence: A PSInSAR analysis of land deformation over a transit corridor in the Los Angeles metropolitan area. *Remote Sensing*, *11*(4), 377.

Kim, J., Kim, D.-J., Kim, S.-W., Won, J.-S., & Moon, W. M. (2007). Monitoring of urban land surface subsidence using PSInSAR. *Geosciences Journal*. https://doi.org/10.1007/bf02910381

Kinniburgh, D. G., Gale, I. N., Smedley, P. L., Darling, W. G., West, J. M., Aldous, P. J., & O'Shea, M. J. (1994). The effects of historic abstraction of groundwater from the London Basin aquifers on groundwater quality. *Applied Geochemistry*. https://doi.org/10.1016/0883-2927(94)90006-X

König, M., Winther, J.-G., & Isaksson, E. (2001). Measuring snow and glacier ice properties from satellite. *Reviews of Geophysics*, *39*(1), 1–27.

Konikow, L. F., & Kendy, E. (2005). Groundwater depletion: A global problem. *Hydrogeology Journal*, *13*(1), 317–320.

Korfali, S., & Jurdi, M. (2010). Deterioration of coastal water aquifers. *European Water*, *29: 3-10*.

Koster, R. D., & Suarez, M. J. (1996). Energy and Water Balance Calculations in the Mosaic LSM. In *NASA Technical Memorandum 104606, Technical Report Series on Global Modeling and Data Assimilation*.

Koster, R. D., & Suarez, M. J. (2001). Soil moisture memory in climate models. *Journal of Hydrometeorology*, *2*(6), 558–570.

Kumar, S. (2017). SAR data format and Acquisition mode webinar. EDUSAT IIRS Dehradun, ISRO. *EDUSAT IIRS Dehradun, ISRO*.

Kuras, O., Wilkinson, P. B., Meldrum, P. I., Oxby, L. S., Uhlemann, S., Chambers, J. E., Binley, A., Graham, J., Smith, N. T., & Atherton, N. (2016). Geoelectrical monitoring of simulated subsurface leakage to support high-hazard nuclear decommissioning at the Sellafield Site, UK. *Science of the Total Environment*, *566*, 350–359.

Kusche, J., & Schrama, E. J. O. (2005). Surface mass redistribution inversion from global GPS deformation and Gravity Recovery and Climate Experiment (GRACE) gravity data. *Journal*

`

of Geophysical Research: Solid Earth. https://doi.org/10.1029/2004JB003556

Kusrini, E., Mualim, N. M., Rahman, A., & Usman, A. (2020). Application of activated Na-zeolite a as a water softening agent to remove Ca2+ and Mg2+ ions from water. *AIP Conference Proceedings*, *2255*(1), 60012.

Kustu, M. D., Fan, Y., & Robock, A. (2010). Large-scale water cycle perturbation due to irrigation pumping in the US High Plains: A synthesis of observed streamflow changes. *Journal of Hydrology*, *390*(3–4), 222–244.

Lakshmanan, V. I., & Gokhale, U. (2020). Clean Water Supply in Rural Odisha--A Case Study. *Smart Villages*, 273.

Lall, U., Josset, L., & Russo, T. (2020). A snapshot of the world's groundwater challenges. *Annual Review of Environment and Resources*, *45*, 171–194.

Lapworth, D. J., Krishan, G., MacDonald, A. M., & Rao, M. S. (2017). Groundwater quality in the alluvial aquifer system of northwest India: new evidence of the extent of anthropogenic and geogenic contamination. *Science of the Total Environment*, *599*, 1433–1444.

Leblanc, M. J., Tregoning, P., Ramillien, G., Tweed, S. O., & Fakes, A. (2009). Basin-scale, integrated observations of the early 21st century multiyear drought in southeast Australia. *Water Resources Research*, *45*(4).

Lee, J.-S., Jurkevich, L., Dewaele, P., Wambacq, P., & Oosterlinck, A. (1994). Speckle filtering of synthetic aperture radar images: A review. *Remote Sensing Reviews*, *8*(4), 313–340.

Lehner, B., Döll, P., Alcamo, J., Henrichs, T., & Kaspar, F. (2006). Estimating the impact of global change on flood and drought risks in Europe: a continental, integrated analysis. *Climatic Change*, *75*(3), 273–299.

Lerner, D. N., & Barrett, M. H. (1996). Urban groundwater issues in the United Kingdom. *Hydrogeology Journal*, *4*(1), 80–89.

Lewis, R. W., & Schrefler, B. (1978). A fully coupled consolidation model of the subsidence of Venice. *Water Resources Research*, *14*(2), 223–230.

Li, M.-G., Chen, J.-J., Xu, Y.-S., Tong, D.-G., Cao, W.-W., & Shi, Y.-J. (2021). Effects of groundwater exploitation and recharge on land subsidence and infrastructure settlement

patterns in shanghai. *Engineering Geology*, *282*, 105995.

Li, X., Zhou, W., Ouyang, Z., Xu, W., & Zheng, H. (2012). Spatial pattern of greenspace affects land surface temperature: evidence from the heavily urbanized Beijing metropolitan area, China. *Landscape Ecology*, *27*(6), 887–898.

Li, Z., Fielding, E. J., Cross, P., & Muller, J.-P. (2006a). Interferometric synthetic aperture radar atmospheric correction: GPS topography-dependent turbulence model. *Journal of Geophysical Research: Solid Earth*, *111*(B2).

Li, Z., Fielding, E. J., Cross, P., & Muller, J.-P. (2006b). Interferometric synthetic aperture radar atmospheric correction: medium resolution imaging spectrometer and advanced synthetic aperture radar integration. *Geophysical Research Letters*, *33*(6).

Liang, X., Lettenmaier, D. P., Wood, E. F., & Burges, S. J. (1994). A simple hydrologically based model of land surface water and energy fluxes for general circulation models. *Journal of Geophysical Research*. https://doi.org/10.1029/94jd00483

Liu, D., Qi, X., Li, M., Zhu, W., Zhang, L., Faiz, M. A., Khan, M. I., Li, T., Cui, S., & others. (2019). A resilience evaluation method for a combined regional agricultural water and soil resource system based on Weighted Mahalanobis distance and a Gray-TOPSIS model. *Journal of Cleaner Production*, *229*, 667–679.

Liu, S., & Li, W. (2019). Zoning and management of phreatic water resource conservation impacted by underground coal mining: A case study in arid and semiarid areas. *Journal of Cleaner Production*, *224*, 677–685.

Liu, Y., Ma, T., & Du, Y. (2017). Compaction of muddy sediment and its significance to groundwater chemistry. *Procedia Earth and Planetary Science*, *17*, 392–395.

Long, D., Shen, Y., Sun, A., Hong, Y., Longuevergne, L., Yang, Y., Li, B., & Chen, L. (2014). Drought and flood monitoring for a large karst plateau in Southwest China using extended GRACE data. *Remote Sensing of Environment*, *155*, 145–160.

Longuevergne, L., Wilson, C. R., Scanlon, B. R., & Crétaux, J. F. (2013). GRACE water storage estimates for the middle east and other regions with significant reservoir and lake storage. *Hydrology and Earth System Sciences*. https://doi.org/10.5194/hess-17-4817-2013

`

Lu, Z., & Danskin, W. R. (2001). InSAR analysis of natural recharge to define structure of a ground-water basin, San Bernardino, California. *Geophysical Research Letters*, *28*(13), 2661–2664.

Lu, Z., & Dzurisin, D. (2010). Ground surface deformation patterns, magma supply, and magma storage at Okmok volcano, Alaska, from InSAR analysis: 2. Coeruptive deflation, July--August 2008. *Journal of Geophysical Research: Solid Earth*, *115*(B5).

Lyu, H.-M., Shen, S.-L., Zhou, A., & Yang, J. (2019). Perspectives for flood risk assessment and management for mega-city metro system. *Tunnelling and Underground Space Technology*, *84*, 31–44.

Lyu, H.-M., Shen, S.-L., Zhou, A., & Yang, J. (2020). Risk assessment of mega-city infrastructures related to land subsidence using improved trapezoidal FAHP. *Science of The Total Environment*, *717*, 135310.

Ma, T., Du, Y., Ma, R., Xiao, C., & Liu, Y. (2018). Water--rock interactions and related eco-environmental effects in typical land subsidence zones of China. *Hydrogeology Journal*, *26*(5), 1339–1349.

MacDonald, A. M., & Allen, D. J. (2001). Aquifer properties of the Chalk of England. *Quarterly Journal of Engineering Geology and Hydrogeology*, *34*(4), 371–384.

Madsen, S. N., Martin, J. M., & Zebker, H. A. (1995). Analysis and evaluation of the NASA/JPL TOPSAR across-track interferometric SAR system. *IEEE Transactions on Geoscience and Remote Sensing*, *33*(2), 383–391.

Makkeasorn, A., Chang, N.-B., Beaman, M., Wyatt, C., & Slater, C. (2006). Soil moisture estimation in a semiarid watershed using RADARSAT-1 satellite imagery and genetic programming. *Water Resources Research*, *42*(9).

Mammen, S. S. (2021). *Delhi's most expensive and posh residential areas*. https://housing.com/news/posh-residential-areas-in-delhi/

Mason, P. J., Ghail, R. C., Bischoff, C., & Skipper, J. A. (2015). *Detecting and monitoring small-scale discrete ground movements across London, using Persistent Scatterer InSAR (PSI)*.

Massonnet, D., Briole, P., & Arnaud, A. (1995). Deflation of Mount Etna monitored by spaceborne

radar interferometry. *Nature*, *375*(6532), 567–570.

Massonnet, D., & Feigl, K. L. (1998). Radar interferometry and its application to changes in the earth's surface. *Reviews of Geophysics*. https://doi.org/10.1029/97RG03139

Massonnet, D., Feigl, K., Rossi, M., & Adragna, F. (1994). Radar interferometric mapping of deformation in the year after the Landers earthquake. *Nature*, *369*(6477), 227–230.

Massonnet, D., Holzer, T., & Vadon, H. (1997). Land subsidence caused by the East Mesa geothermal field, California, observed using SAR interferometry. *Geophysical Research Letters*, *24*(8), 901–904.

Massonnet, D., & Rabaute, T. (1993). Radar Interferometry: Limits and Potential. In *IEEE Transactions on Geoscience and Remote Sensing*. https://doi.org/10.1109/36.214922

Mathers, S. J., Burke, H. F., Terrington, R. L., Thorpe, S., Dearden, R. A., Williamson, J. P., & Ford, J. R. (2014). A geological model of London and the Thames Valley, southeast England. *Proceedings of the Geologists' Association*. https://doi.org/10.1016/j.pgeola.2014.09.001

Mattos, J. B., Cruz, M. J. M., De Paula, F. C. F., & Sales, E. F. (2018). Natural and anthropic processes controlling groundwater hydrogeochemistry in a tourist destination in northeastern Brazil. *Environmental Monitoring and Assessment*, *190*(7), 1–17.

Megdal, S. B. (2018). Invisible water: the importance of good groundwater governance and management. *Npj Clean Water*, *1*(1), 1–5. https://doi.org/10.1038/s41545-018-0015-9

Michael, H. A., & Voss, C. I. (2009). Controls on groundwater flow in the Bengal Basin of India and Bangladesh: regional modeling analysis. *Hydrogeology Journal*, *17*(7), 1561–1577.

Miyawaki, M., Ishii, T., Ohno, S., Fujimura, T., Kimura, T., Harada, K., & Ohki, M. (2017). Evaluation of detection capability of crustal movement by airborne SAR (PI-SAR-L2) repeat-pass interferometry. *2017 IEEE International Geoscience and Remote Sensing Symposium (IGARSS)*, 3818–3821.

MO. (2021). *Met office Seasons*. https://doi.org/25/03/2021

Moeck, C., Affolter, A., Radny, D., Dressmann, H., Auckenthaler, A., Huggenberger, P., & Schirmer, M. (2018). Improved water resource management for a highly complex environment using three-dimensional groundwater modelling. *Hydrogeology Journal*, *26*(1),

133–146.

Mohr, J. J., Reeh, N., & Madsen, S. N. (1998). Three-dimensional glacial flow and surface elevation measured with radar interferometry. *Nature*, *391*(6664), 273–276.

MOL. (2021). *Mayor of London, The London Infrastructure Plan, 2050*. https://www.london.gov.uk/what-we-do/business-and-economy/better-infrastructure/london-infrastructure-plan-2050

Morris, M. D., Berk, J. A., Krulik, J. W., & Eckstein, Y. (1983). A Computer Program for a Trilinear Diagram Plot and Analysis of Water Mixing Systems. *Groundwater*. https://doi.org/10.1111/j.1745-6584.1983.tb00706.x

Mosavi, A., Hosseini, F. S., Choubin, B., Abdolshahnejad, M., Gharechaee, H., Lahijanzadeh, A., & Dineva, A. A. (2020). Susceptibility prediction of groundwater hardness using ensemble machine learning models. *Water (Switzerland)*. https://doi.org/10.3390/w12102770

Motagh, M., Walter, T. R., Sharifi, M. A., Fielding, E., Schenk, A., Anderssohn, J., & Zschau, J. (2008). Land subsidence in Iran caused by widespread water reservoir overexploitation. *Geophysical Research Letters*, *35*(16).

Moujabber, E. M., Samra, B. B., Darwish, T., & Atallah, T. (2006). Comparison of different indicators for groundwater contamination by seawater intrusion on the Lebanese coast. *Water Resources Management*, *20*(2), 161–180.

Munier, S., Becker, M., Maisongrande, P., & Cazenave, A. (2012). Using GRACE to detect groundwater storage variations: the cases of Canning basin and Guarani aquifer system. *International Water Technology Journal*, *2*, 2–13.

Narasimhan, T. N., & Goyal, K. P. (1984). Subsidence due to geothermal fluid withdrawal. *Man-Induced Land Subsidence, Reviews in Engineering Geology*, *6*, 35–36.

NFRA. (2021). *National River Flow Archive, Gauging Station 39001 Thames at Kingston 1883–2020*. http://nrfa.ceh.ac.uk/data/station/info/39001

Niroumand, H. (2021). *Modeling Land Subsidence Processes*. https://www.instagram.com/p/CSUgh56jz40/?utm_medium=copy_link

NISAR. (2020). *NISAR*. https://nisar.jpl.nasa.gov/ Last Accessed: 2020-10-05

`

Nolan, M., & Fatland, D. R. (2003). Penetration depth as a DInSAR observable and proxy for soil moisture. *IEEE Transactions on Geoscience and Remote Sensing*, *41*(3), 532–537.

Ofeigsson, B. G., Hooper, A., Sigmundsson, F., Sturkell, E., & Grapenthin, R. (2011). Deep magma storage at Hekla volcano, Iceland, revealed by InSAR time series analysis. *Journal of Geophysical Research: Solid Earth*, *116*(B5).

Osmanouglu, B., Dixon, T. H., Wdowinski, S., Cabral-Cano, E., & Jiang, Y. (2011). Mexico City subsidence observed with persistent scatterer InSAR. *International Journal of Applied Earth Observation and Geoinformation*, *13*(1), 1–12.

Osmanouglu, B., Sunar, F., Wdowinski, S., & Cabral-Cano, E. (2016). Time series analysis of InSAR data: Methods and trends. *ISPRS Journal of Photogrammetry and Remote Sensing*, *115*, 90–102.

Peltier, A., Bianchi, M., Kaminski, E., Komorowski, J. C., Rucci, A., & Staudacher, T. (2010). PSInSAR as a new tool to monitor pre-eruptive volcano ground deformation: Validation using GPS measurements on Piton de La Fournaise. *Geophysical Research Letters*. https://doi.org/10.1029/2010GL043846

Peng, J., Xu, J., Ma, R., & Wang, F. (2016). Characteristics and mechanism of the Longyao ground fissure on North China Plain, China. *Engineering Geology*, *214*, 136–146.

Pérez, L. G., Vela, N., El Aatik, A., & Navarro, S. (2019). Environmental risk of groundwater pollution by pesticide leaching through the soil profile. *Pesticides-Use and Misuse and Their Impact in the Environment*, 1–28.

Perissin, D., & Wang, T. (2012). Repeat-pass SAR interferometry with partially coherent targets. *IEEE Transactions on Geoscience and Remote Sensing*. https://doi.org/10.1109/TGRS.2011.2160644

Poland. (1984). *Guidebook to studies of land subsidence due to ground-water withdrawal.*

Poland, J. F., & Davis, G. H. (1969). *Land subsidence due to withdrawal of fluids*.

Pratesi, F., Tapete, D., Del Ventisette, C., & Moretti, S. (2016). Mapping interactions between geology, subsurface resource exploitation and urban development in transforming cities using InSAR Persistent Scatterers: Two decades of change in Florence, Italy. *Applied Geography*,

`

77, 20–37.

Pratt, W. E., & Johnson, D. W. (1926). Local subsidence of the Goose Creek oil field. *The Journal of Geology*, *34*(7, Part 1), 577–590.

Price, M. (1987). Fluid flow in the Chalk of England. *Geological Society Special Publication*. https://doi.org/10.1144/GSL.SP.1987.034.01.10

Price, M., Bird, M. J., & Foster, S. S. D. (1976). CHALK PORE-SIZE MEASUREMENTS AND THEIR SIGNIFICANCE. *Water Services*. https://doi.org/10.1016/0148-9062(77)90617-9

Prokopovich, N. P., & Marriott, M. J. (1983). Cost of subsidence to the Central Valley Project, California. *Bulletin of the Association of Engineering Geologists*, *20*(3), 325–332.

Qian, H., Chen, J., & Howard, K. W. F. (2020). Assessing groundwater pollution and potential remediation processes in a multi-layer aquifer system. *Environmental Pollution*, *263*, 114669.

Quincey, D. J., Richardson, S. D., Luckman, A., Lucas, R. M., Reynolds, J. M., Hambrey, M. J., & Glasser, N. F. (2007). Early recognition of glacial lake hazards in the Himalaya using remote sensing datasets. *Global and Planetary Change*, *56*(1–2), 137–152.

Rabus, B., Eineder, M., Roth, A., & Bamler, R. (2003). The shuttle radar topography mission—a new class of digital elevation models acquired by spaceborne radar. *ISPRS Journal of Photogrammetry and Remote Sensing*, *57*(4), 241–262.

Rae, J. E., & Parker, A. (1992). Groundwater quality in the recharged London Basin, England I: Phase associations of iron, manganese, and sulfur in Tertiary Sands. *Environmental Geology and Water Sciences*. https://doi.org/10.1007/BF01797441

Ramillien, G., Frappart, F., Güntner, A., Ngo-Duc, T., Cazenave, A., & Laval, K. (2006). Time variations of the regional evapotranspiration rate from Gravity Recovery and Climate Experiment (GRACE) satellite gravimetry. *Water Resources Research*, *42*(10).

Ramillien, G., Frappart, F., & Seoane, L. (2014). Application of the regional water mass variations from GRACE satellite gravimetry to large-scale water management in Africa. *Remote Sensing*, *6*(8), 7379–7405.

Ramillien, G., Frappart, F., & Seoane, L. (2016). Space Gravimetry Using GRACE Satellite Mission: Basic Concepts. In *Microwave Remote Sensing of Land Surfaces: Techniques and*

`

Methods. https://doi.org/10.1016/B978-1-78548-159-8.50006-2

Rao, V. V. S. G., Rao, G. T., Surinaidu, L., Rajesh, R., & Mahesh, J. (2011). Geophysical and geochemical approach for seawater intrusion assessment in the Godavari Delta Basin, AP, India. *Water, Air, \& Soil Pollution*, *217*(1), 503–514.

Ratner, B. (2009). The correlation coefficient: Its values range between+ 1/− 1, or do they? *Journal of Targeting, Measurement and Analysis for Marketing*, *17*(2), 139–142.

Raucoules, D., Le Mouélic, S., Carnec, C., Maisons, C., & King, C. (2003). Urban subsidence in the city of Prato (Italy) monitored by satellite radar interferometry. *International Journal of Remote Sensing*, *24*(4), 891–897.

Reager, J. T., Thomas, B. F., & Famiglietti, J. S. (2014). River basin flood potential inferred using GRACE gravity observations at several months lead time. *Nature Geoscience*, *7*(8), 588–592.

Refice, A., Bovenga, F., Guerriero, L., & Wasowski, J. (2001). DInSAR applications to landslide studies. *International Geoscience and Remote Sensing Symposium (IGARSS)*. https://doi.org/10.1109/igarss.2001.976084

Richards, J. A. (2009). *Remote sensing with imaging radar* (Vol. 1). Springer.

Richey, A. S., Thomas, B. F., Lo, M.-H., Famiglietti, J. S., Swenson, S., & Rodell, M. (2015). Uncertainty in global groundwater storage estimates in a T otal G roundwater S tress framework. *Water Resources Research*, *51*(7), 5198–5216.

Riley, F. S. (1969). Analysis of Borehole Extensometer Data from Central California. *Land Subsidence, Volume 2*.

Rodell, M., Famiglietti, J. S., Chen, J., Seneviratne, S. I., Viterbo, P., Holl, S., & Wilson, C. R. (2004). Basin scale estimates of evapotranspiration using GRACE and other observations. *Geophysical Research Letters*, *31*(20).

Rodell, M., Velicogna, I., & Famiglietti, J. S. (2009). Satellite-based estimates of groundwater depletion in India. *Nature*. https://doi.org/10.1038/nature08238

Rogers, P. (2008). Facing the freshwater crisis. *Scientific American*, *299*(2), 46–53.

Rose, S., & Long, A. (1988). Monitoring dissolved oxygen in ground water: some basic considerations. *Groundwater Monitoring \& Remediation*, *8*(1), 93–97.

`

Rosen, P. A. (2000). Synthetic aperture radar interferometry. *Proceedings of the IEEE*. https://doi.org/10.1109/5.838084

Royse, K. R., De Freitas, M., Burgess, W. G., Cosgrove, J., Ghail, R. C., Gibbard, P., King, C., Lawrence, U., Mortimore, R. N., Owen, H., & Skipper, J. (2012). Geology of London, UK. In *Proceedings of the Geologists' Association*. https://doi.org/10.1016/j.pgeola.2011.07.005

RPackages. (2021). *R Pacakages and Products*. 22/05/2021

RWM. (2019). London and the Thames Valley: Regional Geology. *Radioactive Waste Management*.

Sahoo, S., & Sahoo, B. (2019). A geomorphology-based integrated stream--aquifer interaction model for semi-gauged catchments. *Hydrological Processes*, *33*(9), 1362–1377.

Sahraoui, O. H., Hassaine, B., & Serief, C. (2006). Radar Interferometry with Sarscape Software. *October*.

Sarkar, A., Ali, S., Kumar, S., Shekhar, S., & Rao, S. V. N. (2016). Groundwater environment in Delhi, India. In *Groundwater environment in Asian cities* (pp. 77–108). Elsevier.

Sarmap. (2014a). *PS Tutorial*.

Sarmap. (2014b). *SARscape help manual*.

Scanlon, B. R., Longuevergne, L., & Long, D. (2012). Ground referencing GRACE satellite estimates of groundwater storage changes in the California Central Valley, USA. *Water Resources Research*, *48*(4).

Schmidt, D. A., & Bürgmann, R. (2003). Time-dependent land uplift and subsidence in the Santa Clara valley, California, from a large interferometric synthetic aperture radar data set. *Journal of Geophysical Research: Solid Earth*, *108*(B9).

Schmidt, R., Flechtner, F., Meyer, U., Neumayer, K.-H., Dahle, C., König, R., & Kusche, J. (2008). Hydrological signals observed by the GRACE satellites. *Surveys in Geophysics*, *29*(4–5), 319–334.

Schulz, W. H., Coe, J. A., Ricci, P. P., Smoczyk, G. M., Shurtleff, B. L., & Panosky, J. (2017). Landslide kinematics and their potential controls from hourly to decadal timescales: Insights from integrating ground-based InSAR measurements with structural maps and long-term

monitoring data. *Geomorphology*, *285*, 121–136.

Scoular, J., Ghail, R., Mason, P., Lawrence, J., Bellhouse, M., Holley, R., & Morgan, T. (2020). Retrospective InSAR analysis of East London during the construction of the Lee Tunnel. *Remote Sensing*, *12*(5), 849.

SCR. (1993). *CEOS SAR Calibration Workshop, ESTEC Noordwijk, The Netherlands, 20–24 Sept. 1993*.

Seasat. (2020). *Seasat*. https://directory.eoportal.org/web/eoportal/satellite-missions/s/seasat Last accessed: 2020-10-01

Shah, T. (2005). Groundwater and human development: challenges and opportunities in livelihoods and environment. *Water Science and Technology*, *51*(8), 27–37.

Shah, T., Roy, A. D., Qureshi, A. S., & Wang, J. (2003). Sustaining Asia's groundwater boom: an overview of issues and evidence. *Natural Resources Forum*, *27*(2), 130–141.

Shand, P., Edmunds, W. M., Lawrence, A. R., Smedley, P. L., & Burke, S. (2007). The natural (baseline) quality of groundwater in England and Wales. In *BGS Research Report RR/07/06*.

Shao, L. (2019). Geological disaster prevention and control and resource protection in mineral resource exploitation region. *International Journal of Low-Carbon Technologies*, *14*(2), 142–146.

Sharma, M. (2021). Groundwater Analytics for Measuring Quality and Quantity. In *Geospatial Technology and Smart Cities* (pp. 415–430). Springer.

Shearer, T. R. (1998). A numerical model to calculate land subsidence, applied at Hangu in China. *Engineering Geology*, *49*(2), 85–93.

Shen, H., Leblanc, M., Tweed, S., & Liu, W. (2015). Groundwater depletion in the Hai River Basin, China, from in situ and GRACE observations. *Hydrological Sciences Journal*, *60*(4), 671–687.

Sidhu, B. S., Sharda, R., & Singh, S. (2021). Spatio-temporal assessment of groundwater depletion in Punjab, India. *Groundwater for Sustainable Development*, *12*, 100498.

Sidiropoulos, P., Dalezios, N. R., Loukas, A., Mylopoulos, N., Spiliotopoulos, M., Faraslis, I. N., Alpanakis, N., & Sakellariou, S. (2021). Quantitative classification of desertification severity

for degraded aquifer based on remotely sensed drought assessment. *Hydrology*, *8*(1), 47.

Siebert, S., Burke, J., Faures, J.-M., Frenken, K., Hoogeveen, J., Döll, P., & Portmann, F. T. (2010). Groundwater use for irrigation--a global inventory. *Hydrology and Earth System Sciences*, *14*(10), 1863–1880.

Sierra, L. A., Yepes, V., & Pellicer, E. (2018). A review of multi-criteria assessment of the social sustainability of infrastructures. *Journal of Cleaner Production*, *187*, 496–513.

Simonetto, E. (2008). DINSAR experiments using a free processing chain. *Image and Signal Processing for Remote Sensing XIV*. https://doi.org/10.1117/12.802508

Simonetto, E., & Follin, J. M. (2012). An overview on interferometric SAR software and a comparison between DORIS and SARSCAPE Packages. *Lecture Notes in Geoinformation and Cartography*. https://doi.org/10.1007/978-3-642-10595-1_7

SLC. (2020). *Sentinel-1A*. https://sentinel.esa.int/web/sentinel/user-guides/sentinel-1-sar/resolutions/level-1-single-look-complex/ Last Accessed: 2020-09-25

Smith, L. C. (2002). Emerging applications of interferometric synthetic aperture radar (InSAR) in geomorphology and hydrology. In *Annals of the Association of American Geographers*. https://doi.org/10.1111/1467-8306.00295

Smith, L. C., Alsdorf, D. E., Magilligan, F. J., Gomez, B., Mertes, L. A. K., Smith, N. D., & Garvin, J. B. (2000). Estimation of erosion, deposition, and net volumetric change caused by the 1996 Skei{\dh}arársandur jökulhlaup, Iceland, from synthetic aperture radar interferometry. *Water Resources Research*, *36*(6), 1583–1594.

Standing, J., & Selman, R. (2001). Building response to Tunnelling - Case studies from construction of the Jubilee Line Extension, London. *Ciria*.

Stigler, S. M. (1989). Francis Galton's Account of the Invention of Correlation. *Statistical Science*, *4*(2), 73–79. https://doi.org/10.1214/ss/1177012580

Strassberg, G., Scanlon, B. R., & Chambers, D. (2009). Evaluation of groundwater storage monitoring with the GRACE satellite: Case study of the High Plains aquifer, central United States. *Water Resources Research*, *45*(5).

Strozzi, T., Farina, P., Corsini, A., Ambrosi, C., Thüring, M., Zilger, J., Wiesmann, A., Wegmüller,

U., & Werner, C. (2005). Survey and monitoring of landslide displacements by means of L-band satellite SAR interferometry. *Landslides*, *2*(3), 193–201.

Strozzi, T., Luckman, A., Murray, T., Wegmuller, U., & Werner, C. L. (2002). Glacier motion estimation using SAR offset-tracking procedures. *IEEE Transactions on Geoscience and Remote Sensing*, *40*(11), 2384–2391.

Stuart, M., Lapworth, D., Crane, E., & Hart, A. (2012). Review of risk from potential emerging contaminants in UK groundwater. *Science of the Total Environment*, *416*, 1–21.

Stumm, W., & Morgan, J. J. (1981). Aquatic chemistry: an introduction emphasizing equilibria in natural waters. *New York, 780p*.

Sun, Q., Zhang, L., Ding, X. L., Hu, J., Li, Z. W., & Zhu, J. J. (2015). Slope deformation prior to Zhouqu, China landslide from InSAR time series analysis. *Remote Sensing of Environment*, *156*, 45–57.

Sun, Z., Long, D., Yang, W., Li, X., & Pan, Y. (2020). Reconstruction of GRACE data on changes in total water storage over the global land surface and 60 basins. *Water Resources Research*, *56*(4), e2019WR026250.

Suthar, S., Bishnoi, P., Singh, S., Mutiyar, P. K., Nema, A. K., & Patil, N. S. (2009). Nitrate contamination in groundwater of some rural areas of Rajasthan, India. *Journal of Hazardous Materials*, *171*(1–3), 189–199.

Swenson, S., Famiglietti, J., Basara, J., & Wahr, J. (2008). Estimating profile soil moisture and groundwater variations using GRACE and Oklahoma Mesonet soil moisture data. *Water Resources Research*, *44*(1).

Syed, T. H., Famiglietti, J. S., & Chambers, D. P. (2009). GRACE-based estimates of terrestrial freshwater discharge from basin to continental scales. *Journal of Hydrometeorology*, *10*(1), 22–40.

Syed, T. H., Famiglietti, J. S., Rodell, M., Chen, J., & Wilson, C. R. (2008). Analysis of terrestrial water storage changes from GRACE and GLDAS. *Water Resources Research*, *44*(2).

Talabi, A. O., Kayode, T. J., & others. (2019). Groundwater pollution and remediation. *Journal of Water Resource and Protection*, *11*(01), 1.

`

Tapley, B., Bettadpur, S., Ries, J., Thompson, P., & Watkins, M. (2004). GRACE measurements of mass variability in the Earth system. *Science*, *305*(5683), 503–505.

Tapley, B., Bettadpur, S., Watkins, C., & Reigber, M. (2004). The gravity recovery and climate experiment: Mission overview and early results. *Geophysical Research Letters*, *31*(9).

Teatini, P., Tosi, L., Strozzi, T., Carbognin, L., Wegmüller, U., & Rizzetto, F. (2005). Mapping regional land displacements in the Venice coastland by an integrated monitoring system. *Remote Sensing of Environment*, *98*(4), 403–413.

Terzaghi, K. (1925). Principles of soil mechanics, IV—Settlement and consolidation of clay. *Engineering News-Record*, *95*(3), 874–878.

Terzaghi Karl. (1943). Theory of consolidation. *Theoretical Soil Mechanics*, 265–296.

Thames Water. (2015). Final Water Resources Management Plan. *Executive Summary*.

Thomas, K. S., Dean, T., O'Leary, C., Sach, T. H., Koller, K., Frost, A., & Williams, H. C. (2011). A randomised controlled trial of ion-exchange water softeners for the treatment of eczema in children. *PLoS Medicine*. https://doi.org/10.1371/journal.pmed.1000395

Tiwari, A. K., & Pal, D. B. (2021). Recent Trends in Groundwater Conservation and Management. *Groundwater Geochemistry: Pollution and Remediation Methods*, 379–391.

Tiwari, V. M., Wahr, J., & Swenson, S. (2009). Dwindling groundwater resources in northern India, from satellite gravity observations. *Geophysical Research Letters*. https://doi.org/10.1029/2009GL039401

Todd, D. . (1959). Ground water hydrology. United States. *John Wiley and Sons Inc.*, 277–294.

Tourian, M. J., Elmi, O., Chen, Q., Devaraju, B., Roohi, S., & Sneeuw, N. (2015). A spaceborne multisensor approach to monitor the desiccation of Lake Urmia in Iran. *Remote Sensing of Environment*. https://doi.org/10.1016/j.rse.2014.10.006

Transport for London, T. (2021). *Northern line extension - Transport for London*. https://tfl.gov.uk/travel-information/improvements-and-projects/northern-line-extension

TWUL. (2020). *Thames Water Utility Ltd. Final Water Resource Management Plan 2015–2040*. https://www.oxford.gov.uk/download/downloads/id/5691/rse11_-_water_resources_management_plan_2015-2040_-_executive_summary.pdf

`

UK Groundwater forum. (1998). Groundwater of hidden assest. *The Thames Groundwater Scheme. Institution of Civil Engineers, London., Britisg Geological Survey, Keyworth*.

UKGW. (2021). *Importance of groundwater, United Kingdom*. http://www.groundwateruk.org/Why-is-Groundwater-Important.aspx

Unavco. (2020). *Synthetic Aperture Radar (SAR) Data*. https://www.unavco.org/data/sar/sar.html Last Accessed: 2020-10-05

UNESCO, I. (1970). Land Subsidence: Proceedings of the First International Symposium on Land Subsidence, Tokyo, 1969. *International Association of Scientific Hydrology (IASH)*.

Ungureanu, N., Vluaduț, V., & Voicu, G. (2020). Water scarcity and wastewater reuse in crop irrigation. *Sustainability*, *12*(21), 9055.

USGS. (2012). Phosphorus and Groundwater: Establishing Links Between Agricultural Use and Transport to Streams. *National Water-Quality Assessment Program, Agricultural Chemicals Team (ACT)*.

USGS. (2021a). *Groundwater Flow Diagram*. USGS. https://www.usgs.gov/media/images/conceptual-groundwater-flow-diagram

USGS. (2021b). *USGS - Content of Natural water*. USGS.

USGS. (2021c). *USGS - What is groundwater*. USGS. https://www.usgs.gov/faqs/what-groundwater?qt-news_science_products=0#qt-news_science_products

Vadon, H., & Sigmundsson, F. (1997). Crustal deformation from 1992 to 1995 at the Mid-Atlantic Ridge, southwest Iceland, mapped by satellite radar interferometry. *Science*, *275*(5297), 194–197.

Victor, C., Fayin, L., S-S, H., & Harry, W. (2006). Micro-Doppler effect in radar: phenomenon, model, and simulation study. *IEEE Transactions on Aerospace and Electronic Systems*, *42*(1), 2–21.

Vieli, A., Payne, A. J., Shepherd, A., & Du, Z. (2007). Causes of pre-collapse changes of the Larsen B ice shelf: Numerical modelling and assimilation of satellite observations. *Earth and Planetary Science Letters*, *259*(3–4), 297–306.

Villholth, K., Giordano, M., & others. (2007). Groundwater use in a global perspective--can it be

managed. *The Agricultural Groundwater Revolution: Opportunities and Threats to Development*, *3*, 393–402.

Vörösmarty, C. J., Green, P., Salisbury, J., & Lammers, R. B. (2000). Global water resources: vulnerability from climate change and population growth. *Science*, *289*(5477), 284–288.

Voss, K. A., Famiglietti, J. S., Lo, M., De Linage, C., Rodell, M., & Swenson, S. C. (2013). Groundwater depletion in the Middle East from GRACE with implications for transboundary water management in the Tigris-Euphrates-Western Iran region. *Water Resources Research*, *49*(2), 904–914.

Wada, Y., Van Beek, L. P. H., Van Kempen, C. M., Reckman, J. W. T. M., Vasak, S., & Bierkens, M. F. P. (2010). Global depletion of groundwater resources. *Geophysical Research Letters*, *37*(20).

Wadge, G., Webley, P. W., James, I. N., Bingley, R., Dodson, A., Waugh, S., Veneboer, T., Puglisi, G., Mattia, M., Baker, D., & others. (2002). Atmospheric models, GPS and InSAR measurements of the tropospheric water vapour field over Mount Etna. *Geophysical Research Letters*, *29*(19), 11.

Wahr, J., Molenaar, M., & Bryan, F. (1998). Time variability of the Earth's gravity field: Hydrological and oceanic effects and their possible detection using GRACE. *Journal of Geophysical Research: Solid Earth*. https://doi.org/10.1029/98jb02844

Wakida, F. T., & Lerner, D. N. (2005). Non-agricultural sources of groundwater nitrate: a review and case study. *Water Research*, *39*(1), 3–16.

Wang, H.-M., Wang, Y., Jiao, X., & Qian, G.-R. (2014). Risk management of land subsidence in Shanghai. *Desalination and Water Treatment*, *52*(4–6), 1122–1129.

Wang, X., De Linage, C., Famiglietti, J., & Zender, C. S. (2011). Gravity Recovery and Climate Experiment (GRACE) detection of water storage changes in the Three Gorges Reservoir of China and comparison with in situ measurements. *Water Resources Research*. https://doi.org/10.1029/2011WR010534

Wang, Y., Wang, L., Zhang, Y., & Yang, T. (2015). Investigation of snow cover change using multi-temporal PALSAR InSAR data at Dagu Glacier, China. *International Geoscience and Remote Sensing Symposium (IGARSS)*. https://doi.org/10.1109/IGARSS.2015.7325872

`

Wang, Y., Yang, J., & Chang, J. (2019). Development of a coupled quantity-quality-environment water allocation model applying the optimization-simulation method. *Journal of Cleaner Production*, *213*, 944–955.

Watson, K. M., Bock, Y., & Sandwell, D. T. (2002). Satellite interferometric observations of displacements associated with seasonal groundwater in the Los Angeles basin. *Journal of Geophysical Research: Solid Earth*, *107*(B4), ETG--8.

Wdowinski, S., Kim, S.-W., Amelung, F., Dixon, T. H., Miralles-Wilhelm, F., & Sonenshein, R. (2008). Space-based detection of wetlands' surface water level changes from L-band SAR interferometry. *Remote Sensing of Environment*, *112*(3), 681–696.

Weast, R. C., & Astle, M. J. (1983). *CRC Handbook of Chemistry and Physics...: 1983-1984*. CRC press.

Webley, P. W., Bingley, R. M., Dodson, A. H., Wadge, G., Waugh, S. J., & James, I. N. (2002). Atmospheric water vapour correction to InSAR surface motion measurements on mountains: results from a dense GPS network on Mount Etna. *Physics and Chemistry of the Earth, Parts A/B/C*, *27*(4–5), 363–370.

Werner, C., Wegmüller, U., Strozzi, T., & Wiesmann, A. (2003). Interferometric Point Target Analysis for Deformation Mapping. *International Geoscience and Remote Sensing Symposium (IGARSS)*. https://doi.org/10.1109/igarss.2003.1295516

WHO. (2017). *Guidelines for drinking-water quality: first addendum to the fourth edition*.

Wilkinson, B., & others. (1985). Rising groundwater levels in London and possible effects on engineering structures. *Proceedings of the 18th Congress of the IAH, Cambridge*, 145–157.

Wilson, J. T., & McNabb, J. F. (1983). Biological transformation of organic pollutants in groundwater. *Eos, Transactions American Geophysical Union*, *64*(33), 505.

Winograd, I. J., & Robertson, F. N. (1982). Deep oxygenated ground water: anomaly or common occurrence? *Science*, *216*(4551), 1227–1230.

Witkowski, M., & Massmann, F. H. (2014). Status GRACE mission operations. GRACE Science Team Meeting. *GSTM Proceedings*.

Wolf, L., Morris, B., & Burn, S. (2007). *Urban Water Resources Toolbox*. IWA Publishing.

`

Wolf, L., Morris, B., & Burn, S. (2015). Urban Water Resources Toolbox - Integrating Groundwater into Urban Water Management. *Water Intelligence Online*. https://doi.org/10.2166/9781780402437

Wouters, B., Bonin, J. A., Chambers, D. P., Riva, R. E. M., Sasgen, I., & Wahr, J. (2014). GRACE, time-varying gravity, Earth system dynamics and climate change. *Reports on Progress in Physics*, *77*(11), 116801.

Wright, T. J., Parsons, B., England, P. C., & Fielding, E. J. (2004). InSAR observations of low slip rates on the major faults of western Tibet. *Science*, *305*(5681), 236–239.

WRMP. (2021). *Water Resource Management Plan, Annual Review Report*. https://www.thameswater.co.uk/media-library/home/about-us/regulation/water-resources/annual-review.pdf

Yamamoto, S., & others. (1995). Recent trend of land subsidence in Japan. *IAHS Publications-Series of Proceedings and Reports-Intern Assoc Hydrological Sciences*, *234*, 487.

Yang, F., Liu, S., Jia, C., Gao, M., Chang, W., & Wang, Y. (2021). Hydrochemical characteristics and functions of groundwater in southern Laizhou Bay based on the multivariate statistical analysis approach. *Estuarine, Coastal and Shelf Science*, *250*, 107153.

Ye, S., Xue, Y., Wu, J., Yan, X., & Yu, J. (2016). Progression and mitigation of land subsidence in China. *Hydrogeology Journal*, *24*(3), 685–693.

Yong, W., Lei, W., Yin, Z., & Taoli, Y. (2015). Investigation of snow cover change using multi-temporal PALSAR InSAR data at Dagu Glacier, China. *International Geoscience and Remote Sensing Symposium (IGARSS)*. https://doi.org/10.1109/IGARSS.2015.7325872

Yu, H., Gong, H., Chen, B., Liu, K., & Gao, M. (2020). Analysis of the influence of groundwater on land subsidence in Beijing based on the geographical weighted regression (GWR) model. *Science of The Total Environment*, *738*, 139405.

Zaitchik, B. F., Rodell, M., & Reichle, R. H. (2008). Assimilation of GRACE terrestrial water storage data into a land surface model: Results for the Mississippi River basin. *Journal of Hydrometeorology*. https://doi.org/10.1175/2007JHM951.1

Zebker, H. A., & Goldstein, R. M. (1986). Topographic mapping from interferometric synthetic

aperture radar observations. *Journal of Geophysical Research: Solid Earth*, *91*(B5), 4993–4999.

Zebker, H. A., Rosen, P. A., & Hensley, S. (1997). Atmospheric effects in interferometric synthetic aperture radar surface deformation and topographic maps. *Journal of Geophysical Research: Solid Earth*, *102*(B4), 7547–7563.

Zebker, H. A., Villasenor, J., & others. (1992). Decorrelation in interferometric radar echoes. *IEEE Transactions on Geoscience and Remote Sensing*, *30*(5), 950–959.

Zebker, H. A., Werner, C. L., Rosen, P. A., & Hensley, S. (1994). Accuracy of topographic maps derived from ERS-1 interferometric radar. *IEEE Transactions on Geoscience and Remote Sensing*, *32*(4), 823–836.

Zektser, I. S., & Everett, L. G. (2004). *Groundwater resources of the world and their use*.

Zhang, H., Yang, R., Wang, Y., & Ye, R. (2019). The evaluation and prediction of agriculture-related nitrate contamination in groundwater in Chengdu Plain, southwestern China. *Hydrogeology Journal*, *27*(2), 785–799.

Zhang, L., Dobslaw, H., Dahle, C., Sasgen, I., & Thomas, M. (2016). *Validation of MPI-ESM decadal hindcast experiments with terrestrial water storage variations as observed by the GRACE satellite mission*.

Zhang, Y.-Q., Wang, J.-H., & Li, M.-G. (2018). Effect of dewatering in a confined aquifer on ground settlement in deep excavations. *International Journal of Geomechanics*, *18*(10), 4018120.

Zhang, Y., Meng, X. M., Dijkstra, T. A., Jordan, C. J., Chen, G., Zeng, R. Q., & Novellino, A. (2020). Forecasting the magnitude of potential landslides based on InSAR techniques. *Remote Sensing of Environment*, *241*, 111738.

Zheng, G., Ha, D., Zeng, C., Cheng, X., Zhou, H., & Cao, J. (2019). Influence of the opening timing of recharge wells on settlement caused by dewatering in excavations. *Journal of Hydrology*, *573*, 534–545.

Zheng, M., Deng, K., Fan, H., & Du, S. (2018). Monitoring and analysis of surface deformation in mining area based on InSAR and GRACE. *Remote Sensing*, *10*(9).

https://doi.org/10.3390/rs10091392

Zhou, X., Chen, M., & Liang, C. (2003). Optimal schemes of groundwater exploitation for prevention of seawater intrusion in the Leizhou Peninsula in southern China. *Environmental Geology*, *43*(8), 978–985.

Zhou, Y., Dong, D., Liu, J., & Li, W. (2013). Upgrading a regional groundwater level monitoring network for Beijing Plain, China. *Geoscience Frontiers*, *4*(1), 127–138.

Zhu, Y., Liu, S., Yi, Y., Qi, M., Li, W., Saifullah, M., Zhang, S., & Wu, K. (2021). Spatio-temporal variations in terrestrial water storage and its controlling factors in the Eastern Qinghai-Tibet Plateau. *Hydrology Research*, *52*(1), 323–338.

Zimmerman, R. W. (1990). *Compressibility of sandstones*.

Zou, Q., Zhou, J., Zhou, C., Song, L., & Guo, J. (2013). Comprehensive flood risk assessment based on set pair analysis-variable fuzzy sets model and fuzzy AHP. *Stochastic Environmental Research and Risk Assessment*, *27*(2), 525–546.

Zuoding, L. (2002). RESEARCH ON GROUNDWATER EXPLOITATION, UTILIZATION AND ANALYSIS. In *Bureau of Hydrology, Ministry of Water Resources, Beijing 100053, China*. http://www.iugg.org/members/nationalreports/china2002/chinaIAHS/CHAPTER 2 RESEARCH ON GROUNDWATER EXPLOITATION.htm